Carbon fixation in the Hydrosphere: Quantification for the Indian region using ^{13}C & ^{15}N isotopes

A THESIS

submitted for the Award of Ph. D. degree of

MOHANLAL SUKHADIA UNIVERSITY

in the

Faculty of Science

by

Naveen Gandhi

Under the Supervision of

Prof. R. Ramesh

Senior Professor
Geosciences Division
Physical Research Laboratory, Ahmedabad, India.

DEPARTMENT OF PHYSICS

MOHANLAL SUKHADIA UNIVERSITY

UDAIPUR

2010

CERTIFICATE

I feel great pleasure in certifying the thesis entitled "**Carbon fixation in the Hydrosphere: Quantification for the Indian region using ^{13}C and ^{15}N isotopes**" by Mr. Naveen Gandhi under my guidance. He has completed the following requirements as per Ph.D. regulations of the University

(a) Course work as per the university rules.

(b) Residential requirements of the university.

(c) Presented his work in the departmental committee.

(d) Published/accepted minimum of one research paper in a referred research journal,

I am satisfied with the analysis of data, interpretation of results and conclusions drawn.

I recommend the submission of thesis.

Date: 2010

Prof. R. Ramesh
(Supervisor)
Senior Professor
Physical Research Laboratory
Ahmedabad, India.

DECLARATION

*I Mr Naveen Gandhi, S/o Mr. Bhagwan Dass Gandhi, resident of A-4, PRL residences, Navrangpura, Ahmedabad - 380009, hereby declare that the research work incorporated in the present thesis entitled "***Carbon fixation in the Hydrosphere: Quantification for the Indian region using ^{13}C and ^{15}N isotopes***" is my own work and is original. This work (in part or in full) has not been submitted to any University for the award of a Degree or a Diploma. I have properly acknowledged the material collected from secondary sources wherever required. I solely own the responsibility for the originality of the entire content.*

Date:

Naveen Gandhi

(Author)

To my

Maa and Papa

Acknowledgments

This thesis arose in part out of years of research that has been done since I came to PRL. By that time, I have worked with a great number of people whose contribution in assorted ways to the research and the making of the thesis deserved special mention. It is a pleasure to convey my gratitude to them all in my humble acknowledgment. In the first place, I would like to record my gratitude to my thesis supervisor Prof. R. Ramesh for his supervision, advice, and guidance from the very early stage of this research as well as giving me extraordinary experiences through out the work. Above all and the most needed, he provided me unflinching encouragement and support in various ways. His intuition has made him as a constant oasis of ideas in science, which exceptionally inspired and enriched my growth as a student, a researcher and a scientist I want to be. I am indebted to him.

I gratefully acknowledge Prof. M. M. Sarin for his advice, and critical comments during various stages of this thesis work. I also benefitted from him by doing a project under him during my course work at PRL. His involvement with his originality has triggered and nourished my scientific understanding.

I am very much indebted to Drs. J. S. Ray, M. G. Yadava and all the members of Planetary and Geosciences Division for their constructive comments and suggestions during various area seminars and reviews. Their guidance always helped to improve the quality of the research work.

I would like to thank N. B. Vaghela for being the first person who taught me how to work with vacuum systems. I am proud to record that I had several opportunities to work with an exceptionally experienced person like him.

I am grateful to Dr. M. S. Sheshshayee for providing all the facilities for my sample analyses at University of Agricultural Sciences, Bangalore. My special thanks to Bhushana for his help in various ways during my stay at Bangalore.

Collective and individual acknowledgments are also owed to my colleagues Satya, Shreyas, Ashutosh, Rohit, Arvind and Amzad whose present somehow perpetually refreshed, helpful, and memorable.

I would like to show my gratitude to Dr. P. Sharma and for his help and care during course work at PRL. I also thank Dr. B. Vaishnav for advice and help during reviews at PRL and Ph.D. registration at Udaipur.

I acknowledge with thanks Drs. S. Prasanna Kumar (National Institute of Oceanography; NIO, Goa), M. Sudhakar, N. Anil Kumar, M. M. Subramaniam, Ravi Mishra (National centre for Antarctic and Ocean Research; NCAOR, Goa), R. M. Dwivedi, Prakash Chauhan, Mini Raman (Space Application Centre, Ahmedabad) for giving me the opportunity to participate in various research cruises. Thanks are due to Drs. S. W. A. Naqvi, M. V. M. Wafar, Prabhu

Matondakar (NIO, Goa), for nitrate, Chlorophyll and cell counts data during Arabian Sea cruises. My special thanks to Suhas (NCAOR, Goa) for nutrients and chlorophyll measurements during Bay of Bengal, Equatorial Indian Ocean and Southern Ocean cruises. I thank Dr. S. Mukhopadhyay, formaly at Central Salt and Marine Chemicals Research Institute, Bhavnagar, for teaching me nutrient analysis. Thanks are due to my friends P. V. Nagamani, Arvind Sahay, Suraksha, Swetali, Racheal, Sharon, Ratna, Shramik, Sunil Shukla, Rahul, Bhuvaneswari, Elizabeth, Zeena, Padma Kumar, Nivedita, and Madhumita for making the cruises memorable. I also thank ISRO-GBP for funding provided for the cruises.

I would also like to thank all the reviewers and editors for reviewing and providing critical comments to improve my manuscripts (published and/or under review in different journals).

I owe a special appreciation to Prof. Rajesh Pandey for encouragement during various stages, which has helped me to improve this work. The Physics Department and the Ph.D. section of Mohan Lal Sukhadia University, Udaipur has provided the support I have needed to produce and complete my thesis.

The generous support from Janiji, D. K. Rao, Navin Juyal, R. D. Deshpande, Ravi Bhushan, R. Rengarajan, A. K. Sudheer, A. D. Shukla, Mahajanji, Neeraj Srivastava, Dipak Panda, and Pranav bhai is greatly appreciated.

I am very grateful to all the members of the Computer center, especially Jigar bhai, Tejas, Alok, Mishra Ji for the help in computer related works. My special thanks go to Mrs. Nandini Rao for her help during procuring chemicals and instruments for my thesis work. Furthermore, I would like to thank Uma madam, Nishtha madam, Pragya, Alam, and all the supporting staff of PRL library. I would also acknowledge people from different sections of PRL: G. P. Patel, Gopi, Parul madam, D. H. Gandhi, Priti madam, Pauline, Jayashree, Ranganathan, R. S. Gupta, Bankim, Atul Manke, Keyur, Senthil Babu, Manan Shah, and Sivadasan for their help in various stages.

I also benefited by outstanding works, from my seniors at PRL, those inspired me throughout my thesis work. I thank to Drs. Sanjeev Kumar, Neeraj Rastogi, Santosh Rai, Anirban Das, Lokesh Sahu, Harish Gadhavi, Y. C. Nagar, Morthekai, R. S. Gauda, Amit Misra, Antra, Vandana, Sanat, Uma, Subimal, Sasadhar, Ritesh, Rajesh, and A. S. Mauraya.

In my daily work, I have been blessed with a friendly and cheerful group of fellow students. I thank to Anil, Ashwini, Gyana, Alok, Shuchita, Sumanta, Rahaman, Kirpa, Sanjeev, Ramji, Bhavik, Vishal, Manan, Harinder, Timmy, Chandramohan (CM), Jitendra bhatt for creating lively atmosphere at PRL and hostel.

I was fortunate to have wonderful juniors at PRL. I sincerely thank Shinde, Naveen Chauhan, Rabiul, Vimal, Anand, Bhaswar, Soumya, Pankaj, Vineet, Suman, Shreekanth, Rohit, Ashok, Suratna, Neeraj, Ashish, Jayati, Patra, Arvind Singh Rajpurohit, Prashant, Arvind Saxena, Srinivas, Satinder, Chinmay, Yogita, Moumita, Tapas and many others for

making me feel at home.

Where would I be without my family? My parents deserve special mention for their inseparable support and prayers. My Mother, Mrs. Madhu Gandhi, in the first place is the person who put the fundament my learning character, showing me the joy of intellectual pursuit ever since I was a child. She has always supported my dreams and aspirations. I thank her for all she is and all she has done for me. My Father, Mr. Bhagwan Dass Gandhi, is the one who sincerely raised me with his caring and gently love. Kavita, my sister, thanks for being supportive and caring. My special thanks to my jijaji, Mr. Chandresh Vijay, who was always there for me whenever it mattered the most. The acknowledgment cannot be finished without mentioning cute smiles of my nephew and niece (Pratham and Prakriti) who always relaxed and made me cheer up.

I am particularly indebted to my childhood friend Jitendra. I have found him standing with me always when I required. He has been a constant source of support and encouragement.

Words fail me to express my appreciation to my wife Sumita whose dedication, love and persistent confidence in me, has taken the load off my shoulder. I owe her for being unselfishly let her intelligence, passions, and ambitions collide with mine. Therefore, I would also like to thank Mr. and Mrs. Bishwanath Kedia for letting me take her hand in marriage, and accepting me as a member of the family. I also thank Sunita-Nilu bhaiya, Sunil and Monika for their love and affection for me.

Finally, I would like to thank everybody who was important to the successful realization of thesis, as well as expressing my apology that I could not mention personally one by one.

Naveen Gandhi

Abstract

^{13}C and ^{15}N tracer techniques have been used to measure total and new productivity in different oceanic regions viz., the Arabian Sea (AS), the Bay of Bengal (BOB), the equatorial Indian Ocean (EIO), and the Indian sector of the Southern Ocean (SO) during different seasons between 2006 and 2009. The AS remains low productive during spring and shows higher new productivity during late winter. Different plankton species dominate during different seasons here. However, diatoms invariably remain significant in all the seasons and regions. Preliminary results show that the north-western AS is known to be dominated by *Noctiluca miliaris* blooms and the eastern AS, by diatoms. The present study provides the first evidence of photo-inhibition in the surface waters of the region. When light intensity exceeds 1200 mol $m^{-2}s^{-1}$, surface productivity decreases due to photo-inhibition. Further, the highest specific uptake rate is found in the morning, followed by the evening and the noon during winter. The BOB shows east-west variation in productivity with the western BOB exhibiting higher productivity. NO_3 is found to be the most preferred nitrogen compound followed by urea and NH_4 by phytoplankton during spring. The BOB has larger contribution relative to the AS in the sequestration of CO_2 from the atmosphere, particularly during spring. During early winter, eddy-pumping supplies nutrients from the deep and enhances the new productivity. Integrated new productivity is more than two times higher at the center of the eddy than its value outside, which suggests that eddies are capable of exporting most of the total production to the deep. The EIO shows comparable new productivity and f-ratios to that obtained from the other parts of the Indian Ocean. A comparison of earlier findings with the present study rules out any significant change in productivity in the EIO over the past 3-decades. In the SO, the highest surface chl a (>0.5 mg m^{-3}) is found at the Subtropical convergence. On either side of the Subtropical convergence, surface chl a is lower. The new productivity covaries with the overall productivity, while uptake of reduced forms of nitrogen (NH_4 and urea) shows opposite trends. The SO shows a large latitudinal variability in chlorophyll, productivity, new productivity and

f-ratios. Preference to different nitrogenous compounds also varies with latitude in the region. The present study provides a valuable data set for this region. This can be combined with the biological models to ascertain the role of the region in the global nitrogen and carbon budgets.

Key words: Indian region; ^{13}C *and* ^{15}N *tracer techniques; new productivity; f-ratio; nutrients; eddy-pumping; light intensity.*

Contents

List of Figures

List of Tables

Chapter 1

Introduction

1.1 Background

The total carbon on the earth is distributed among four main reservoirs: the atmosphere, the hydrosphere (mainly the oceans), land, and fossil fuels. The global carbon budget is the balance of the exchanges (incomes and losses) of carbon between these reservoirs (e.g., atmosphere↔hydroshpere). In the atmosphere, the globally averaged concentration of CO_2 is nearly 0.0387% (387 ppmv), equivalent to approximately 805 PgC (1 Pg = 1 Gt = 10^{15} g). The total amount of carbon in the world oceans is approximately 38,000 Pg, nearly 50 times more than in the atmosphere. Most of this is present in intermediate and deep waters; only 700-1000 PgC is in the surface ocean and in direct contact with the atmosphere. There are also 6000 Pg of carbon locked up in ocean sediments. The amount of carbon contained in terrestrial vegetation (550±100 Pg) is of the same order as in the atmosphere (800 Pg). The organic matter in soils is two to three times this amount [1500-2000 PgC in the top meter and as much as 2300 PgC in the top 3 m (*Jobaggy and Jackson*, 2000)]. The amount of carbon stored in reserves of coal, oil, and gas, which are the residuals of organic matter formed millions of years ago by plants, is estimated to be 5000-10,000 Pg, larger than any other reservoir except the deep sea, and about ten times the carbon content of the atmosphere

(*Houghton*, 2007). The exchanges of carbon within and among these reservoirs is called the global carbon cycle. The exchanges may occur in seconds (for example, the fixation of atmospheric CO_2 through photosynthesis) or over millennia [for example, the accumulation of fossil carbon (coal, oil, gas) through the deposition and diagenesis of organic matter]. The global carbon cycle is shown in a simplified form in Fig 1.1.

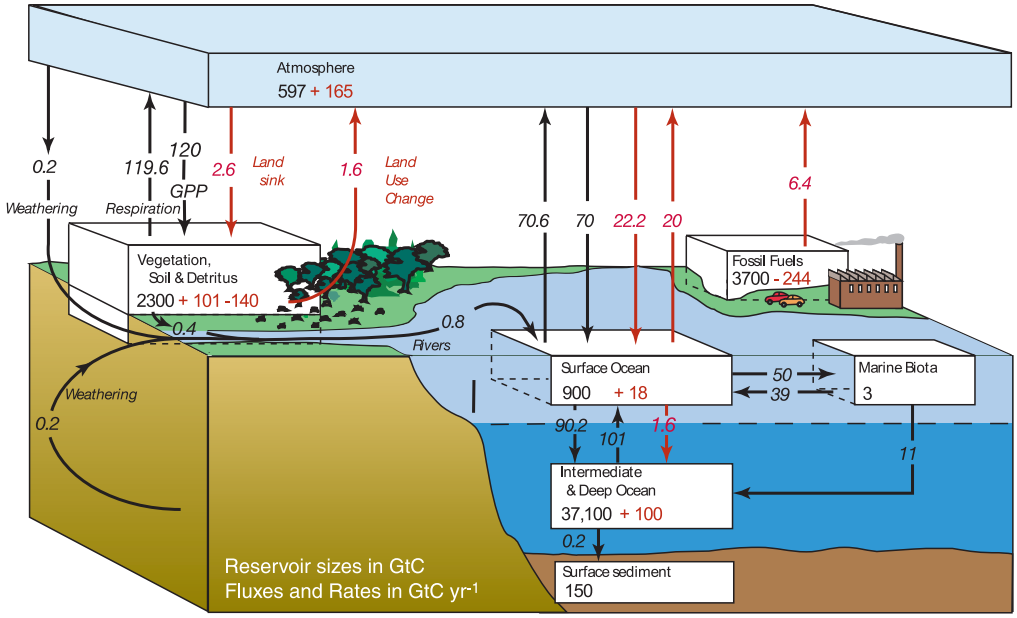

Figure 1.1: *Schematic of the global carbon cycle for the 1990s, showing the main annual fluxes in GtC* yr^{-1}*: pre-industrial natural fluxes in black, and anthropogenic fluxes in red; other uncertainties given in their Table 1).(Source: Fourth Assessment Report of the Intergovernmental Panel on Climate Change (IPCC) 2007; Denman et al., 2007)*

Each year, CO_2 released to the atmosphere by human activity including fossil fuel combustion and land use change, perturbs the global carbon cycle. These perturbations (shown in red in Fig 1.1) are the dominant drivers of the present day climate change because of their persistent effect on the atmosphere. Only 57 to 60% of the CO_2 emitted from human activity remains in the atmosphere. A significant part of the deficit is taken up by the hydroshpere. Some dissolves into

the oceans and some is incorporated into plants as they grow. Here we discuss the continuous exchange between the ocean and the atmosphere by two main processes. First, in winter, cold, dense waters at high latitudes, enriched in dissolved CO_2 (as dissolved inorganic carbon; DIC), sink from the surface to the depths of the ocean. This localized sinking, associated with the Meridional Overturning Circulation is termed the solubility pump. Over time, it is roughly balanced by a distributed diffuse upward transport of DIC primarily into warm surface waters. In the second process, oceanic phytoplankton take up atmospheric CO_2 through photosynthesis. They are present in the upper sunlit layer, the euphotic zone, of the ocean. In the presence of sunlight phytoplankton convert inorganic CO_2 into organic carbon. The process lowers the partial pressure of CO_2 in the upper ocean and thereby promotes the diffusion of CO_2 from the atmosphere. Once formed, this organic matter faces the immediate possibility of decomposition back to CO_2, PO_4, ammonia and other nutrients through consumption by herbivorous zooplankton and degradation by bacteria. However, approximately 25% of the carbon fixed in the upper ocean may sink into the interior (*Falkowski et al.*, 2000; *Laws et al.*, 2000) by this biological pump. Once the organic C sinks beneath the main ocean thermocline, it is effectively sequestered from the atmosphere for centuries to millennia.

The export of organic carbon from the surface to the ocean interior presently accounts for roughly 11 to 16 PgC per year (*Falkowski et al.*, 1998). This process keeps atmospheric CO_2 concentrations 150 to 200 ppmv lower than it would be if all the phytoplankton in the ocean were to stop photosynthesis (*Falkowski et al.*, 2000; *Laws et al.*, 2000). After several decades of measurements in the atmosphere and the oceans, the global atmospheric CO_2 budget is still surprisingly uncertain. A better understanding of their behavior is the key to predict, and hopefully mitigate, the future impact of anthropogenic CO_2. Therefore, the primary productivity in the Hydrosphere needs to be quantified in different seasons and regions, which is one of the aims of this work.

1.2 Estimation of new (export) and total production

1.2.1 Different methods to estimate new (export) production

Export production can be independently measured using sediment traps (*Nair et al.*, 1989) and ^{234}Th deficiency in the water column (*Buesseler*, 1991; *Buesseler et al.*, 1998; *Ramaswamy et al.*, 2005). Sediment traps are generally deployed in the open ocean, at depths ranging from 200 m to more than 1000 m where they collect particulate matter exported to the deep. Here, trap hydrodynamics, the problem of zooplankton "swimmers", and the dissolution of material after collection are the major issues of concern. Trap hydrodynamics include: (1) trap Reynolds number, $R_t = u_f \times D \times v^{-1}$ where u_f is the horizontal current velocity, D is the trap diameter, and v is the fluid kinematic viscosity, (2) trap aspect ratio, $A = H \times D^{-1}$ where H is the trap height and D is the inside diameter of the trap mouth, and (3) the ratio of current speed to particle fall velocity, $u \times W^{-1}$, where W is the gravitational sinking speed of the particles. Neutrally buoyant sediment traps are preferred to minimize hydrodynamic bias. By using meshed collection chambers in traps the influence of swimmers can be minimized and dissolution effects can be overcome by proper calibration e.g., by the U-Th calibration method. However, the observed data do not show a very encouraging correlation between the measured ^{234}Th flux in the sediment traps and calculated ^{234}Th flux based upon water column ^{234}Th and ^{238}U data from the world oceans (*Buesseler et al.*, 2007). Further, a factor of 3-10 difference has been observed between the trap-derived and ^{234}Th derived export fluxes (*Buesseler*, 1991). Therefore it is still a challenge for oceanographers to overcome these problems and obtain accurate estimates of sinking particle flux using sediment traps.

Net community production (NCP), a measure of the balance of autotrophic and

heterotrophic processes comparable to new (export) production, can also be estimated using total dissolved inorganic carbon in the surface water (*Bates et al.*, 2006; *Lee*, 2001) or using oxygen accumulated in the euphotic zone (*Codispoti et al.*, 1986; *Minas et al.*, 1986; *Platt et al.*, 1989; *Sarma*, 2004). NCP is approximately equivalent to new/export production only when recycled production balances respiration, under quasi-steady state conditions. The oxygen balance in the upper layer remains zero under convective mixing so any new production would not be detected which may lead to an underestimation of new production (*Lipschultz et al.*, 2002). However, this approach is still under development.

Luz and Barkan (2000) proposed a new method to measure oceanic productivity with the triple-isotope composition of dissolved oxygen. In this approach $\triangle^{17}O$ (where, the $\triangle^{17}O = 1000\ (\delta^{17}O - 0.521\delta^{18}O)$ value of dissolved O_2 is considered as a measure of gross biological production. $\triangle^{17}O$ value of dissolved O_2 ($\triangle_{diss}$) depends on the rate of air-water gas exchange and the rate of *in situ* production of biological O_2. The air-water gas exchange tends to bring $\triangle_{diss}$ to an equilibrium value with air (by definition, $\triangle^{17}O$ of air $O_2 = 0$). On the other hand, biologically produced O_2 tends to bring $\triangle_{diss}$ to a maximum value. In natural aquatic systems, $\triangle_{diss}$ varies between these two extremes. Therefore, gross biological production can be calculated from $\triangle_{diss}$ if the rate of air-sea gas exchange is known (*Luz and Barkan*, 2000). This approach has been used with the O_2/Ar method to estimate net and gross production (e.g., *Reuer et al.*, 2007). It has been noticed that the uncertainty in gross production estimated from the $\triangle_{diss}$ sharply increases as $\triangle_{diss}$ values approach the biological limit of $\triangle^{17}O$. In general, the estimation of gross production by this approach has an uncertainty of the order of 30%. Generally, this method provides estimates only for the mixed layer, as vertical mixing with deeper water introduces variability in the air-sea gas exchange rate, which makes the estimation somewhat erroneous. Further, in the cases of very shallow and deeper mixed layers the method does not provide precise estimations (*Luz and Barken*, 2000). It might provide an alternative method to measure productivity if

it is improved further.

New and regenerated productivity may be directly measured using the ^{15}N tracer technique (*Dugdale and Goering*, 1967; *UNESCO*, 1994). The relevant mass spectrometric techniques and instrumentation have been improved enormously in the recent past, thus offering a better way to quantify marine biological productivity. The advancements include sub-microgram level ^{15}N determination which has become increasingly popular to differentiate between new and regenerated marine productivity, even in oligotrophic waters. The validity of the underlying assumptions of the method and the experimental procedures followed in the present study are discussed in the next chapter.

1.2.2 ^{15}N tracer technique and new (export) production

Nitrogenous nutrients are available in different forms e.g., NO_3, NH_4, and urea and support primary productivity in the surface ocean, where their relative concentrations depend upon the pH and redox state of seawater. They are also influenced by biological and physical processes e.g., upwelling, mixing, advection and diffusion. Part of the oceanic primary productivity which is supported by NO_3, brought into the euphotic zone from deeper waters through physical processes, is termed as 'new' productivity; whereas, productivity supported by NH_4 and urea, derived from biological processes occurring within the euphotic zone, is called 'regenerated' productivity (*Dugdale and Georing*, 1967). Under steady state for nitrogen in the euphotic zone, losses trough sinking particles, mixing, and by predation, balance the flux of 'new' nitrogen supporting primary production in the euphotic zone (*Eppely and Peterson*, 1979; *Lewis et al.*, 1986; *Platt et al.*, 1992) i.e., export production equals new production under steady state (*Eppely and Peterson*, 1979) in the absence of significant lateral transport (*Plattner et al.*, 2005). However, on longer time scales new production is known to be coupled to export production even otherwise (i.e. non-steady state; *Eppely and Peterson*, 1979) and they are referred to interchangeably as new production (*Sarmiento and Siegenthaler*,

1992). In addition to the NO_3 flux to the euphotic zone, N_2-fixation can also be a substantial factor in the new production (*Karl et al.*, 2002). N_2-fixation is particularly important in the tropical and sub-tropical oceans (*Capone et al.*, 2005). The fraction of the total nitrogen uptake that is 'new' is called *f*-ratio, defined as the ratio of new to total production and represents the probability that a nitrogen atom is assimilated by phytoplankton due to new production; likewise (1-*f*) is the probability of assimilation by regenerated production. (1-*f*)/*f* provides a measure of number of times nitrogen recycles in the euphotic zone before sinking out of the system as particulate matter (*Eppley and Peterson*, 1979). Theoretically *f*-ratio can vary between 0 and 1.

Sources of error in new production estimated using ^{15}N

Some of the main sources of error in classical ^{15}N uptake experiments are still being debated, such as nitrogen regeneration and the release of dissolved organic nitrogen (DON) (*Fernandez and Raimbault*, 2007). Ammonium regeneration is the main source of regenerated nitrogen to the euphotic zone. By studying NH_4 isotopic dilution (recycling of unlabeled substrate) during ^{15}N incubation experiments, *Glibert et al* (1982a), and *Harrison et al* (1987) showed that NH_4 regeneration can result in significant underestimations of regenerated production, which would also bias the assessment of the *f*-ratio.

Nitrification (the oxidation of NH_4 to NO_3 mediated by nitrifying bacteria) is also an important variable, now not only considered responsible for the deep NO_3 reservoir but also believed to provide a source of in situ regenerated NO_3 near the surface. *Yool et al* (2007) suggested that for much of the world ocean a substantial fraction of the NO_3 taken up is generated through recent nitrification near the surface. Thus, a significant part of the available NO_3 could account for regenerated rather than new production. This can have a significant impact in the calculation of the *f*-ratio.

On an average, 25 to 41% of the dissolved inorganic nitrogen taken up by phy-

toplankton is released as dissolved organic nitrogen (*Bronk et al.*, 1994). This leads to an underestimation of measured new and regenerated productions by up to 74 and 50%, respectively. Larger the release rate, larger the underestimation of uptake rates. The degree of underestimation also depends upon the natural and induced release of DON because any condition that imparts a stress to cells, such as changes in temperature, light, or salinity, that can induce the release of DON. To minimize this, extreme care is taken during incubation and filtration. The rate of release also varies at different stages of a bloom, such as emergent plateau and decay stages. It is also found that the release of DON increases sevenfold when the bloom begins to decline. The released DON can also be incorporated in the organic substrate, which can further complicate matters. The estimation of DON uptake by phytoplankton is still a challenge to the oceanographic community (*Bronk et al.*, 1994; *Slawyk and Raimbault*, 1995), probably related to schedule constraints and the labour intensive nature of the methods involved.

Estimation of the nitrification rate and NH_4 regeneration was not undertaken in the present study. According to the Joint Global Ocean Flux Study (JGOFS) protocol (*UNESCO*, 1994), followed in the present study, NH_4 and DON emission, nitrification rate into the waters would be minimal for short-time incubations ($\sim$4 hours). Therefore, the possible uncertainty in the estimation of new production and *f*-ratio due to the above-mentioned processes is likely to be small.

1.2.3 Estimation of total production

Marine primary production in the oceanic waters is usually estimated by the ^{14}C-tracer technique (*Nielsen*, 1952). The high sensitivity of this technique allows us to determine productivity even in low productive oceanic waters (*Slawyk et al.*, 1977). *MacIsaac and Dugdale* (1972) compared carbon and nitrogen uptake data obtained from different oceanic regions and found discrepancies between the dissolved inorganic carbon to nitrogen ratio in water and carbon to nitrogen assimilation ratios in plant tissue obtained using ^{14}C and ^{15}N techniques. These discrepancies could

be due to the loose coupling between photosynthesis and inorganic nitrogen uptake (*MacIsaac and Dugdale*, 1972) or due to the differences in the measurement techniques (*Slawyk et al.*, 1977) e.g., incubations of ^{14}C and ^{15}N samples are generally carried out in bottles of different sizes (125-250 ml vs. 1-2 L), and for different durations (12-24 vs. 4-6 hours), and different depth ranges (up to 120 m vs. up to 1% light level). Further, the instruments are also different (scintillation counter vs. mass spectrometer). Hence, the instrumental errors associated with the measurements are also different (*Slawyk et al.*, 1977).

To overcome these issues a method of estimating carbon assimilation by mass spectrometry was developed (*Slawyk et al.*, 1977) using the stable isotope ^{13}C. This technique can be combined with the ^{15}N technique and simultaneous measurements of carbon and nitrogen assimilation can be made on the same sample. These improvements may minimize some of uncertainties associated with the nitrogen and carbon assimilation rates, particularly the uncertainty due to the difference in the measurements techniques. In the present study, ^{13}C tracer is used to estimate total primary production, and ^{15}N for new production.

1.3 Summary of earlier studies on new productivity

In this section, earlier work on the subject in the different parts of the world ocean, including our study area, is presented. The uptake rates of different forms of nitrogen (i.e., NO_3, NH_4 and urea) obtained from different parts of the world ocean are listed in Table 1.1. The productivity of marine waters is highly variable, both temporally and spatially. This variability ranges over orders of magnitude, across ocean-basin scales, and diel to decadal scales. The availability of light and nutrients are the critical factors underlying this variability. Apart from light, nitrogen is the most important macro-nutrient controlling marine productivity. The concentrations of inorganic forms of nitrogen vary spatially and temporally to a

large extent in the marine environment. For example, NO_3 concentrations may vary from >20 μM during late winter to <100 nM during summer in mid to high latitude ocean regions. Similarly, its concentrations range from ∼100 nM year round in the oligotrophic gyres of the Pacific Ocean, to >25 μM in the surface Southern Ocean. Physical and biological processes are responsible for such variations, which indeed control the variability in productivity around the world oceans (Table 1.1). The most important feature seen in this table is the extreme variability exhibited within each of the different regions. Oceanic gyres (regions on either side of the Equator in all the major oceans) exhibit very low new productivity (NO_3 uptake). These oceanic gyres are oligotrophic and typically exhibit nitrogen concentrations in the nanomolar range and low phytoplankton biomass (e.g. *Eppley and Koeve*, 1990; *Lewis et al.*, 1986; *Planas et al.*, 1999; *McCarthy et al.*, 1996; *Wilkerson and Dugdale*, 1992; *Aufdenkampe et al.*, 2002; *Elskens et al.*, 2008). These regions are permanently thermally stratified and thus are isolated from the deep ocean. There are also no significant river inputs to these regions. These two facts together are responsible for the low new productivity in gyres.

Temperate and high latitude regions show high new productivity during spring and early summer; later they tend towards very low new productivity due to the low supply of new nitrogen as a result of thermal stratification (e.g. *Smith*, 1993; *Smith*, 1995; *Smith et al.*, 1997; *Varela et al.*, 2005; *Lipschultz*, 2001). Upwelling regions also show a temporal variations in the new productivity because they receive large amounts of new nitrogen during the upwelling season; when the new nitrogen gets exhausted, these regions tend towards regenerated production (*Owens et al.*, 1993). There are regions like the subarctic north Pacific and the Southern Ocean, where surface NO_3 is high but biomass level is low, and these are known as "high-nutrient, low-chlorophyll (HNLC)" regions (*Cullen*, 1991). In general, new productivity has been reported to be low in HNLC regions (*Sambrotto and Mace*, 2000; *Mengesha et al.*, 1998; *Savoye et al.*, 2004).

Table 1.1: *Summary of uptake rates of NO_3 (ρNO_3), NH_4 (ρNH_4), and urea ($\rho Urea$) from the major ocean basins measured using the ^{15}N tracer technique. Uptake rates have been converted to common units (mmol N $m^{-2} d^{-1}$) using data provided in the original publication or using conversion factors specified in the footnotes. Some places only surface uptake rates are given, for which units are specified in the footnotes.*

Location	Season	ρNO_3	ρNH_4	ρUrea	Reference
		Atlantic Ocean			
North*	Fall	0.3-0.5	0.9-1.9	0.9-1.3	*Varela et al., 2005*
Northeast	Summer	0.2-10.0	1.2-12.0		*Donald et al., 2001*
Northeast	Spring	2.5-13.6	1.8-4.4		*Bury et al., 2001*
Northwest×	Summer	<2	1-10		*Lipschultz, 2001*
Northwest×	Winter	15-170	<12		*Lipschultz, 2001*
Subtropical Gyre	Spring	0.6-2.6			*Eppley and Koeve, 1990*
Subtropical Gyre	June	0.8			*Lewis et al., 1986*
Equatorial*	Fall	381-1900	61-79	451-522	*Varela et al., 2005*
N Subtropical Gyre×	Mar-Apr	2.1-37.7	5.6-52.4		*Planas et al., 1999*
E Subtropical Gyre×	Mar-Apr	1.1-71.4	6.5-69.6		*Planas et al., 1999*
S Subtropical Gyre×	Mar-Apr	0.1-22.8	3.1-49.9		*Planas et al., 1999*
South*	Spring	104-135	56-123	478-642	*Varela et al., 2005*
Northeast	Winter	1-7	1-4		*Fernandez et al., 2005*
Northeast	Spring	2-8	1-8		*Fernandez et al., 2005*
Northeast	late summer	1-3	1-4		*Fernandez et al., 2005*
		Pacific Ocean			
Subarctic**	May	3.6±1.8			*Wheeler, 1993*
Subarctic**	June	3.1±1.0			*Wheeler, 1993*
Subarctic**	Aug	3.2±1.7			*Wheeler, 1993*
Subarctic**	Sep	2.9±0.9			*Wheeler, 1993*
Northeast	Winter	0.8-1.8	1.9-3.6	0.4-1.6	*Varela and Harrison, 1999*
Northeast	Spring	1.6-3.6	4.9-9.7	2.2-6.1	*Varela and Harrison, 1999*
Northeast	Summer	0.3-3.2	2.4-7.5	0.9-9.1	*Varela and Harrison, 1999*
Northeast	Jan-Feb	0.7-0.8	5.3-8.4		*Harrison et al., 1992*
Northeast	May,July	0.2-0.8	2.7-13.1		*Harrison et al., 1992*
Northeast	Oct-Nov	0.55	2.7-3.7		*Harrison et al., 1992*
Eastern Tropical	Winter	1.3-5.9	0.9-5.3		*Maclsaac and Dugdale, 1972*
Eastern Tropical	Spring	0.3-20.8	0.9-6.5		*Maclsaac and Dugdale, 1972*
N Equatorial	April	0.4-0.8	1.6-22.8		*Pena et al., 1992*
Equatorial	April	1.2-3.5	0.3-20.8		*Pena et al., 1992*
S Equatorial	April	0.7-1.4	1.4-44.9		*Pena et al., 1992*
Tropical	Aug-Sept	0.4-0.7	3.0-6.0		*McCarthy et al., 1996*
Tropical	Feb-Mar	0.2-0.8	1-21		*McCarthy et al., 1996*
Equatorial	Aug-Sep	0.5-1.0	5-7		*McCarthy et al., 1996*
Equatorial	Feb-Mar	1.2-4.7	15-21		*McCarthy et al., 1996*
Equatorial	Summer (eutrophic)	1.5-2.7	7.0-12.5		*Raimbault et al., 1999*
Equatorial	Summer (mesotrophic)	0.9-1.6	7.5-8.2		*Raimbault et al., 1999*

(continued)

Location	Season	ρNO_3	ρNH_4	ρUrea	Reference
Equatorial	Summer (oligotrophic)	0.5-1.6	4.4-10.7		*Raimbault et al., 1999*
N Tropical*	Winter	0.02-0.2	0.5-2.8		*Wilkerson and Dugdale, 1992*
Equatorial*	Winter	0.1-1.7	0.5-6.0		*Wilkerson and Dugdale, 1992*
S Tropical*	Winter	0.2-0.3	1.7-6.9		*Wilkerson and Dugdale, 1992*
Equatorial	Apr-May	0.8-3.7			*Aufdenkampe et al., 2002*
Equatorial	Oct	2.0-3.8			*Aufdenkampe et al., 2002*
NW Subarctic Gyre*	July-Aug	1.4±0.2	4.9±0.2		*Elskens et al., 2008*
NW Subarctic Gyre*	Aug	0.8±0.1	5.3±0.4		*Elskens et al., 2008*
South China Sea[a]	Spring	1.6±1.1			*Chen and Chen, 2006*
South China Sea[a]	Summer	1.3±0.9			*Chen and Chen, 2006*
South China Sea[a]	Fall	1.0±0.5			*Chen and Chen, 2006*
South China Sea[a]	Winter	2.8±1.5			*Chen and Chen, 2006*
Indian Ocean					
Arabian Sea	Spring	0.4-5.2	0.9-42.1[⊗]		*Sambrotto, 2001*
Arabian Sea	SW monsoon	4.3-6.4	15.2-51.8[⊗]		*Sambrotto, 2001*
Western IO[b]	Fall	2.7-88.9	20.3-49.1		*Owens et al., 1993*
Western IO	Nov-Dec	0.3-9.8	0.1-11.8	0-3.6	*Watts and Owens, 1999*
Arabian Sea	Jan	0.6-7.2	5.4-37.0		*McCarthy et al., 1999*
Arabian Sea	Oct-Nov	0.3-4.4	3.3-21.0		*McCarthy et al., 1999*
Western IO[×]	June-July	0-9	50-1080		*Mengesha et al., 1999*
Western IO[×]	Fall	17-90	40-370		*Mengesha et al., 1999*
Arabian Sea	NE monsoon	1.7-3.5	10.9-20.6‡		*Dickson et al., 2001*
Arabian Sea	SW monsoon	1.2-8.5	3.5-31.1‡		*Dickson et al., 2001*
NE Arabian Sea	Jan	1-4.3	3.8-23.3	1.3-7.3	*Kumar et al., 2010*
NE Arabian Sea	Feb-Mar	5.7-23.2	6.2-9.0	3.8-7.8	*Kumar et al., 2010*
NE Arabian Sea	Feb-Mar	0.63-20.9	0.4-3.3	0.6-3.9	*Prakash et al., 2008*
Bay of Bengal	Sep-Oct	0.2-8.8	0.3-0.8	0.3-1.3	*Kumar et al., 2004*
Bay of Bengal	Apr-May	0.9-10.7	0.7-1.8	0.2-1.1	*Kumar et al., 2004*
Arctic Ocean					
Greenland Sea*	Spring	4.5-263	5.6-74.1		*Smith, 1993*
NE Polynya*	Summer	0.2-29.1	0.1-1.8		*Smith, 1995*
NE Polynya*	May-July	0.1-5.6	0.01-2.2	0.01-2.1	*Smith et al., 1997*
Polar Sea*	July-Aug	0.05-7.5	0.05-3.2		*Smith et al., 1997*
Southern Ocean					
Antarctic Polar Front	Summer	0.9-12.5	12.2-54.8	0.7-10.8	*Sambrotto and Mace, 2000*
Scotia/Weddell Sea	Nov-Dec	0.2-6.7			*Goeyens et al, 1991*
Scotia/Weddell Sea	Winter	0.3-2.5	0.7-9.7		*Coat et al., 1992*
Weddell Sea[×]	Nov-Jan	22-910	9-110		*Semeneh et al., 1998*
Prydz Bay[×]	Jan-Mar	27-61	11-85		*Semeneh et al., 1998*
Indian Sector[×]	Jan-Mar	22±15	39±16		*Semeneh et al., 1998*
Indian Sector	Mar	0.4-1.4			*Slawyk, 1979*
Indian Sector[×]	Spring	0.3-100	10-30	6-22	*Mengesha et al., 1998*
Indian Sector[×]	Summer	5-22	4-33		*Mengesha et al., 1998*
Indian Sector[×]	Summer	0.9-7.7	0.5-3.3	0.2-1.9	*Prakash, 2008*
Pacific Sector	Spring	0.9-7.6	2.1-3.0	0.5-1.8	*Savoye et al., 2004*

*Multiplied by 12 to get daily rate; [×]Surface uptake rates (μmolm^{-3}d^{-1}); **Divided by 14; [a]Using the Redfield Ratio (C:N=106:16; Redfield et al 1963); [⊗]The values are the sum of NH_4 and urea uptake rates calculated using given NO_3 uptake rate and *f*-ratio; [b]Calculated using the given total N uptake rate and *f*-ratio; [c]Calculated using the given N uptake and fractions; [‡]The values are the regenerated productivity calculated using the given total N and NO_3 uptake rate.

^{15}N based new productivity measurements were carried out in the western and central Arabian Sea (AS) under the JGOFS programme. A significant seasonal and geographical variation in new productivity was observed in the AS. *Owens et al* (1993) reported a large variation in the NO_3 uptake rates, from 2.7 mmol N $m^{-2}d^{-1}$ in the central AS to 88.9 mmol N $m^{-2}d^{-1}$ in the coastal upwelling region. New productivity varied between 0.6-7.2 mmol N $m^{-2}d^{-1}$ during winter and between 0.3-4.4 mmol N $m^{-2}d^{-1}$ during early winter in the central AS (*McCarthy et al.*, 1999). New productivity measurements in the eastern AS have been initiated in 2003 by *Kumar et al* (2010). Similar to the central AS, the eastern AS also shows a seasonal variability in the new productivity. The new productivity varies between 1-4.3 mmol N $m^{-2}d^{-1}$ during early winter, and between 5.7-23.2 mmol N $m^{-2}d^{-1}$ during late winter, with spatial variations within the region. An increasing trend from south to north in the new productivity, 5.7 to 20.9 mmol N $m^{-2}d^{-1}$, has been reported by *Prakash et al* (2008) during late winter. In the Bay of Bengal, new productivity measurements were initiated in 2002 under Bay of Bengal Processes Studies (BOBPS) programme by *Kumar et al* (2004): a large variation in the new productivity has been found in the coastal and open ocean regions during both fall and spring (*Kumar et al.*, 2004). Localized eddies also play a significant role in enhancing new productivity during both the seasons. Although new productivity in some parts of the northern Indian Ocean have been measured during some major programmes, e.g. JGOFS and BOBPS, a large part of the Indian Ocean such as the equatorial and the Southern Indian Oceans still remain to be fully explored.

1.4 Rationale behind the present study

As discussed earlier, each year CO_2 is released to the atmosphere from human activity, both fossil fuel combustion and land use change. Thus during the Anthropocene (since AD 1800), about 244±20 PgC has been emitted into the atmosphere. However, the atmospheric CO_2 has increased only by 165 Pg C (from 597 PgC in 1800 to 762 PgC in 1994, *Sabine et al* (2004)). The anthropogenic CO_2 that did

not accumulate in the atmosphere must have been taken up by the ocean, and the land biosphere.

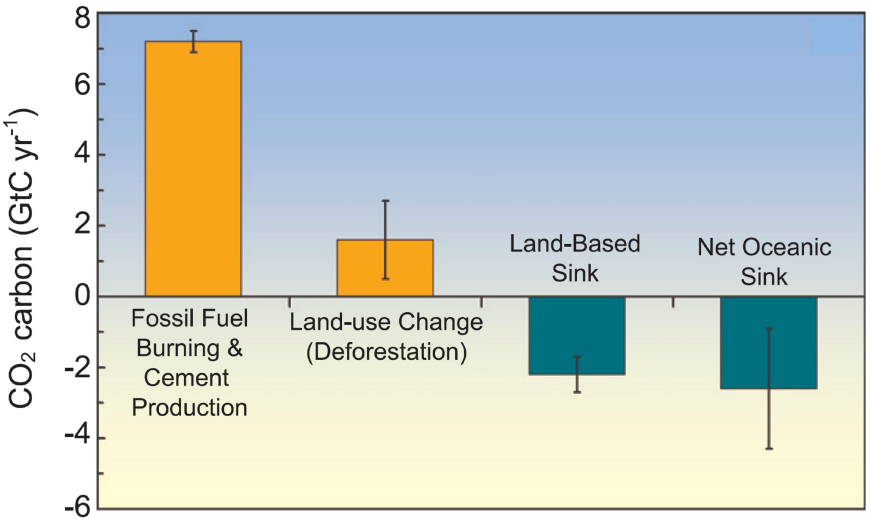

Figure 1.2: *Sources and sinks of CO_2. Land-related fluxes are for the 1990s; fluxes due to fossil fuel combustion and cement production and the net ocean uptake are for the period 2000 to 2005 CE. Uncertainties in the estimates represent 1 standard deviation (Source: Fourth Assessment Report of the IPCC, 2007; Denman et al, 2007)*

The relative roles of the ocean and land biosphere as sinks for anthropogenic CO_2 over the Anthropocene are poorly understood. The global carbon sources and sinks of carbon are shown in Fig 1.2. *Sabine et al* (2004) synthesized the individual ocean estimates to provide a data-constrained global estimate of the cumulative oceanic sink for anthropogenic CO_2 during 1800 to 1994 CE. They found that the highest vertically integrated concentrations are in the North Atlantic. As a result, this ocean basin stores 23% of the global oceanic anthropogenic CO_2, despite covering only 15% of the global ocean area. By contrast, the Southern Ocean south of 50^{o}S has very low vertically integrated anthropogenic CO_2 concentrations, containing only 9% of the global inventory. More than 40% of the global inventory is found in the region between 50^{o}S and 14^{o}S because of the substantially higher vertically integrated concentrations and the large ocean area in these latitude bands. About 60% of the total oceanic anthropogenic CO_2 inventory is stored in the Southern

Hemisphere oceans, roughly in proportion to the larger ocean area of this hemisphere. A large variability, in both spatial and temporal, exists in the different ocean basins with regard to anthropogenic CO_2 uptake (*Sabine et al.*, 2004). In addition, seasonal and interannual variations are not included in the estimates for oceans in the IPCC (2007) (*Denman et al.*, 2007) (Fig 1.2). *Sarma et al* (1998) have shown that the central and eastern Arabian Sea are a perennial source of CO_2 and suggested that they could release ∼45 Tg C y^{-1} to the atmosphere. On the other hand, it has also been shown that the deep waters of the Arabian Sea receive higher amounts of both organic and inorganic carbon through sinking matter from the euphotic zone. The accumulation of DIC in deep waters is found to be the highest in the North Indian Ocean compared to that elsewhere (*Sarma et al.*, 2006). This confirms that a large variability exists in this small basin with regard to estimations of carbon fluxes. Therefore, to obtain large scale estimations for the carbon export fluxes, sustained observations over several years of ^{15}N based new (export) productivity measurements are needed, particularly in the Indian Ocean, whose biogeochemical budget still remains inadequately characterized. The present study is an attempt to fill this gap and provide high quality data for the regional carbon budget. All the major basins viz., the Arabian Sea, the Bay of Bengal, the Equatorial Indian Ocean and the Indian sector of the Southern Ocean, have been investigated in the present study, with a larger spatial coverage compared to previous studies. Further, the present study is the first of its kind in which ^{13}C and ^{15}N tracers have been used simultaneously, thus gaining a better handle with which to understand assimilation of nitrogen and carbon in phytoplankton.

1.5 Major questions addressed in present study

The main objective of the present work is to quantify the new and total production, *f*-ratio by using ^{13}C and ^{15}N isotopes tracer techniques in the Indian region during different seasons. The specific objectives are:

1. To study different types of blooms, e.g. *Trichodesmium* bloom (during

inter monsoon) and *Noctiluca miliaris* bloom (during late winter monsoon) in the Arabian Sea, to evaluate their effect on the biogeochemistry of the basin. *Trichodesmium* is an important diazotrophic plankton that fixes atmospheric N_2 and introduces 'new' nitrogen to the euphotic zone (*Capone et al.*, 1997). The net loss or gain of nitrogen from the ocean directly influences the carbon budget of the region, which has a bearing on the global carbon budget. Although *Trichodesmium* blooms have been observed every year during the spring and fall inter-monsoons (e.g. *Devassy et al.*, 1978, *Matondkar et al.*, 2006) in the NE Arabian Sea region, earlier work pertains only to temporal and spatial variations in their community structure. ^{15}N based N uptake rate measurements were not made during *Trichodesmium* blooms. *Noctiluca miliaris* is a heterotrophic plankton that occurs in the northern Arabian Sea during late winter. *Gomes et al* (2008) claimed that diatom blooms have replaced recently by the *Noctiluca miliaris* blooms. The effect of such plankton community shift on nitrogen cycling has not been fully investigated.

2. To understand the winter mixing and its role in the NO_3 supply and subsequent uptake in surface waters of the Arabian Sea. During winter, dry and cool north-easterly trade winds intensify evaporation and cool the sea surface, and trigger the sinking and convective mixing of surface water in the northern Arabian Sea. This mixing leads to the deepening of the mixed layer and an upward transport of nutrients into the surface waters, leading to the winter blooms (*Madhupratap et al.*, 1996). Investigation of intra-seasonal and inter-annual variation in N uptake rates is lacking for bloom conditions.

3. To study the role of eddies in the nutrient dynamics and new production in the Bay of Bengal. Ocean eddies are the storms in the ocean, playing an important role in ocean dynamics, as well as the transport of heat, salt, nutrients and other chemical properties. Mesoscale eddies are a ubiquitous and energetic feature of the open ocean and are frequently observed in the Bay of Bengal, but their role in the new (export) production remains to be quantified.

4. To understand the nitrogen and carbon cycling in the equatorial Indian Ocean and its role in the global context. The equatorial regions of the other major oceans are oligotrophic and show low new productivity (Table 1.1). Such estimates are not available for the equatorial Indian Ocean.
5. Quantify the nitrogen and carbon uptake rates in the Southern Indian Ocean. The region, characterized as an HNLC region, is less studied in comparison to the other oceanic regions because of the extreme environmental conditions which often restrict sampling.

1.6 Outline of the thesis

The thesis consists of six chapters, the details of which are given below.

Chapter 1

This chapter gives a brief introduction on the role of the ocean in the global carbon cycle/budget, nitrogen cycle and its biogeochemistry, biogeochemical processes controlling them and the responsible physical mechanisms. Further, the chapter briefly reviews the work done earlier on this subject in different parts of the world oceans. The last section of this chapter highlights the importance of the present study and the scientific questions addressed.

Chapter 2

Chapter 2 gives a brief description of the ^{13}C and ^{15}N tracer techniques. The chapter also contains the detailed information on the study areas, seasons and durations of sampling, experimental procedures and the method used for the measurement of particulate organic nitrogen/carbon (PON/POC) and their isotope ratios. Analytical uncertainties are also discussed.

Chapter 3

In Chapter 3, results of new and primary productivity from the Northern Indian Ocean are presented, in four parts. In the first two parts, results from the Arabian

Sea during April 2006 and Mar 2007 are discussed. Results from the Bay of Bengal during May-June 2007 and Nov-Dec 2007 are presented in the third and fourth parts.

Chapter 4

Chapter 4 discusses the results of new and primary productivity from the Equatorial Indian Ocean.

Chapter 5

Chapter 5 deals with the results of new and primary productivity from the Indian sector of the Southern Ocean.

Chapter 6

This chapter summarizes the results obtained from the present study and suggests scope for future work.

Chapter 2

Materials and Methods

In the present study, measurements of new, regenerated and total primary production using ^{15}N and ^{13}C tracers were carried out in the Arabian Sea, Bay of Bengal, Equatorial Indian Ocean and Indian sector of Southern Ocean. For this, six cruises were undertaken, two each in the Arabian Sea and the Bay of Bengal and one each in the Equatorial Indian Ocean and the Indian sector of Southern Ocean. The basic principles of ^{15}N and ^{13}C tracer techniques, sampling procedures, and mass spectrometric measurements are presented here. Details of the cruises undertaken are given in Table 2.1.

Table 2.1: *Details of cruises undertaken in the present study.*

Cruise No./Ship	Duration	Season
Arabian Sea		
SS-244/ FORV *Sagar Sampada*	15 Apr-29 Apr, 2006	Spring*
SS-253/ FORV *Sagar Sampada*	1 Mar-19 Mar, 2007	Late Winter*
Bay of Bengal		
SK-234/ ORV *Sagar Kanya*	14 May-4 June, 2007	Spring*
SK-242/ ORV *Sagar Kanya*	25 Nov-16 Dec, 2007	Winter*
Equatorial Indian Ocean		
SK-248/ ORV *Sagar Kanya*	15 July-19 Aug, 2008	Summer*
Southern Ocean		
ABP-35/ RV *Akedemik Boris Petrov*	12 Feb-14 Apr, 2009	Austral Summer

*Boreal seasons.

2.1 Estimation of new, regenerated and total primary production

Joint Global Ocean Flux Study (JGOFS) protocol (*UNESCO*, 1994) was followed for the estimation of new and regenerated production using ^{15}N tracer. Total primary production was estimated using ^{13}C tracer following the procedure of *Slawyk et al* (1977).

Basic principle

The measurements of new and regenerated production rely on the determination of the rate of uptake of the 'trace' ^{15}N-labelled nitrogen compound by phytoplankton during deck incubation. New productivity is measured as the rate of incorporation of the 'trace' ^{15}N-labelled NO_3 by phytoplankton during incubation. The estimation of regenerated production is, likewise, based on the measurement of the rate of ^{15}N-labelled NH_4 and urea incorporations. Similarly, total primary productivity is measured as the rate of incorporation of the 'trace' ^{13}C-labelled $NaH^{13}CO_3$ by phytoplankton during incubation.

2.2 Sampling Regions

2.2.1 The Arabian Sea

Sampling in the Arabian Sea was done in collaboration with Space Application Center (SAC), Ahmedabad. Cruises were undertaken in two seasons: spring (Apr, 2006) and late winter (Mar, 2007). During both, sampling was done onboard FORV *Sagar Sampada* in the north-eastern (NE) Arabian Sea.

Spring (Apr, 2006)

The main aim of the sampling was to study nitrogen cycling during the *Trichodesmium* blooms. Only ^{15}N-labelled tracers were used to measure new and regenerated productivity. Water samples were collected at 8 different stations,

shown in the Fig 2.1.

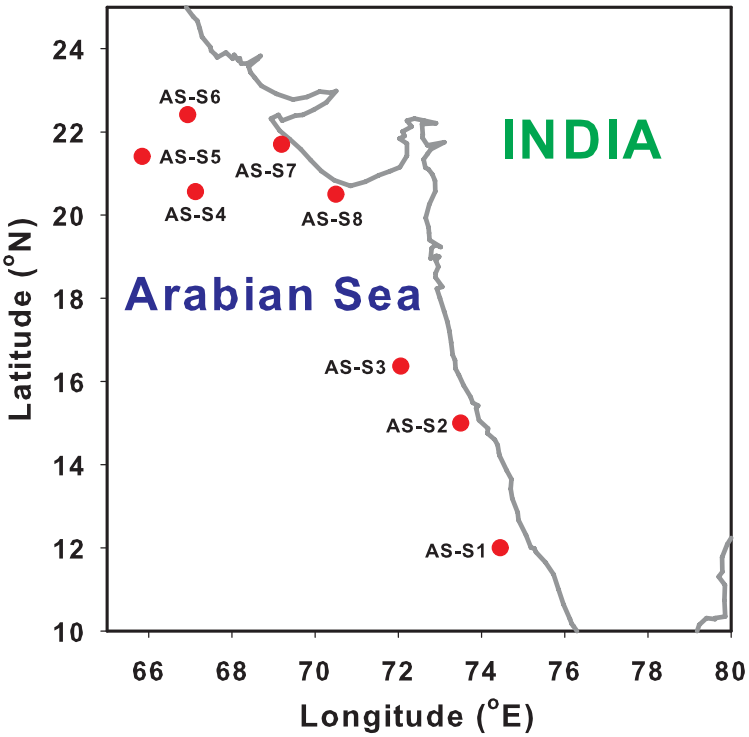

Figure 2.1: *Sampling locations in the NE Arabian Sea during spring (Apr, 2006).*

AS-S1 to AS-S8 denote productivity stations 1 to 8. The details of sampling locations with dates are listed in Table 2.2.

Table 2.2: *Sampling dates, station codes, and locations of the sampling stations in the NE Arabian Sea during spring (Apr, 2006).*

Sampling Date (Apr, 2006)	Station Code	Lat (^{o}N)	Lon (^{o}E)
17	AS-S1	12.0	74.4
19	AS-S2	15.0	73.5
20	AS-S3	16.4	72.1
23	AS-S4	20.6	67.1
24	AS-S5	21.4	65.8
25	AS-S6	22.4	66.9
26	AS-S7	21.7	69.2
27	AS-S8	20.5	70.5

Late winter (Mar, 2007)

The cruise was aimed to investigate the role of plankton species *Noctiluca miliaris*, also called *Noctiluca scintillans*, on the export production in the region during the late winter.

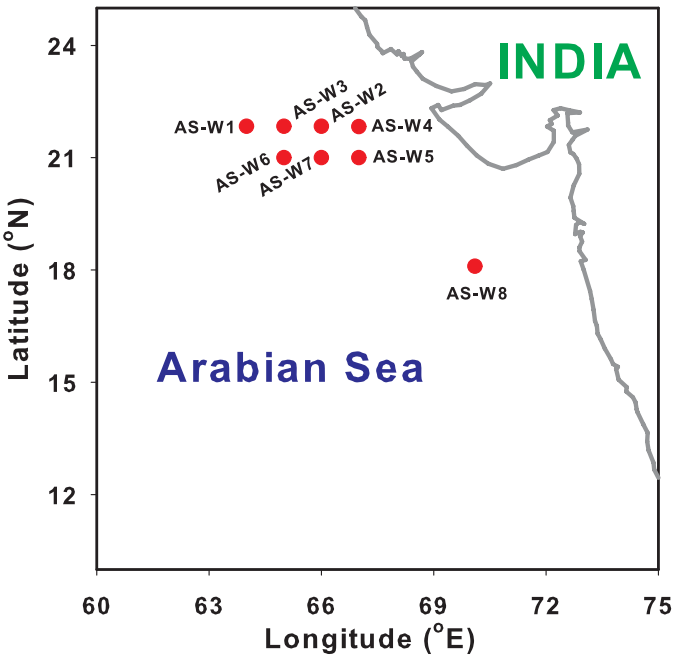

Figure 2.2: *Sampling locations in the NE Arabian Sea during late winter (Mar, 2007).*

Table 2.3: *Sampling dates, station codes, and locations of the sampling stations in the NE Arabian Sea during late winter (Mar, 2007).*

Sampling Date (Mar, 2007)	Station Code	Lat (°N)	Lon (°E)
7	AS-W1	21.9	64.0
8	AS-W2	21.9	66.0
9	AS-W3	21.9	65.0
10	AS-W4	21.9	67.0
11	AS-W5	21.0	67.0
12	AS-W6	21.0	65.0
13	AS-W7	21.0	66.0
15	AS-W8	18.1	70.0

Both ^{15}N and ^{13}C-labelled tracers were used to measure new (also regenerated) and total primary productivity, respectively. Water samples were collected at 8 different stations, as shown in the Fig 2.2. At station AS-W8, only ^{13}C-labelled tracer was used. The sampling dates and locations are listed in Table 2.3.

2.2.2 The Bay of Bengal

Sampling in the Bay of Bengal was done in two different seasons; during spring (May-June, 07) in collaboration with National Center for Antarctic and Ocean Research (NCAOR), Goa and during early winter (Nov-Dec, 07) in collaboration with National Institute of Oceanography (NIO), Goa. Sampling during both the seasons was done onboard ORV *Sagar Kanya*

Spring (May-June, 2007)

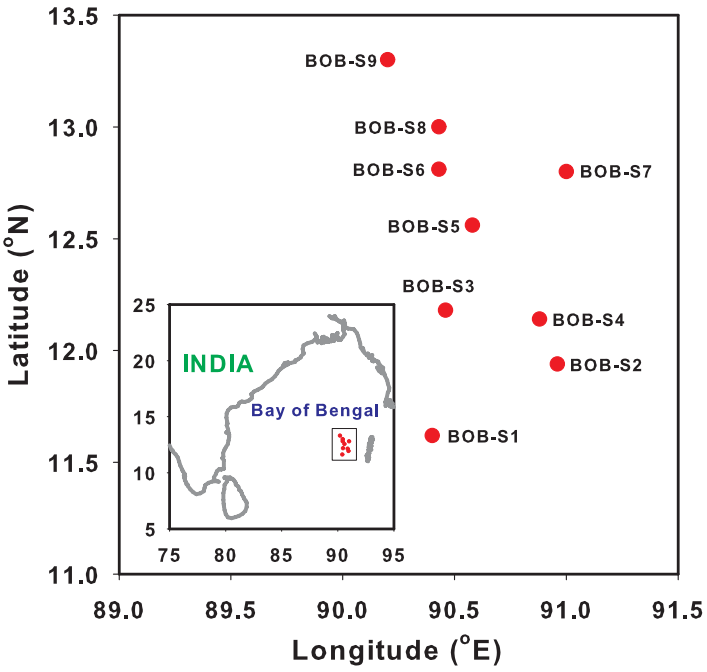

Figure 2.3: *Sampling locations in the Bay of Bengal during spring (May-June, 2007).*

In this cruise, ^{15}N-labelled tracers were used to measure new and regenerated productivity. ^{13}C-labelled tracer was used only to measure surface productivity.

Water samples were collected at 9 different stations, shown in the Fig 2.3. The details of sampling locations along with dates of sampling are listed in Table 2.4. At BOB-S2, BOB-S7 and BOB-S9, only surface productivity measurements were carried out.

Table 2.4: *Sampling dates, station codes, and locations of the sampling stations in the Bay of Bengal during spring (May-June, 2007).*

Sampling Date (May, 2007)	Station Code	Lat (^{o}N)	Lon (^{o}E)
21	BOB-S1	11.6	90.4
23	BOB-S2	11.9	90.9
24	BOB-S3	12.2	90.4
25	BOB-S4	12.1	90.9
26	BOB-S5	12.6	90.6
27	BOB-S6	12.8	90.4
28	BOB-S7	12.8	91.0
29	BOB-S8	13.0	90.4
30	BOB-S9	13.3	90.2

Early Winter (Nov-Dec, 2007)

The main aim of sampling during this season was to study the role of eddies in the nutrient dynamics and new production in the region. In this cruise, water samples were collected at 4 different stations (Fig 2.4); one right at the center of an eddy, two in the proximity of the eddy and one outside the eddy. The sampling locations and dates are listed in Table 2.5.

Table 2.5: *Sampling dates, station codes, and locations of the sampling stations in the Bay of Bengal during early winter (Nov-Dec, 2007).*

Sampling Date (2007)	Station Code	Lat (^{o}N)	Lon (^{o}E)
29 Nov	BOB-F1	18.6	88.6
4 Dec	BOB-F2	19.0	88.0
8 Dec	BOB-F3	17.8	87.5
11 Dec	BOB-F4	15.6	87.4

Total primary productivity measurements (using ^{13}C -labelled tracer) were carried out at all the four locations, whereas, at BOB-F3 and BOB-F4, only new and regenerated productivity measurements were carried out (using ^{15}N-labelled tracer)

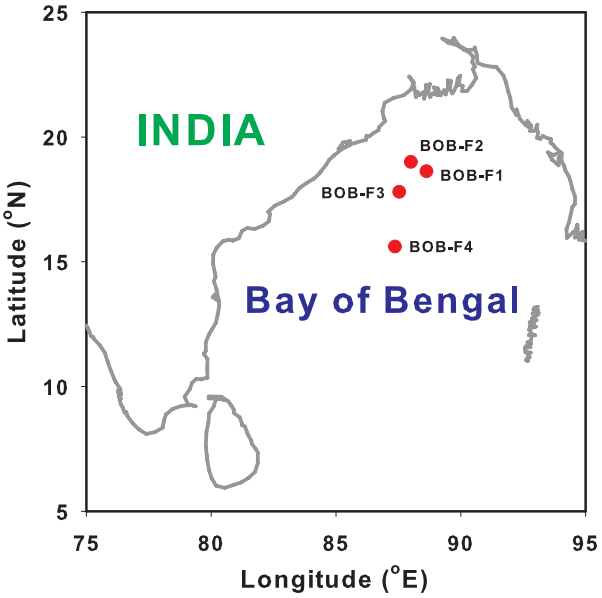

Figure 2.4: *Sampling locations in the Bay of Bengal during early winter (Nov-Dec, 2007).*

2.2.3 The Equatorial Indian Ocean

Sampling in the Equatorial Indian Ocean (EIO) was done in the summer, (July-Aug, 2008) in collaboration with NCAOR, Goa. The sampling was done onboard ORV *Sagar Kanya* (SK-248) during 15 July-19 Aug, 2008.

Table 2.6: *Sampling dates, station codes, and locations of the sampling stations in the Equatorial Indian Ocean (EIO) during summer (July-Aug, 2008).*

Sampling Date (Aug, 2008)	Station Code	Lat (^{o}N)	Lon (^{o}E)
1	EIO-S1	-9.0	65.0
4	EIO-S2	-6.0	65.0
8	EIO-S3	-3.0	66.0
9	EIO-S4	-3.0	65.0
12	EIO-S5	2.0	65.0

In this cruise, ^{15}N and ^{13}C-labelled tracers were used to measure new (also regenerated) and total primary productivity, respectively. Water samples were collected at 5 different stations, as shown in Fig 2.5.

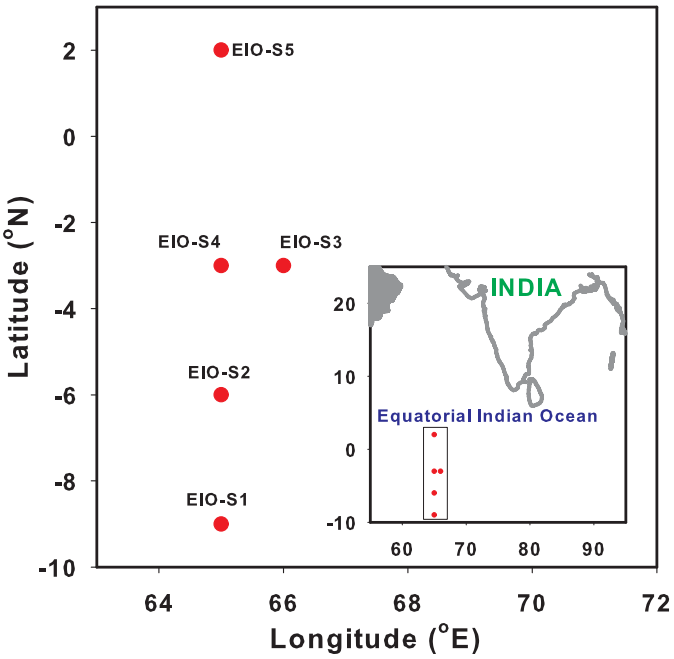

Figure 2.5: *Sampling locations in the Equatorial Indian Ocean (EIO) during summer (July-Aug, 2008).*

The sampling locations and dates are listed in Table 2.6. At all the five locations total primary productivity measurements were carried out (using ^{13}C-labelled tracer), whereas, at EIO-S2, EIO-S3 and EIO-S5, only new and regenerated productivity measurements were carried out (using ^{15}N-labelled tracer).

2.2.4 Indian sector of the Southern Ocean

Sampling in the Indian sector of Southern Ocean was done in austral summer (12 Feb-14 Apr, 2009) in collaboration with NCAOR, Goa. The sampling in the Southern Ocean was done onboard RV *Akedemik Boris Petrov* (35 ABP).
In this cruise, ^{15}N and ^{13}C-labelled tracers were used at 14 different stations (Fig 2.6). The dates and sampling locations are listed in Table 2.7.

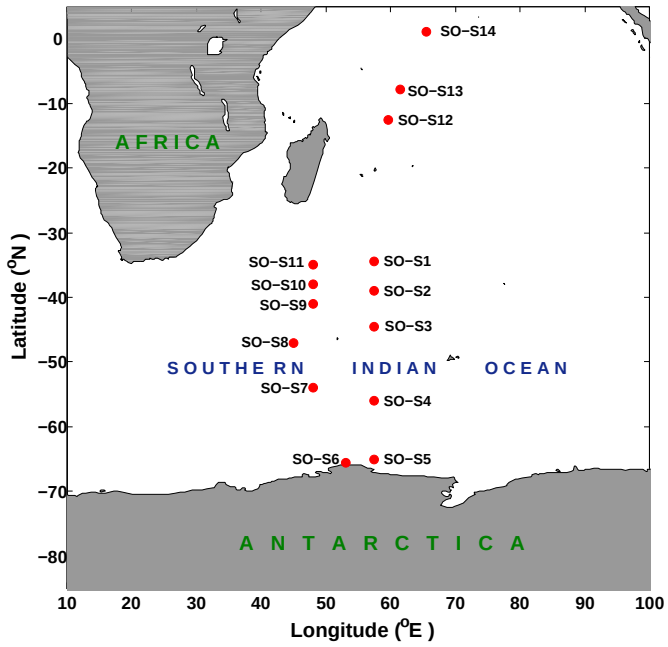

Figure 2.6: *Sampling locations in the Indian sector of the Southern Ocean during austral summer (Feb-Apr, 2009).*

Table 2.7: *Sampling dates, station codes, and locations of the sampling stations in the Indian sector of the Southern Ocean during the austral summer (Feb-Apr, 2009).*

Sampling Date (2009)	Station Code	Lat (^{o}N)*	Lon (^{o}E)
17 Feb	SO-S1	-34.5	57.5
19 Feb	SO-S2	-39.0	57.5
22 Feb	SO-S3	-44.5	57.5
28 Feb	SO-S4	-56.0	57.5
4 Mar	SO-S5	-65.0	57.5
7 Mar	SO-S6	-65.5	53.0
13 Mar	SO-S7	54.0	48.0
16 Mar	SO-S8	-47.0	45.0
20 Mar	SO-S9	-41.0	48.0
21 Mar	SO-S10	-38.0	48.0
22 Mar	SO-S11	-35.0	48.0
31 Mar	SO-S12	-12.5	59.7
2 Apr	SO-S13	-7.9	61.4
9 Apr	SO-S14	1.0	65.5

*minus sign denotes southern hemisphere locations.

2.3 Measurement procedure

The measurement of productivity involved the preparation of tracers, selection of sampling depths for the required light levels, collection of water samples, measurement of nutrients, addition of ^{15}N and ^{13}C labelled tracers, incubation, filtration, preservation, mass spectrometric analysis, and the calculation of nitrogen and carbon uptake rates. The same measurement procedures were followed for analysing samples collected during all the cruises, as elaborated in the following subsections.

2.3.1 Tracer preparation

^{15}N-labelled Tracers

The ^{15}N-labelled (99 atom% enriched) NO_3 ($Na^{15}NO_3$), NH_4 ($^{15}NH_4Cl$) and urea ($^{15}NH_2$-CO-$^{15}NH_2$) salts in dry chemical form were procured from Sigma-Aldrich (USA). 250 ml of stock solutions were prepared, which contained $\sim$ 2.0 mmol N L^{-1}. For this, 43.4 mg of $Na^{15}NO_3$ (molecular weight $\sim$85.98 g), 27.3 mg of $^{15}NH_4Cl$ (molecular weight $\sim$54.48 g), and 16.8 mg of urea (molecular weight $\sim$62.04 g) were added in three different volumetric flasks, made upto 250 ml with deionized Milli-Q water and mixed thoroughly to make a homogeneous solution. These were later transferred to 250 ml polycarbonate bottles (procured from Nalgene, USA) for further use. The working solutions were prepared from the stock solution in three different concentration levels: 0.01, 0.05 and 0.1 mmol N L^{-1} for each tracer. To prepare the first, 5 ml of stock solution was diluted to 1000 ml deionized Milli-Q water. The second solution was prepared by diluting 6.2 ml of the stock solution to 250 ml deionized Milli-Q water. Similarly, the third solution was prepared by diluting 12.4 ml of the stock solution to 250 ml deionized Milli-Q water. The weighing of the salts was done using Thomas Scientific weighing paper on Sartorius microbalance (model no: MC-5; Germany).

^{13}C-labelled Tracer

The ^{13}C-labelled (99 atom% enriched) carbon ($NaH^{13}CO_3$) salt in dry chemical

form was procured from Cambridge Isotope Laboratories, Inc. (USA). The working solution of ∼0.2 mol C L^{-1} was prepared. For this, 5 g of $NaH^{13}CO_3$ (molecular weight ∼85 g) was added in a volumetric flask containing 300 ml of deionized Milli-Q water and mixed thoroughly to make a homogeneous solution. This was later transferred to a polycarbonate bottle (procured from Nalgene, USA) for further use.

2.3.2 Irradiance measurement

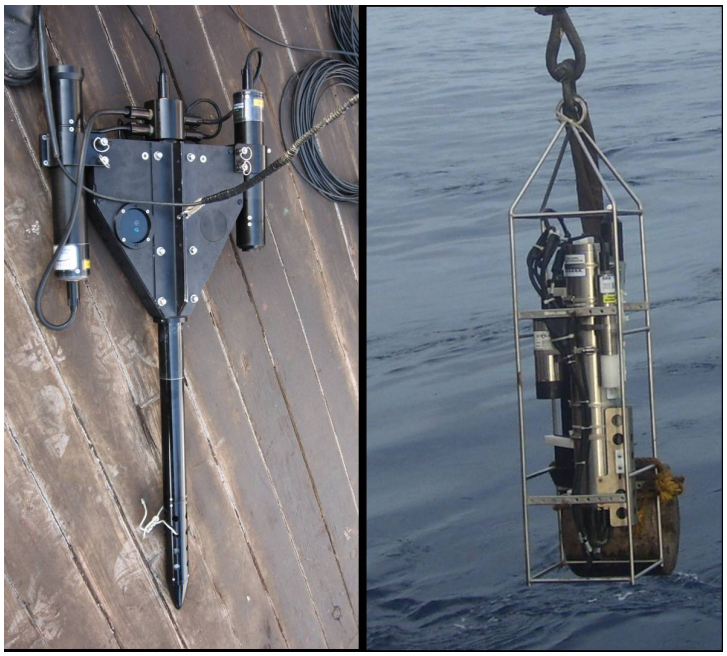

Figure 2.7: *Underwater radiometer (Satlantic Inc., Canada) (left) and portable CTD (right).*

A Hyperspectral underwater radiometer (Satlantic Inc., Canada) was used during sampling (Apr, 2006 and Mar, 2007) in the Arabian Sea to measure irradiance levels at different depths within the euphotic zone (zone between the surface and the depth at which irradiance value falls to 1% of its surface value). The radiometer (Fig 2.7) was operated by scientists from SAC, Ahmedabad, at each sampling location prior to the sample collection. Based on these light measurements, six different depths were chosen for collecting water samples. The corresponding light

levels were 100%, 80%, 64%, 20%, 5% and 1% of the surface value.

A Biospherical, photosynthetically-active-radiation (PAR) sensor (QSP-2300 S/N 70102) attached to a portable conductivity, temperature, and density (CTD) sensor system (SBE 19plus) was used for the measurement of irradiance levels. The PAR sensor was used in the Bay of Bengal (during Nov-Dec, 2007), Equatorial Indian Ocean (during July-Aug, 2008) and Southern Ocean (during Feb-Apr, 2009). Similar to the radiometer operation, the portable CTD (Fig 2.7) operated prior to the seawater sample collection for determining the sampling depths corresponding to the light levels 100%, 80%, 64%, 20%, 5% and 1% of the surface value.

In the Bay of Bengal during May-June, 2007, a *Secchi* disk was operated during noon time to estimate the euphotic depth for each sampling station, a day prior to the sampling (also verified on the sampling location later in the day during noon). Euphotic depth was determined as ∼2.8**Secchi* depth (*d*), where *Secchi* depth was determined by appearance or disappearance of *Secchi* disk in the water column. This euphotic depth was then used to calculate an attenuation coefficient '*k*' (i.e., extinction coefficient) for the available light averaged over the euphotic zone by applying the Beer-Lambert law,

$$\frac{I_z}{I_0} = exp(-k * z) \tag{2.1}$$

Here, I_z and I_0 are the intensities of light at a given depth 'z' and the ocean surface, respectively. Using equation 2.1, the value of '*k*' was calculated as

$$k = \frac{1.64}{d} \tag{2.2}$$

Then the depths from which the samples were to be collected for the above light levels were estimated using the relation

$$z = \frac{4.60 - ln(I_z)}{k} \tag{2.3}$$

2.3.3 Meteorological parameters

Wind speed, wind direction, atmospheric pressure, relative humidity, dew point, insolation, and air temperature were recorded by an automatic weather station installed onboard the ships.

2.3.4 Seawater sampling

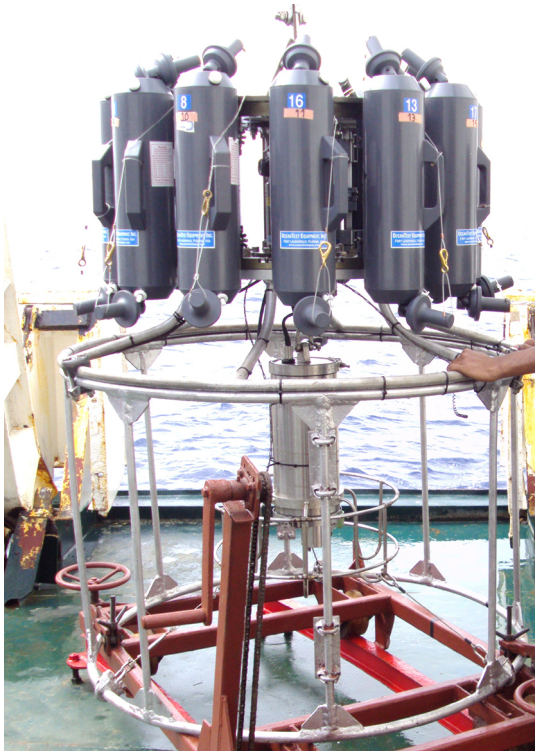

Figure 2.8: *CTD sensors and rosette sampler system (SeaBird 911 plus).*

During all the cruises, water samples were collected using clean Go-Flo/Niskin bottles (General Oceanic, Miami, Florida, USA), to avoid trace metal contamination. These bottles were attached to a CTD sensors and rosette sampler system (SeaBird 911 plus; see Fig 2.8). The CTD sensors were used to obtain conductivity-temperature-depth profiles. The temperature and pressure (i.e., depth) sensors were calibrated before each cruise. The SEASOFT software package was used to process the raw CTD data. The CTD-attached rosette was first lowered to the lowest required depth and water samples were collected while hauling up by clos-

ing the bottles one by one at the required depths. To ensure that the samples were collected from the desired depths, the CTD rosette was allowed to stabilize at that particular depth for a minute. Once the rosette was hauled back to the deck, the samples were immediately transferred to pre-washed polycarbonate incubation bottles of two (or one) liter capacity. Individual water samples were collected for NO_3 (2L volume), NH_4 (2L) and urea (1L) enrichment experiments, each in duplicate. Generally, carbon tracer experiments were carried out together with the NO_3 tracer experiments. Samples were also collected at each station for blank corrections for all the tracers.

2.3.5 Nutrient measurements

An automated segmented flow analyzer was used to measure dissolved inorganic nutrients such as NO_3, NO_2, PO_4 and SiO_4 in sea water samples during all the cruises. 100 ml of sea water sample was separately collected for nutrient measurements from all the six depths at each sampling location. Standard techniques (*UNESCO*, 1994) for nutrient analysis in sea water were followed. Detection limits for NO_3, NO_2, PO_4, and SiO_4 were 0.1 μM, 0.02 μM, 0.01 μM, and 0.1 μM, respectively. Error in the nutrient measurements is less than 1 % for the concentrations >1 μM, while it reaches as high as 5 % for very low ambeint values. Ambient NH_4 and urea could not be measured because of logistic reasons.

2.3.6 Chlorophyll measurements

1 L of water sample from each depth at each sampling location was collected for chlorophyll measurement and filtered on 47 mm GF/F 0.7 μm pore size filters under low vacuum. Chlorophyll was then extracted using 10 ml of 90% acetone (AR grade) and was measured using Turner Design fluorometer.

2.3.7 Tracer addition

According to the JGOFS protocol (*UNESCO*, 1994) and suggested by *Dugdale and Wilkerson* (1986) for the ^{15}N tracer enrichment measurements, ^{15}N tracer was

added at less than 10% of its ambient concentration. A similar condition is also applicable for the ^{13}C tracer (*Slawyk et al.*, 1977). Therefore, ambient concentration of dissolved NO_3, NH_4, urea, and inorganic carbon were required prior to tracer addition. Generally, NO_3 was measured onboard during the cruises; SK-234, SK-242, SK-248. So, NO_3 ($Na^{15}NO_3$) tracer solution was added at less than 10% of its ambient value at each depth. However, during SS-244, SS-253 and 35 ABP cruises, such measurements could not be done onboard because of logistic problems. For these cruises the samples were kept frozen and the NO_3 measurements were done immediately at the end of the cruise. Therefore, fixed concentrations of NO_3 ($Na^{15}NO_3$) tracer solution was added on the basis of the available data of NO_3 concentration from the region proximal to the present sampling locations. Later it turned out that majority of the times we had indeed added <10 % of ambient value.

Ambient NH_4 and urea were not measured; so fixed, small, amounts of NH_4 ($^{15}NH_4Cl$) and urea ($^{15}NH_2$-CO-$^{15}NH_2$) tracers were added following *Owens et al* (1993). The fixed amount was decided using prior knowledge of about the area and season of sampling.

During the cruises SS-244, SS-253, SK-234, SK-242, and 35 ABP, NH_4 ($^{15}NH_4Cl$) and urea ($^{15}NH_2$-CO-$^{15}NH_2$) tracers were added to final concentrations of 0.01 μM to each sample. While during the cruise SK-242, the amount was 0.02 μM. In the case of ^{13}C tracer, a fixed amount of $NaH^{13}CO_3$ solution was added to a final concentration of 0.2 mM to each sample during cruises in which total productivity was measured.

2.3.8 Incubation

After addition of tracers, 4 hours incubation was performed as suggested in the JGOFS protocol (*UNESCO*, 1994). To simulate the irradiance at the depths from which samples derived, well-calibrated neutral density filters were put on the sample bottles. The neutral density filters were calibrated using lux-meter in both

dry and wet conditions. Subsequently sample bottles covered with neutral density filters were kept in a big plastic tub on the deck and seawater from a depth of 6 m was circulated to regulate the temperature during the incubation from 10:00 to 14.00 Hrs local time at each station. Immediately after the incubation, samples were transferred to the shipboard laboratory for filtration and were kept wrapped in a thick black cloth and in dark till the filtration was over.

2.3.9 Filtration and preservation

All samples were filtered in dim light, sequentially through precombusted (4 hr at 400^{o}C) 47 mm diameter and 0.7 μm pore size Whatmann GF/F filters. Samples were filtered under low vacuum (<70mm Hg) using a manifold filtration unit and vacuum pump (procured from Millipore, USA) (see Fig 2.9).

Figure 2.9: *Dark filtration by the author onboard using a manifold and vacuum pump (Millipore, USA).*

Separate glass cups were used for each tracer to avoid any cross contamination. After filtration, GF/F filters were rinsed using filtered sea-water. The filters were

preserved in 47 mm petrislides (procured from Millipore, USA) with the help of clean forceps (separate forceps were used for different tracers). After this, filters were dried in an oven at 50 ^{o}C overnight and stored for further analysis on mass spectrometer. For the blank correction, zero time enrichment was estimated. For this, the same concentrations of isotopically enriched tracers as in samples, were added to the individual blank samples. Immediately after the addition, the blank samples were filtered and dried for isotopic analysis.

2.3.10 Mass spectrometric analysis

Figure 2.10: *Thermo Quest's Finnigan Delta plus continuous flow Isotope Ratio Mass Spectrometer (IRMS) at the National Facility, University of Agricultural Sciences, Bangalore, India.*

To calculate the uptake rate of N (or C), it is required to measure two parameters (a) total N (or C) content and (b) atom $\%^{15}$N (or $\%^{13}$C) in the post incubation samples. To measure these parameters on GF/F filter samples, Thermo Quest's Finnigan Delta plus continuous flow Isotope Ratio Mass Spectrometer (IRMS) at the National Facility, University of Agricultural Sciences, Bangalore, India (Fig 2.10) was used. All mass-spectrometric measurements were made by the author. The peripherals attached with the mass spectrometer were Elemental Analyzer

(Flash EA 1112 Series, CE Instruments, Italy) and ConFlo III. The instrument and its working are discussed below.

Elemental Analyzer (EA)

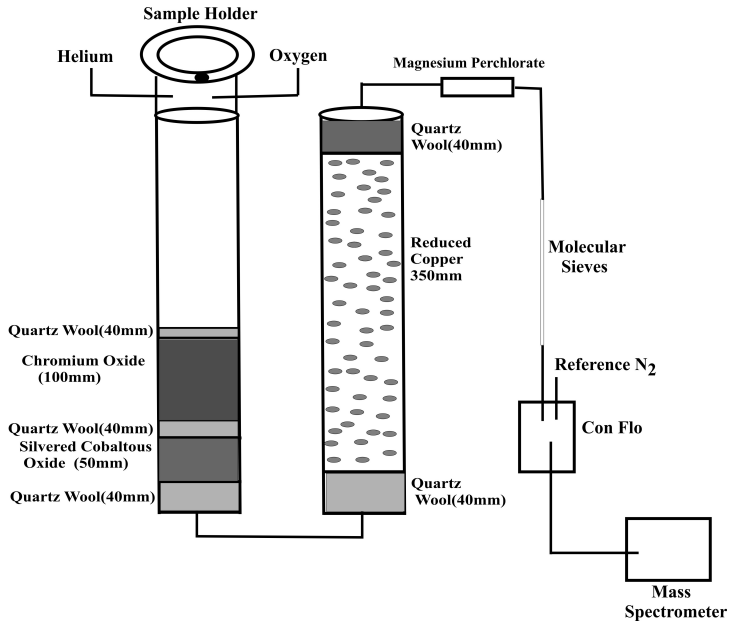

Figure 2.11: *Schematic diagram of Elemental Analyzer interfaced with IRMS.*

Elemental analyzer uses the Dumas combustion method for high temperature flash combustion. It consisted of two reactors (an oxidation or combustion column and a reduction column), a water absorber column, and a Gas Chromatograph (GC). Both the combustion and reduction columns, were made of quartz (melting point ∼1800 ^{o}C) tubes, which were 45 cm in length, with 18 mm outer diameter, and 14 mm inner diameter. Combustion column was prepared by filling quartz tube with chromium oxide (layer thickness ∼10 cm) and silvered cobaltous oxide (layer thickness ∼5 cm), separated (layer thickness ∼1 cm) and bracketed by quartz wool (layer thickness ∼5 cm). Reduction column was prepared by filling quartz tube with reduced copper (layer thickness ∼12 cm) with quartz wool at the top and bottom (∼5 cm). The chemicals required for combustion and reduction columns were procured from IVA Analysentechnik e.K., Meerbusch (Germany). Water absorber

column, 10 cm in length, with 5 mm inner diameter, was filled with magnesium perchlorate anhydrous granulate (6 ÷ 18 mesh). A molecular sieve made up of zeolite was used in the GC, 100 cm in length, with 4 mm outer diameter, and 1.6 mm inner diameter.

Conflo III

ConFlo III is a device coupling EA and IRMS. It works with an open-split arrangement whereby a gas flow of ∼80-100 ml min^{-1} coming from EA is reduced to ∼0.3 ml min^{-1}, the rate at which gas is introduced into the IRMS. ConFloIII contains two open split cells: one 'sample section' and the other 'reference section', which split the gases coming from EA and the reference gas cylinder, respectively.

Mass Spectrometer

Thermo Quest's Finnigan Delta plus continuous IRMS is a gas source mass spectrometer. In the source, ions are generated by electron (80 eV) impact in high vacuum, and are accelerated by a ∼3 keV potential difference. The accelerated ion beam exits the ion source through a slit (width 0.3 mm), and enters the magnetic sector of field strength 0.75 Tesla. The direction of the uniform magnetic field is perpendicular to the direction of the moving ions. The geometry of the magnetic sector is such that the ion beam enters and exits the magnetic sector at an angle of 26.5^o. This is done in order to maintain the radius of flight to be 9 cm. The collector consists of three Faraday cups connected to amplifiers. The elemental analyzer and mass spectrometer are fully automated and are controlled by the Finnigan MAT software ISODAT.

Measurement procedure

For isotopic analysis, a quarter of each of the GF/F filter samples was packed into a pellet using a clean silver foil. The rest was preserved for replicate analysis. Samples were then loaded on a turret (sample holder had the capacity of 62 samples) kept on the top of the oxidation chamber. Typically, 62 samples (56 GF/F filter

samples and 6 standards) were analyzed in a single run. Standards were kept at 1st, 17th, 32th, 47th, 48th and 62th positions. An automated mechanism allowed the samples to fall one by one into the oxidation chamber. The temperature of the oxidation chamber was maintained at 1100 ^{o}C with the help of an electric furnace. As soon as a sample fell, a one-second pulse of oxygen was given at a flow rate of 175 mls^{-1}. The temperature inside the column increased to 1800 ^{o}C for a moment, an oxygen pulse, lead to combustion of the sample with a flash. A constant flow of pure He gas (grade 5, 99.999%, procured from *Hydragas*, Bangalore) was maintained. Combustion of the sample produced oxides of mainly C, N and H in the presence of oxygen and oxidizing agents (chromium oxide and silvered cobaltous oxide). Therefore, the main gases coming out of the column were CO_2, NO_x and H_2O. Helium carried these gases to the reduction column. The reduction column contained reduced copper at 680 ^{o}C. Here different oxides of nitrogen were reduced to N_2 gas. CO_2 remained in its oxidized form because of high affinity of carbon for oxygen. Gases coming out of the column, mainly N_2, CO_2 and H_2O, were passed through the magnesium perchlorate column, which absorbed moisture. The remaining gases were then carried to GC column (maintained at 60 ^{o}C). The gas mixture passed at different rates through the GC column, depending on their various chemical and physical properties and their interaction with the molecular sieve. The function of the molecular sieve was to separate different gases. The retention time for N_2 was less than that for CO_2, as a result of which N_2 moved faster than CO_2 and came out earlier from the chromatographic column. Once the N_2 or CO_2 exited the column, it was injected into the mass spectrometer through the ConFlo.

A method of instructing the timing of different events (i.e., on and off times of reference gas, on and off times of elemental analyser and He dilution) was followed. The total data acquisition time for each sample was 450 sec.

For nitrogen measurements, the amplitudes of 28, 29 and 30 mass peaks and their ratios (29/28 and 30/28) were recorded, while for carbon measurements, the am-

plitudes of 44, 45 and 46 mass peaks and their ratios (45/44 and 46/44) were monitored. Area under the different mass peaks were proportional to the amounts of nitrogen (or carbon) present in the sample. The ratios were measured as atom $\%^{15}N$ (or $\%^{13}C$). Standards were loaded in varying amounts, ranged from 0.02 to 0.1 mg N (or 0.1 to 0.5 mg C) to calibrate the mass spectrometer for estimating PON (or POC).

Typically, the combustion and reduction columns were changed after ∼300 samples, followed by degassing of the system overnight. After checking for leak in the connections, background levels were measured. After this, internal precision of the mass spectrometer was checked by 'ZERO ENRICHMENT or Standard ON/OFF' method in which a reference N_2 or CO_2 gas was injected repeatedly and its $\delta^{15}N$ or $\delta^{13}C$ was measured. The reference gas injections gave an internal precision better than 0.1‰. This was followed by $\delta^{15}N$ or $\delta^{13}C$ measurements of external standards.

Table 2.8: *Atom percent and its precision for standard materials used (* 1-sigma standard deviation).*

Standard	Quoted atom % ^{15}N (or ^{13}C)	Measured % ^{15}N (or ^{13}C)
	Nitrogen	
$(NH_4)_2SO_4$ (IAEA-N-2)	0.373883	0.375116 ± 0.00066*(n=21)
KNO_3 (IAEA-N-3)	0.368188	0.367129 ± 0.00163* (n=17)
KNO_3 (USGS-32)	0.432152	0.432442 ± 0.00244* (n=15)
	Carbon	
Starch	1.081719	1.067496 ± 0.00096* (n=73)

For nitrogen, calibrated in-house casein and international standards $(NH_4)_2SO_4$ (IAEA-N-2) and KNO_3 (IAEA-NO-3) were used for checking the external precision. While for carbon, calibrated in-house starch and international standard ANU sucrose were used. The external precisions of the measurements were consistently better than 0.5‰. Error associated with the estimation of amount of nitrogen or carbon present in the sample was less than 10%. While the error was less than 1% in estimating atom $\%^{15}N$ and $\%^{13}C$.

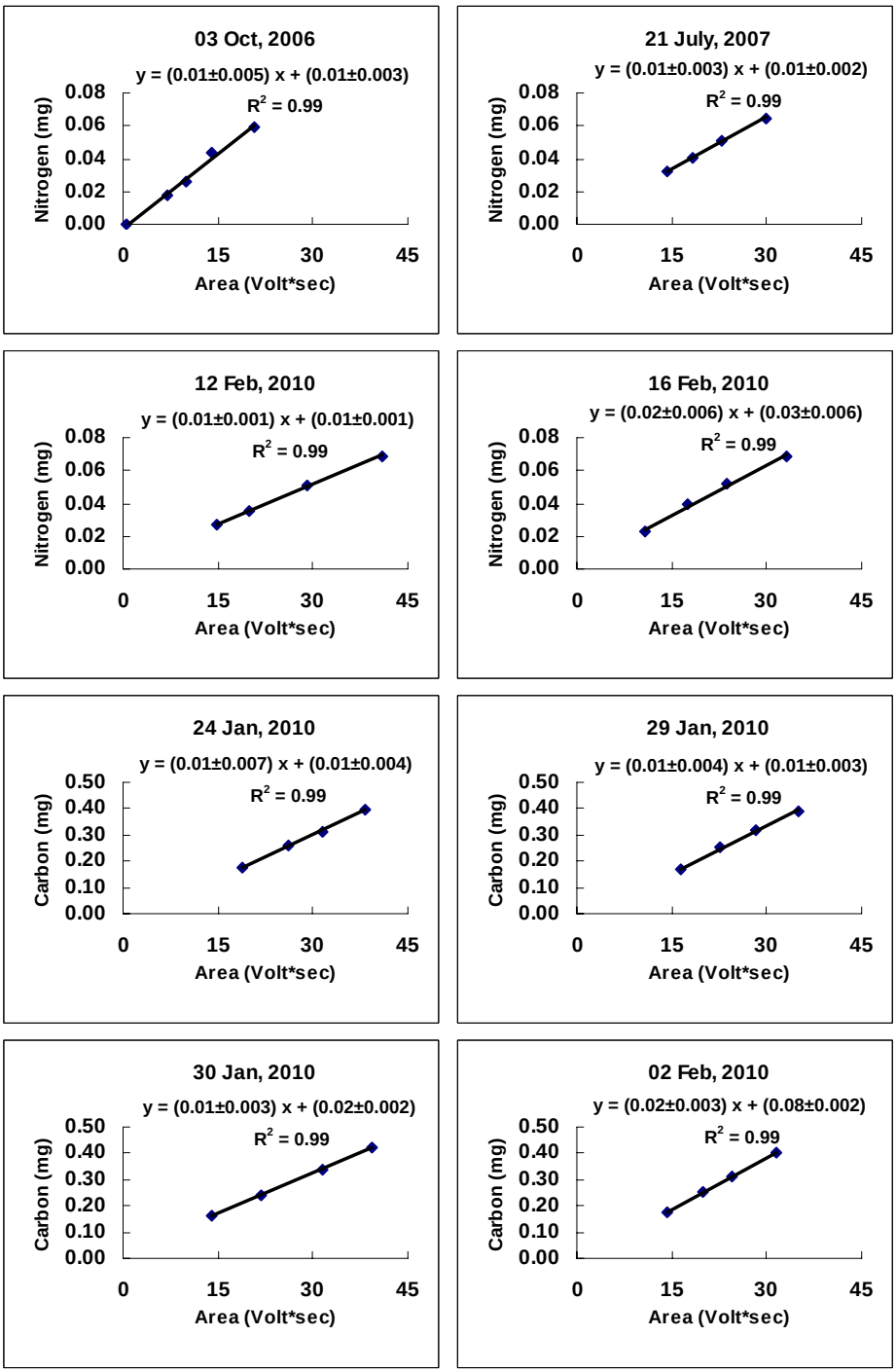

Figure 2.12: *Examples of calibration plots for estimating the amount of nitrogen (or carbon) present in the sample filters.*

The laboratory standards with their quoted and measured isotopic compositions, with the precision obtained during the present study are as listed in Table

2.8. Some examples of calibration plots, which were constructed to estimate the amount of nitrogen and carbon in the sample filters are shown in Fig 2.12. The mass spectrometer showed good stability during carbon measurements. However, it was observed that sensitivity of the mass spectrometer changed with time, in the case of nitrogen isotopic measurements (Fig 2.12). Three filaments were replaced over the four year period (between 2006 and 2010), which could be the reason for the variation in the sensitivity. Therefore, to get better and precise results, the mass spectrometer was calibrated for each sample batch using international standards. Linearity check using different amounts of international standards was usually performed before the commencement of measurements. For both carbon and nitrogen, the slopes of regression lines for such checks were found to be better than 0.6‰ per volt.

2.3.11 Equations to calculate N and C uptake rates

Nitrogen uptake rate equation

Several equations (*Neess et al.*, 1962; *Dugdale and Goering*, 1967; *Eppley et al.*, 1977) have been proposed to calculate nitrogen uptake rates with some inherent assumptions e.g., neglecting isotope dilution by unlabeled NH_4 produced from remineralization of organic matter and exchange of particulate nitrogen during the incubation. *Dugdale and Wilkerson* (1986) proposed an equation for specific uptake rate based on a constant transport model (*Grunseich et al.*, 1980). The specific uptake rate (in the unit of hr^{-1} or d^{-1}) is calculated based on the isotope ratio of sample measured at the end of incubation.

$$V_N = \frac{^{15}N_{xs}}{(^{15}N_{enr} - ^{15}N_{natural}) \times T} \tag{2.4}$$

Where, $^{15}N_{xs}$ is the excess atom % ^{15}N relative to the natural abundance of atom % ^{15}N in the particulate form, $^{15}N_{enr}$ is the atom % ^{15}N in the initially labeled fraction in the dissolved form, $^{15}N_{natural}$ is the abundance of (atom %) ^{15}N in the

natural unlabeled fraction in the dissolved form, and T is the duration of incubation.

The N uptake rate in concentration units (mmol N $m^{-3}d^{-1}$) is calculated by multiplying the specific uptake rate and PON_t particulate organic nitrogen (PON) at the end of incubation.

$$\rho_N = V_N \times PON_t \tag{2.5}$$

The following assumptions are made for the sake of simplicity. During incubation,
(i) there exists only a single nitrogen source for phytoplankton.
(ii) there is no excretion of nitrogen by phytoplankton.
(iii) Isotopic discrimination is negligible.
(iv) Atom % ^{15}N in the dissolved phase remains constant, as a consequence of (ii) and (iii).

Equation (2.5) provides the most accurate estimate of uptake rate among all other proposed equations if the isotope ratio and the PON can be measured on the same sample. Still, the presence of detrital nitrogen and an increase in PON during incubation leads to an underestimation of specific uptake rate with the equation (2.4) but the latter does not lead to a large inaccuracy as the difference in the PON measured before and after incubation is usually small. However, equation (2.5) is insensitive to the presence of detrital nitrogen in the filter, and to the simultaneous uptake of labelled and unlabeled nutrients (*Dugdale and Wilkerson*, 1986). Perturbation of uptake rates by addition of isotopically labeled tracers requires correction according to the Michaelis-Menten kinetics but it would not introduce much inaccuracy if the tracer amount is less than ∼10% of the ambient value (*Dugdale and Wilkerson*, 1986; *UNESCO*, 1994). Usually error in the ambient nitrate measurement affects the $^{15}N_{enr}$ used in the denominator of the equation (2.4). Error is more (around 5 %) in the case of low ambeint nitrate values. However, it reduces (<2 %) for higher nitrate levels (>1 μM). Error in atom % ^{15}N

measurements introduces <1 % error. Error in PON estimation is generally found <10 %, which only affects estimation of ρ_N. In general, error in the estimation of specific uptake rate and uptake rate of nitrogen is found less than <2 % and <10 %, respectively.

In the present study, the total nitrogen uptake rate was calculated as the sum of NO_3, NH_4 and urea uptake rates. Depth-integrated uptake rates (in the unit of mmol N $m^{-2}d^{-1}$) were calculated by trapezoidal integration.

New productivity was considered equivalent to NO_3 uptake rate and regenerated productivity, equivalent to the sum of NH_4 and urea uptake rates; f-ratio was the ratio of new productivity to total productivity, calculated as the ratio of NO_3 uptake to the total nitrogen uptake rate (*Sambrotto*, 2001).

Carbon uptake rate equation

Slawyk et al (1977) showed the importance of the coupled ^{13}C and ^{15}N tracer technique. They also found a consistency between the results obtained by the ^{13}C and ^{14}C methods. The main advantage of using ^{13}C is that it can be combined with the ^{15}N technique to get a better insight into the relationship between photosynthesis and inorganic nitrogen uptake by marine phytoplankton. Similar to specific uptake rate of nitrogen, specific uptake rate of carbon can be calculated using the following relation:

$$V_C = \frac{^{13}C_{xs}}{(^{13}C_{enr} - ^{13}C_{natural}) \times T} \tag{2.6}$$

where $^{13}C_{xs}$ is the excess atom % ^{13}C relative to the natural abundance of atom % ^{13}C in the particulate form, $^{13}C_{enr}$ is the atom % ^{13}C in the initially labeled fraction in the dissolved form, $^{13}C_{natural}$ is the abundance of (atom %) ^{13}C in the natural unlabeled fraction in the dissolved form, and T is the duration of incubation.

Also, carbon uptake rate in concentration units (mmol C $m^{-3}d^{-1}$) is calculated by multiplying the specific uptake rate and POC_t particulate organic carbon (POC) at the end of incubation.

$$\rho_C = V_C \times POC_t \tag{2.7}$$

Depth-integrated uptake rates (in the unit of mmol C $m^{-2}d^{-1}$) are calculated by trapezoidal integration. As in the case of nitrogen measurements, error in atom % ^{13}C measurements introduces <1 % error in the estimation of ρ_C and V_C. Usually error in the dissolved inorganic carbon measurement is low (<1 %), which affects the $^{13}C_{enr}$ used in the denominator of the equation (2.6). Error in POC estimation is generally found <10 %, which only affects estimation of ρ_C. In general, error in the estimation of ρ_C and V_C is found less than <10 % and <1 %, respectively.

2.3.12 Experimental precautions

Precautions to avoid contamination during measurements are of utmost importance. Good quality polycarbonate bottles were filled directly from the Go-Flo/Niskin bottles, to avoid any trace metal contamination. No carboys were used to store water samples. Bottles were thoroughly rinsed with the sample seawater before collection. Samples were covered with thick black cloth after the collection. New pipette tips were used for tracer each addition to each bottle. The samples were kept in dark before incubation; they were not exposed suddenly to light when taking out for incubation, to avoid possible light shock to phytoplankton. Filtration was also done in a near dark environment. During the filtration, only the sample to be filtered was taken out and rest were kept in dark. Different filtration cups and forceps were used for different tracers and for samples which monitored natural atom % ^{15}N and % ^{13}C. These cups were thoroughly rinsed with filtered seawater. GF/F filters were handled using clean and separate forceps for each tracer. Once the filtration was over, the polycarbonate bottles were cleaned with 5% HCl and three times with Milli-Q water before raching the next sampling location. For the mass spectrometric analysis samples were packed in clean silver foils. Blanks of cleaned silver foils were found insignificant, as found by testing in the mass spectrometer during every batch.

Chapter 3

New and Primary productivity in the northern Indian Ocean

3.1 Introduction

The northern Indian Ocean comprises mainly of two tropical basins (the Arabian Sea and the Bay of Bengal). Its uniqueness is that it is bounded to the north by the Asian continent, preventing northward oceanic heat export and only allowing a weak ventilation of the northern Indian Ocean thermocline. The hydrography and circulation of the northern Indian Ocean have been studied by many oceanographers (e.g., *Wyrtki*, 1973; *Schott*, 1983; *Shetye et al.*, 1993; *Schott and MaCreary*, 2001; *Shankar et al.*, 2002, and the many references therein). The winds over the northern Indian Ocean reverse direction twice a year; they blow from northeast during December to February (NE monsoon), and reverse direction towards the end of May and start blowing from the southwest (SW monsoon), persisting till September. Oct-Nov and Mar-May are the months of transition, with weaker winds. The winds are much stronger during the summer monsoon than during the winter monsoon (*Shankar et al.*, 2002).

These seasonally reversing monsoon winds over the northern Indian Ocean force a seasonally reversing circulation in the upper ocean. During summer (winter) the

Somali current flows poleward (equatorward) along the coast of Somalia (*Schott and McCreary*, 2001). During Apr-May and Oct-Nov, eastward surface jets are observed in the Equatorial current (*Wyrtki*, 1973). The currents along the east coast of India viz., the East India Coastal Current (EICC) (*Shetye et al.*, 1993) and the currents along the west coast of India, called the West India Coastal Current (WICC) (*Shetye et al.*, 1990) prevail in some seasons. The Summer Monsoon Current (SMC) flows eastward as a continuous current from the western Arabian Sea to the Bay of Bengal during summer, while the Winter Monsoon Current (WMC) flows westward, from the Bay of Bengal to the Arabian Sea during winter (*Shankar et al.*, 2002). These two monsoonal currents transfer water between, the Bay of Bengal and the Arabian Sea.

Both the Arabian Sea (AS) and the Bay of Bengal (BOB) are land locked in the north and forced by seasonally reversing monsoon winds and the surface circulations of both the basins undergo seasonal reversal. Despite these striking similarities, the basins show differences in many aspects e.g., the BOB receives fairly large quantities of fresh water from the Indian rivers (1.6×10^{12} m^3 yr^{-1} compared to 0.3×10^{11} m^3 yr^{-1} to the AS; *Subramanian*, 1993), which exerts a strong influence on the surface water circulation and stratification of the sea surface (*Shetye et al.*, 1991), the BOB remains cloudy throughout the year while cloudiness observed only during the SW monsoon in the AS. On an annual scale the BOB receives excess precipitation over evaporation $\sim$2 myr^{-1} (*Prasad*, 1997) while the AS shows excess of evaporation (>100 mm/month) over fresh water inputs (precipitation and river discharge) during summer and winter (*Prasanna Kumar and Narvekar*, 2005).

3.1.1 Productivity in the Arabian Sea

The AS shows strong seasonal cycle with high chlorophyll biomass as well as productivity. The AS shows high productivity during the SW monsoon (0.6 g C m^{-2}d^{-1}), moderate during the NE monsoon (0.3 g C m^{-2}d^{-1}), and low ($\sim$0.1 g C m^{-2}d^{-1}) during the intermonsoon period (*Bhattathiri et al.*, 1996; *Madhupratap et*

al., 1996). Higher productivity during summer in the Arabian Sea is driven by a combination of processes such as upwelling along the coasts of Somalia, Arabian and southern part of the west coast of India, advection from the upwelling region to the central Arabian Sea, Ekman pumping associated with the cyclonic wind stress curl north of the Findlater Jet and wind-driven mixing; all of which supply subsurface nutrients to the euphotic zone (*Prasanna Kumar and Prasad*, 1996; *Madhupratap et al.*, 1996). During winter, higher productivity in the Arabian Sea is triggered by winter cooling and convective mixing, which deliver nutrients to the euphotic zone.

Apart from witnessing changes in physical and biogeochemical conditions in time, the AS also exhibits considerable spatial variation, not seen in any other ocean (*Smith and Bottero*, 1977). Asymmetric monsoonal effect creates a strong gradient in biogeochemical processes within the basin (*Burkill et al.*, 1993). Geographically, the coastal locations (e.g., off Oman) are more productive than open ocean locations. Phytoplankton growth is found to exceed zooplankton grazing more in the western AS than in the eastern AS. This points the existence of different ecosystems in the east and west, probably due to different physical forcings (*Sarma*, 2004). In general, picoplankton are more dominant in the eastern AS, probably due to low NO_3 concentration; whereas diatoms are major contributors to primary production in the western AS. Therefore, *Sarma* (2004) argued that most of the produced organic carbon is recycled in the euphotic zone in the eastern AS, whereas it is exported to the deeper layers in the western AS. He further suggested that on an annual scale, western AS is net autotrophic, whereas eastern AS is net heterotrophic.

Sarma et al (1998) found high pCO_2 in surface waters of the AS than that in the atmosphere throughout the year; they estimated that this region is a perennial source of atmospheric CO_2 and it emits an average of $\sim$45 Tg C yr^{-1} to the atmosphere. *Sarma et al* (2003) estimated that the sinking organic matter flux from the surface accounts for about 30% of the total photosynthetic production

rate. They suggested that intense remineralization of organic matter takes place in the surface layers of the AS, and that the grazing and excretion of carbon by the microzooplankton and mesozooplankton sustain supersaturation of carbon dioxide in surface waters and hence promote the emission of carbon to the atmosphere. On the other hand, the sinking fluxes of particulate organic and inorganic carbon are the highest in the northern Indian Ocean (*Sarma et al.*, 2006). The rates of bacterial respiration, mineralization of organic carbon and inorganic carbon dissolution are also the highest in the northern Indian Ocean than elsewhere. Further, *Sarma et al* (2006) suggested that the biological pump operating in the northern Indian Ocean is the most efficient that transports surface-derived organic/ inorganic carbon to deeper layers.

Since the formulation of the concept of new and regenerated productivity (*Dugdale and Goering*, 1967) and the use of new productivity as a measure of export production, the ^{15}N tracer technique has been extensively used to characterize the biogeochemistry of the surface ocean and to asses the ocean's role in carbon sequestration. To assess the new productivity and f-ratios in the western and central AS, ^{15}N based new productivity measurements were carried out under US JGOFS program. New productivity measurements were initiated in the eastern part of the AS by *Kumar et al* (2010) in 2003. Significant seasonal and geographical variations in the new production and f-ratios are observed in the AS. *Owens et al* (1993) reported a large variation in the NO_3 uptake rates, from 2.7 mmol N $m^{-2}d^{-1}$ in the central AS to 88.9 mmol N $m^{-2}d^{-1}$ in the coastal upwelling region during fall, 1986. The f-ratio varied from a low of 0.09 at an open ocean station to as high as 0.92 at a coastal station. N-uptake rates varied from 9.2 mmol N $m^{-2}d^{-1}$ to 40 mmol N $m^{-2}d^{-1}$ during the winter monsoon, and from 3.9 mmol N $m^{-2}d^{-1}$ to 24 mmol N $m^{-2}d^{-1}$ during the late summer/early winter monsoon in the central AS (*McCarthy et al.*, 1999). Here the mean N-uptake rate is significantly higher in winter ($\sim$26 mmol N $m^{-2}d^{-1}$) than in late summer (11 mmol N $m^{-2}d^{-1}$). The f-ratio varied from 0.03 to 0.31 and from 0.04 to 0.29 during winter and the late

summer, respectively. Large variations in the N-uptake rate from 1.1 mmol N $m^{-2}d^{-1}$ to 23.6 mmol N $m^{-2}d^{-1}$ have also been found for the north-western AS during an inter-monsoon period (*Watts and Owens*, 1999). It is found that the f-ratios varied from a low of 0.07 in the open ocean region to a high of 0.52 at a coastal station. A large variation in the N-uptake rate, ranging from 0.1 to 13 mmol N $m^{-2}d^{-1}$ has also been reported during the spring inter-monsoon and the SW monsoon for the northern AS (*Sambrotto*, 2001).

Very high new production has been observed in the north-eastern Arabian Sea (NE-AS) during winter ranging from 1 to 4.3 mmol N $m^{-2}d^{-1}$ with a lower f-ratio, averaging around 0.19 (*Kumar et al.*, 2010). A general trend of spatial increase in the new production from south to north has been observed. During late winter monsoon, new production and f-ratio were significantly different in bloom (23 mmol N $m^{-2}d^{-1}$, 0.65) and non-bloom (5.7 mmol N $m^{-2}d^{-1}$, 0.54) regions. *Prakash et al* (2008) found the presence of two different biogeochemical provinces in eastern Arabian Sea during the late winter monsoon: less productive southern (non-bloom) and more productive northern (*Noctiluca miliaris* bloom) regions. The southern sector is characterized by low column N-uptake and very low f-ratio ($\sim$5.5 mmol N $m^{-2}d^{-1}$ and 0.4, respectively). The f-ratio, although low, increased progressively towards north. The northern part is a highly productive zone, with very high N-uptake and significantly high f-ratio ($\sim$19 mmol N $m^{-2}d^{-1}$ and 0.8, respectively) (*Prakash et al.*, 2008). The link between winter mixing with the nutrient supply to the surface and its role in the winter blooms have been studied extensively (*Madhupratap et al.*, 1996; *Prasanna Kumar and Narvekar*, 2005). The present study is an attempt to enhance our understanding of winter mixing and its impact on new productivity. The present results, in the foreground of previous findings allows us to observe any intra-seasonal and/or inter-annual variation in new productivity during winter. Further, the link between entrainment of nutrients due to winter cooling and the observed new productivity has also been investigated.

Recent observations based on ocean color show that summer productivity in the

western Arabian Sea has been increasing from year 1997 to 2004 (*Goes et al.*, 2005). The observed trend in Chlorophyll has been attributed to the warming of the Eurasian land mass. However, such a trend is not observed in the NE-AS (*Prakash and Ramesh*, 2007). *Naqvi et al* (2010), on the basis of *in situ* hydrographic and chlorophyll measurements as well as a reanalysis of ocean color data extending to 2009, have also ruled out the conclusions put forward by *Goes et al* (2005). In this context, it is worthwhile to observe any annual trend in the new productivity, which has a direct link with the removal of carbon to the deep. Towards this, as mentioned earlier, a comparison of the present results with the previous findings has been made in the present study.

It is evident that a large spatio-temporal variability exists in the biogeochemical characteristics of the response of this basin to climate change. The region is one of the major quasi-permanent sites for water column denitrification and loses ∼60 Tg N yr^{-1} through this process (*Codispoti*, 2007). Further, *Trichodesmium* blooms are frequently seen in the area (*Devassy et al.*, 1978, *Capone et al.*, 1998, *Parab et al.*, 2006), and nitrogen fixation within such blooms can be substantial (∼130 μmol N $m^{-2}d^{-1}$ between surface and 0.5 m depth; *Capone et al.*, 1998). In addition to *Trichodesmium* blooms, the presence of diazotrophic γ-proteobacteria in the Arabian Sea has also been reported (*Bird et al.*, 2005), which are believed to release fixed nitrogen to the ocean water, making it available to the other non-diazotrophic species (*Letelier and Karl*, 1996). However, the lack of N_2-fixation measurements in the region leads to a significant uncertainty in the nitrogen balance. Furthermore, ^{15}N based N uptake rate measurements during inter-monsoon periods in the NE-AS are very limited particularly during *Trichodesmium* blooms. The present study reports the first measurements of ^{15}N-based NO_3, NH_4 and urea uptake rates in the NE-AS during spring. In the absence of direct measurements of N_2-fixation, several authors e.g. *Karl et al* (1995), *Tyrrell* et al (2003) and *Poulton et al* (2009) have used *Trichodesmium* abundance and published values of specific rates of N_2-fixation, and estimated the potential magnitude of N_2-fixation associ-

ated with it. A similar approach has been adopted here. Further, NO_3 based new production has been combined with the estimated N_2-fixation rates to re-estimate new production. The study also provides a rough estimate of nitrogen gained by the water column due to *Trichodesmium* growth.

3.1.2 Productivity in the Bay of Bengal

In contrast to the AS, in the BOB, surface chlorophyll and productivity show a weaker seasonality. The chlorophyll and the productivity are the highest during winter, followed by spring intermonsoon; both are the lowest during summer. This low productivity in the BOB is due to strong stratification of the upper waters under the influence of fresh water influx from rivers as well as direct overhead precipitation during the monsoon. Despite this, sediment trap data show that the average annual vertical fluxes of organic carbon are comparable in both basins (*Ramaswamy and Nair*, 1994). This has been attributed to scavenging of organic matter from the water column in association with mineral particles (the "ballast" hypothesis; *Ittekkot et al.*, 1991). *Naqvi et al* (1996) measured respiration rates in both the regions and found that the rates are almost two times higher in the AS than in the BOB. This suggests that the faster vertical removal of organic matter in the BOB. The comparable downward organic carbon fluxes in the highly productive AS and the moderately productive BOB can also be understood with the help of independent estimates of new production based on nitrogen uptake because, on a longer time scale, new production is considered to be equal to the export production. The new production measurements using ^{15}N tracer technique were carried out in the BOB for the first time under the program Bay of Bengal Process Studies (BOBPS) (*Kumar et al.*, 2004), who found consistently high new productivity in two different seasons (Sep-Oct, 2002 and Apr-May, 2003), which could be one of the reasons for the relatively higher downward organic carbon flux in the moderate/low productive BOB. They observed that the new productivity during the pre-monsoon is higher than that during the post-monsoon. Overall, the

new production for the region during the pre-monsoon averaged around 5.4 (±3.7) mmol N $m^{-2}d^{-1}$, that is almost twice the average value observed during the post-monsoon (2.6±2.7 mmol N $m^{-2}d^{-1}$). However, the average f-ratio estimated for the entire region increased to 0.70 (±0.1) during pre-monsoon, compared to 0.5 during the post-monsoon.

Prasanna Kumar et al (2007) proposed eddy pumping by the subsurface cold core eddies as a possible mechanism of nutrient injection to the oligotrophic waters in the Bay of Bengal during summer. It has been found that eddy enhances the biological productivity 2 to 8 times compared to the non-eddy region. *Madhu et al* (2002) observed enhanced primary production along the south-western BOB due to the October 1999 super-cyclone. Therefore, such mixing by cyclones or by eddies could be a cause of higher new production in the Bay. Though the existence of eddies and their role in enhancing productivity in the BOB has been studied by *Prasanna Kumar et al* (2007), their role in the context of new (export) productivity is yet to be explored fully. An attempt has been made in the present study to measure new (export) and total productivity in and outside an eddy to understand its role in the carbon export to the deep. New productivity measurements have been carried out in the eastern BOB (Andaman Sea) to explore the region as well. This has an overall implication to our understanding of the cause of comparable annual fluxes of organic carbon in the high-productive AS and the low-productive BOB.

3.2 Part I: Sampling in the NE-AS (spring 2006)

3.3 Environmental conditions

Typical spring conditions are observed during the study period. Weak winds, clear sky, intense sun light, and low sea state conditions are found. The region shows low productivity during spring, as evidenced by the chlorophyll image (Fig 3.1). Sampling locations are superimposed on the chlorophyll image.

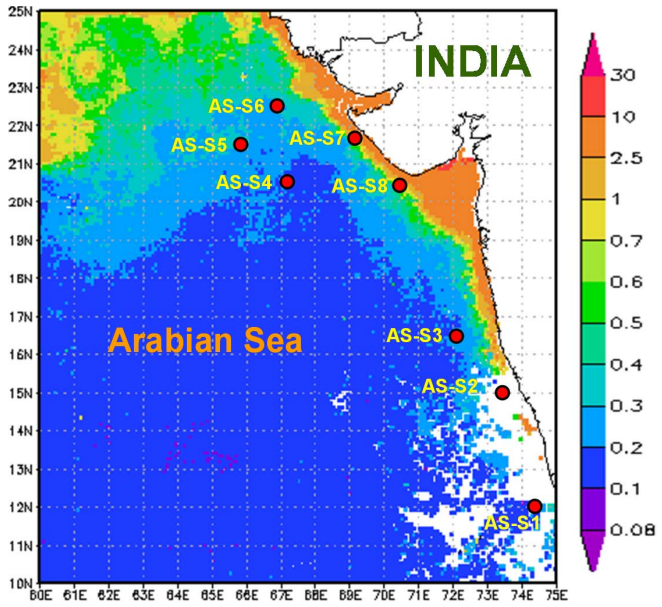

Figure 3.1: *Composite SeaWiFS Chlorophyll image for 15-30 Apr, 2006 (source: http://reason.gsfc.nasa.gov/OPS/Giovanni/ocean.swf8D.shtml) corresponding to cruise in the NE-AS during spring with superimposed station locations.*

Here, stations with water depth <500 m have been considered as coastal locations viz., AS-S1, AS-S2, AS-S7, and AS-S8. While the stations with water depth >500 m have been considered as open ocean locations viz., AS-S3, AS-S4, AS-S5, and AS-S6. Surface temperature, salinity, winds, mixed layer depth (MLD) and euphotic depth (ED) data are listed in Table 3.1.

Table 3.1: *Station codes, locations of the stations, sea surface temperature (^oC; SST), surface salinity (psu), mixed layer depth (m; MLD), euphotic depth (m; ED) and wind speed (ms^{-1}; V_w) in the NE-AS during spring (Apr, 2006).*

Station Code	Lat (^{o}N)	Lon (^{o}E)	SST	Salinity	MLD	ED	V_w
AS-S1	12.0	74.4	29.9	33.7	39	67	3.1
AS-S2	15.0	73.5	29.2	34.8	25	34	5.7
AS-S3	16.4	72.1	28.8	34.6	27	48	6.6
AS-S4	20.6	67.1	28.2	35.3	37	58	6.0
AS-S5	21.4	65.8	27.5	35.9	28	48	5.8
AS-S6	22.4	66.9	27.5	35.9	28	47	7.4
AS-S7	21.7	69.2	27.3	35.9	29	35	6.5
AS-S8	20.5	70.5	27.4	35.7	16	18	7.0

Surface winds are generally low in the study area, from 3.1 to 7.4 ms^{-1} with an average of ~5.5 ms^{-1}.

3.3.1 Temperature and salinity

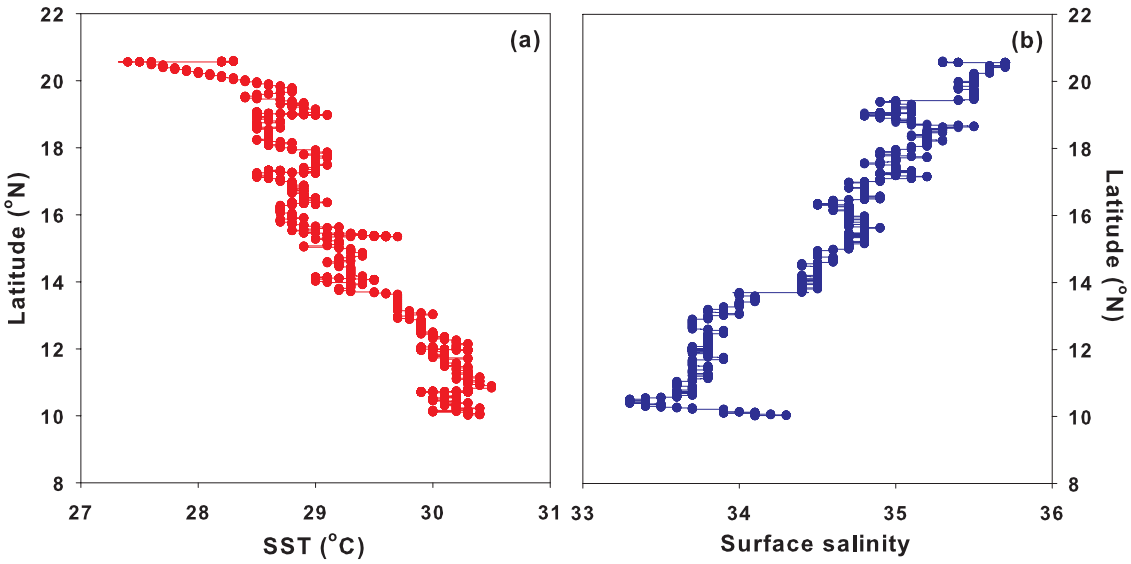

Figure 3.2: *Latitudinal variation of (a) SST and (b) surface salinity in the NE-AS during SIM.*

Sea surface temperatures (SST) are high, and range from 27.3 to 30.4 ^{o}C. A decreasing trend is observed in SST from the south to the north, whereas surface salinity shows the opposite trend (Fig 3.2). Surface water is highly stratified at all the stations. *Prasanna Kumar and Narvekar* (2005) reported similar environment conditions which led to a shallow mixed layer in the region. At the coastal locations, mixed layer depth (the depth at which temperature decreased by 1 ^{o}C of its surface value; MLD) varies from 16 to 39 m. No significant difference is observed in the MLD values between coastal and open ocean locations (Table 3.1). The deepest and the shallowest ED are observed at the stations AS-S1 and AS-S8 (both coastal). Overall, it varies from 47 to 58 m and 18 to 67 m for the open ocean and coastal stations, respectively. The ED is deeper than the MLD at all stations (Table 3.1).

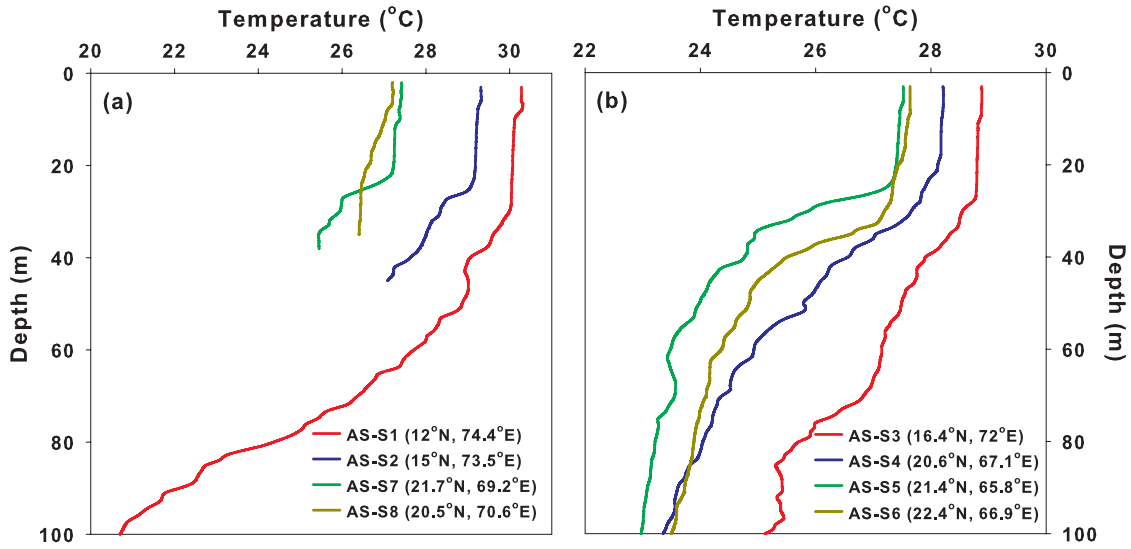

Figure 3.3: *Depth profiles of temperature at (a) coastal (water depth <500 m) and (b) open ocean (water depth >500 m) locations in the NE-AS during spring.*

SST decreases by ∼0.3 ^{o}C per degree latitude towards the north (Fig 3.2); whereas, surface salinity increases by ∼0.2 psu per degree latitude towards the north (Fig 3.2). This north-south trend is a typical feature of the AS (*Prasanna Kumar and Narvekar*, 2005; *Prakash et al.*, 2008).

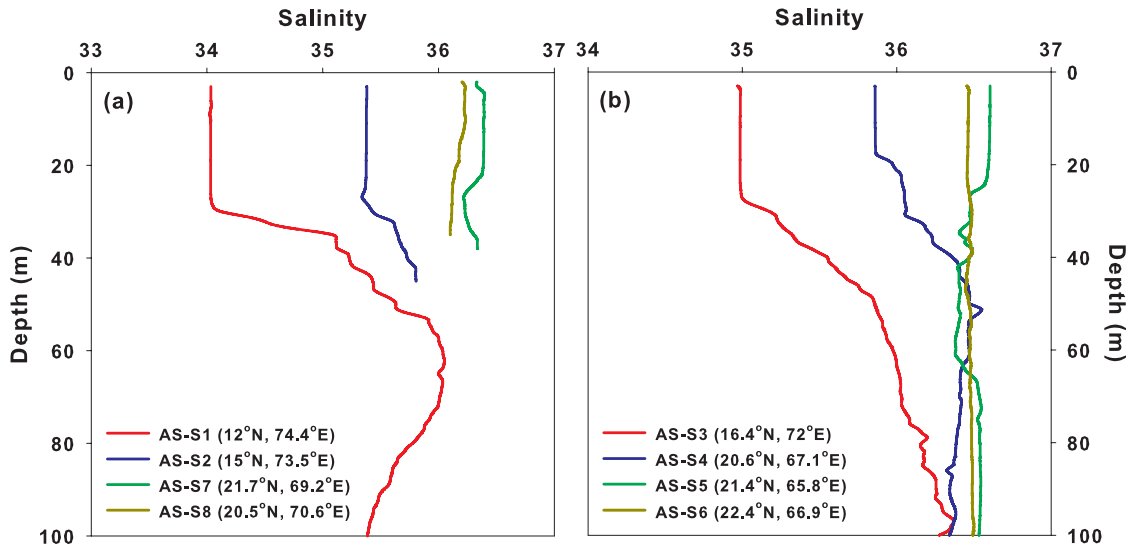

Figure 3.4: *Depth profiles of salinity at (a) coastal and (b) open ocean locations in the NE-AS during spring.*

The gradient is a consequence of the transfer of water masses between the BOB and the AS by monsoonal currents and the differential solar heating in the region. Depth profiles of temperature and salinity are shown in Figs 3.3 and 3.4, respectively. No signature of mixing/upwelling or turbulence in the surface layers is seen. The thermocline shoals up towards the north at open ocean stations (Fig 3.3b) while such signatures are not clearly seen at the coastal locations because of shallow depth profiles from the CTD (limited by water depth). Nevertheless, surface water is found to be highly stratified at all the coastal as well as open ocean locations (Figs 3.3 and 3.4).

3.3.2 Nutrients

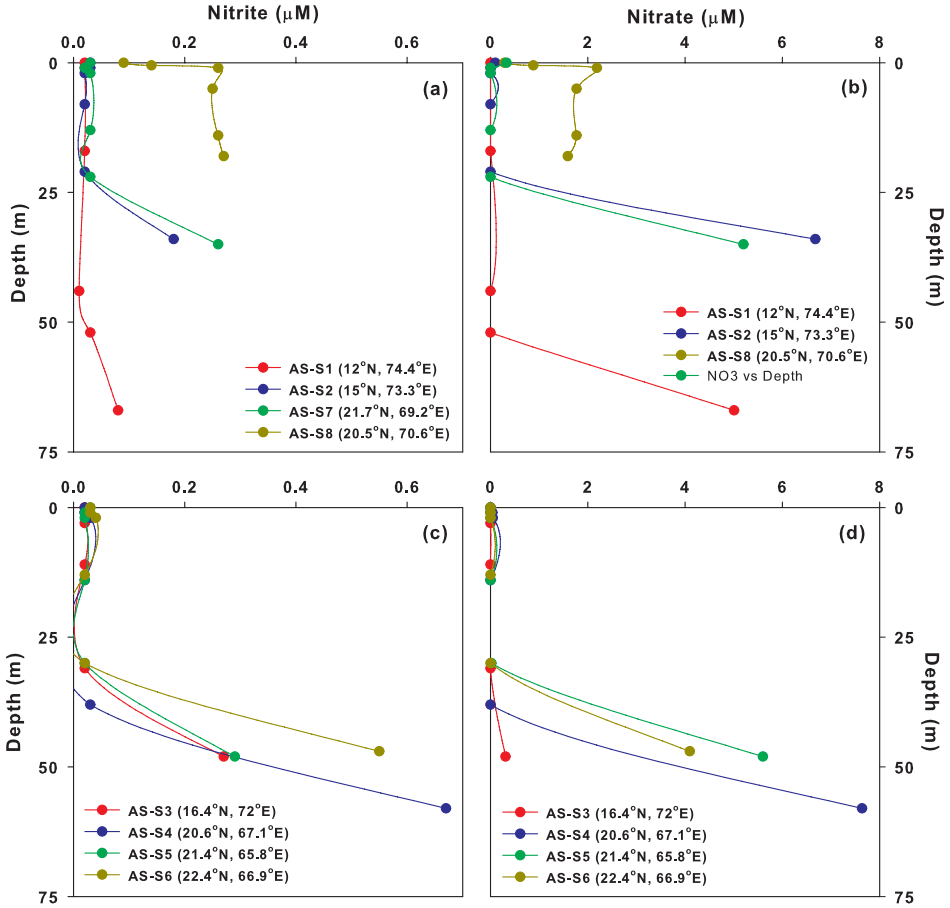

Figure 3.5: *Depth profiles of NO_2 (left) and NO_3 (right) at different (a and b) coastal and (c and d) open ocean locations in the NE-AS during spring.*

Different nutrient (NO_2, NO_3, PO_4, and SiO_4) profiles are shown in Figs 3.5 and 3.6. NO_2, and NO_3 are found to be mostly near or below to detection limit (<0.01μM) at all stations except AS-S8. Nitrite concentration is below 0.1 μM at all the locations. No significant difference is observed between the coastal and open ocean locations for NO_2, and NO_3 values (Fig 3.5). The upper ~20 m water column is completely devoid of NO_2 and NO_3 over the study area. Below ~20 m depth, NO_2, and NO_3 values increase at all the locations.

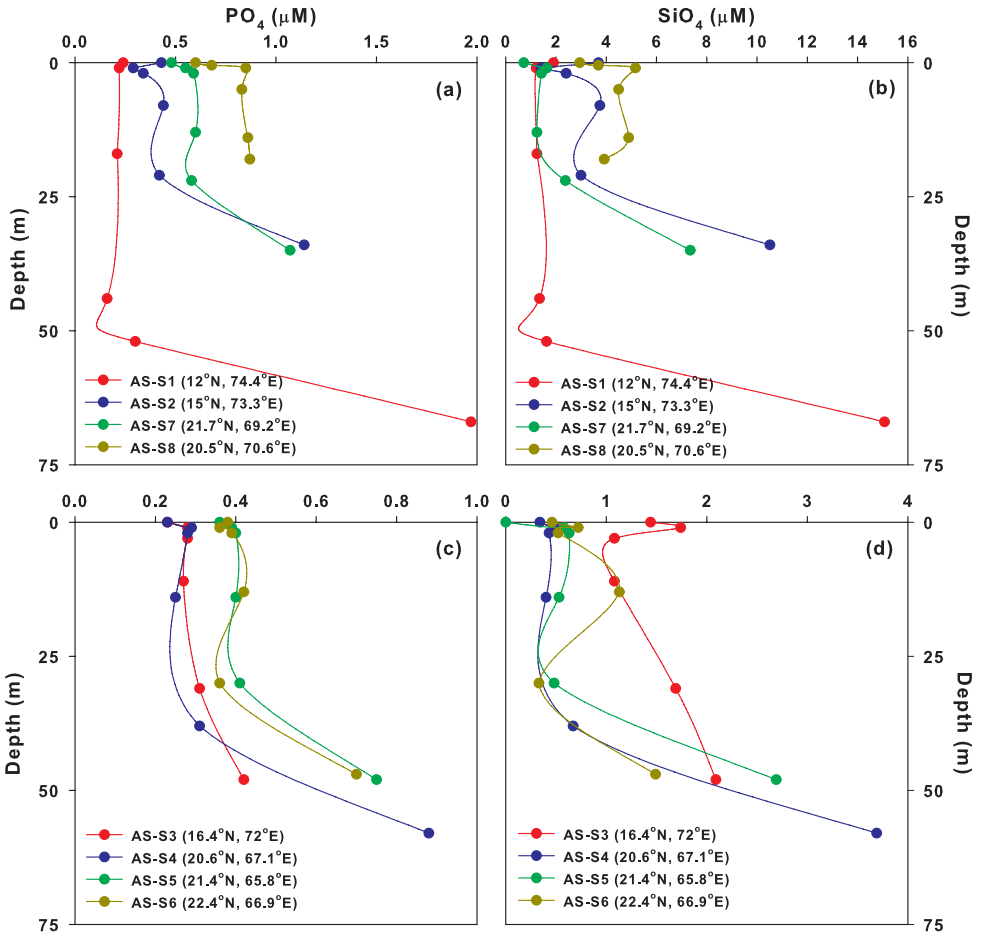

Figure 3.6: *Depth profiles of PO_4 (left) and SiO_4 (right) at different (a and b) coastal and (c and d) open ocean locations in the NE-AS during spring.*

Surface PO_4 concentration is significant (>0.2 μM) (Fig 3.6), similar at coastal and open ocean locations; whereas a significant difference in the sub-surface values is observed (Fig 3.6), with higher values at coastal locations. A similar pattern is

also found in SiO_4. This indicates the supply of these nutrients to be continental.

3.3.3 Phytoplankton

Dr. Prabhu Matondkar from the National Institute of Oceanography, Goa provided the phytoplankton cell data. Total phytoplankton (including *Trichodesmium*) cell counts (cell L^{-1}) and *Trichodesmium* counts (trichomes L^{-1}) are shown in Fig 3.7. Total plankton cell counts vary from 180 cells L^{-1} to 8338 cells L^{-1}. At the coastal locations, the average cell counts are 3291 cells L^{-1}, whereas in the open ocean it was 766 cells L^{-1}.

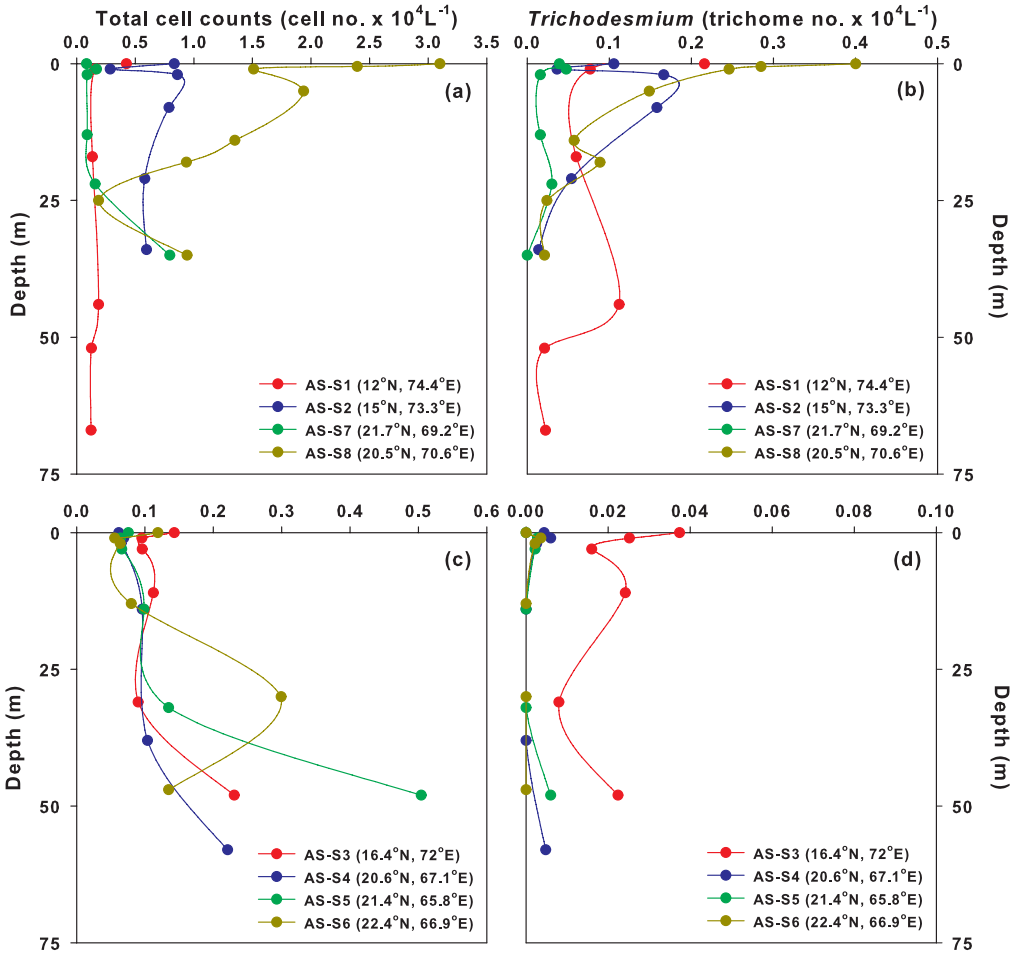

Figure 3.7: *Depth profiles of total phytoplankton cells (left) and Trichodesmium (right) at different (a and b) coastal and (c and d) open ocean locations in the NE-AS during spring.*

The presence of diatoms, dinoflagellate and cyanobacteria are observed at all the locations with varying proportions. Overall, diatoms dominate the plankton population (more than 50%) and the species were *Navicula* sp., *Thalassiothrix frauenfeldii*, *Skeletonema costatum*, *Rhizosolenia setigera*. After diatoms, cyanobacteria is the most abundant plankton and dominate in the coastal region. Deficiency of phosphorus and iron are the well known key factors restraining the growth of *Trichodesmium* (*Karl et al.*, 2002). The former is not the limiting nutrient during the study period (Fig 3.6a and b). Iron is not measured in the present study. However, during the spring, winds are predominantly from the Arabian Peninsula and other parts of the Middle East and the wind-blown dust is known to supply bioavailable Fe (*Johansen and Hoffmann*, 2003). Such environmental conditions including gentler winds, shallow mixed layer and lower NO_3 favor the growth of *Trichodesmium* in the study area. Both *Trichodesmium erythraeum* and *Trichodesmium thibautii* are found in the region with the slight dominance of the former. *Scripsiella trachoidea* is the main dinoflagellate found in the region. *Trichodesmium* abundance varied from 0 to 4004 trichomes L^{-1}, generally abundant in coastal stations (Fig 3.7); however, at one open ocean station (station AS-S3) significantly higher *Trichodesmium* cells (374 trichomes L^{-1}) are found in surface water. More than 1000 trichomes L^{-1} are observed at stations AS-S1, AS-S2, and AS-S8 with the highest found at AS-S8. The highly varying concentration of *Trichodesmium* suggests that *Trichodesmium* growth is highly dependent on very localized environment parameters. Its appearance at open ocean locations indicates that open ocean can also be a favorable environment for *Trichodesmium* in addition to the coastal region. Overall, concentration of total cells are higher at the coastal locations. *Trichodesmium* abundance in the present study is comparable to that previously reported from the central Arabian Sea ($\sim$104 trichomes L^{-1}; *Capone et al.*, 1998) but lower than that reported from the west coast of India ($>$107 filaments L^{-1}; *Devassy et al.*, 1978).

3.3.4 Chlorophyll

Surface Chl *a* is found to be low (0.11 to 0.85 mg C m^{-3}) at all the stations except AS-S8 (6.63 mg C $^{-3}$). At the coastal locations, surface chl *a* is higher than at the open ocean locations and it varies from 0.15 to 6.63 mg C m^{-3} (average of 1.38 mg C m^{-3}) at the former and 0.11 to 0.23 mg C m^{-3} (average of 0.16 mg C m^{-3}) at the latter.

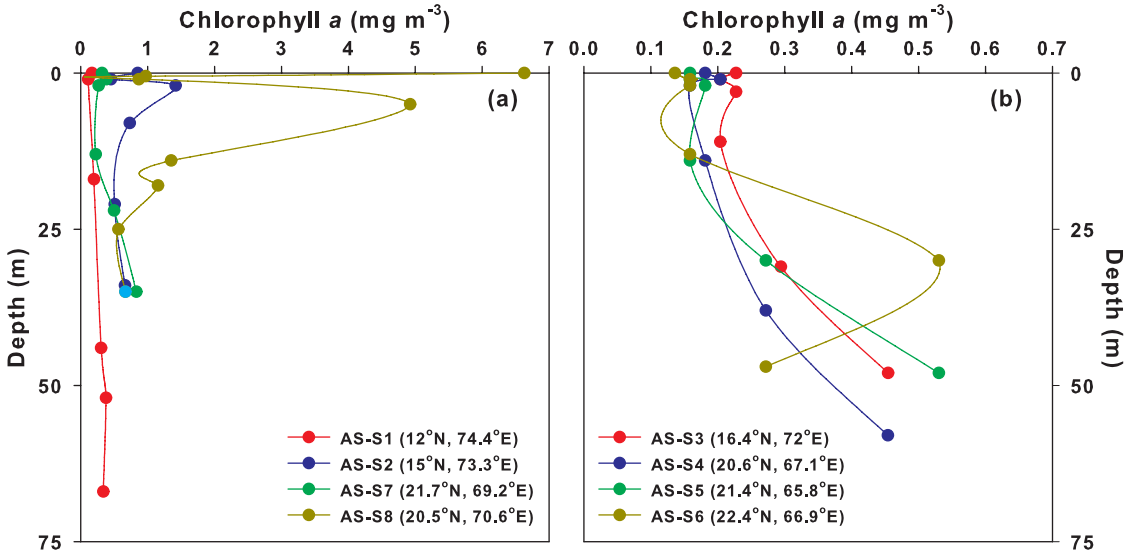

Figure 3.8: *Depth profiles of chlorophyll a at different (a) coastal and (b) open ocean locations in the NE-AS during spring.*

Unlike NO_3, Chl *a* is lower throughout the euphotic zone (Fig 3a and b), and shows a slight increase below mixed layer, at all stations but AS-S8. There is a no signature of sub-surface chl *a* maximum over the study area except at AS-S6. In general, chl *a* follows the pattern of total cell content at all the locations. Lower cell content and chl *a* are the consequence of lower NO_3 values in the ED, which indicate nitrogen limiting conditions. Higher NO_3 below the MLD supports a slight increase in chl *a* and plankton cell counts at those depths, particularly at open ocean locations (Figs 3.7 and 3.8). However, such a pattern is not seen at the coastal locations, suggesting different environment conditions with different nutrient and plankton regimes.

3.4 Nitrogen uptake rates

^{15}N based new and regenerated productivity is measured at eight stations (Fig 3.1). Here, the measured NO_3 uptake rates are treated as new production, apart from nitrogen fixed by *Trichodesmium*. As *Trichodesmium* presence is observed in the study area, it is required to incorporate N_2 fixation associated with the *Trichodesmium* with the measured NO_3 uptake rates to calculate new production. Direct measurement of N_2-fixation is not performed, so potential magnitude of N_2-fixation associated with the *Trichodesmium* is estimated based on the observed *Trichodesmium* abundance and the reported cell specific N_2-fixation rate. There exist some data on cell specific N_2-fixation rates from field and laboratory experiments; e.g., *Fu and Bell* (2003) reported N_2-fixation rate 2 pg N cell^{-1} h^{-1} from cultured strain of *Trichodesmium* sp. (GBRTRLI101) from the Great Barrier Reef Lagoon, *McCarthy and Carpenter* (1979) measured N_2-fixation rates (1.9 pg N trichome^{-1} h^{-1}) for *Oscillatoria thiebautii* (Gom.) in the subtropical north Atlantic Ocean. *Capone et al* (1998) observed an extensive bloom of *Trichodesmium* N_2-fixation in the central AS and measured specific N_2-fixation rate (1.5 pmol N trichome^{-1} h^{-1}). The specific N_2-fixation rates given by *Capone et al* (1998) have been used here, as their measurements are from the AS and the abundance of *Trichodesmium* in both studies are also comparable.

3.4.1 New productivity

Nitrate uptake rate

Depth profiles and their euphotic-depth-integrated NO_3 uptake rates at different locations are shown in Fig 3.9. Depth profiles of NO_3 uptake rates almost follow the pattern of ambient NO_3 concentration. Surface uptake rates of NO_3 are generally very low throughout the study area. Nitrate uptake rate increases below the MLD with increase in the ambient NO_3 levels (Fig 3.9). As in NO_3 values, no significant difference has been observed in NO_3 uptake rates between the coastal and open

ocean locations. This indicates the strong coupling of the NO_3 uptake and its availability in the region. Euphotic-depth-integrated NO_3 uptake rates vary from 0.22 to 1.29 mmol N m^{-2} d^{-1}. Similar to Chl *a*, most of the NO_3 uptake is found below the mixed layer at all the stations (Fig 3.9).

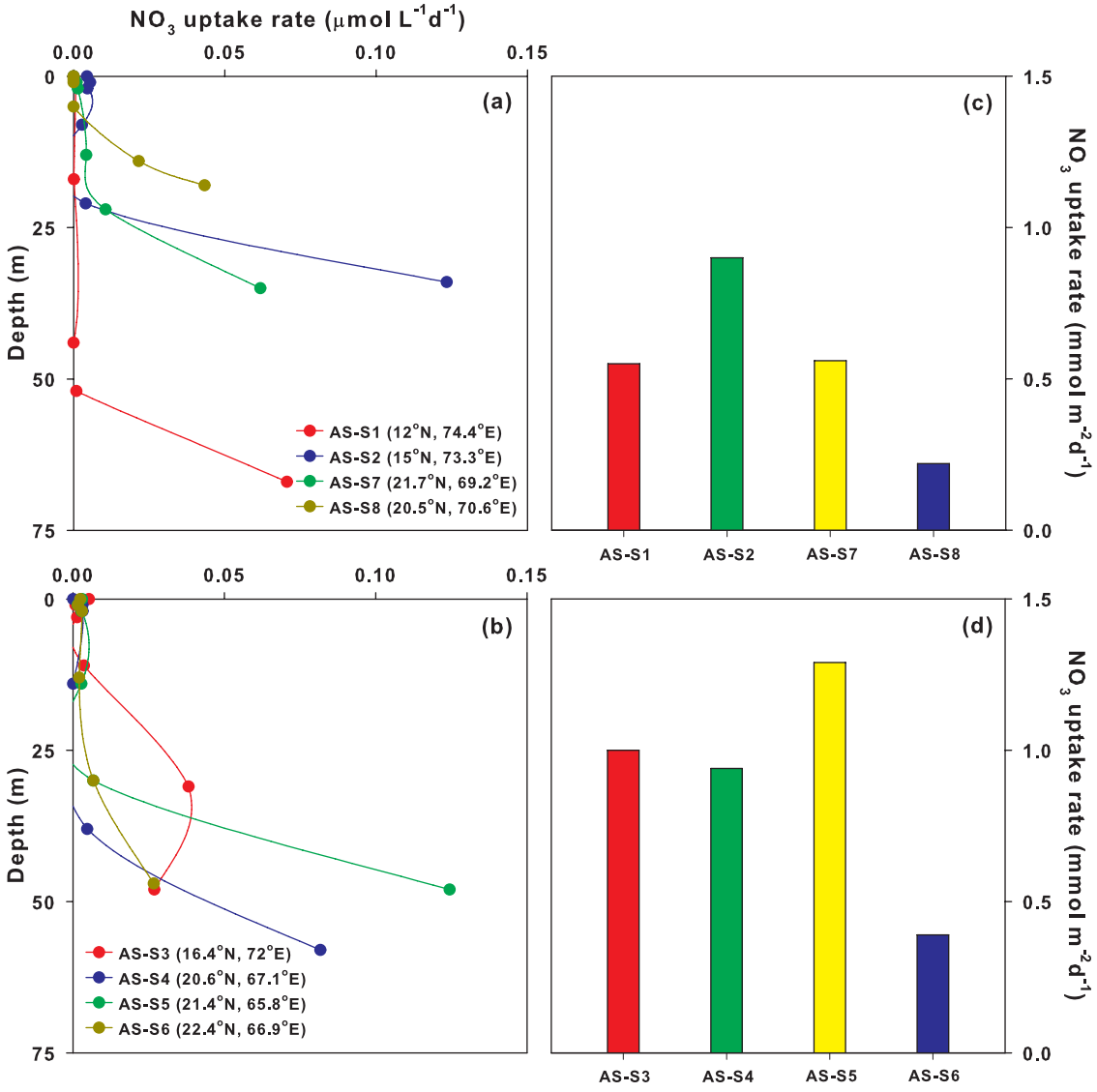

Figure 3.9: *Depth profiles of NO_3 uptake rate (left) and their euphotic-depth-integrated values (right) at different (a and c) coastal and (b and d) open ocean locations in the NE-AS during spring.*

Euphotic NO_3 uptake rates are 0.22 to 0.56 mmol N m^{-2} d^{-1} (with an average of 0.52 mmol N m^{-2} d^{-1}) and 0.39 to 1.29 mmol N m^{-2} d^{-1} (with an average of 1.07

mmol N m^{-2} d^{-1}) at coastal and open ocean stations, respectively. No north-south trend is observed in the NO_3 uptake rate. Overall, NO_3 uptake at the open ocean locations is twice the value at coastal locations, with the highest value at station AS-S5. Interestingly, the lowest NO_3 uptake is observed at station AS-S8, at which the highest abundance of *Trichodesmium* is found. This is in contrast to the observations of *Kumar et al* (2010), who found that new productivity at the coastal region was twice that at open ocean during winter in the NE-AS; this suggests the coastal and open ocean regions behave differently and the new productivity varies with seasons. *Watts and Owens* (1999) reported new productivity 0.3-0.9 mmol N m^{-2} d^{-1} off the Oman and 0.9-4.3 mmol N m^{-2} d^{-1} for the central AS during inter-monsoon. *Sambrotto* (2001) measured a new productivity of 3.1 mmol N m^{-2} d^{-1} in the Oman coastal upwelling zone and 0.4 mmol N m^{-2} d^{-1} in the south-eastern AS during spring. Our values from the NE-AS are comparable to those reported from the north-western and south-eastern AS, but lower than those for the central AS. The observed values are lower than the values reported by *Kumar et al* (2010) and *Prakash et al* (2008) during winter from the NE-AS.

N_2-fixation rate

N_2-fixation rates associated with *Trichodesmium* (estimated from their abundance and cell specific uptake rate) are shown in Fig 3.10. As *Trichodesmium* is abundant in the coastal region, the associated N_2-fixation rate is also higher. N_2-fixation rate is mostly confined to the first few meters of the surface with the highest value at AS-S8; it decreases with depth (Fig 3.10). Similar observations were made by *Capone et al* (1998) in the central AS; they reported that N_2-fixation was 3-fold higher in the upper 0.5 m than that between 0.5 and 40 m. N_2-fixation rates were higher than the NO_3 uptake rates in the MLD, particularly at the coastal locations. Euphotic-depth-integrated N_2-fixation is also shown in Fig 3.10. These rates vary from 0.002 to 0.54 mmol N m^{-2} d^{-1}; they are 0.08 to 0.54 mmol N m^{-2} d^{-1} (with an average of 0.33 mmol N m^{-2} d^{-1}) and 0.002 to 0.10 mmol N m^{-2} d^{-1}

(with an average of 0.03 mmol N m^{-2} d^{-1}) for coastal and open ocean stations, respectively. Although the abundance of *Trichodesmium* is comparable to that of *Capone et al* (1998), our values being slightly higher. Their estimates were based on the direct measurements of N_2-fixation by the C_2H_2 reduction method whereas our values are obtained from the *Trichodesmium* cells counts and their potential uptake rates; this could be the reason for the observed difference.

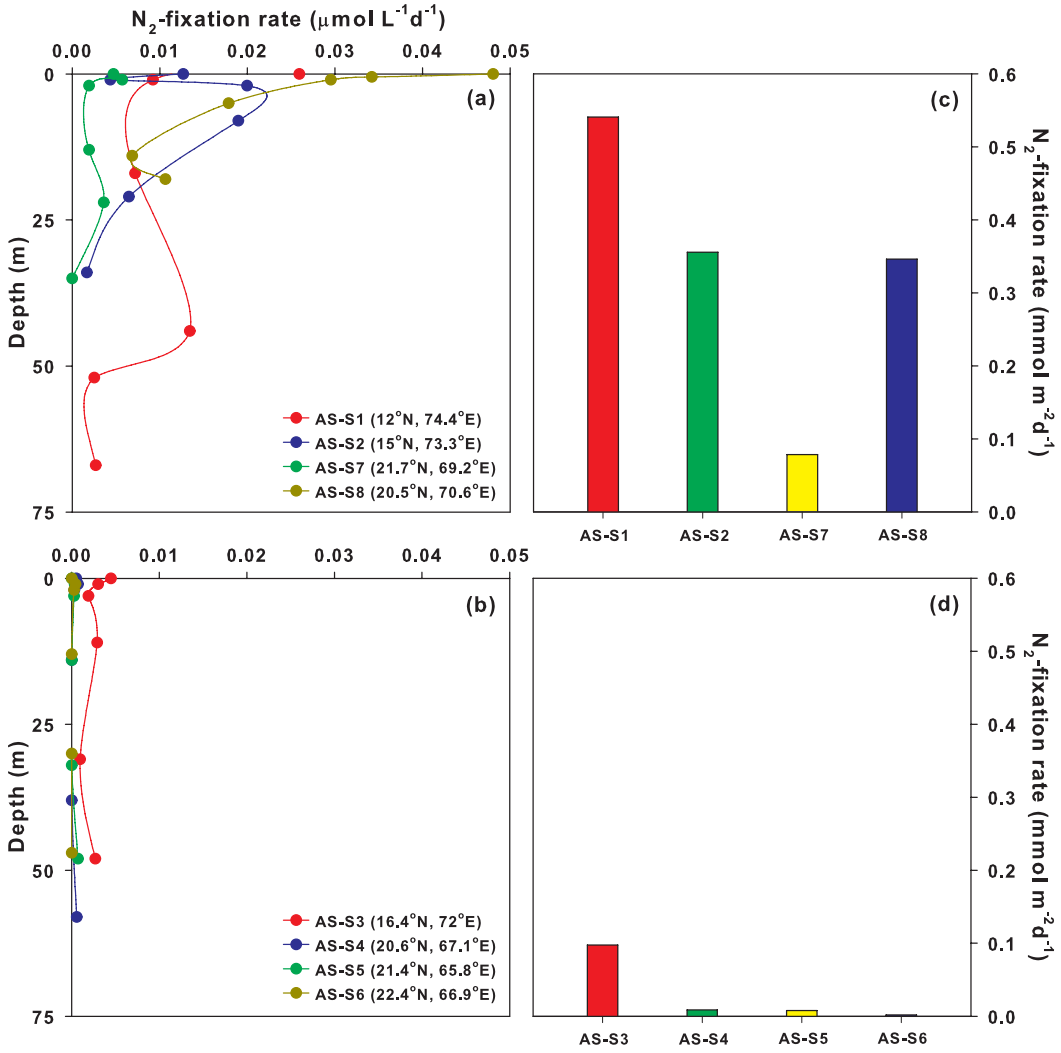

Figure 3.10: *Depth profiles of estimated N_2-fixation rate (left) and their euphotic-depth-integrated values (right) at different (a and c) coastal and (b and d) open ocean locations in the NE-AS during spring.*

Although the surface abundance of *Trichodesmium* at station AS-S8 is nearly

4 times than that at AS-S1, N_2-fixation is more at the latter. The integrated N_2-fixation rate depends on the abundance of *Trichodesmium* cells as well as the ED for which the integration is done. As *Trichodesmium* are in bloom at AS-S8, they limit the penetration of light and hence reduce the ED at the location. Therefore, the estimate of N_2-fixation is higher at station AS-S1 (ED = 67 m) than that at AS-S8 (ED = 18 m). An open ocean location (AS-S3) also shows a significant N_2-fixation rate.

3.4.2 Regenerated productivity

As mentioned in the earlier chapter, the sum of NH_4 and urea uptake rates is considered as regenerated productivity. Ambient NH_4 and urea concentrations are not measured, and for the calculation of regenerated production, it is assumed that the tracer added is the only source of nutrient for the plankton. Therefore, uptake rates given here are the conservative lower estimates for NH_4 and urea uptake.

NH_4 uptake rate

Depth profiles of NH_4 uptake rates at different sampling locations are given in Fig 3.11. Surface uptake rate of NH_4 at both open ocean as well as coastal locations shows very low values and remains between 0.001 and 0.006 μmol N $L^{-1}d^{-1}$ (with an average of 0.003 μmol N $L^{-1}d^{-1}$). These values are much lower than those observed for N_2-fixation rates. Nevertheless, these are comparable to NO_3 uptake rates. The highest surface NH_4 uptake is found at the location AS-S1, which also shows a higher surface N_2-fixation rate. A slight increasing trend with depth has been observed for NH_4 uptake within the MLD. At all the locations, the maximum NH_4 uptake rate is associated with the mid-depths. Euphotic-depth-integrated NH_4 uptake rates are shown in Fig 3.11. This decreases to the north in the coastal locations and varies from 0.07 to 0.39 mmol N $m^{-2}d^{-1}$ (with an average of 0.19 mmol N $m^{-2}d^{-1}$). No spatial trend is observed at the open ocean locations which show values from 0.08 to 0.13 mmol N $m^{-2}d^{-1}$ (with an average of 0.10 mmol N $m^{-2}d^{-1}$).

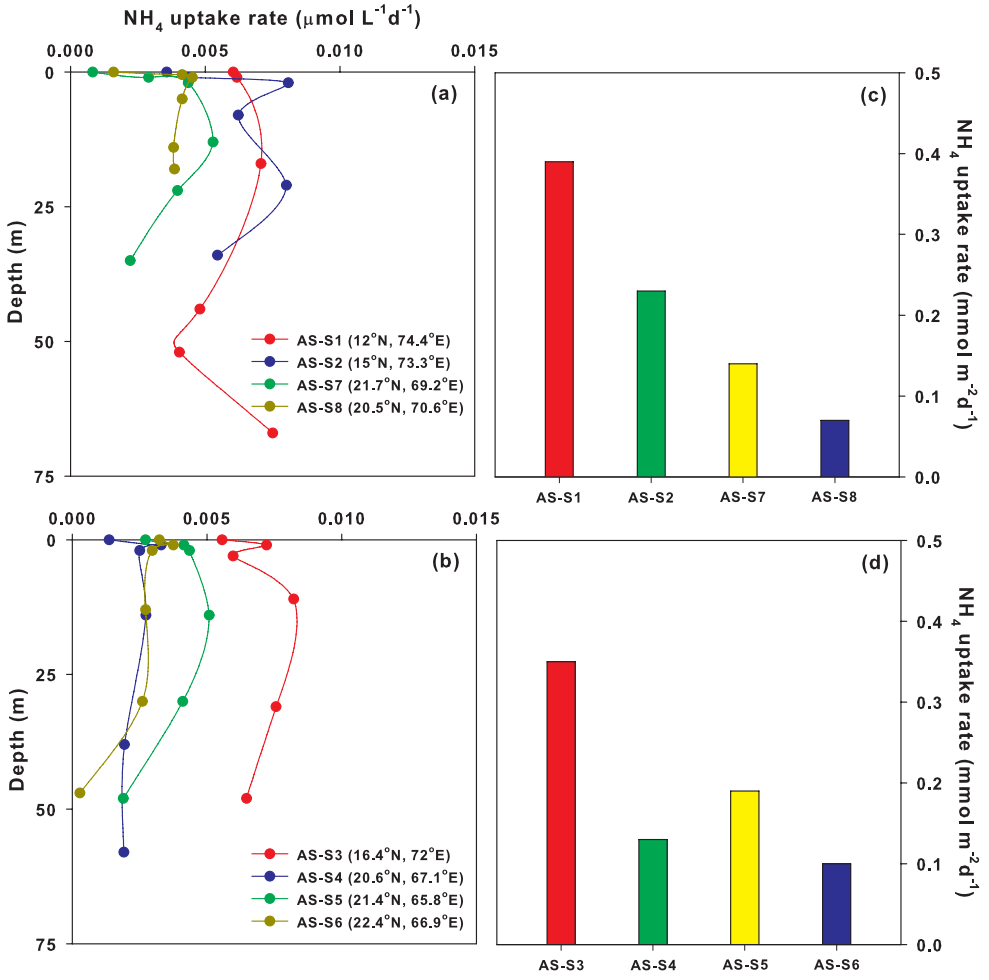

Figure 3.11: *Depth profiles of NH_4 uptake rate (left) and their euphotic-depth-integrated values (right) at different (a and c) coastal and (b and d) open ocean locations in the NE-AS during spring.*

Unlike the NO_3 uptake rates, the uptake rates of NH_4 at the coastal locations are almost twice as high as that at open ocean locations. Overall, NH_4 uptake rates are almost 3 times lower than the NO_3 uptake. N_2-fixation is also twice of the NH_4 uptake at the coastal locations. As in the case of NO_3 uptake, the lowest NH_4 uptake was observed at AS-S8, at which the highest abundance of *Trichodesmium* was observed. The average NH_4 uptake reported here is less than the average NH_4 assimilation rate of 3.7 mmolN $m^{-2}d^{-1}$ reported by *Watts and Owens* (1999) during inter-monsoon at the north-western AS. The values are also lower than

those reported by *Kumar et al* (2010) and *Prakash et al* (2008) in winter at the same region.

Urea uptake rate

Depth profiles of urea uptake rates at different sampling locations are shown in Fig 3.12.

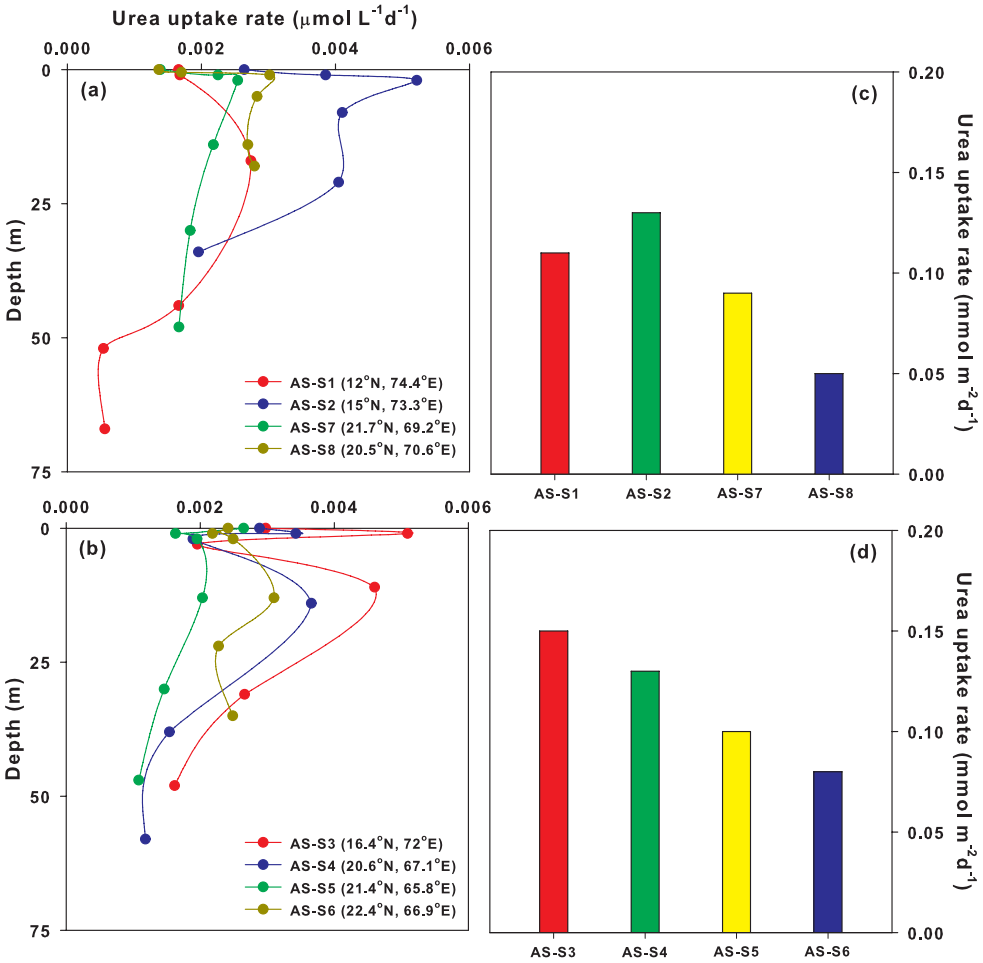

Figure 3.12: *Depth profiles of urea uptake rate (left) and their euphotic-depth-integrated values (right) at different (a and c) coastal and (b and d) open ocean locations in the NE-AS during spring.*

Surface uptake rate of urea at both open ocean as well as coastal locations show very low values and variation. Surface urea uptake varies from 0.001 to 0.003, much lower than that observed for other nitrogenous compounds (NO_3, NH_4, and N_2).

The highest value is found at AS-S3. Like in case of NH_4 uptake, a slight increasing trend with depth is observed for urea uptake within the MLD and the maximum rate is associated with the mid-depths. This indicates that plankton community responds similarly to NH_4 and urea availability with a slightly higher preference for the former. Euphotic-depth-integrated urea uptake rates vary from 0.05 to 0.15 mmol N $m^{-2}d^{-1}$ (with an average of 0.11 mmol N $m^{-2}d^{-1}$) and 0.08 to 0.13 mmol N $m^{-2}d^{-1}$ (with an average of 0.10 mmol N $m^{-2}d^{-1}$) for coastal and open ocean stations, respectively. Here, south-north decreasing trend is observed at the open ocean locations (Fig 3.11). Among all, urea is found to be the least preferred nitrogen substrate by phytoplankton. Similar to NO_3 uptake rate, the lowest (euphotic depth) NH_4 and urea uptake rates are also found at AS-S8. Regenerated productivity (the sum of NH_4 and urea uptake rates) integrated over the euphotic depth, ranges from 0.12 to 0.51 mmol N $m^{-2}d^{-1}$. The highest rate is found at station AS-S1 and the lowest at AS-S8 (both coastal locations). It varies from 0.12 to 0.51 mmol N $m^{-2}d^{-1}$ (with an average of 0.31 mmol N $m^{-2}d^{-1}$) and 0.19 to 0.50 mmol N $m^{-2}d^{-1}$ (with an average of 0.31 mmol N $m^{-2}d^{-1}$) at coastal and open ocean locations, respectively. Unlike new productivity, no difference is observed in the average regenerated productivity between coastal and open ocean locations.

3.4.3 *f*-ratio

f-ratios integrated over the euphotic zone range from 0.52 to 0.71 (with an average of 0.65) and 0.67 to 0.82 (with an average of 0.74) at coastal and open ocean locations, respectively. It shows that average f-ratio at open ocean is 14% higher than that at coastal locations. Inclusion of N_2-fixation related to the *Trichodesmium* significantly changed (increased) the f- ratio in the coastal stations as *Trichodesmium* was more abundant there. Including N_2-fixation, f- ratios range from 0.69 to 0.83 (with an average of 0.76) at coastal locations. The average value of f-ratio increases by $\sim$18% at the coastal locations. However, inclusion of N_2-fixation does not make a significant impact on the f-ratios at open ocean stations where *Tri-*

chodesmium is not as abundant. Including N_2-fixation, f-ratios range from 0.69 to 0.82 (with an average of 0.75) at open ocean locations. An important highlight is that f-ratios at coastal and open ocean locations become equal after the inclusion of N_2-fixation. It shows the importance of N_2-fixation for the estimation of new productivity and f-ratios during spring in this region.

Nitrate uptake rates are higher below the mixed layer (Fig 3.9), where NO_3 and Chl *a* concentrations are also higher (Figs 3.5 and 3.8). However, N_2-fixation is confined to the mixed layer (Fig 3.10) where most *Trichodesmium* is found (Fig 3.7). The above observations suggest that in the surface layers N_2-fixation, and below the mixed layer, NO_3 uptake, dominate the new production, at least in the coastal region. *Sambrotto* (2001) reported f-ratios <0.2 for the north-western AS during spring, lower than those presented here. *McCarthy et al* (1999) also reported lower f-ratios (<0.2) for the Oman coast and 0.13 to 0.29 for the central AS. The f-ratios reported here are based on the conservative estimates of regenerated productivity. In addition, the mentioned studies were not carried out in bloom conditions as ours. These could explain a part of the difference between the present and other studies but not the whole as the ambient concentration of NH_4 generally remains low in the NE-AS but it could increase during blooms (*Wafar et al.*, 1986). Therefore, the present study along with the previous results indicate a large spatial variation in the preferred nitrogenous nutrient between the north-western, central and NE-AS.

3.5 δ^{15}N of surface natural PON

The isotopic composition of nitrogen (δ^{15}N) of natural particulate organic nitrogen (PON) are shown in Fig 3.13. A large variation is observed in the δ^{15}N of surface PON, range from 2.5 to 11.4‰. *Trichodesmium* fixes nitrogen of an isotopic composition (∼0‰) close to that of atmospheric N_2 (*Brandes et al.*, 1998), thus, it has the lowest δ^{15}N among the marine phytoplankton. δ^{15}N of PON varies with the abundance of *Trichodesmium* in the surface waters and its minimum value is

found at station AS-S8 (*Trichodesmium* bloom station).

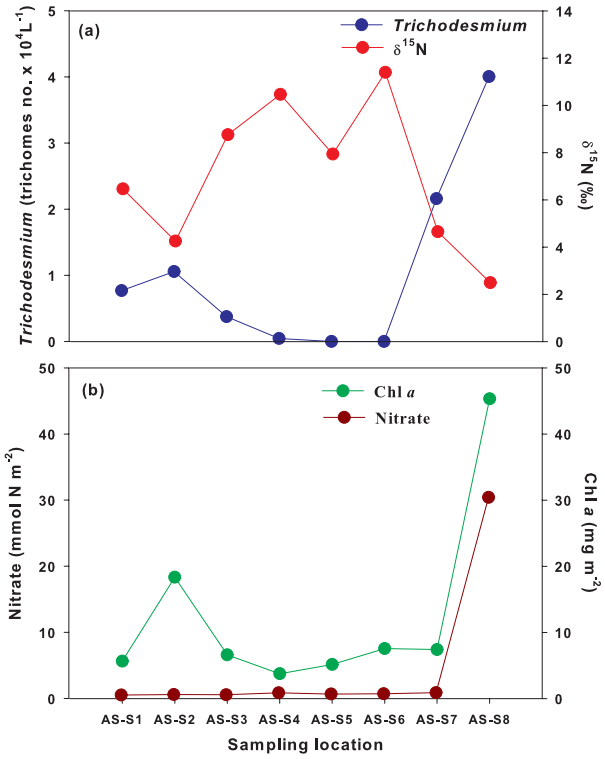

Figure 3.13: *Variation of (a) $\delta^{15}N$ and Trichodesmium and (b) chlorophyll and column NO_3 at different sampling locations in the NE-AS during SIM.*

δ^{15}N of PON in the coastal water ranges from 2.5 to 7.4‰(average 5.1‰); whereas in the open ocean, it ranges from 5.5 to 11.4‰(average 8.0‰). The difference in δ^{15}N of PON between coastal and open ocean is mainly because of the difference in the abundance of *Trichodesmium*: *Trichodesmium* is found to be an order of magnitude more abundant in the coastal region (an average of 1387 trichomes L^{-1}) than in the open ocean (an average of 134 trichomes L^{-1}).

3.6 Input of nitrogen by *Trichodesmium*

3.6.1 Approach 1: Based on δ^{15}N of surface natural PON

Capone et al (1998) used a simple mass balance equation to estimate the contribution of recently fixed nitrogen to the surface pool of suspended particles as well as

to the sinking organic matter collected by sediment traps. They used the nitrogen isotopic composition of natural surface PON in their calculation. They assumed the nitrogen isotopic compositions of *Trichodesmium* (δ^{15}N = 0‰by definition) and NO_3 below mixed layer (δ^{15}N = 10‰). Using a similar approach, our isotopic data suggest that the recently fixed nitrogen contributes to as high as ∼79 % of the nitrogen in surface PON The total surface area covered by blooms is more than 20% of the area of the AS (*Capone et al.*, 1998) and their persistence is for more than 30% of the time (*Westberry and Siegel*, 2006); the estimated N_2-fixation rates can be used to extrapolate the nitrogen input by *Trichodesmium* blooms for the Arabian Sea. Taking these data at face value, the estimated annual nitrogen gain for the region by such blooms is ∼0.9 Tg N in good agreement with that reported by *Capone et al* (1998) (∼1 Tg N yr^{-1}).

3.6.2 Approach 2: Based on higher NO_3 associated with *Trichodesmium* bloom

Trichodesmium is generally abundant in the low NO_3 waters (*Capone et al.*, 1997). However, at station AS-S8, *Trichodesmium* is detected with higher concentrations of NO_3 (Figs 3.13). Fig 3.13 shows the δ^{15}N of natural surface PON and *Trichodesmium* abundance (upper panel) along with the mixed layer depth-integrated NO_3 and Chl *a* (lower panel) at different stations. The lowest δ^{15}N of PON coincides with the highest *Trichodesmium* abundance in the surface at station AS-S8, a clear indication of the dominance of *Trichodesmium* in the total phytoplankton population. Further, the highest mixed-layer-integrated Chl *a* is also observed here showing the intensity of *Trichodesmium* bloom. Similar abundance of *Trichodesmium* bloom was observed by *Capone et al* (1998) in the central AS with very low concentrations of NO_3 in the water column. *Devassy et al* (1978) also observed development of such blooms is a low NO_3 environment. However, we have observed a significantly higher concentration of NO_3 in the mixed layer at station AS-S8. Atmospheric deposition, river discharge, upwelling/deep mixing, or

nitrification of NH_4 released by *Trichodesmium* (*Montoya and Voss*, 2006) could be considered as the possible sources of the observed NO_3 at station AS-S8.
No simultaneous observations are available for the atmospheric deposition during the study period. However, any atmospheric contribution should be observable over a wider region; but no other station, not even the nearby AS-S7, showed a measurable concentration of NO_3 at the surface. This indicates that the contribution of atmospheric aerosols is minor to the observed NO_3 at AS-S8. There are some rivers e.g. Mahi, Narmada and Tapi (major rivers; annual mean discharge >300 m^3s^{-1}), Sabarmati (smaller river; annual mean discharge <50 m^3s^{-1}) that debouch into the region (Fig. 1). However, all the rivers have very low discharge, <5% of the SW monsoon discharge, during April (source: *www.grdc.sr.unh.edu*). Further, river water (salinity 0 psu) lowers the salinity of sea water. However, no such signature was observed at AS-S8. Salinity was high (>35.5 psu; Table 1) at AS-S8 and was similar to the nearby stations. It is also known that significant amounts of nutrients are removed during the passage of the river through the estuarine ecosystem. Therefore, the contribution of NO_3 from river discharge is likely to be negligible. It is possible that a short term upwelling had occurred in the area before the sampling time. Winds were also not high during the period (Table 3.1). To the best of our knowledge neither a cyclone passed through the area nor any rough sea condition was reported from the region just before and during sampling. Furthermore, no earlier evidence is available for upwelling/deep mixing in the region during this time of the year. Therefore, nitrification of the released NH_4 could be the most likely source of the observed higher concentration of NO_3 at the station AS-S8. *Devassy et al* (1978) also reported a progressive accumulation of dissolved inorganic nitrogen with increase in *Trichodesmium* abundance in surface water during 1975 and 1977. If *Trichodesmium* is indeed the source of the observed NO_3, it can be termed as new nitrogen input to the water column. This input is scaled to 30 mmol N m^{-2} after normalizing with the column NO_3 of the nearest station AS-S7. Higher *Trichodesmium* was observed at other stations as

well e.g. stations AS-S1, AS-S2 and AS-S3 but such accumulation of NO_3 was not observed at these stations. Therefore, it is suggested that this preliminary evidence significant new nitrogen addition must be verified by future measurements; similar measurements, along with direct measurements of N_2-fixation.

3.7 Part I: Conclusion

Low wind strength, shallow MLD, and low mixed layer NO_3 during spring result in low productivity in the NE-AS. Both the open ocean and coastal stations show very low NO_3, NH_4 and urea uptake rates, due possibly to the strong stratification and low ambient nutrient concentrations. This is also evidenced by low chlorophyll values seen in the chlorophyll image obtained from SeaWiFS weekly 9-km data (source: *http://reason.gsfc.nasa.gov/OPS/Giovanni/ocean.swf8D.shtml*) corresponding to the measurement period. During spring, the NE-AS is found to be well stratified and most of the NO_3 uptake takes place below the mixed layer. Nitrate is the most preferred nitrogenous nutrient during spring, followed by NH_4 and urea (Figs 3.9, 3.11, and 3.12). Urea is the least preferred nitrogenous nutrient. Inclusion of N_2-fixation associated with *Trichodesmium* significantly changes (increases) the f-ratio, particularly in the coastal stations, whereas NO_3 uptake and N_2-fixation are the dominant factors of new production below the mixed layer and surface layers, respectively. The lowest $\delta^{15}N$ of surface PON coincides with the highest *Trichodesmium* abundance at surface, confirming that *Trichodesmium* fixes atmospheric N_2 ($\delta^{15}N = 0$) and adds new nitrogen to the ocean. $\delta^{15}N$ of surface PON suggests that the recently fixed nitrogen contributes to as high as $\sim$79 % to the nitrogen in the surface suspended organic matters. An annual input of nitrogen from the growth of *Trichodesmium* is $\sim$0.9 Tg N, calculated using the estimated N_2-fixation rate, and the possible areal extent of such blooms and their persistence. This estimate is comparable to that earlier reported from the region; however, direct determination of N_2-fixation rates are needed to obtain a more reliable estimate. Higher NO_3 observed during *Trichodesmium* bloom could be as

much as 30 mmol N m^{-2}. The f-ratios presented here are higher than that of reported for the north-western AS (<0.2; *Sambrotto*, 2001), for the Oman coast (<0.2; McCarthy et al., 1999), and for the central AS (0.13 to 0.29; McCarthy et al., 1999) for the same season. Therefore, based on present results and the values reported by *Watts and Owens* (1999) and *Sambrotto* (2001) it can be concluded that the different parts of the AS show different new productivity and f-ratios during spring. The difference is could be due to the bloom and non-bloom conditions and/or due to the difference in plankton community in different parts of the AS.

3.8 Part II: Sampling in the NE-AS (late winter 2007)

3.9 Environmental conditions

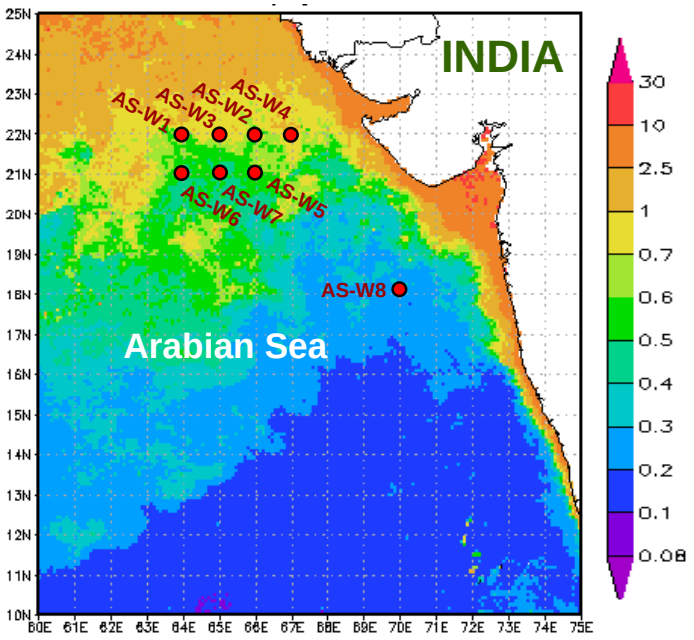

Figure 3.14: *Composite SeaWiFS Chlorophyll image for 26 Feb-21 Mar, 2007 (source: http://reason.gsfc.nasa.gov/OPS/Giovanni/ocean.swf8D.shtml) corresponding to cruise in the NE-AS during late winter with superimposed station locations.*

Earlier measurements of carbon and nitrogen uptake rates were carried out during the early and middle phases of winter in the NE-AS (*Madhupratap et al.*, 1996; *Prakash et al.*, 2008; *Kumar et al.*, 2010). The present study aims to carry out the first simultaneous measurements of carbon and nitrogen uptake rates in the NE-AS. Sampling is done mainly along two latitudinal transects (21^{o}N and 22^{o}N). One station is chosen south of these (AS-W8) to detect spatial variation, if any in the uptake rates (Fig 3.14).

Dry and cool northeasterly trade winds intensify evaporation and cool the sea surface, triggering the sinking and convective mixing of surface water. This mixing leads to the deepening of the mixed layer and an upward transport of nutrients into the surface waters, leading to winter blooms (*Madhupratap et al.*, 1996). Such blooms are also observed in chlorophyll images captured by satellites sensors. Satellite based studies reveal that the winter bloom in the region generally appears by the end of February and disappears by the end of March every year (e.g., *Dwivedi et al.*, 2006).

Table 3.2: *Station codes, locations of the stations, sea surface temperature (^{o}C; SST), surface salinity (psu), mixed layer depth (m; MLD), euphotic depth (m; ED), PAR (μmol $m^{-2}s^{-1}$) and wind speed (ms^{-1}; V_w) in the NE-AS during late winter (Mar, 2007).*

Station Code	Lat (^{o}N)	Lon (^{o}E)	SST	Salinity	MLD	ED	PAR	V_w
AS-W1	22	64.0	25.9	36.1	50	51	1699	1.1
AS-W2	22	66.0	25.7	35.9	43	48	1719	2.4
AS-W3	22	65.0	25.7	36.1	34	45	1731	5.5
AS-W4	22	67.0	25.6	35.9	23	45	1826	4.8
AS-W5	21.0	67.0	25.5	36.0	39	74	1690	6.2
AS-W6	21.0	65.0	26.0	36.0	40	85	1653	9.0
AS-W7	21.0	66.0	25.8	36.1	39	48	1844	3.3
AS-W8	18.1	70.0	27.9	35.6	72	108	1782	4.6

The sampling is done during late winter to check the persistence of winter cooling effect till this period. The wind speed is not as high as reported for early winter

in the previous studies (*Madhupratap et al.*, 1996; *Prasanna Kumar and Narvekar.*, 2005), it varies between 1.1 and 9.0 ms^{-1} (with an average of 4.6 ms^{-1}). Dense patches of phytoplankton blooms are seen in the study area, also evidenced by high chlorophyll in the SeaWiFS Level-3 Version 4 weekly 9-km image (source: *http://reason.gsfc.nasa.gov/OPS/Giovanni/ocean.swf8D.shtml*) corresponding to the cruise period (Fig 3.14). The blooms are found to be limited to the north. Clear sky conditions are observed in the region with intense sunlight, PAR varies from 1653 to 1844 μmol $m^{-2}s^{-1}$ during the study period.

Due to winter mixing, MLD deepens to as much as 120 m (*Madhupratap et al.*, 1996; *Prasanna Kumar and Narvekar*, 2005; *Prakash et al.*, 2008; Kumar et al., 2010) during early winter. However, subsequently as the winter cooling weakens, the mixed layer starts shoaling. This puts the system back again towards stratification, as confirmed by in the present study; temperature based MLD values varied from 23 to 50 m (with an average of 38 m) in the northern locations (Table 3.2), an indicator of weakening of winter mixing effect. However, the MLD at the southernmost station (AS-W8) was 72 m. Generally, euphotic depth (ED) is found to be deeper than the MLD at all the stations, it varies from 45 to 75 m (with an average of 57 m) at the northern stations and reaches as high a value as 108 m at the southernmost station (AS-W8). Interestingly, the ED is deeper at 21^{o}N than at 22^{o}N, it varies from 48 to 85 m (with an average of 69 m) at 21^{o}N and from 45 to 51 m (with an average of 47 m) at 22^{o}N. The difference could be due to the higher chlorophyll content at the latter, which absorbs solar radiation and hence reduces the ED. The SeaWiFS chlorophyll image shows that the stations at 22^{o}N contain higher chlorophyll (Fig 3.14), supporting the above inference.

3.9.1 Temperature and salinity

Surface salinity and temperature at the different stations in the north show no significant variation (Table 3.2). They are limited to 0.3 ^{o}C and 0.2 psu, respectively. Depth profiles of temperature are shown in Fig 3.15. Although winter mixing

started weakening during the study period, significant undulations are observed in the depth profiles of temperature and salinity to varying degrees. Undulations in the temperature profiles are more at 21^{o}N than at 22^{o}N. Depth profiles of salinity are shown in Fig 3.16. Salinity profiles show more undulations than temperature profiles. The undulations in salinity and temperature indicate mixing but not as prominent as reported for the early winter (e.g., *Prasanna Kumar and Narvekar*, 2005).

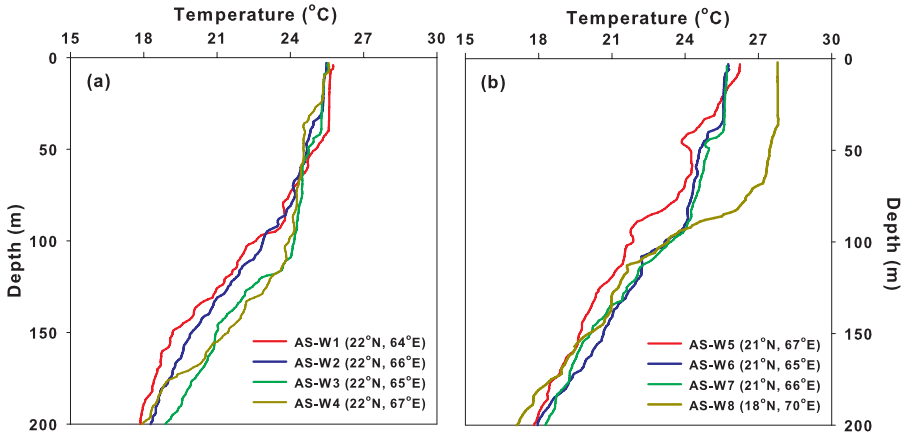

Figure 3.15: *Dept profiles of temperature along (a) 22^{o}N and (b) 21^{o}N latitudes in the NE-AS during late winter. Note: AS-W8 is at the 18^{o}N.*

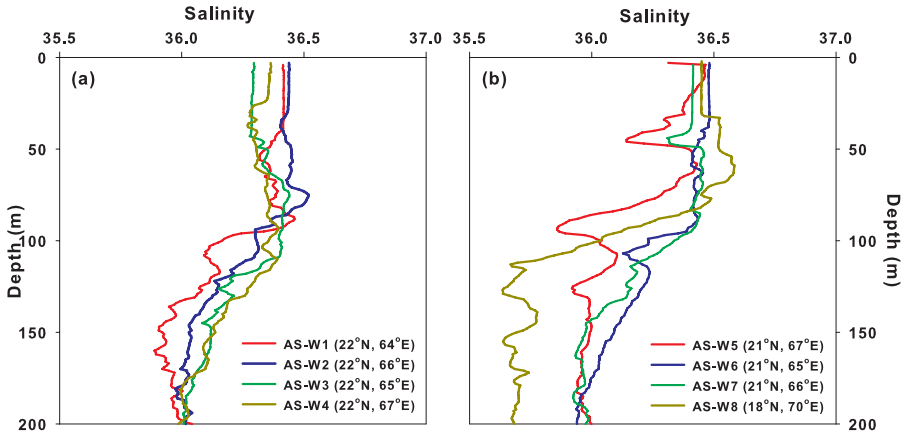

Figure 3.16: *Depth profiles of salinity along (a) 22^{o}N and (b) 21^{o}N latitudes in the NE-AS during late winter. Note: AS-W8 is at the 18^{o}N.*

The southernmost station shows higher sea surface temperature (SST) and lower surface salinity than those observed at the northern locations (Figs 3.15 and

3.16). Large fresh water discharge by major rivers result in the low salinity of the BOB surface waters (*Prasanna Kumar et al.*, 2002). The winter monsoon current, which flows from the BOB to the western AS during winter (*Shankar et al.*, 2002), could be responsible for the low salinity at the AS-W8 location.

3.9.2 Nutrients

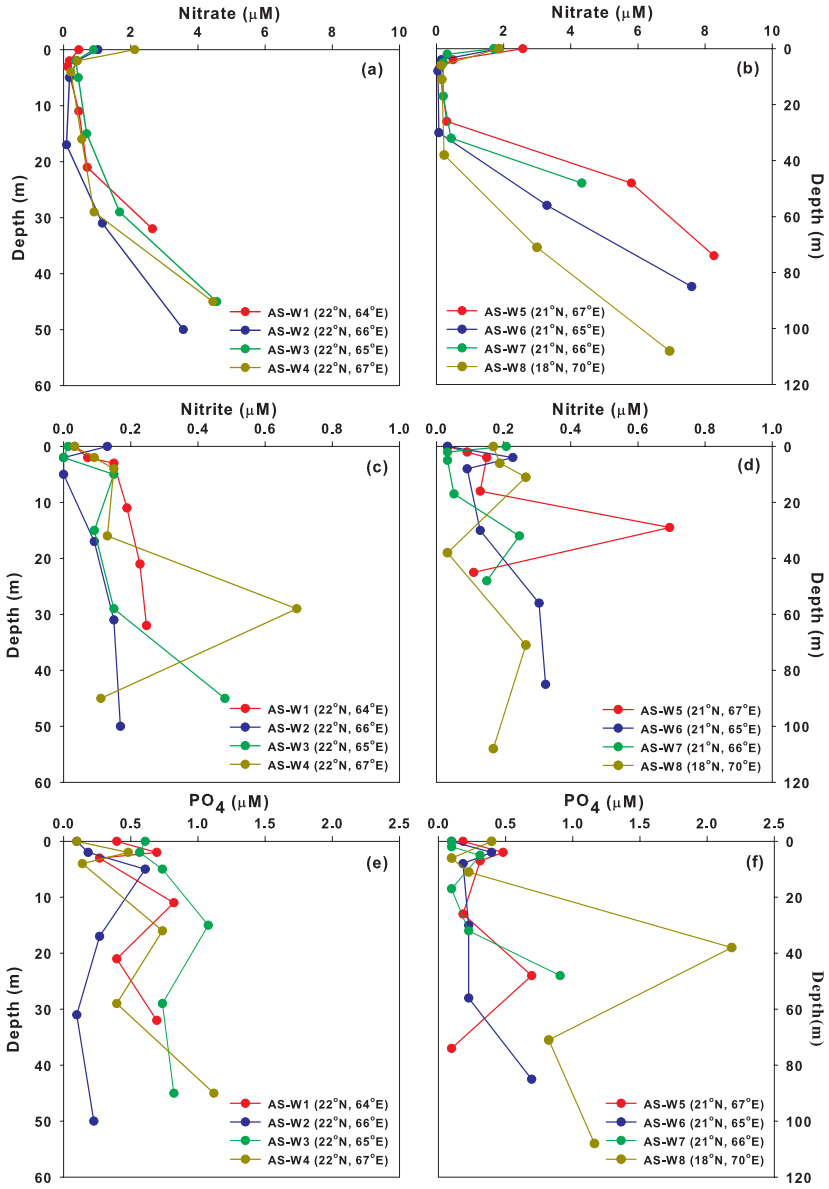

Figure 3.17: *Depth profiles of different nutrients: (a and b) NO_3, (c and d) NO_2, and (e and f) PO_4 along the (left) 22°N and (right) 21°N latitudinal locations in the NE-AS during late winter.*

In the northern region, surface NO_3 concentrations are higher. It varies from 0.5 to 2.6 μM (Fig 3.17). Nitrate concentration decreases in the sub-surface layers and the lowest values are found in the mid-depths (Fig 3.17). No significant variation is observed for surface values between 21^{o}N and 22^{o}N. However, surface NO_3 values are higher towards the east at both the latitudes (Fig 3.17). The southernmost station (AS-W8) also shows higher NO_3 concentration throughout the euphotic zone. Nitrite (NO_2) is almost ten times lower than NO_3. Surface NO_2 concentrations are slightly higher at 21^{o}N than at 22^{o}N. Unlike NO_3, no regular pattern is observed for NO_2 with depth (Fig 3.17). No latitudinal variation is observed in PO_4, its surface values are generally lower than 0.5 μM (Fig 3.17). Unlike NO_3 and NO_2, the sub-surface PO_4 concentration at AS-W8 is higher than at northern locations. As in case of NO_2, no regular pattern is observed for PO_4 concentration with depth.

3.9.3 Dissolved oxygen

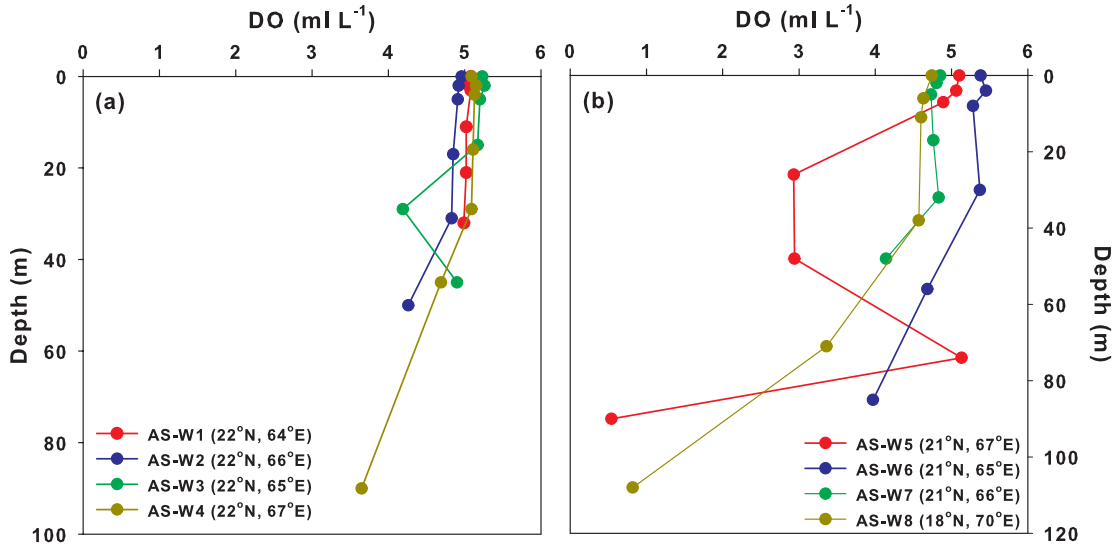

Figure 3.18: *Depth profiles of dissolved oxygen along (a) 22^{o}N and (b) 21^{o}N latitudes in the NE-AS during late winter.*

Fig 3.18 presents the depth profiles of dissolved oxygen (DO) at different locations: It varies from 4.8 to 5.4 ml L^{-1} (Fig 3.17) in the surface. The highest value is

found at AS-W6, and the lowest, at AS-W8. No significant variation is observed in DO in the upper 30 m, except at AS-W5, where a sharp decline is seen (Fig 3.18b); this coincides with an abrupt increase in nitrite concentration (Fig 3.17d). This indicates the shoaling of oxygen-poor water, which carries higher nitrite due to mixing at the location. Mid-depth oxygen deficiency in the Arabian Sea is perhaps the most severe observed anywhere in the world oceans (*Naqvi*, 1987). Our observation suggests that winter mixing signature persists till mid-March despite the weakening of winter cooling. Overall, not much difference has been observed in DO between the northern and the southern locations.

3.9.4 Chlorophyll

Surface chlorophyll *a* (chl *a*) is different along both the latitudes (Fig 3.19). The highest surface chl *a* (>0.5 mg m^{-3}) is found at AS-W2 and AS-W4 along 22^{o}N.

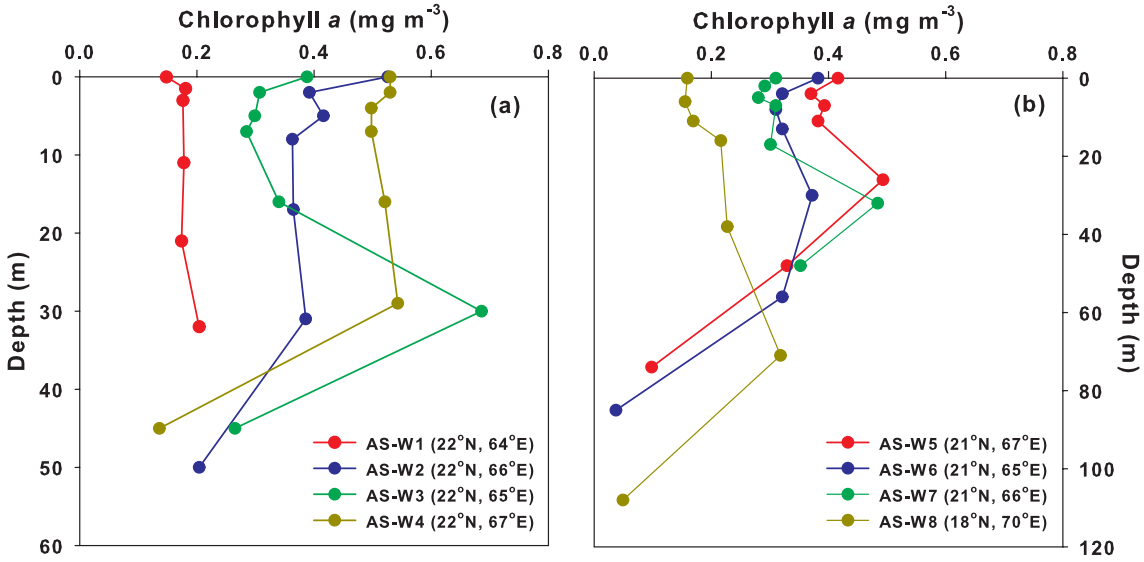

Figure 3.19: *Depth profiles of Chlorophyll along (a) 22^{o}N and (b) 21^{o}N latitudes in the NE-AS during late winter.*

In the northern region, the lowest surface chl *a* is observed at AS-W1, which is comparable that observed at the southernmost location (AS-W8). A similar pattern can also be seen in the SeaWiFS chlorophyll image (Fig 3.14). The Deep

Chlorophyll Maximum (DCM) is located at 30 m depth along 21^{o}N, while it is slightly shallower at 22^{o}N. It has been suggested that winter mixing (*Madhupratap et al.*, 1996) and higher chlorophyll are mostly found in the northern AS (*Banse and McClain* 1986), as confirmed by our study. In general, winter blooms form in late Jan and persist until mid March north of 20^{o}N in the AS, where winter convective mixing is the strongest (*Madhupratap et al.*, 1996).

3.9.5 Phytoplankton

Phytoplankton cell data are obtained from Dr. Prabhu Matondkar from NIO, Goa. Total phytoplankton, diatoms, and *Noctiluca* cell counts (cell L^{-1}) are shown in Fig 3.20. Total plankton cell counts vary from 200 cells L^{-1} to 9520 cells L^{-1}. At 22^{o}N, the average cell counts are 4000 cells L^{-1}, whereas, at 21^{o}N it is 1200 cells L^{-1}. This is in tune with the measured chl *a* (Fig 3.19) and SeaWiFS chlorophyll images (Fig 3.14). The highest cell concentration is observed at AS-W3, while it is the lowest at the southernmost location (AS-W8) (Fig 3.20). The presence of diatoms, dinoflagellate and *Noctiluca miliaris* is observed at all the locations in varying proportions.

Overall, diatoms dominate the plankton population in the region (more than 60%) and the species are *Rhizosolenia alata*, *Navicula hyalina*, and *Leptocylindrus mediterranian*. *Prorocentrum minimus*, *Oxytoxum scolopax*; *Gyrodinium spirale* is the dominant dinoflagellate species. *Madupratap et al* (1996) also reported the dominance of diatoms here during winter. However, at two locations (AS-W2 and AS-W4), *Noctiluca miliaris* dominates over other plankton (more than 80% in surface at AS-W4). It has been proposed that the plankton community is shifting from diatoms to *Noctiluca miliaris*-dominant community in the region (*Gomes et al.*, 2008). Mesoscale eddy activity in the western Arabian Sea has been linked to the appearance of *Noctiluca miliaris* blooms in the Gulf of Oman, and the western Arabian Sea.

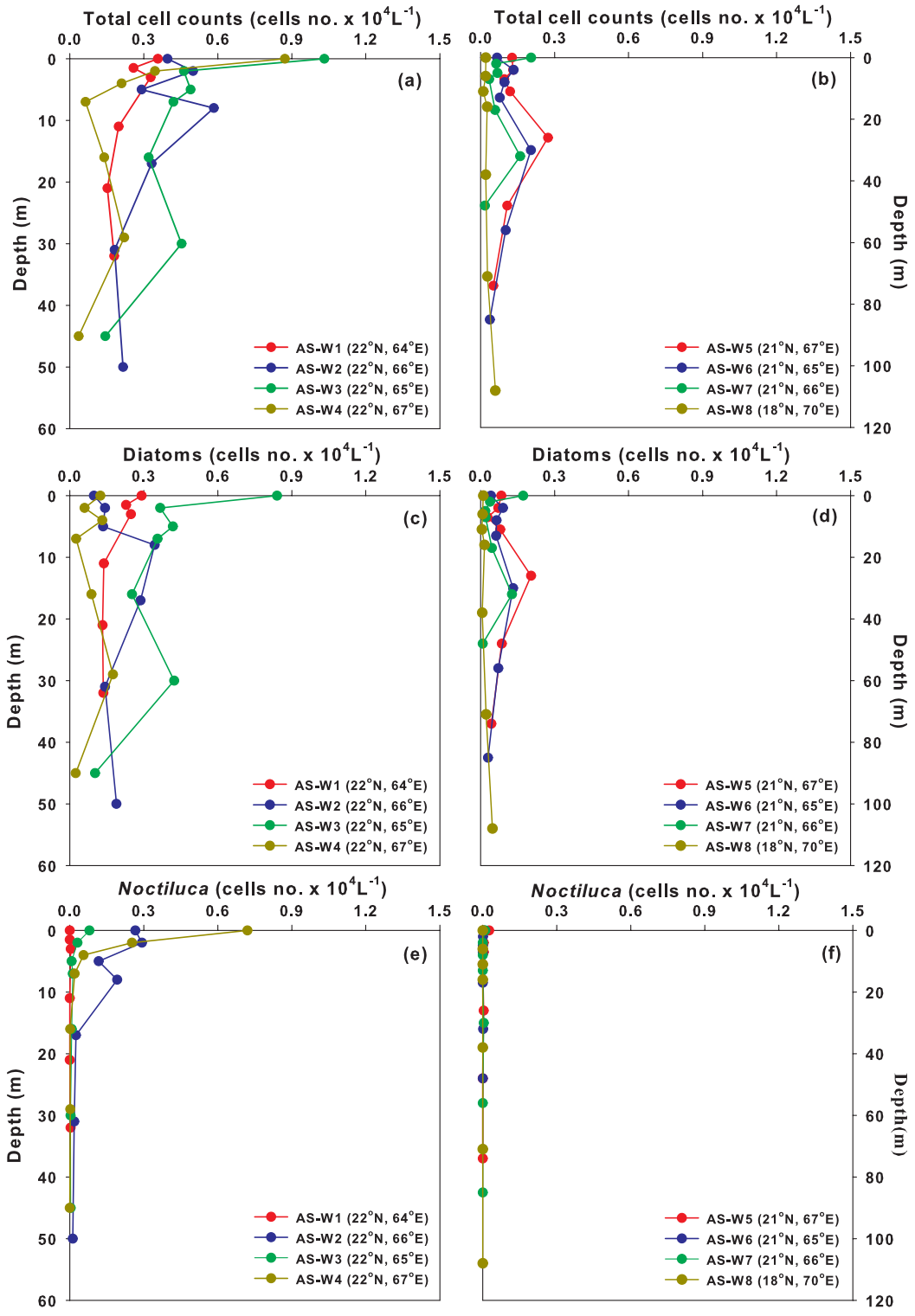

Figure 3.20: *Depth profiles of (a and b) total phytoplankton, (c and d) diatoms, and (e and f) Noctiluca miliaris cells counts along the (left) 22°N and (right) 21°N latitudinal locations in the NE-AS during late winter.*

Gomes et al (2008) suggest that winter blooms are initiated in the Gulf of Oman via a cold-core eddy, which brings nutrients and oxygen-poor subsurface waters (depth 100-300 m) to the surface, facilitates the genesis and evolution of *Noctiluca miliaris* blooms. However, in the present study, higher *Noctiluca miliaris* abundance is observed at AS-W2 and AS-W4, at which DO and nitrate concentrations are found to be similar to that at other locations. Indian JGOFS studies were concentrated on the 65^{o}E transect in the eastern Arabian Sea. JGOFS studies concluded that the region is diatom-dominated, also confirmed by the present study. *Noctiluca miliaris* is limited to the west of 65^{o}E and the northern region. *Noctiluca miliaris* blooms have been observed in the north-western Arabian Sea near the Gulf of Oman as fa back as 1962 by *Dugdale et al* (1964). This suggests the north-western Arabian Sea is known to be dominated by *Noctiluca miliaris* blooms while the eastern AS is dominated by diatoms. Therefore, it is too early, on the basis of limited observations, to infer a community shift in this region.

3.10 Carbon and Nitrogen uptake rates

Productivity measurements are made at 8 different stations as shown in Fig 3.14. At all the eight locations total primary productivity measurements are measured (using ^{13}C-labelled tracer). At seven locations (AS-W1 to AS-W7), new and regenerated productivity measurements are carried out (using ^{15}N-labelled tracer).

3.10.1 Carbon uptake rates

Depth profiles of carbon uptake rates at different sampling locations are shown in Figs 3.21a and 3.21c. Carbon uptake rates vary from 0.08 to 0.64 μmol C L^{-1}d^{-1} in the surface. The highest surface productivity is observed at AS-W2, while it is the lowest at AS-W6, both being northern locations. The average surface productivity at 22^{o}N (0.37 μmol C L^{-1}d^{-1}) is a factor two higher than that at 21^{o}N (0.15 μmol C L^{-1}d^{-1}). The large difference in the surface productivity between the nearby latitudes can be explained with the help of chlorophyll image (Fig 3.14), which

shows higher biomass at 22^{o}N than that at 21^{o}N.

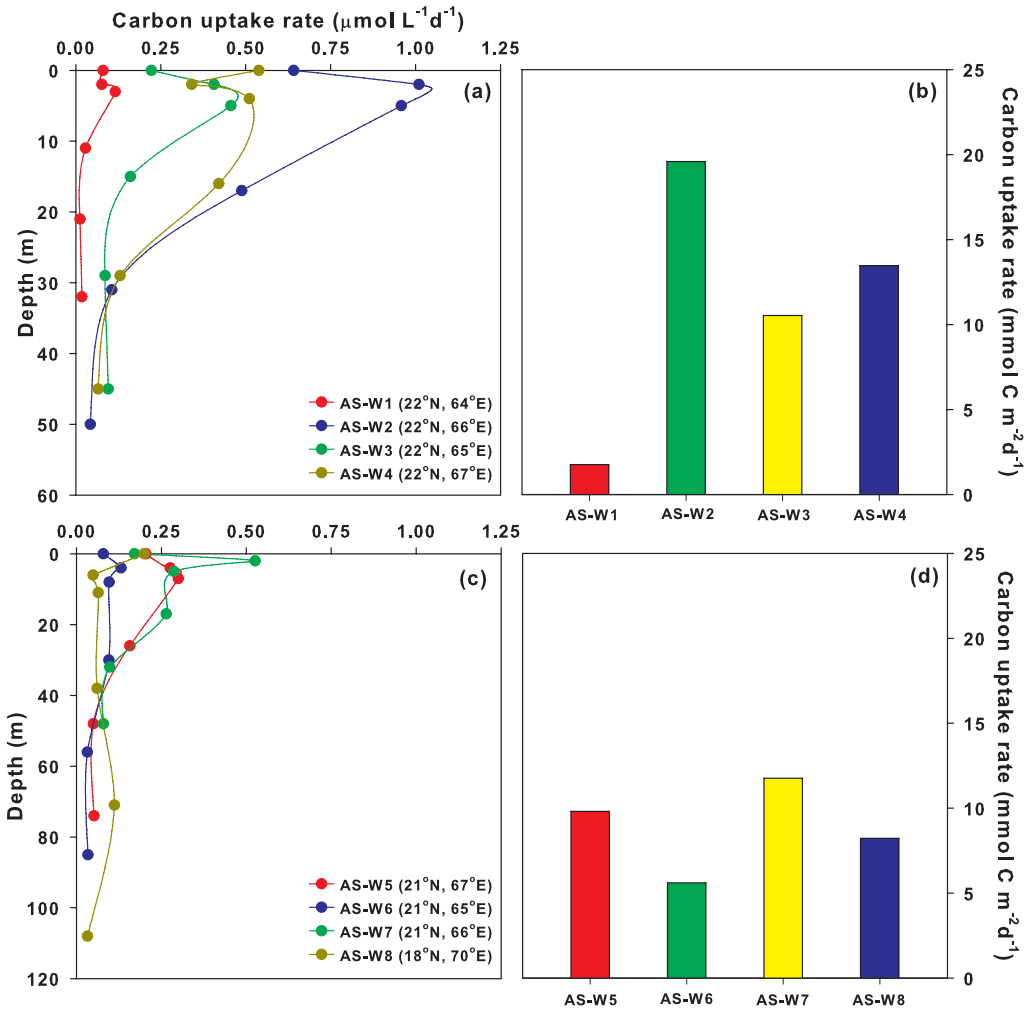

Figure 3.21: *Depth profiles of carbon uptake rate (left) and their euphotic-depth-integrated values (right) along the (a and c) 22^{o}N and (b and d) 21^{o}N latitudinal locations in the NE-AS during late winter.*

The southernmost location also shows very low surface productivity (∼0.1 μmol C L^{-1}d^{-1}), also evidenced by the chlorophyll image (Fig 3.14) and cell counts at the location (Fig 3.20c). One interesting observation is that at all the locations the highest productivity is found just below the surface (Figs 3.20a and 3.20c). This is in contrast to what is seen in the cell counts and nitrate values, which are higher at the surface than that at the sub-surface. Excess light intensity could be a reason for the lower surface productivity compared to the sub-surface. The role of light

intensity over the surface productivity is discussed in detail in the next section. Euphotic-depth-integrated carbon uptake rates are shown in Figs 3.21b and 3.21d. This varies from 1.76 to 19.59 mmol C $m^{-2}d^{-1}$, equivalently, 21.1 to 235.1 mg C $m^{-2}d^{-1}$ (with an average of 10.1 mmol C $m^{-2}d^{-1}$ or 121.2 mg C $m^{-2}d^{-1}$). The highest and the lowest productive locations are at 22^oN (Fig 3.21b). The average productivity at 22^oN, except at AS-W1, is found to be $\sim$14 mmol C $m^{-2}d^{-1}$. At 21^oN, the average productivity is lower ($\sim$10 mmol C $m^{-2}d^{-1}$) than that at 22^oN. Nutrients are found to be comparable at both the latitudes (Fig 3.17) and so is the light intensity. Therefore, the difference in productivity between these two latitudes could be due to the difference in plankton cell counts and chl *a*. Although plankton cells and chl *a* are low at AS-W8, the productivity at this location is found to be comparable to that observed at locations at 21^oN (Fig 3.21d). Lower plankton concentration in upper layers allows light to penetrate to the deeper layers (ED = 108 m at AS-W8) which enhances the overall integrated productivity here. *Madhupratap et al.* (1996) reported productivity between 335 and 807 mg C $m^{-2}d^{-1}$ during Feb 1995, more than thrice that observed in the present study (maximum of 235 mg C $m^{-2}d^{-1}$). Their measurements were mainly carried out during early February (peak of winter cooling), whereas, the present work was done during March (the waning phase of winter cooling). Inter-annual variations could also be a reason for the discrepancy. However, *Prakash and Ramesh* (2007) found no significant inter-annual variation in chlorophyll during 1997-2005 in the NE-AS. Productivity values reported by *Madhupratap et al.* (1996) are integrated from surface to 120 m depth, whereas the present values are integrated over the euphotic zone, which varies from 45 to 108 m. The difference in the depths to which the integration is done may also contribute to the discrepancy.

Effect of light intensity on productivity

An experiment was carried out at station AS-W8 to quantify the effect of solar intensity on surface productivity. Surface water was collected in six 1L polycar-

bonate bottles (Nalgene, USA) and a constant amount (∼0.2 mM) of $NaH^{13}CO_3$ tracer was added to all the six bottles. To vary the light intensity, six different neutral light density filters were used. Different bottles received different light intensities: 100, 80, 64, 20, 5 and 1% of the surface intensity (1782 μmol $m^{-2}s^{-1}$). Incubation was done on deck for 4 hours symmetrical to local noon. A continuous flow of seawater from 5 m depth was maintained to regulate the temperature. As in case of uptake rate measurements, samples were filtered and preserved for mass spectrometric analysis. Mass spectrometric analysis and the calculations (using equation 2.7) were done as explained in Chapter 2.

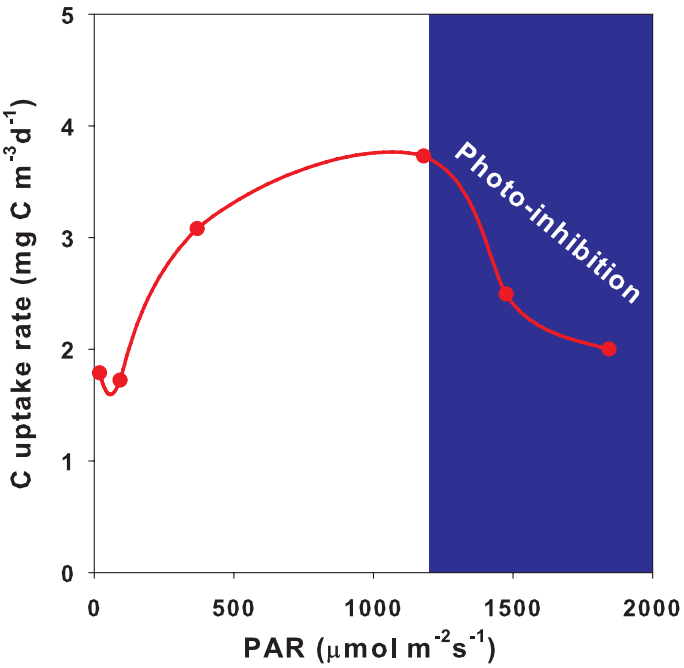

Figure 3.22: *Variation of the surface carbon uptake rate with the different PAR values at the AS-W8 in the NE-AS during late winter.*

Fig 3.22 presents the variation of surface productivity under different light intensities. Initially, surface productivity increases with increase in light intensity. When light intensity exceeds 1200 μmol $m^{-2}s^{-1}$, surface productivity declines. The decline in productivity is a consequence of the shrinkage of the chloroplast of phytoplankton due to the excess light, termed as photo-inhibition. This shows that

the surface light available in the NE-AS during late winter is much more than the optimum value required for photosynthesis by phytoplankton. Photo-inhibition has been observed in different regions e.g., the central Atlantic (*Hu and Smith*, 1998), the Ross Sea (*Planas et al.*, 1999). Photo-inhibition is one of the reasons offered for the observed lower surface productivity in the AS compared to that in the BOB (*Qasim*, 1977) based on the 12-hours *in situ* ^{14}C productivity measurements. This did not entail time-course experiments so as to observe the effect of sunlight during different times of a clear day. In this respect, the present result is the first to quantify the photo-inhibition in the NE-AS during the noon of a clear day. The result also explains the lower productivity observed (Figs 3.21a and 3.21c) in the surface than at sub-surface, despite higher concentration of plankton (Figs 3.20a and 3.20b) and higher nitrate values (Figs 3.17a and 3.17b) at the surface.

Effect of time of the day on productivity measurement

To check the effect of 4-hr incubations at different times of a day, an experiment was performed at AS-W8. Surface water samples were collected pre-dawn in 6 one liter polycarbonate bottles. Two samples were incubated from 06:00 to 10:00 Hrs. after adding $NaH^{13}CO_3$ tracer with the final concentration $\sim$0.2 mM. The rest were kept in the dark. At 10:00 Hrs, another two were incubated till 14:00 Hrs. followed by the next two from 14:00 to 18:00 Hrs. The samples were filtered as soon as the respective incubations ended and were preserved for mass spectrometric analysis. Mass spectrometric analysis and calculations for estimation of specific uptake rate of carbon (using equation 2.6) were performed as explained in Chapter 2.
Results are shown in Fig 3.23. Specific uptake rate in the morning (06:00 to 10:00 Hrs) is higher and remains low for noon (10:00 to 14:00 Hrs) and again increases in the evening (14:00 to 18:00 Hrs) incubations (Fig 3.23). The highest specific uptake rate is found during morning, followed by evening and noon. Photo-inhibition due to excess surface light intensity could be a reason for the reduction in the specific uptake rates during noon. During morning hours, PAR is found to be $\sim$1050 μmol

$m^{-2}s^{-1}$ and it increased to 1825 μmol $m^{-2}s^{-1}$ during noon and it decreases again in the afternoon.

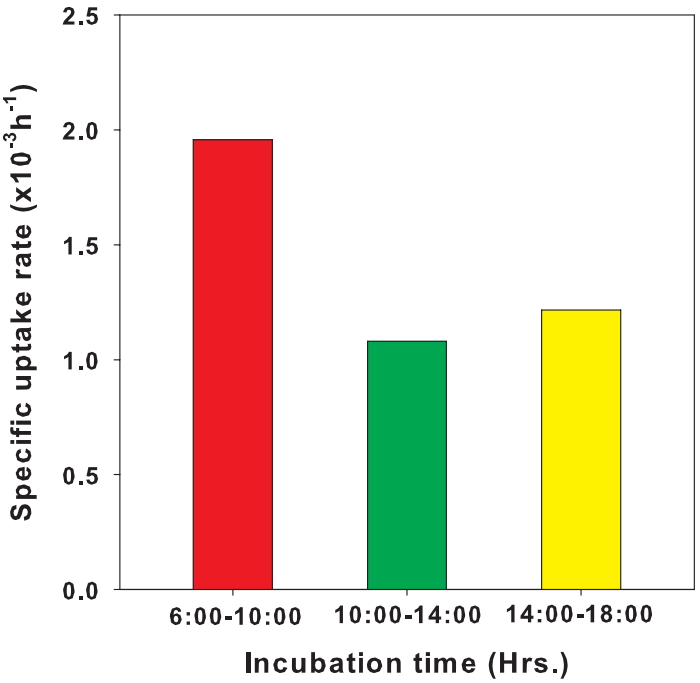

Figure 3.23: *Variation of specific uptake rate of carbon with the different incubation time at the AS-W8 in the NE-AS during late winter.*

Morning PAR value is in the range of optimum requirement for photosynthesis, while it increases to photo-inhibition region during noon (Fig 3.22). The ratio of specific uptake rates during morning, noon and evening is 3.4: 1: 2. Similarly, the ratio of productivities during morning, noon and evening is 4.5: 1: 2.3. Both the experiments indicate that the surface light intensity in the NE-AS is more than that required for photosynthesis in the noon hours during late winter under clear sky conditions. Further, the present results and analyses suggest that ^{13}C experiments carried out around local noon are likely to underestimate surface productivity by as much as $\sim$35 %. Error introduced due to this on the euphotic-depth-integrated productivity values reported in the present study is well within the uncertainty quoted. Therefore, no correction was made in the measured values of column productivity. However, the results have a serious implication to the algorithm for

calculating column productivity based on surface chlorophyll values obtained from satellites.

3.10.2 New productivity

Depth profiles of NO_3 uptake rate, termed as new productivity, at different sampling locations are shown in Figs 3.24a and 3.24c. New productivity varies from 0.03 to 0.12 μmol N $L^{-1}d^{-1}$ in the surface waters.

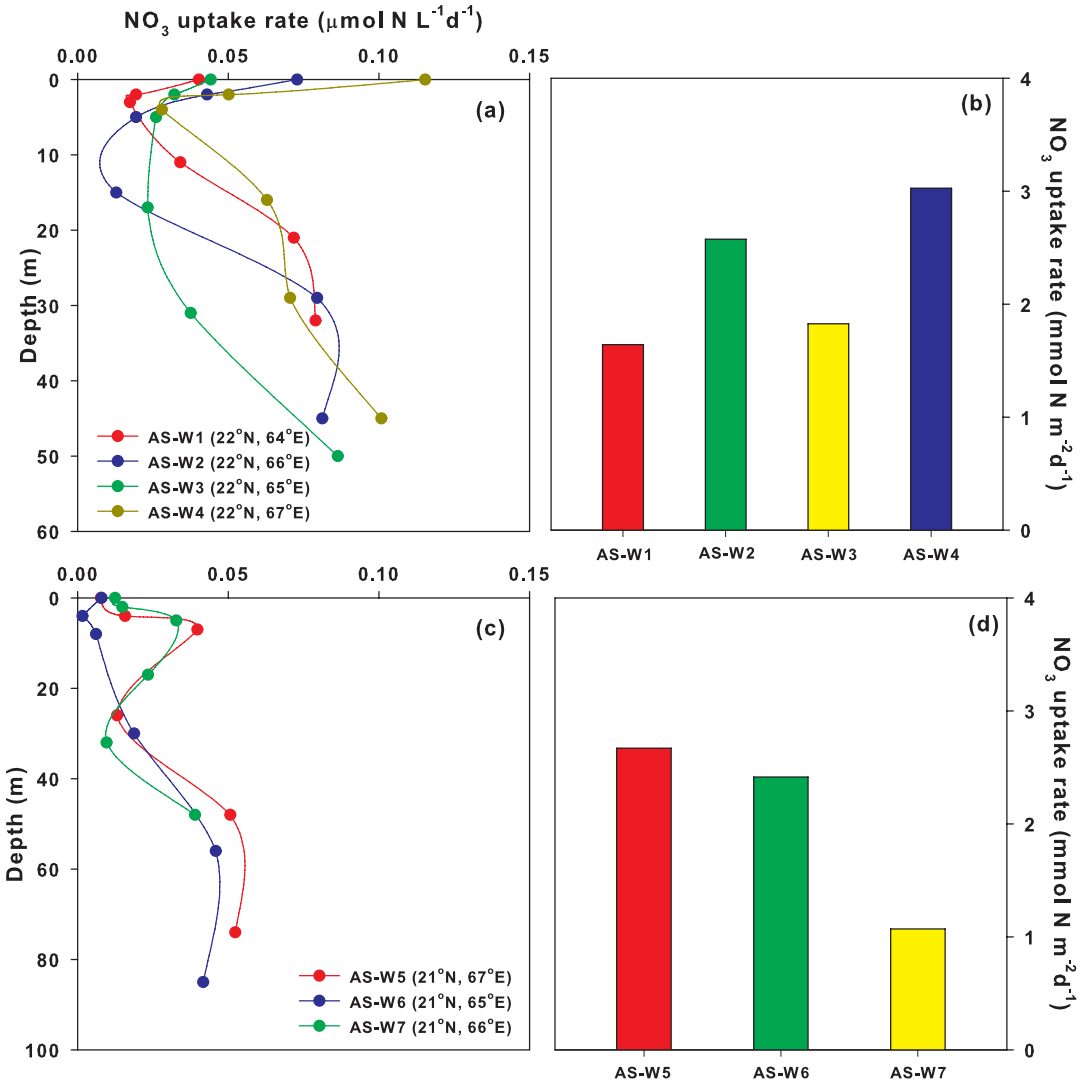

Figure 3.24: *Depth profiles of NO_3 uptake rate (left) and their euphotic-depth-integrated values (right) along the (a and c) 22°N and (b and d) 21°N latitudinal locations in the NE-AS during late winter.*

The highest surface productivity is observed at AS-W4, while it is the lowest at AS-W5. Unlike carbon uptake, no difference is seen for average surface new productivity (0.07 μmol N $L^{-1}d^{-1}$) at both the latitudes. New productivity could not be measured at AS-W8, which restricts the comparison between northern and southern locations. One more contrasting observation regarding new productivity vis-a-vis carbon uptake is that the highest new productivity is at surface or at the base of euphotic zone (1% of surface light intensity value) at 22^oN (Figs 3.24a). However, at 21^oN higher new productivity is found at sub-surface layers. Higher new productivity at surface and at the base of euphotic zone show the loose coupling between the light availability and nitrate assimilation. Overall, new productivity follows the pattern of available nitrate rather than available light in the euphotic zone. *Harrison et al* (1996) suggested that the nitrogen fuelling the primary productivity maximum was derived from regenerative processes in the euphotic zone. Productivity associated with the Chl *a* maximum, associated with the nitracline, was fuelled by NO_3 upwelled from below (*Harrison et al.*, 1996). The decoupling of carbon uptake and new productivity observed here confirms this.
Euphotic-depth-integrated new productivity is shown in Figs 3.24b and 3.24d. Integrated productivity varies from 1.6 to 9.0 mmol N $m^{-2}d^{-1}$ (with an average of 6.7 mmol N $m^{-2}d^{-1}$). The highest and the lowest productive locations are AS-W5 and AS-W1, respectively (Figs 3.24b and 3.24d).
The average productivity at 22^oN is $\sim$2.3 mmol N $m^{-2}d^{-1}$. In contrast to our observations on carbon uptake, at 21^oN, the average productivity is higher ($\sim$6.7 mmol N $m^{-2}d^{-1}$) than that at 22^oN. Light and nutrients values are comparable at both the latitudes. Therefore, the difference in new productivity between these two longitudes are could be due to the difference in plankton cell count and chl *a*, which are lower at 21^oN than that at 22^oN. Satellite chlorophyll image also confirms lower chlorophyll at 21^oN (Fig 3.14). Lower cell and chl *a* at surface allow light to penetrate to deeper layers, which enhances euphotic depth and hence the depth-integrated new productivity. *Kumar et al* (2010) reported euphotic-zone-

integrated NO_3 uptake rates, ranging from 1.0 to 4.2 mmol N $m^{-2}d^{-1}$ with an average of 2.3 mmol N $m^{-2}d^{-1}$ in January 2003. They also measured depth-integrated NO_3 uptake rates during Feb-March 2003 and found that new productivity ranged from 5.7 to 23.2 mmol N $m^{-2}d^{-1}$ with an average of 12.7 mmol N $m^{-2}d^{-1}$, more than five times that observed in January 2003. During JGOFS studies, *Watts and Owens* (1999) found average NO_3 uptake rate of 9.8 mmol N $m^{-2}d^{-1}$ during November-December, while *McCarthy et al* (1999) observed new productivity of 1.52 mmol N $m^{-2}d^{-1}$ in January. The present results are comparable to the results obtained by *Kumar et al* (2010) for NE-AS during early winter and are lower than that observed during other times. *Prakash et al* (2008) reported a large spatial variation in new productivity from south to north in the NE-AS. They observed higher new production in the north than in the south to be low new productive region. *Prakash and Ramesh* (2007) ruled out any significant temporal trend in the productivity in the NE-AS; the present study, along with the earlier findings, points towards intra-seasonal variation in new productivity during winter: low new production during early and late winter with higher mid-winter new productivity. Differences in the new productivity at different latitudes observed here was also observed by *Prakash et al* (2008), who demonstrated spatial variation in new productivity within the basin during winter.

3.10.3 Regenerated productivity

Here, the sum of NH_4 and urea uptake rates is considered as regenerated productivity. Ambient NH_4 and urea concentrations are not measured during the present study. For the calculation of regenerated production, it is assumed that the tracer added is the only source of nutrient for the plankton. Therefore, uptake rates given here are the conservative estimates for NH_4 and urea. Depth profiles of NH_4 uptake rate at different sampling locations are shown in Figs 3.25a and 3.25c. It varies from 0.003 to 0.012 μmol N $L^{-1}d^{-1}$ in the surface. It is almost an order of magnitude less than the surface new productivity.

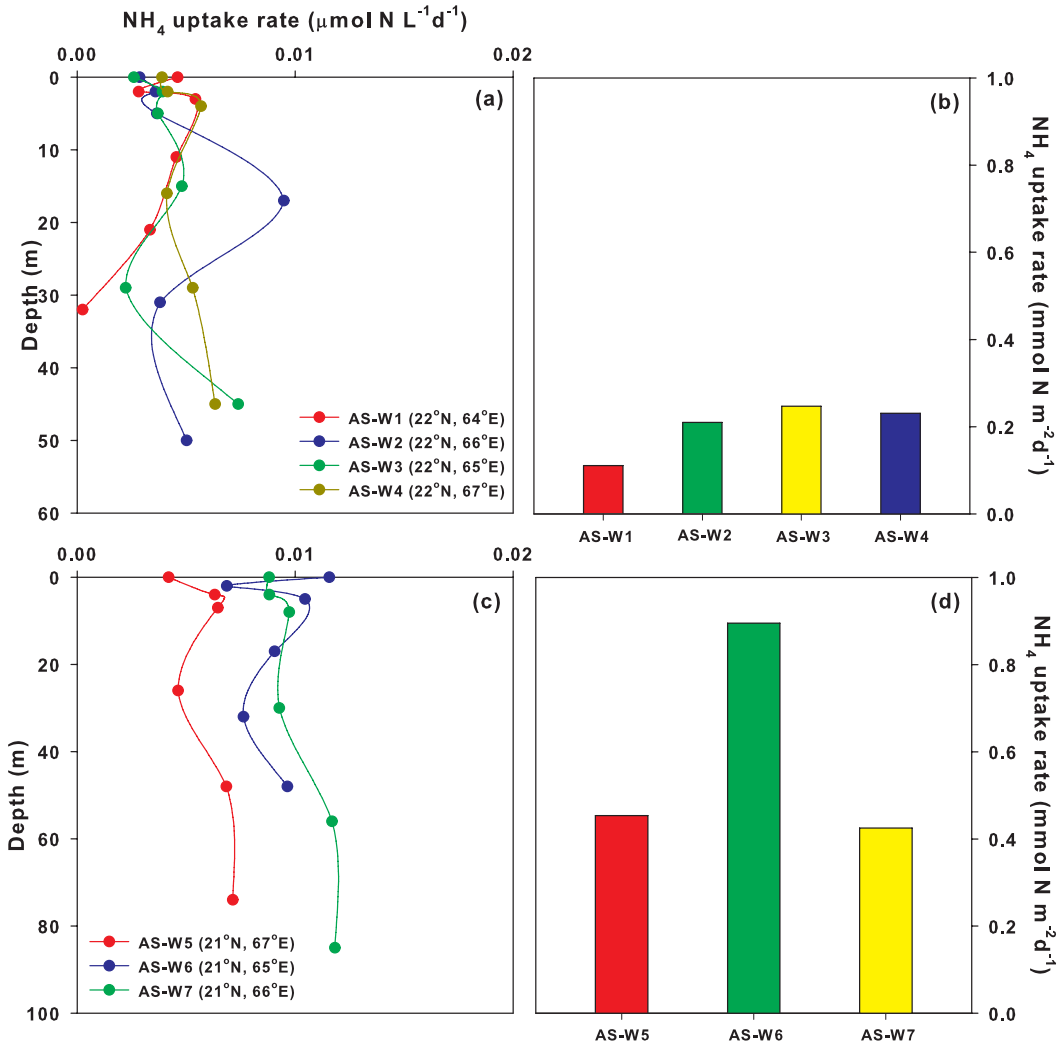

Figure 3.25: *Depth profiles of NH_4 uptake rate (left) and their euphotic-depth-integrated values (right) along the (a and c) 22°N and (b and d) 21°N latitudinal locations in the NE-AS during late winter.*

The highest surface NH_4 uptake is observed at AS-W7. Like new productivity, no significant variation is observed for NH_4 uptake between 21°N and 22°N. However, one contrasting observation on NH_4 uptake from that on new productivity is that its highest value is found to be at sub-surface at both the latitudes (Figs 3.25a and 3.25c). Overall, NH_4 uptake is very low. The values reported here are conservative estimates of NH_4 uptake, which represent the lower bound for NH_4 uptake. This could be one of the reasons for the large difference between NH_4

uptake and new productivity. However, not much NH_4 has been reported for this region (*Wafar et al.*, 1986; *Devassy et al.*, 1978), generally it remains below 1 μM. If we consider on its face value, it can explain only half of the difference between NH_4 and NO_3 uptakes, indicating the preference of NO_3 to NH_4 by phytoplankton during late winter.

Euphotic-depth-integrated NH_4 uptake values are shown in Figs 3.25b and 3.25d; it varies from 0.11 to 0.42 mmol N $m^{-2}d^{-1}$ (with an average of 0.37 mmol N $m^{-2}d^{-1}$). The highest and the lowest productive locations are AS-W1 and AS-W6, respectively (Figs 3.24b and 3.24d). In contrast to the observation for NO_3 uptake, the NH_4 uptake at 21^oN is higher ($\sim$0.6 mmol N $m^{-2}d^{-1}$) than that at 22^oN ($\sim$0.2 mmol N $m^{-2}d^{-1}$). The average NH_4 uptake rate during January 2003 was found 5.6 mmol N $m^{-2}d^{-1}$ (*Kumar et al.*, 2010), which is considerably higher than the average value presented here. The present values are much lower than that reported by *McCarthy et al* (1999) for early winter, 25 mmol N $m^{-2}d^{-1}$. *Prakash et al* (2008) reported NH_4 uptake between 0.36 and 3.28 mmol N $m^{-2}d^{-1}$ in mid-winter. The present study reports the lowest NH_4 uptake rates compared to earlier findings, indicating intra-seasonal and spatial variation in NH_4 uptake during winter.

Depth profiles of urea uptake rate at different sampling locations are shown in Figs 3.26a and 3.26c. Urea uptake in the surface varies from 0.003 to 0.009 μmol N $L^{-1}d^{-1}$ (with an average of 0.005 μmol N $L^{-1}d^{-1}$). As for NH_4 uptake, urea uptake is also an order of magnitude less than the surface new productivity. Like new productivity, no significant variation is observed in urea uptake between latitudes and depths (Figs 3.26a and 3.26c). As in the case of NH_4, urea uptake is also low. As for NH_4, the values reported here for urea uptake are conservative estimates, which represent its lower bounds. No data are available on ambient urea in the region. Therefore, it is difficult to pin-point the exact reason for the large difference between new productivity and urea uptake. Nevertheless, the present data suggest that urea is the least preferred nitrogenous compound by phytoplankton

during late winter.

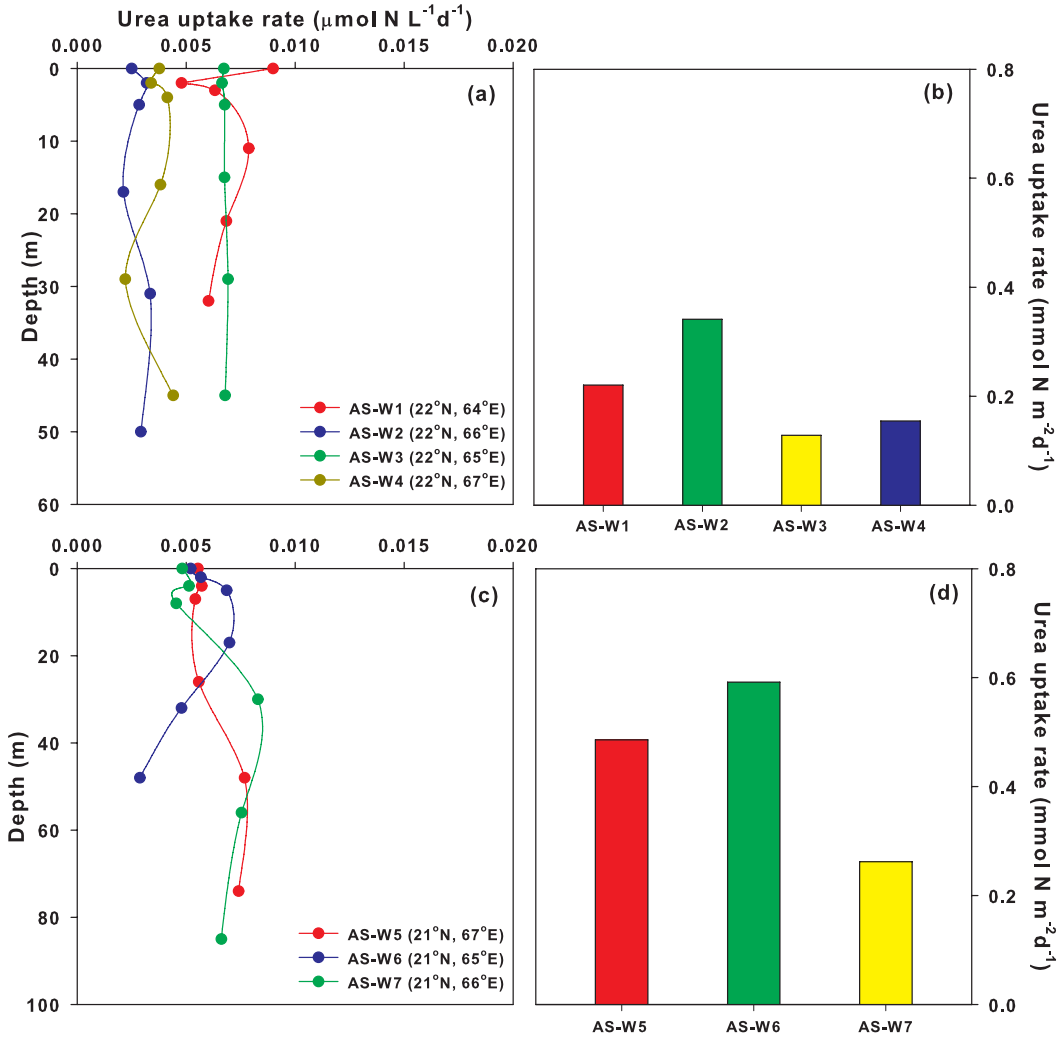

Figure 3.26: *Depth profiles of urea uptake rate (left) and their euphotic-depth-integrated values (right) along the (a and c) 22°N and (b and d) 21°N latitudinal locations in the NE-AS during late winter.*

Euphotic-depth-integrated urea uptake values are shown in Figs 3.26b and 3.26d. Integrated uptake varies from 0.13 to 0.59 mmol N $m^{-2}d^{-1}$ (with an average of 0.31 mmol N $m^{-2}d^{-1}$). The average urea uptake at 22°N is found to be ∼0.21 mmol N $m^{-2}d^{-1}$. As in the case of NO_3 and NH_4, at 21°N, the average urea uptake is higher (∼0.45 mmol N $m^{-2}d^{-1}$) than that at 22°N.

Prakash et al (2008) reported euphotic-zone-integrated urea uptake rates, between

0.63 and 3.99 mmol N $m^{-2}d^{-1}$ with an average of 1.86 mmol N $m^{-2}d^{-1}$ in Feb-Mar 2004. They found that urea was the least preferred nitrogenous substrate during winter in the NE-AS. In the present study too, ammonium uptake rates are generally higher than urea uptake and nitrate is the most preferred nitrogenous nutrient in this region. In contrast, NH_4 was found be the most preferred nitrogenous nutrient during late winter in the north-western AS (*McCarthy et al.*, 1999). An overall comparison of present study with *McCarthy et al* (1999) suggests that ammonium uptake and role of ammonium as a nutrient is more prevalent in the north-western AS than the NE-AS during late winter. It is also notable that the present values for uptake rates are lower than those reported by *Prakash et al* (2008) for the same region. This indicates that the variation of uptake rate of nitrogen during the course of winter in the NE-AS, as inter-annual variations are not very significant (*Prakash and Ramesh*, 2007).

3.10.4 *f*-ratio

f-ratios integrated over the euphotic zone at the stations vary from 0.80 to 0.91 (with an average of 0.85). f-ratios are found to be similar at 21^oN and 22^oN. *McCarthy et al* (1999) reported f-ratios in the range of 0.01 to 0.31 during early and late winter for the NW and central AS. *Watts and Owens* (1999) found f-ratios 0.07 to 0.52 during early winter in the NW-AS. However, Prakash et al (2008) found higher f-ratios ($\sim$0.82), comparable to the present study, during winter in the northern AS (*Prakash et al.*, 2008). *Kumar et al* (2010) also reported high f-ratios ($\sim$0.52), but somewhat less than that reported here. f-ratios reported by *McCarthy et al* (1999) and *Watts and Owens* (1999) earlier are lower than those reported here, based on the conservative estimates of regenerated productivity. This could be a reason for the difference between the present and earlier estimates from other parts of the AS. Nevertheless, our results are consistent with earlier findings, suggesting that ammonium and urea are the preferred nitrogenous nutrients in the NW and central Arabian Sea. In contrast, nitrate is the preferred nutrient in the NE-AS,

particularly in winter. Further, the present study, along with the earlier results from the region, show persistently high new production year after year and f-ratios more than 0.5 during winter suggest enhanced downward transport of newly formed organic matter, which has direct implications to the sequestration of carbon in the deeper ocean.

3.10.5 C:N consumption ratio

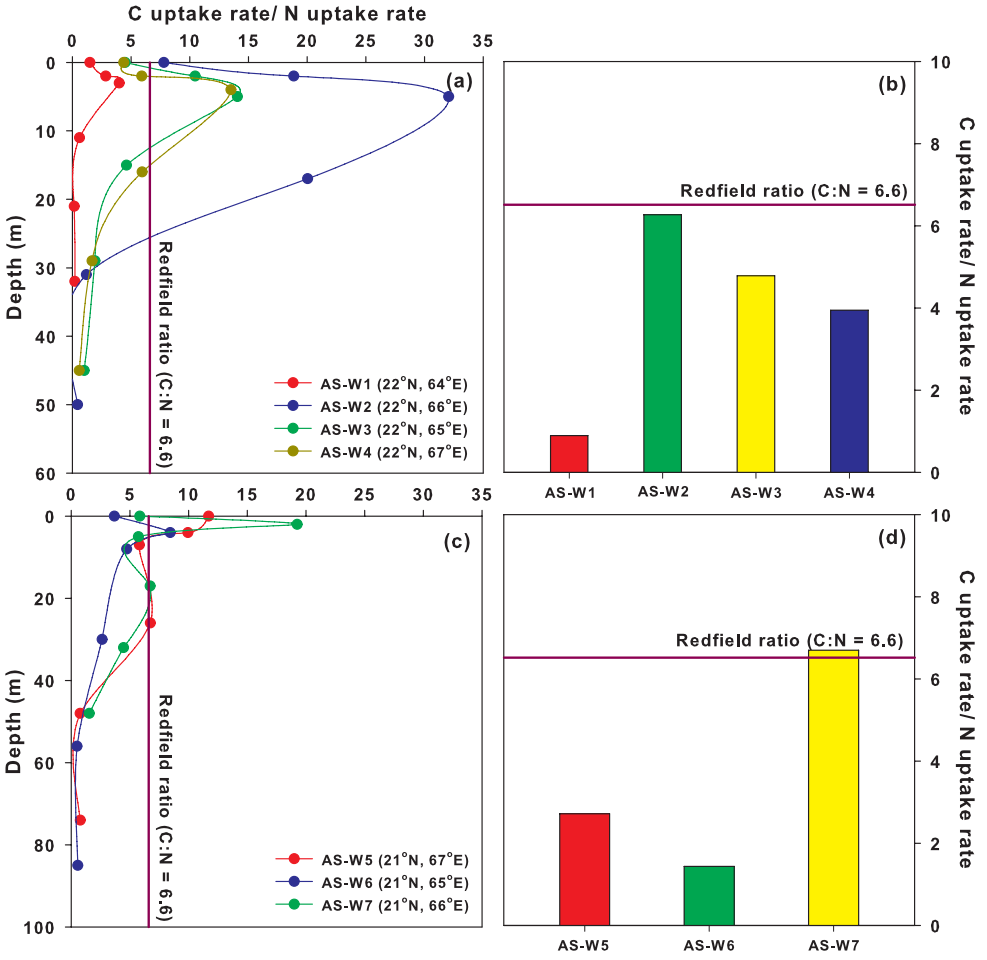

Figure 3.27: *Depth profile of the ratio of the observed C to N uptake rate (left) and the ratio of their euphotic-depth-integrated C to N uptake rates at different locations (right) along the (a and b) 22°N and (c and d) 21°N latitudes in the NE-AS during late winter. Pink lines represent the Redfield ratio (C:N = 6.6).*

Figs 3.27a and 3.27c present the depth profiles of the ratio of carbon to nitrogen uptake rates (C:N) at different sampling locations. The ratio at the surface varies

from <1 to 7.8 during the study period. The average ratio at 22^oN is found to be 4.5, close to the Redfield ratio (C:N = 6.6). Layers just below the surface, and middle layers show higher ratios than the Redfield ratio and again lower values are seen in the depths correspond to < 5% light level from the surface. Variation in the ratio is mainly controlled by the available light and nutrients, composition of plankton and microbial metabolism (e.g., N_2 fixation, denitrification and anammox etc.) (*Arrigo*, 2005).

Nutrients are not limited during the period (Fig 3.17). At the surface, photo-inhibition suppresses assimilation of carbon, which results in the lower C:N ratio. In contrast, light limitation in the deeper depths decreases the carbon uptake and hence reduces the C:N ratio. Therefore, extreme light conditions are responsible for the deviation of the C:N ratio from the Redfield ratio. However, mid-depths show C:N as high as 32.

Diatoms dominated the plankton community. At AS-W2 and AS-W4, *Noctiluca miliaris* is found to be dominant plankton species. The highest C:N ratio is associated with AS-W4. AS-W2 also shows a higher ratio, comparable to that observed at AS-W3. Therefore, it is difficult to conclude that *Noctiluca miliaris* promotes the assimilation of more carbon relative to nitrogen. Nevertheless, both AS-W2 and AS-W4, *Noctiluca* bloom locations, give some indication for the preferential uptake of carbon over nitrogen at mid-depths. The ratio of euphotic-depth-integrated uptake rates of carbon and nitrogen varies between <1 and 6.3. Overall, the ratio is found to be lower than the Redfield ratio at all the locations. This indicates the importance of the type of plankton present, and the availability of light, as the assimilation of nitrogen compounds are known to be affected by light (*Arrigo*, 2005).

3.11 Part II: Conclusion

Varying wind strength, shallow MLD, high mixed layer NO_3 during late winter results in moderate productivity in the NE-AS. Most locations are populated by

diatoms, as expected in the region during winter. At two locations, *Noctiluca miliaris* is quite abundant. The present study and earlier reports suggest that northern AS off Oman is populated by *Noctiluca miliaris*, whereas, at the same time diatoms dominate in the eastern AS. A large variation in productivity is observed between two nearby latitudes (21^oN and 22^oN), as also seen in SeaWiFS chlorophyll images. Northern locations are more productive than the southern locations. The north-south variation observed here is consistent with the earlier findings from the region (e.g., *Madhupratap et al.*, 1996; *Prasanna Kumar and Narvekar*, 2005). Surface cell counts control the overall depth of the euphotic zone and hence the column integrated productivity. The present study also provides the first evidence of photo-inhibition in the surface waters of the region using time course- and varying light intensity- experiments: when light intensity exceeds 1200 μmol $m^{-2}s^{-1}$, the surface productivity decreases. This indicates that the surface light available during this season is much more than the optimum value required for photosynthesis. This result is further supported by another experiment in which the highest specific uptake rate is found in the morning hours, followed by evening and noon. During morning hours PAR is $\sim$1050 μmol $m^{-2}s^{-1}$ and it increases to 1825 μmol $m^{-2}s^{-1}$ during the noon and decreases again in the afternoon. New productivity is higher than that observed during spring (this study). However, the values are lower than that reported during early and mid-winter in different years (*Prakash et al.*, 2008; *Kumar et al.*, 2010), so is the regenerated productivity. As inter-annual variations are not very prominent in the region, a comparison of the present results with the earlier reported values indicates that new productivity varies significantly in the course of winter. Higher f-ratios are consistent with earlier findings, which suggest that the region is effectively contributing to the sequestration of excess atmospheric carbon to the deep ocean. A comparison of the present results with the results obtained from the different parts of the AS shows that preference for different nitrogenous substrates varies from the west to the east.

3.12 Part III: Sampling in the BOB (spring 2007)

3.13 Environmental conditions

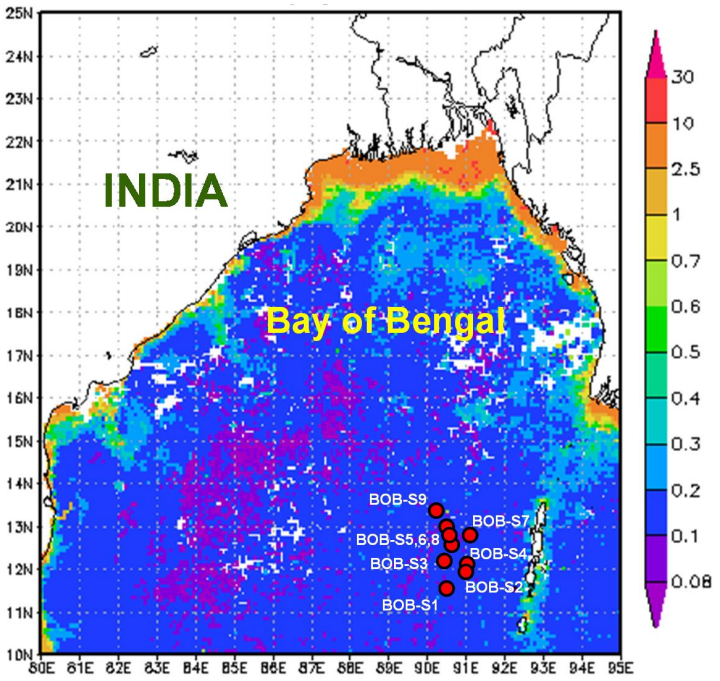

Figure 3.28: *Composite SeaWiFS Chlorophyll image for May-June 2007 (source: http://reason.gsfc.nasa.gov/OPS/Giovanni/ocean.seawifs.shtml) corresponding to cruise in the BOB during spring with superimposed station locations.*

Measurements of nitrogen uptake rates in the BOB were initiated under BOBPS programme (*Kumar et al.*, 2004; *Kumar and Ramesh*, 2005). Measurements were carried out in the coastal and central BOB during BOBPS. To improve our understing of the nitrogen uptake in the region, the present study aims to carry out measurements of nitrogen uptake rate in the southern BOB west of the Andaman Sea.

In addition, ^{13}C based surface productivity is also measured at nine locations. Depth profiles of carbon uptake rates could not be measured due to logistic prob-

lems. Sampling is done mostly in a small region ($2^o \times 1^o$) shown in Fig 3.28.

Table 3.3: *Station codes, locations of the stations, sea surface temperature (^oC; SST), surface salinity (psu), mixed layer depth (m; MLD), euphotic depth (m; ED), and PAR ($\mu mol\ m^{-2}s^{-1}$) in the BOB during spring (May-June, 2007).*

Station Code	Lat (^{o}N)	Lon (^{o}E)	SST	Salinity	MLD	ED	PAR
BOB-S1	11.6	90.4	29.6	32.7	35	65	1380
BOB-S2	11.9	90.9	29.4	32.8	ND	ND	1600
BOB-S3	12.2	90.4	29.4	32.8	52	69	1690
BOB-S4	12.1	90.9	29.6	32.8	60	74	434
BOB-S5	12.6	90.6	29.7	32.8	60	77	1130
BOB-S6	12.8	90.4	29.9	32.8	56	66	1450
BOB-S7	12.8	91.0	29.8	32.8	ND	ND	200
BOB-S8	13.0	90.4	29.9	32.9	48	75	1220
BOB-S9	13.3	90.2	29.9	32.8	ND	ND	1200

ND-no data available (see text for details).

Sea surface temperature (SST) is found to be high at all the locations (Table 3.3), ranging from 29.4 to 29.9 ^{o}C. Surface salinity varies from 32.7 to 32.9 psu (Table 3.3), lower than that observed in the NE-AS during spring (this study). Although the sampling locations are confined to a small region ($2^o \times 1^o$), temperature based mixed layer depth (MLD) varies significantly from 35 to 60 m. The BOB is known to remain cloudy most of the year (e.g. *Qasim*, 1977; *Radhakrishna*, 1978; *Gomes et al.*, 2000), confirmed in the present study too. Cloudiness controls the light reaching the sea surface. PAR varies from 200 to 1690 μmol m^{-2}s^{-1}. However, on a clear day the surface light intensity (at locations BOB-S2 and BOB-S3) is comparable to that observed during spring in the NE-AS (this study). Euphotic depth (ED) varies from 65 to 77 m. Overall, the MLD is found to be shallower than the ED at all the locations. SeaWiFS (Level-3 Version 4 weekly 9-km data, source: http://reason.gsfc.nasa.gov/OPS/Giovanni/ocean.swf8D.shtml) chlorophyll corresponding to the measurement period (Fig 3.28) shows no evidence of variation in chlorophyll at this location, with very low chlorophyll values.

3.13.1 Temperature and salinity

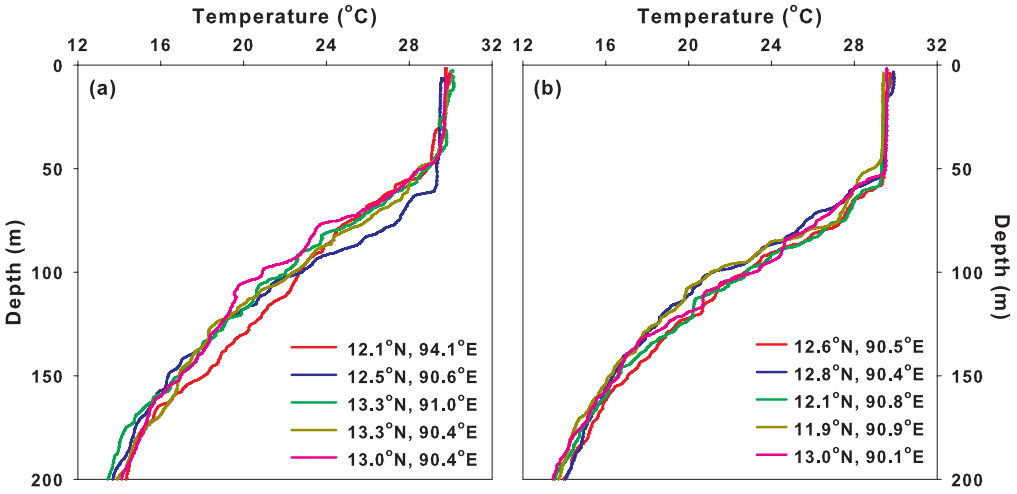

Figure 3.29: *Depth profiles of temperature at different locations in the BOB during spring.*

Depth profiles of temperature at different locations are shown in Fig 3.29, with no significant variation. Surface water is found to be very stable and stratified, no change is observed in temperature from the surface to 50 m depth (Figs 3.29a and 3.29b).

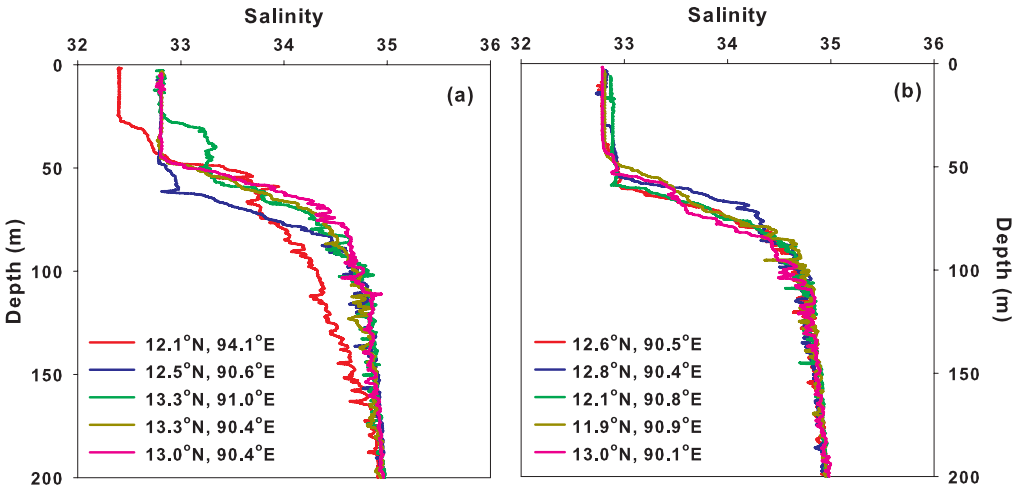

Figure 3.30: *Depth profiles of salinity at different locations in the BOB during spring.*

A similar scenario exists for salinity, whose depth profiles are presented in Fig 3.30: Except at 12.1^{o}N, 94.1^{o}E there is no significant variation. Lower salinity is

found in the surface here compared to other locations.

Prasanna Kumar et al (2007) also observed higher SST >29^{o}C during spring 2003. They also observed surface salinity values similar to that observed in the present study during spring. The strong stratification is a result of large river run-off and higher E-P values for the region, which lead to a low nutrient supply to the surface and hence lower productivity (*Prasanna Kumar et al.*, 2002). In the present study, similar conditions are seen.

3.13.2 Nutrients and chlorophyll

Depth profiles of NO_3 and PO_4 are given in Fig 3.31. At all the locations NO_3 concentration is close to 0.5 μM. It remains the same upto the depth 60 m. Only one location (BOB-S1) shows a slightly different pattern below the MLD for NO_3 (Fig 3.31a).

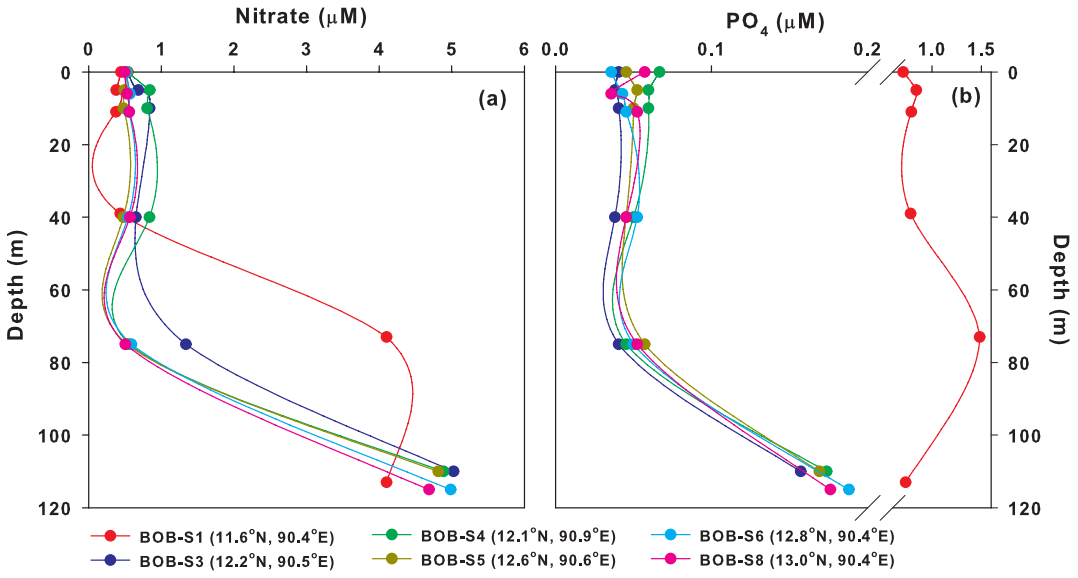

Figure 3.31: *Depth profiles of different nutrients: (a) NO_3, and (b) PO_4 at different locations in the BOB during spring.*

NO_3 values in the surface observed here are marginally higher than that reported by *Prasanna Kumar et al* (2007) for spring 2003. NO_3 concentrations were near the detection limit in the top 20 m during their study. Like NO_3, PO_4 con-

centrations are also found to be invariable (∼0.05 μM) in the first 60 m at all the locations, except at BOB-S1 (Fig 3.31b). Higher concentration of PO_4 is found at BOB-S1 compared to other locations. This location also shows the lowest surface salinity, the MLD and euphotic depth. However, SST at this location is found to be comparable to that at other locations.

Depth variations of chl *a* are shown in Fig 3.32. Most of the locations show very low chl *a* values, consistent with the chlorophyll image for the sampling period (Fig 3.28). However, a few locations show significant chl *a* values in surface (∼0.8 mg m^{-3}). A remarkable feature of the profiles is that Deep Chlorophyll Maximum (DCM) is invariably situated between 50 and 70 m at all the locations.

This is a typical feature of the region and is also consistent with the earlier reports from this region (*Gomes et al.*, 2000; *Prasanna Kumar et al.*, 2007; *Jyothibabu et al.*, 2008).

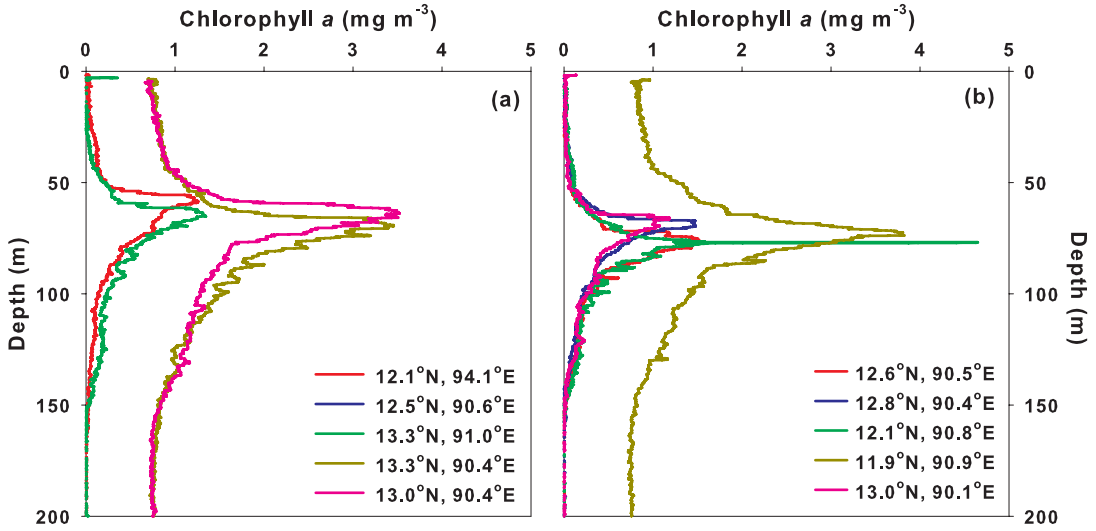

Figure 3.32: *Depth profiles of chlorophyll at different locations in the BOB during spring.*

Surface light intensity, except at two locations (BOB-S2 and BOB-S3), is not very intense. Therefore, lower chl *a* values in the surface is a consequence of low nutrient availability. But, light limitation at the deeper layers results in low a

chlorophyll content. In the middle depths, both light and nutrients are optimally available, which leads to higher chlorophyll values at these depths. This is a typical characteristic of an oligotrophic region.

3.14 Carbon and Nitrogen uptake rates

New productivity and regenerated productivity measured at 9 different stations are shown in Fig 3.28. At six locations (BOB-S1, BOB-S3, BOB-S4, BOB-S5, BOB-S6, and BOB-S8), samples were collected from six depths each to cover the whole euphotic zone. But, at the other three locations, only surface samples were collected. Samples for ^{13}C based surface productivity measurements were collected at eight locations (BOB-S2, BOB-S3, BOB-S4, BOB-S5, BOB-S6, BOB-S7, BOB-S8, and BOB-S9).

3.14.1 Carbon uptake rate

Surface productivity values are given in Table 3.4. It varies from 0.03 to 0.25 μmol C $L^{-1}d^{-1}$ (with an average of 0.09 μmol C $L^{-1}d^{-1}$ or 1.14 mg C $m^{-3}d^{-1}$).

Table 3.4: *Station codes, surface carbon productivity ($\mu mol\ C\ L^{-1}d^{-1}$; ρC), surface uptake rates of NO_3 (ρNO_3), NH_4 (ρNH_4) and urea ($\rho urea$) (in the unit of $\mu mol\ N\ L^{-1}d^{-1}$) in the BOB during spring (May-June, 2007).*

Station Code	ρC	ρNO_3	ρNH_4	ρurea
BOB-S1	ND	0.031	0.006	0.010
BOB-S2	0.07	0.046	0.004	0.005
BOB-S3	0.09	0.023	0.002	0.006
BOB-S4	0.25	0.022	0.003	0.013
BOB-S5	0.07	0.008	0.002	0.001
BOB-S6	0.03	0.012	0.003	0.005
BOB-S7	0.10	0.136	0.001	0.002
BOB-S8	0.08	0.040	0.001	0.004
BOB-S9	0.05	0.199	0.002	0.008

ND-no data available (see text for details).

BOB-S4 and BOB-S7 show higher values, 0.25 and 0.10 μmol C $L^{-1}d^{-1}$, re-

spectively, compared to the other locations. Interestingly, at these locations surface light intensities are minimum (Table 3.3). This suggests a significant effect of light intensity over the surface productivity in this basin.

Qasim (1977) reported that primary productivity in the surface (first 1 m) is < 1 mg C $m^{-3}hr^{-1}$ in off-shore BOB. *Radhakrishna* (1978) reported primary productivity in the range of 1.56 to 9.78 mg C $m^{-3}d^{-1}$ during March-April 1975. Comparable surface productivity has been observed for summer (16.1 mg C $m^{-3}d^{-1}$ for in-shore and 7.5 mg C $m^{-3}d^{-1}$ for off-shore), winter (8.6 mg C $m^{-3}d^{-1}$ for in-shore and 4.0 mg C $m^{-3}d^{-1}$ for off-shore), and spring (<6 mg C $m^{-3}d^{-1}$) (*Madhu et al.*, 2006). Surface productivity values ranged from 2.4 to 4.0 mg C $m^{-3}d^{-1}$ and from 1.9 to 9.7 mg C $m^{-3}d^{-1}$ during spring for the central and western BOB (*Prasanna Kumar et al.*, 2007). Values observed during the present study are on the lower side of the range reported earlier. Earlier results are mostly concentrated on the coastal and central BOB, while the present results are from the eastern part. No trend is found for surface productivity with time when comparing all the earlier data. Therefore, it is unlikely to conclude that the lower values of the present study are a consequence of inter-annual variations or a temporal trend in productivity. Nevertheless, the present results suggest that the eastern BOB is less productive than the western BOB. This east-west variation in productivity is similar to that found in the AS.

3.14.2 Nitrogen uptake rate

New productivity (NO_3 uptake rate) and regenerated productivity (the sum of NH_4 and urea uptake rates) results (using ^{15}N-labelled tracer) at the 6 locations are shown in Figs 3.33, 3.34, and 3.35.

New productivity

Surface NO_3 uptake rates are given in Table 3.4 and its depth profiles are shown in Fig 3.33a. It varies from 0.008 to 0.199 μmol N $L^{-1}d^{-1}$ (with an average of 0.057 μmol N $L^{-1}d^{-1}$) with the highest at BOB-S9. Similar values were obtained

under the BOBPS programme during April-May 2003 (*Kumar*, 2004). The values are also comparable to those observed during spring in the NE-AS (this study). In general, sub-surface maxima for NO_3 uptake rate vary from 40 to 80 m depth at different locations, except at BOB-S6 (Fig 3.33a). This is similar to the depth profile of chlorophyll in which deep chlorophyll maximum (DCM) is found to be situated between 50 and 70 m.

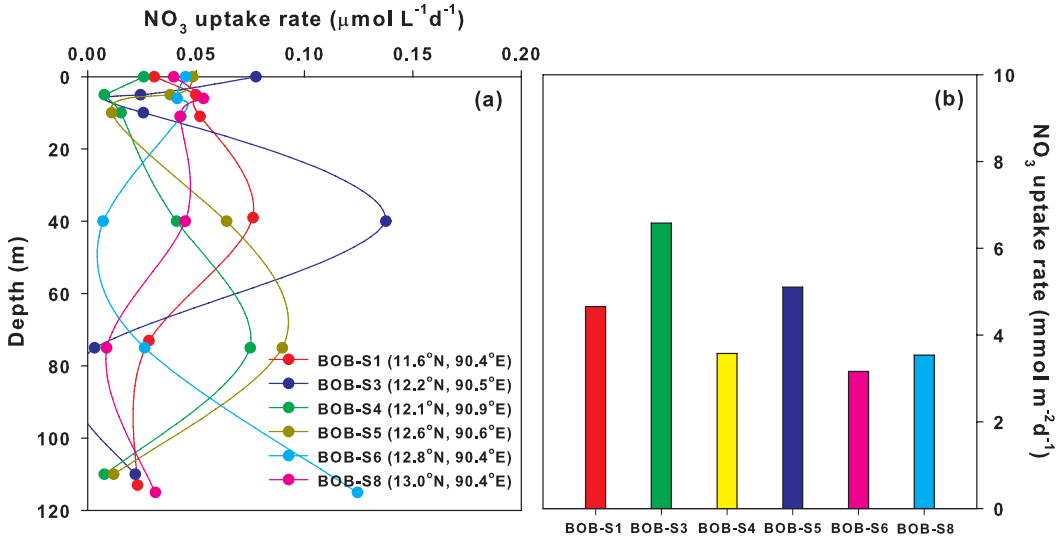

Figure 3.33: *Depth profiles of NO_3 uptake rate (left) and their euphotic-depth-integrated values (right) at different locations in the BOB during spring.*

Euphotic-depth-integrated NO_3 uptake rates at different locations are presented in Fig 3.33b. Column new productivity varies from 3.2 to 6.6 mmol N $m^{-2}d^{-1}$ (with an average of 4.4 mmol N $m^{-2}d^{-1}$). *Kumar et al* (2004) reported new productivity minimum of 0.98 mmolN $m^{-2}d^{-1}$ (offshore) to 10.67 mmolN $m^{-2}d^{-1}$ (shelf location) in April-May 2003. Overall, the new productivity for the region during spring 2003 was 5.44 ($\pm$3.66) mmolN $m^{-2}d^{-1}$ (*Kumar et al.*, 2004). Although the present study region is different from that of *Kumar et al* (2004), the present results are comparable to their new productivity estimates. This is in contrast to the surface carbon uptake results, which suggests a spatial variation exists in the BOB. The range as well as the average integrated NO_3 uptake rate found here are around four

times higher than those measured during spring in the NE-AS. This suggests that the BOB has a potentially larger contribution in the sequestration of CO_2 from the atmosphere than that of the AS during spring.

Regenerated productivity

Uptake rates given here are the conservative estimates for NH_4 and urea as the ambient concentrations of NH_4 and urea were not measured during the present study. Here, the sum of NH_4 and urea uptake rates are equivalent to regenerated productivity. NH_4 and urea uptake rate data are presented in Figs 3.34 and 3.35, respectively.

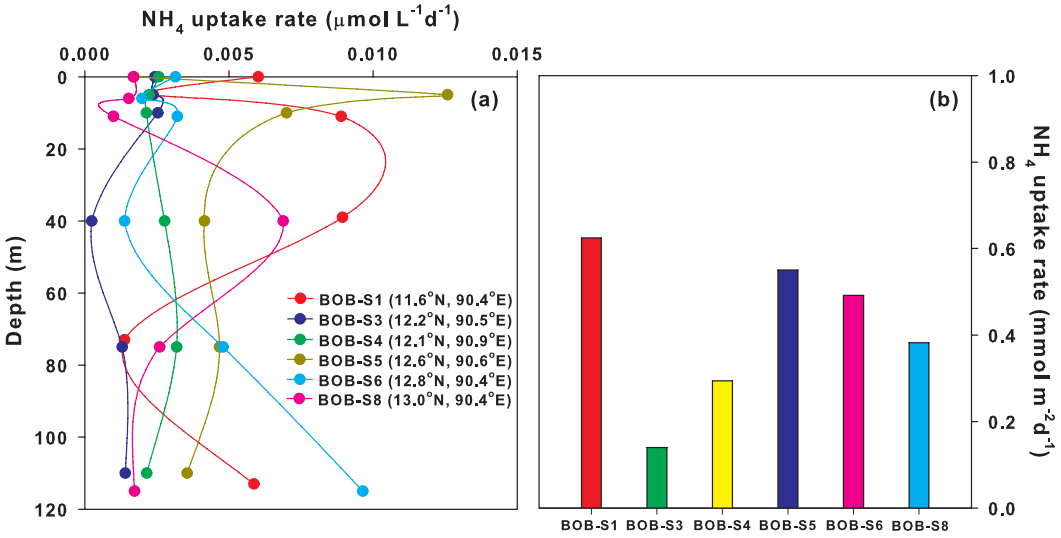

Figure 3.34: *Depth profiles of NH_4 uptake rate (left) and their euphotic-depth-integrated values (right) at different locations in the BOB during spring.*

Surface NH_4 uptake varies from 0.001 to 0.006 μmol N $L^{-1}d^{-1}$ (Fig 3.34a). Overall, the surface NH_4 uptake averages around 0.003 μmol N $L^{-1}d^{-1}$, an order of magnitude less than the average NO_3 uptake at surface. A similar observation is also made during spring in the NE-AS (this study). *Kumar* (2004) also reported similar surface NH_4 uptake in spring 2003. NH_4 uptake does not show any pattern with depth as was the case with NO_3 uptake. Nevertheless, three locations (BOB-S1, BOB-S5 and BOB-S8) do show higher values at middle depths (between 5 and

40 m). Euphotic-depth-integrated values are presented in Fig 3.33b. It varies from 0.14 to 0.62 mmol N $m^{-2}d^{-1}$. Overall, the average value is found to be 0.41 mmol N $m^{-2}d^{-1}$. As in case of NO_3 uptake, the average euphotic-depth-integrated NH_4 uptake value is higher than that observed during spring in the NE-AS (this study). *Kumar* (2004) reported NH_4 uptake rates more than twice higher than that the present study. They reported NH_4 uptake rate range from 0.67 to 1.80 mmol N $m^{-2}d^{-1}$ (with an average of 1.18 mmol N $m^{-2}d^{-1}$) in spring 2003. This comparison is similar to that observed in the case of NO_3 uptake rate values.

Urea uptake varies from 0.001 to 0.013 μmol N $L^{-1}d^{-1}$ in surface (Fig 3.35a). Overall, the surface urea uptake averages around 0.006 μmol N $L^{-1}d^{-1}$, twice higher than the average NH_4 uptake, but it is much less than the NO_3 uptake. This is in contrast to the results obtained during spring in the NE-AS (present study).

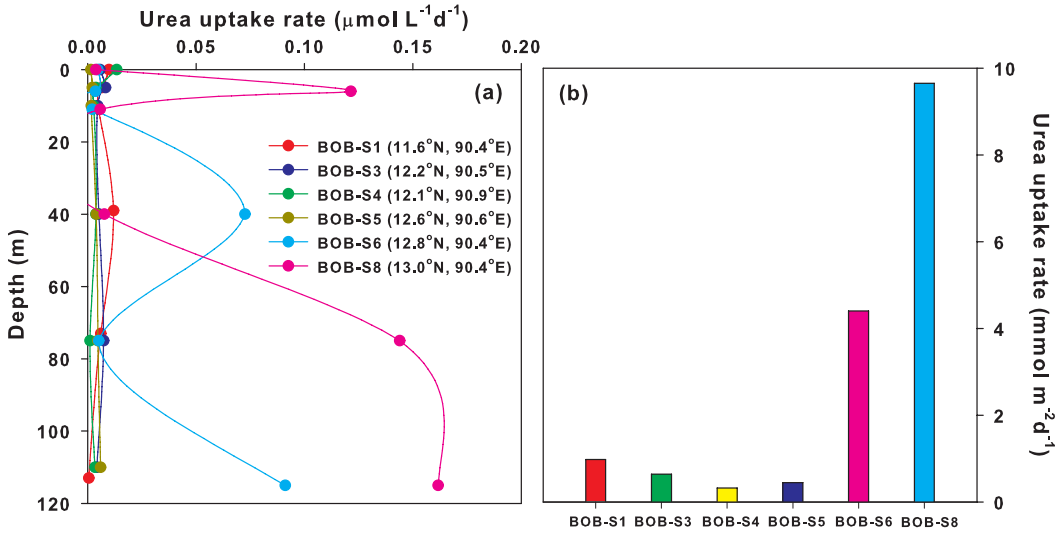

Figure 3.35: *Depth profiles of urea uptake rate (left) and their euphotic-depth-integrated values (right) at different locations in the BOB during spring.*

In the NE-AS, urea is found to be the least preferred nitrogenous substrate in the surface waters. Surface values observed here are similar to that found during spring 2003 (*Kumar* 2004). However, in 2003, the urea uptake never exceeded 0.016 μmol N $L^{-1}d^{-1}$, whereas, the highest value during present study is found

to be 0.162 μmol N $L^{-1}d^{-1}$ at the base of euphotic zone at BOB-S8 (Fig 3.34a). BOB-S6 and BOB-S8 show very high urea uptake rates in the sub-surface layers compared to the other locations. This is also reflected in the chlorophyll profiles, which show quite different, and higher chlorophyll values at a few locations (Fig 3.32).

Euphotic-depth-integrated NH_4 uptake values are shown in Fig 3.34b. It varies from 0.33 to 9.65 mmol N $m^{-2}d^{-1}$. Overall, the average value is found to be 0.60 mmol N $m^{-2}d^{-1}$ (by excluding BOB-S6 and BOB-S8) in the study area. Inclusion of BOB-S6 and BOB-S8 values increased the average to 2.74 mmol N $m^{-2}d^{-1}$. At these two locations, urea uptake is even higher than NO_3 uptake, otherwise it remains lower than NO_3 uptake at other locations. In general, NO_3 is the most preferred nitrogenous compound by phytoplankton, followed by urea and NH_4. However, at BOB-S6 and BOB-S8, the sequence changed to urea followed by NO_3 and NH_4. The average value (by excluding BOB-S6 and BOB-S8) of urea uptake of the present study matches well with the values obtained during spring 2003 for this region (*Kumar et al.*, 2004), an average value of $\sim$0.60 mmol N $m^{-2}d^{-1}$. As in the cases of NO_3 and NH_4, the values presented here are higher than that observed during spring in the NE-AS (present study). The total nitrogen uptake rate (the sum of NO_3, NH_4 and urea uptake rates) varies from 4.19 to 13.57 mmol N $m^{-2}d^{-1}$ (with an average of 7.59 mmol N $m^{-2}d^{-1}$), much higher than that observed during spring in the NE-AS (present study). It varies from 0.35 to 1.58 mmol N $m^{-2}d^{-1}$ (with an average of $\sim$1 mmol N $m^{-2}d^{-1}$). The comparison suggests that the BOB is more productive than the AS during spring, particularly the eastern BOB. However, the BOB remains less productive during other seasons (*Prasanna Kumar et al.*, 2002; *Gauns et al.*, 2005).

3.14.3 *f*-ratio

Euphotic-depth-integrated *f*-ratio varies from 0.26 to 0.89 with the highest value at BOB-S3. The estimated average *f*-ratio for the region is 0.66. The results indicate

that the BOB is capable of high new/export production. BOB-S6 and BOB-S8 show relatively lower values 0.39 and 0.26, respectively. This is because of very high urea uptake at these locations. It has been observed that new productivity is generally higher than the regenerated productivity. *Kumar et al* (2004) also observed high f-ratio (range from 0.50 to 0.87) during spring in the region. The average f-ratio is comparable to that estimated during the same season but lower than that during winter in the NE-AS (this study). New productivity values and f-ratio measured during the present study suggest that the eastern part of BOB is also capable of high new/export production as observed for its coastal and western parts during the BOBPS programme (*Kumar et al.*, 2004).

3.15 Part III: Conclusion

The light reaching the sea surface is mainly controlled by cloudiness. PAR varies from 200 to 1690 μmol $m^{-2}s^{-1}$. However, clear day surface light intensity at some locations is comparable to that observed during spring in the NE-AS. Nutrient availability is the key factor which controls surface productivity, as light remains moderate in the region. Higher chlorophyll at mid-depths is the consequence of moderate light and higher nutrients. Surface productivity observed during the present study is on the lower side of the range reported earlier from the coastal and central BOB. The present results do not indicate any significant inter-annual variation or decrease in productivity with time in the region. This confirms that the eastern BOB is less productive that the western BOB. The east-west variation in productivity is similar to that found in the AS. NO_3 is found to be the most preferred nitrogen compound followed by urea and NH_4. However, at some locations, phytoplankton do show higher preference for urea. The BOB shows higher nitrogen uptake compared to the NE-AS during spring. Comparison with the results of *Kumar et al* (2004) and those from the NE-AS (this study) reveals that the BOB has a larger contribution as compared to the NE-AS in the sequestration of CO_2 from the atmosphere, particularly during spring.

3.16 Part IV: Sampling in the BOB (early winter 2007)

3.17 Environmental conditions

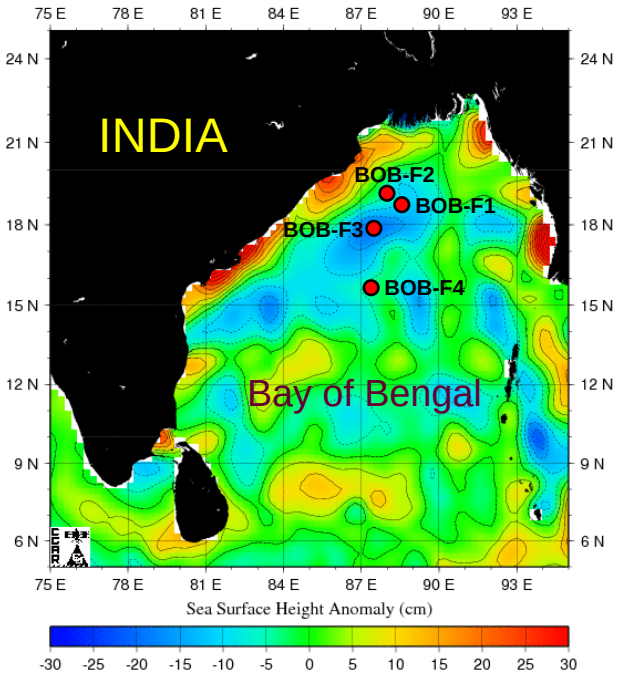

Figure 3.36: *Sea Surface Height Anomaly image for 25 Nov 2007 (source:http://argo.colorado.edu/∼realtime/gsfc–global-real-time–ssh/) corresponding to cruise in the BOB during early winter with superimposed station locations.*

The main aim of sampling during early winter was to study the role of eddies in the new/export production in the region. Cold-core eddies are capable of pumping subsurface waters to the upper layers. Eddy-pumping could cause an upward displacement of the nutricline along constant density surfaces and inject nutrients to the surface (*Falkowski et al.*, 1991; *Seki et al.*, 2001). This enhances biological productivity and the carbon export out of the euphotic zone. The existence of eddies in the Bay of Bengal has been reported by several authors

(*Ramasastry and Balaramamurty*, 1957; *Babu et al.*, 1991; 2003; *Murty et al.*, 1993; *Shetye et al.*, 1993; *Prasanna Kumar et al.*, 2004; 2007). *Prasanna Kumar et al* (2007) observed an increase in NO_3 and SiO_4 during both fall and spring intermonsoons in the region of eddies. The increase in nutrients resulted in higher concentrations of chl *a*. They also observed that eddy-pumping shallows the subsurface chlorophyll maximum (SCM). To further enhance our understating about the role of eddies in the new and export production, an eddy was identified at 17.8 ^{o}N, 87.5 ^{o}E, with the help of sea surface height anomaly image (source: *http://argo.colorado.edu/∼realtime/gsfc–global-real-time–ssh/*). Water samples were collected at 4 different stations (Fig 3.36); one right at the center of the eddy, two in the proximity of the eddy and one outside the eddy.

Table 3.5: *Station codes, locations of the stations, sea surface temperature (^{o}C; SST), air temperature (^{o}C; T_A), and euphotic depth (m; ED) in the BOB during early winter (Nov-Dec, 2007).*

Station Code	Lat (^{o}N)	Lon (^{o}E)	SST	T_A	ED
BOB-F1	18.6	88.6	28.0	26.0	∼50
BOB-F2	19.0	88.0	27.0	25.5	∼50
BOB-F3	17.8	87.5	27.0	24.0	∼50
BOB-F4	15.6	87.4	27.0	27.5	∼50

During the study period sea surface temperature (SST) varied between 27 and 28 ^{o}C (Table 3.5). No significant variation is observed in the SST between eddy and non-eddy locations. The SST at all the locations are found to be uniform (27 ^{o}C) except at BOB-F1. Constancy of the SST is a consequence of the strong stratification in the BOB due to the influx of fresh water from major rivers (e.g., Ganga, Brahmaputra). *Prasanna Kumar et al* (2007) reported that cyclonic eddies were unable to break the stratification of the top 20 m layer during Fall 2002 and Spring 2003. Although the SST is uniform between eddy and non-eddy locations a large variation in the surface NO_3 concentrations has been observed. Surface NO_3 concentration at BOB-F3 (at the center of the eddy) is found to be ∼1 μM while

it is low (0.3 μM) at BOB-F4 (outside the eddy). Further, NO_3 concentration in the upper 20 m at BOB-F3 is found to be six times higher compared to that at BOB-F4. Euphotic depth is found to be uniform at all the locations in the present study (Table 3.5). However, air temperature shows a large variation from 24.0 to 27.5 ^{o}C.

3.18 Carbon and nitrogen uptake rates

Total primary productivity measurements (using ^{13}C -labelled tracer) were carried out at all the four locations, whereas, at BOB-F3 and BOB-F4, only new and regenerated productivity measurements were carried out (using ^{15}N-labelled tracers).

3.18.1 Carbon uptake rate

Depth profiles of carbon uptake rates are shown in Fig 3.37a. Surface productivity varies from 0.89 to 2.71 μmol C m^{-2}d^{-1} (with an average of 1.53 μmol C m^{-2}d^{-1}). The highest value is found in BOB-F3 (at the center of the eddy) while, the lowest is at BOB-S4 (outside the eddy).

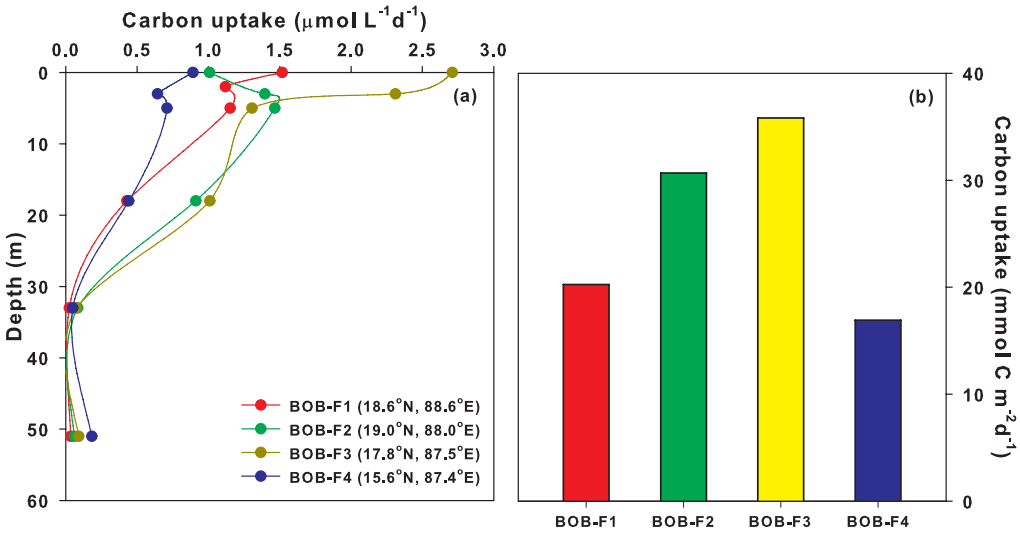

Figure 3.37: *Depth profiles of carbon uptake rate (left) and their euphotic-depth-integrated values (right) at different locations in the BOB during early winter.*

The intermediate surface productivity values are associated with the locations proximal to the eddy. This clearly indicates the role of eddy in enhancing productivity in the BOB. It has been found that the BOB receives minimum light during winter (*Narvekar and Prasanna Kumar*, 2006). During spring (this study) lower light levels are associated with higher surface productivity, the same has been found in early winter too. Higher productivity values are at surface, and they decrease with depth. Although the supply of nutrients by eddy-pumping is higher in the sub-surface (*Prasanna Kumar et al.*, 2007), productivity is lower at those depths. Light limitation in the deep may be responsible for the lower productivity. Similar observations have been made during the late winter in the NE-AS (this study).

Euphotic-depth-integrated carbon uptake rates are presented in Fig 3.37b. It varies from 16.9 to 35.8 mmol C $m^{-2}d^{-1}$ or 202.1 to 429.6 mg C $m^{-2}d^{-1}$ (with an average of 25.9 mmol C $m^{-2}d^{-1}$ or 310.8 mg C $m^{-2}d^{-1}$). At the center of the eddy (BOB-F3), productivity is twice higher than that outside the eddy (BOB-F4). A similar range of productivity ($\sim$180 to $\sim$500 mg C $m^{-2}d^{-1}$) was observed during Fall 2002, under the BOBPS programme. The present study confirms and quantifies that the eddies in the BOB supply nutrients to the surface and thus enhance biological productivity.

3.18.2 Nitrogen uptake rate

New productivity (NO_3 uptake rate) and regenerated productivity (the sum of NH_4 and urea uptake rates) measurements were carried out (using ^{15}N-labelled tracer) at two locations, BOB-F3 and BOB-F4.

New productivity

Depth profiles of NO_3 uptake rate are shown in Fig 3.38a. At the center of the eddy (BOB-F3), surface NO_3 uptake rate is found to be lower than that observed outside the eddy (BOB-F4). This is in contrast to the measured surface productivity. Sub-surface values of NO_3 uptake are higher at BOB-F3 than at BOB-F4.

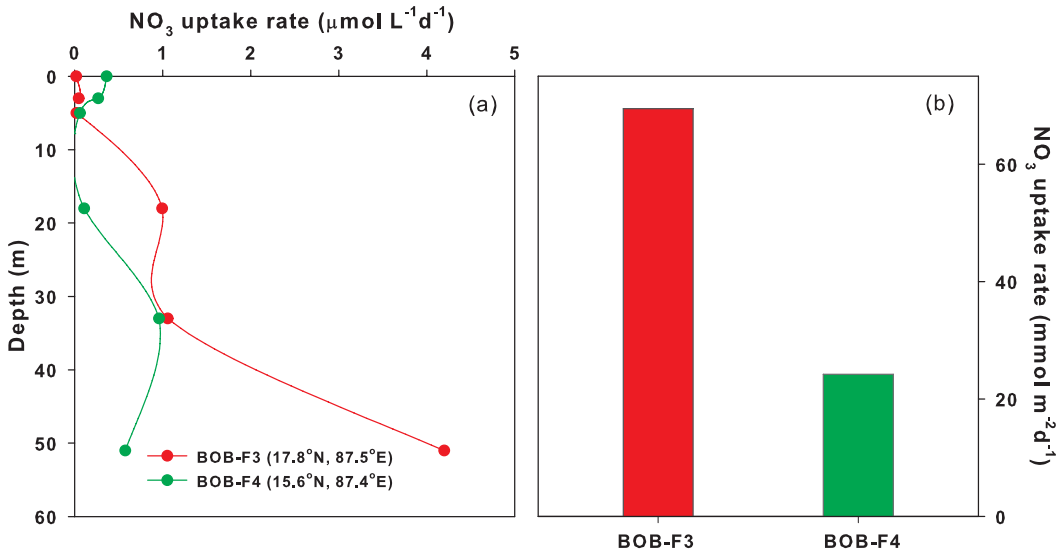

Figure 3.38: *Depth profiles of NO_3 uptake rate (left) and their euphotic-depth-integrated values (right) at different locations in the BOB during early winter.*

This suggests that the higher productivity in the surface at the BOB-F3 is supported by nitrogen from a source other than NO_3, or NO_3 uptake at the surface may be suppressed by some environmental factor (e.g., patchiness of the plankton distribution).

Euphotic-depth-integrated NO_3 uptake for both the locations are presented in Fig 3.38b. It clearly shows that new productivity is much higher at the center of the eddy (BOB-F3) than at outside the eddy (BOB-F4). Eddy-pumping supplies nutrients from deeper depths and enhances new productivity as well. Integrated new productivity is more than twice higher at the center of the eddy than at outside the eddy. In the first 20 m depth, NO_3 concentration is almost seven times higher at the center of the eddy than at outside. The subsequent increase in new productivity in the upper 20 m at the center of the eddy is only thrice compared to that outside. Diminished surface NO_3 uptake rate at the center of the eddy could be the reason for the observed difference in the supply of NO_3 and its subsequent uptake in the first 20 m. Nevertheless, the results clearly show eddy-enhancement of new productivity. This has implications to understand

the comparable downward fluxes of carbon in the BOB and the AS, despite the productivity in the former being lower (for details regarding this "BOB paradox" see *Kumar et al* (2004)).

Regenerated productivity

As before, the uptake rates of NH_4 and urea presented here are the conservative estimates.

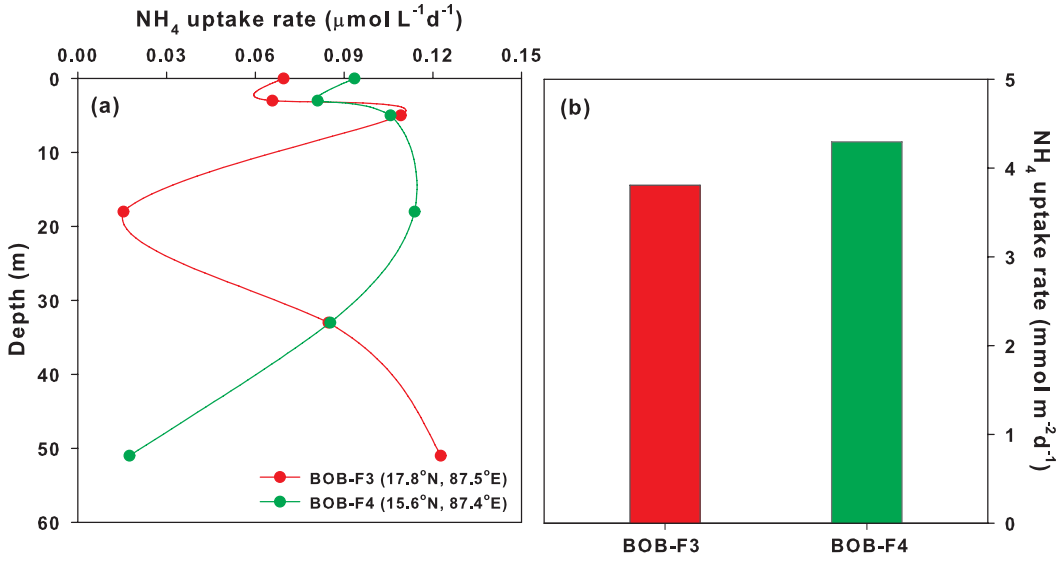

Figure 3.39: *Depth profiles of NH_4 uptake rate (left) and their euphotic-depth-integrated values (right) at different locations in the BOB during early winter.*

Depth profiles of NH_4 uptake rates at both the locations are presented in Fig 3.39a. Surface NH_4 uptake rates are comparable at both the locations. The average surface NH_4 uptake rate is found to be 0.08 μmol N $m^{-2}d^{-1}$, which is lower than the average NO_3 uptake rate. As in the case of NO_3, higher values are associated with the middle depths at the center of the eddy. Euphotic-depth-integrated NH_4 uptake rate is slightly higher outside the eddy than at its center. This is in contrast with carbon uptake and new productivity, both of which show higher values at the center. Denitrification is not prominent in the BOB and thus, the deeper waters in the BOB are in general not depleted in NO_3. Therefore, as a result of eddy-pumping, deeper water mostly carries oxidized forms of nitrogen (e.g., NO_3) to the

surface. This is reflected in the observed higher NO_3 uptake at the center of the eddy. In other words, uptake rates of NH_4 could be suppressed by eddy-pumping in the region.

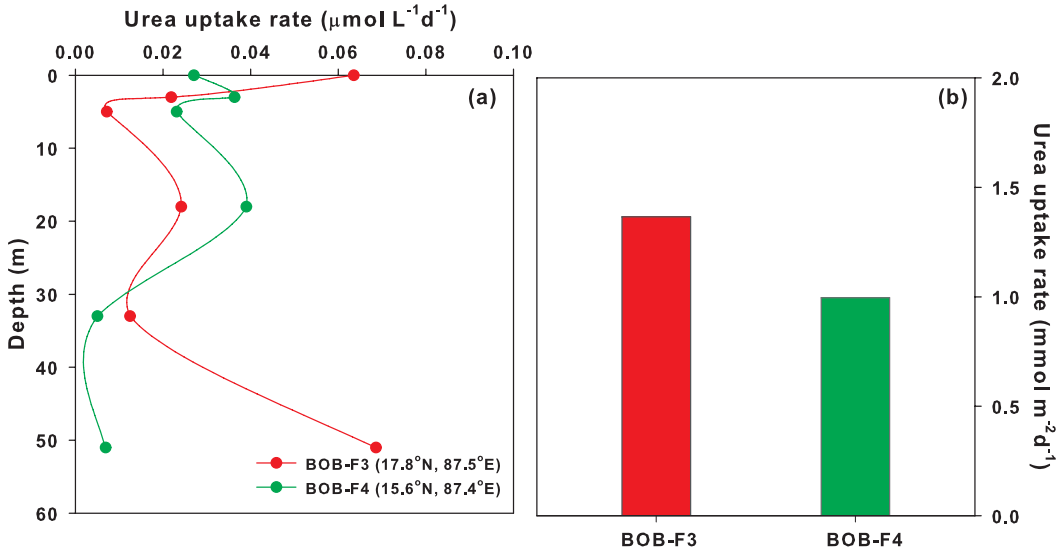

Figure 3.40: *Depth profiles of urea uptake rate (left) and their euphotic-depth-integrated values (right) at different locations in the BOB during early winter.*

Depth profiles of urea uptake rate at both the locations are presented in Fig 3.40a. Its surface value at the center of the eddy is half of that outside. The average surface urea uptake rate is found to be 0.05 μmol N $m^{-2}d^{-1}$, lower than the average NO_3 and NH_4 uptake rates. As in the cases of NO_3 and NH_4, higher values are associated with mid-depths at the center of the eddy. In contrast to NH_4 uptake, euphotic-depth-integrated values of urea uptake are slightly higher at the center of the eddy than outside (Fig 3.40b). Nevertheless, the urea uptake rates are much less than the NO_3 and NH_4 uptake rates. This suggests that urea is the least preferred nitrogenous substrate during early winter, which is also seen during spring in the BOB.

3.18.3 *f*-ratio

As the NH_4 and urea uptake rates are the conservative estimates, the f-ratio estimated here is the upper bound of f-ratio in the region. At both the locations f-

ratio is found to be quite high >0.8. The difference between the center and outside the eddy is minor. The NH_4 and urea uptake rates are conservative estimates, and this could be a reason for such higher f-ratio here. However, *Kumar et al* (2004) also reported f-ratios close to 0.8 during fall 2002 at some locations in the central BOB. Supply of NO_3 to the surface by the eddy contributes to the higher new production at the center of the eddy, while the transport of unutilized NO_3 from the center to the surrounding areas may contribute to the new production there. Therefore, both the locations show high new production as well as f-ratios. The higher f-ratio implies that the BOB can transfer most of its total production to the deep when assisted by eddies.

3.18.4 C:N consumption ratio

Depth profiles of the ratio of the measured carbon and total nitrogen (the sum of NO_3, NH_4 and urea) uptake rates are presented in Fig 3.41.

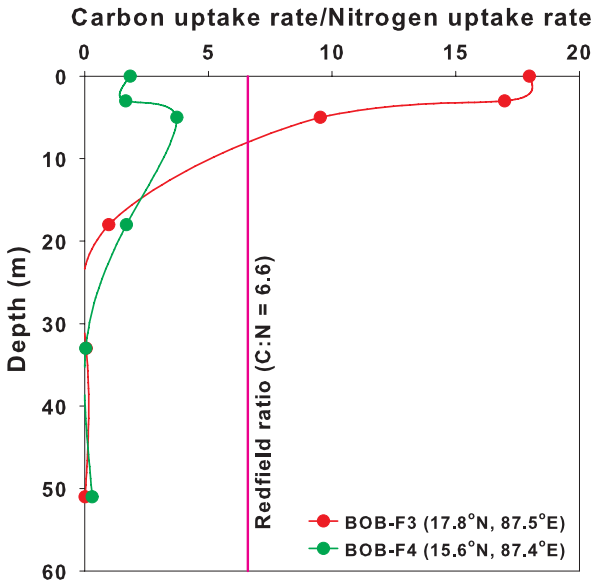

Figure 3.41: *Depth profile of the ratio of the observed C to N uptake rate at different locations in the BOB during early winter. Pink line represents the Redfield ratio (C:N = 6.6).*

A large variation is seen in the C:N ratio between the center and outside the eddy. At the center its value is more than 17, while outside it is low (∼2). The

common feature at both the locations is that the ratio is higher in the surface layers and it decreases with depth (Fig 3.41). As discussed earlier, the ratio mainly depends on the relative availability of nitrogenous nutrients, the plankton composition, and the availability of sun light. It quite evident that at the center and outside the eddy, nitrogenous compounds are in different proportions. This might significantly contribute to the observed difference in the C:N ratios.

3.19 Part IV: Conclusion

An eddy was identified at 17.8 ^{o}N, 87.5 ^{o}E in the northern BOB during early winter 2007 for productivity measurements. Eddy and non-eddy locations show a large variation in the surface NO_3 concentrations. NO_3 concentration in the upper 20 m at the center is found to be six times higher than that outside. The highest surface productivity is found to be at the center of the eddy while the lowest, outside. The intermediate surface productivity values are associated with the locations proximal to the eddy. Euphotic-depth-integrated productivity is found to be twice higher at the center of the eddy than that outside. The observed values are consistent with earlier reported values from an eddy region in the BOB under the BOBPS programme. This confirms the role of eddies in enhancing productivity in the BOB. As seen in carbon uptake, the integrated new productivity is also more than twice higher at the center than outside. Such variations are not seen in the NH_4 and urea uptake rates, which were much lower. Overall, NO_3 is the most preferred nitrogenous substrate by phytoplankton within the eddy. Higher new productivity and f-ratios observed within eddy suggest that eddies aid in exporting most of the total production to the deep.

Chapter 4

New and Primary productivity in the equatorial Indian Ocean

4.1 Introduction

The Equatorial Indian Ocean (EIO, 10^oN to 10^oS) lies to south of the Indian subcontinent and is quite far from coastal influences . The EIO is different from other equatorial regions of the world ocean because of the reversal of the monsoon winds twice a year due to which the surface currents reverse semiannually. Unlike the Pacific and the Atlantic, the equatorial undercurrent here exists only during winter (Dec-Mar). The general oceanic circulation and water masses are described in this section.

4.1.1 Climatology and circulation patters

Winds and oceanic currents

In the EIO, winds are weaker during the peak monsoon seasons (Fig 4.1). Climatological winds in the EIO are related to the seasonal north-south migration of the Tropical Convergence Zone (TCZ). The TCZ is centered around the equator in spring and fall, leading to strong westerlies during these seasons (*Beaufort et al.*, 1999). In both seasons the winds are zonal, blowing from the west as a response to the pressure gradient between the western Indian Ocean (highs), and the Indone-

sian tropical warm pool (lows). The strongest intra-seasonal westerly winds are located a few degrees north (south) of the equator in Jun-Sep (Jan-Mar). Intra-seasonal convection over the EIO is centered more or less on the equator in summer, but somewhat to the south of the equator in Jan-Mar (*Senan et al.*, 2003). In the EIO, a strong jet like current flows to the east in response to the westerlies, causing the thermocline to rise in the west and depression in the east (*Wyrtki*, 1973). This surface jet flows with velocities of 0.7 ms^{-1} or more. These jets are equatorially trapped and approximately 500 km wide. *Senan et al* (2003) show westerly wind-bursts lasting 10-40 days, associated with atmospheric convection in the eastern EIO, which have the potential to produce intra-seasonal eastward equatorial jets in the ocean. They also observed that the strong westerly bursts associated with summer monsoon intra-seasonal oscillations can drive monsoon jets in the eastern EIO. The summer monsoon winds dominate the annual cycle, so that the annual-mean wind field has a structure much like that in July. Because of this forcing, significant upwelling does not occur along the equator in the Indian Ocean, but rather in the northern hemisphere off Somalia, Oman, and India. The upwelled water comes from depths of 200- 300 m, occasionally with temperatures colder than 15 ^oC and densities in excess of 26.5 kg m^{-3} (*Schott and McCreary*, 2001). These temperatures and densities correspond to those in southern mid-latitudes near 40^oS, and the relatively low salinity of the water upwelled off Somalia also clearly identifies it as being of southern-hemispheric origin (*Fischer et al.*, 1996). Hence, the zonally integrated meridional circulation has a shallow overturning cell, with a northward subsurface branch supplying the northern-hemisphere upwelling and a southward surface branch returning it to the southern Indian Ocean. Moreover, there is a net southward heat transport associated with this flow since the subsurface branch imports cool water into the northern hemisphere and the surface branch exports warm water. This circulation is called the cross-equatorial cell (CEC). There are two other shallow overturning cells in the Indian Ocean. One is closed by upwelling in a band from 5^oS to 10^oS in the central and western parts,

called the subtropical cell (STC). It is driven by the negative wind-stress curl in the region associated with the equatorward weakening

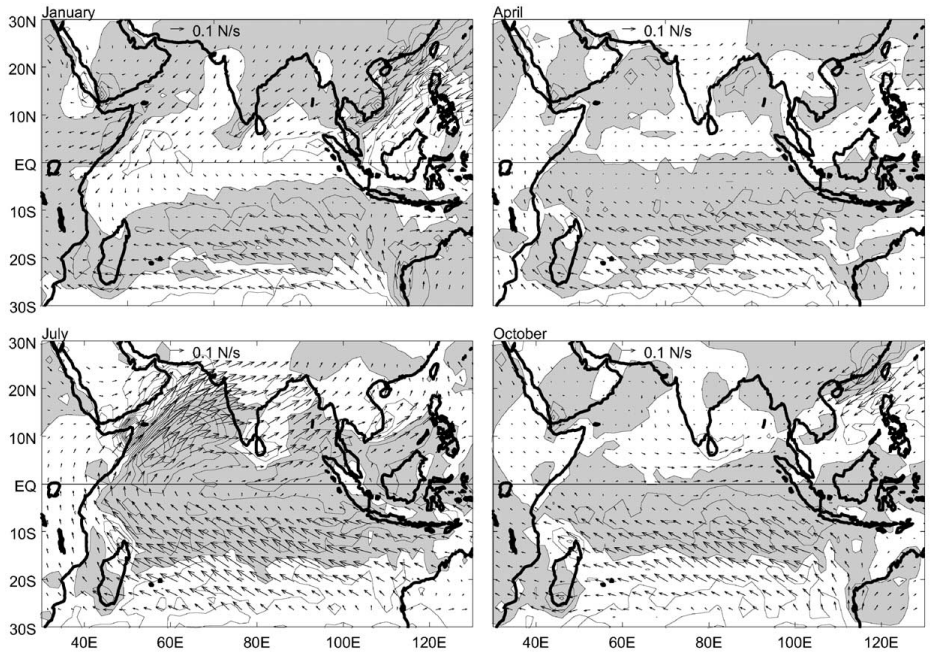

Figure 4.1: *Wind-stress (arrows) and wind-curl (contours) fields for the Indian Ocean. The contour interval for wind curl is 10^{-7} N m^{-3}, and negative values are shaded. (Source: Miyama et al., 2003).*

of the Southeast Trades. The isopycnals rise close to the surface in the region, but sea surface temperature (SST) does not show any indication of upwelling in the region (*Spencer et al.*, 1982; *Wyrtki*, 1988; *Levitus and Boyer*, 1994; *Levitus et al.*, 1994). While satellite ocean colour data indicates the presence of phytoplankton bloom (*Murtugudde et al.*, 1999) in this band, attributable to the upwelling caused by the overturning cells. The other cell is associated with upwelling in the eastern equatorial ocean, along the Java and Sumatran coasts, in the Arafura Sea, and occasionally along the equator; it can be viewed as an eastern branch of the STC (eastern STC).

Water masses

You and Tomczak (1993) have reviewed the water masses in the Indian Ocean and their characteristics in the upper Indian ocean. They observed the presence

of the Bay of Bengal water in the surface layer of the EIO. They also described that the Red Sea water and Persian Gulf water (Arabian Sea High Salinity Water, ASHSW), the Australasian Mediterranean water (AAMW) which originates from the deep basins of the Australasian Mediterranean Sea and the Indian Central water (ICW) subducted in the subtropical Convergence of the Southern Hemisphere. *Sardessai et al* (2010) observed four water masses in the eastern EIO. The surface layer with low salinity waters is dominated mainly by the waters from the northeastern Indian Ocean and the Indonesian through flow (ITF). The surface waters are also enriched with nutrients with SiO_4, showing the highest enrichment in winter, spring and summer. The subsurface waters, the depth of which varies temporally and spatially, are strongly influenced by the ASHSW and carries the signatures of NO_3 deficits and oxygen minimum layer and low Nitrate/Phosphate (N:P) ratio. Two distinct water masses were identified below the subsurface waters (>200m) towards the north and south of the equator. Below the subsurface waters (>200m), the Australasian Mediterranean Waters towards the south is identified by relatively less saline waters and higher oxygen, whereas the water mass towards the north of the equator identified as the Indian Central water, is characterized by higher salinity, lower oxygen levels and higher nutrients at shallower depths. In general, nutrients are higher towards the north than to the south of the equator. This is attributed to physical forcings such as zonal currents, equatorial under currents and elevation of the thermocline to shallower depths. Nitrate deficits and low N:P ratio waters from the Arabian Sea are found below 1000 m in the eastern EIO (*Sardessai et al.*, 2010).

In terms of biological productivity, satellite ocean colour data suggest that the equatorial Atlantic and Pacific are more productive than the equatorial Indian ocean. Spatial variation is observed in the exchange of CO_2 with atmosphere in the region. The regions between 10^oN-20^oS appears as perennial sources of CO_2 to the atmosphere (*Bates et al.*, 2006), while the region between 20^oS-35^oS acts as sink. Further, seasonal variation also persists in the Net community production

(NCP). The maximum rates of NCP are observed during the winter and spring. In addition, during summer and fall, the trophic status appears to shift from net autotrophy to net heterotrophy in the 10^{o}N-20^{o}S zone. In spite of the above unique features of the EIO, the upper ocean variability in terms of primary productivity is poorly studied and understood. The primary reason for this is the inadequacy of observations. The present study of simultaneous measurements of carbon and nitrogen uptake rates using ^{13}C and ^{15}N tracers is the first of its kind from this important basin.

4.2 Hydrographic and meteorological parameters

Typical summer monsoonal conditions were observed during the study period. Strong winds, precipitation and cloudiness were observed. Environmental parameters recorded at the sampling locations (Fig 4.2) are listed in Table 4.1.

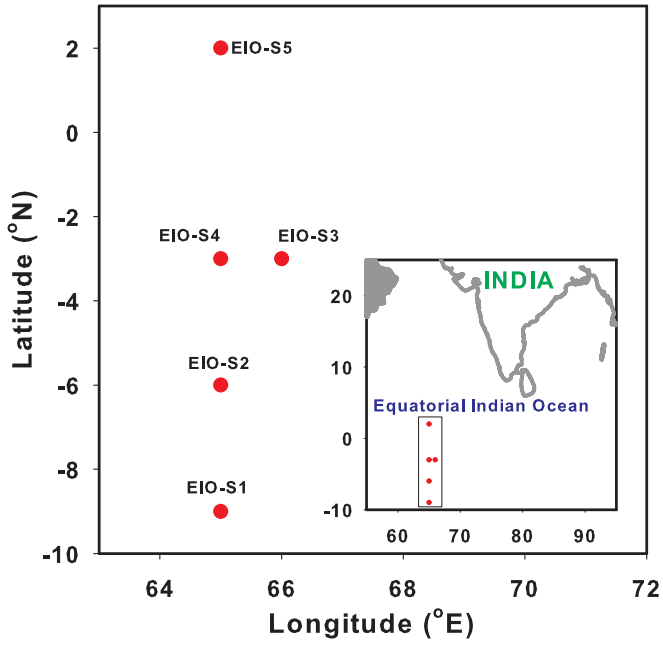

Figure 4.2: *Sampling locations in the Equatorial Indian Ocean (EIO) during summer (July-Aug, 2008).*

Winds were stronger to the south of the equator and varied from 2 to 6.5

ms^{-1}. Strong cloudiness suppressed photosynthetically active radiation (PAR) (Table 4.1). PAR was as low as 164 μmol $m^{-2}s^{-1}$ at the southern most sampling location. The highest PAR was observed near the equator. No north-south pattern was seen in the PAR values, which varied with the presence of clouds. Euphotic depth varied from 80 to 103 m. Mixed layer depth (MLD) was found to be always shallower than the euphotic depth, varying between 60 and 75 m. Variations in temperature and salinity are discussed in the next section.

Table 4.1: *Station code, station location, sea surface temperature (^oC; SST), surface salinity, mixed layer depth (m; MLD), euphotic depth (m; ED), Photosynthetically active radiation ($\mu mol\ m^{-2}s^{-1}$; PAR), and surface wind speed (ms^{-1}; V_w) at different sampling locations.*

Station code	Lat (^{o}N)	Lon (^{o}E)	SST	Salinity	MLD	ED	PAR	V_w
EIO-S1	-9	65	26.0	35.0	60	80	164	6.5
EIO-S2	-6	65	27.0	34.4	65	84	401	5.5
EIO-S3	-3	66	28.0	34.9	60	100	198	3.3
EIO-S4	-3	65	28.0	35.1	75	88	213	4.0
EIO-S5	2	65	28.5	35.2	75	103	580	2.5

4.2.1 Temperature and salinity

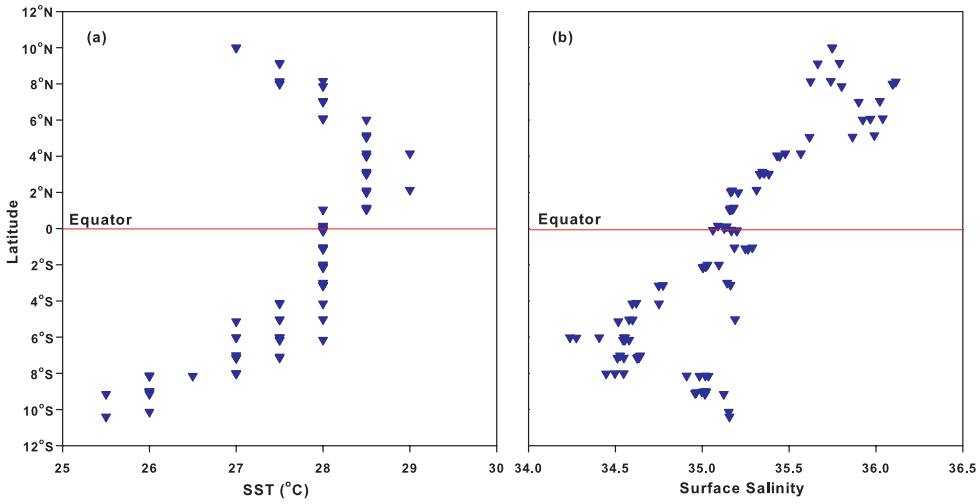

Figure 4.3: *Latitudinal variation in (a) SST, and (b) surface salinity across the equator at 65^{o}E longitude.*

During the present study sampling was done along the 65^{o}E transect. Meteorological parameters were recorded at every 3 hours interval. Sea state was 8 (near "Gale" conditions) and the sea quite rough, particularly to south of the equator. Latitudinal variations in sea surface temperature (SST) and salinity are shown in Fig 4.3. High SST at the equator and a gradual decrease in either side indicate convergence of water masses at the equator (Fig 4.3a). Similarly, a general increasing trend in salinity is found on either side, away from the equator (Fig 4.2b). The highest SST (>29 ^{o}C) is observed near the equator, while the lowest SST is associated with 10^{o}S. In contrast, surface salinity value is the lowest near the equator. To the south of 6^{o}S, low salinity and SST indicate the advection of low saline and colder water to the region.

The low salinity surface water mass in the EIO could have originated from the Bay of Bengal. *Sengupta et al* (2006) reported that the low salinity surface water mass in the EIO is formed due to excess precipitation over evaporation, which characterizes the northeastern part (Bay of Bengal) of the Indian Ocean.

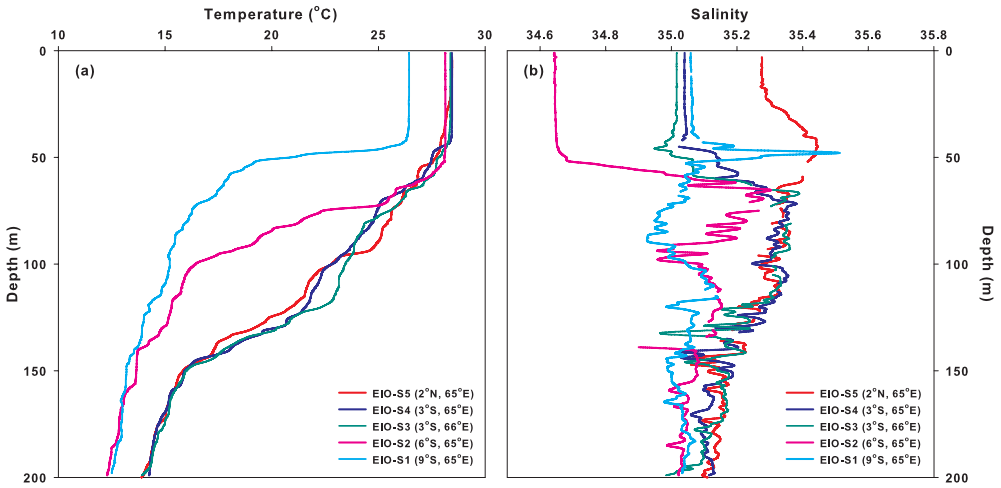

Figure 4.4: *Depth profiles of (a) temperature and (b) salinity at different sampling locations in the EIO.*

Depth profiles of temperature and salinity are shown in Fig 4.4. Thermocline shoals up towards south of the equator (Fig 4.3a), as also reported by *Sardessai et*

al (2010). A signature of rigorous mixing is seen in the depth profiles of salinity (Fig 4.3b). Large variations in the salinity profiles are observed between 2^{o}N-9^{o}S, suggesting mixing of different water masses in this small latitudinal belt, as reported by *Sardessai et al* (2010).

4.2.2 Nutrients and dissolved oxygen

In the EIO, nutrients generally show an asymmetric distribution at different depths and are regulated by the seasonally varying physical processes such as thermocline elevation, meridional and zonal transports, equatorial undercurrent and elevation of nutrient replete waters north of the equator, and sinking of nutrient-poor water towards the equator driven by tropical wave instability (*Evans et al.*, 2009).

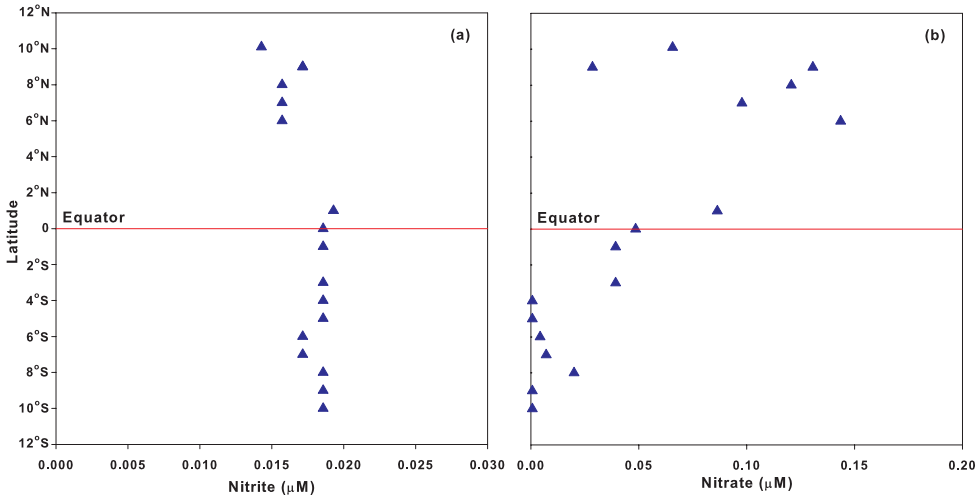

Figure 4.5: *Latitudinal variation of surface concentrations of (a) NO_3 and (b) NO_2 across the Equator at 65^{o}E longitude.*

The latitudinal variation of surface concentrations of NO_3 and NO_2 across the equator at 65^{o}E longitude is shown in Fig 4.5. NO_3 concentrations were lower throughout the transect with a large variation on either side of the equator. An increasing trend is seen from north to south in the surface NO_3; no such variation is ob served for the surface NO_2. The longitudinal variation of NO_3 shows the prominent oligotrophic conditions in the south compared to the north.

The distribution of nutrients (NO_2, NO_3, PO_4, and SiO_4) down to 200 m at the 65^{o}E transect are shown in Fig 4.6. To the south of the equator, the surface layer is devoid of nutrients.

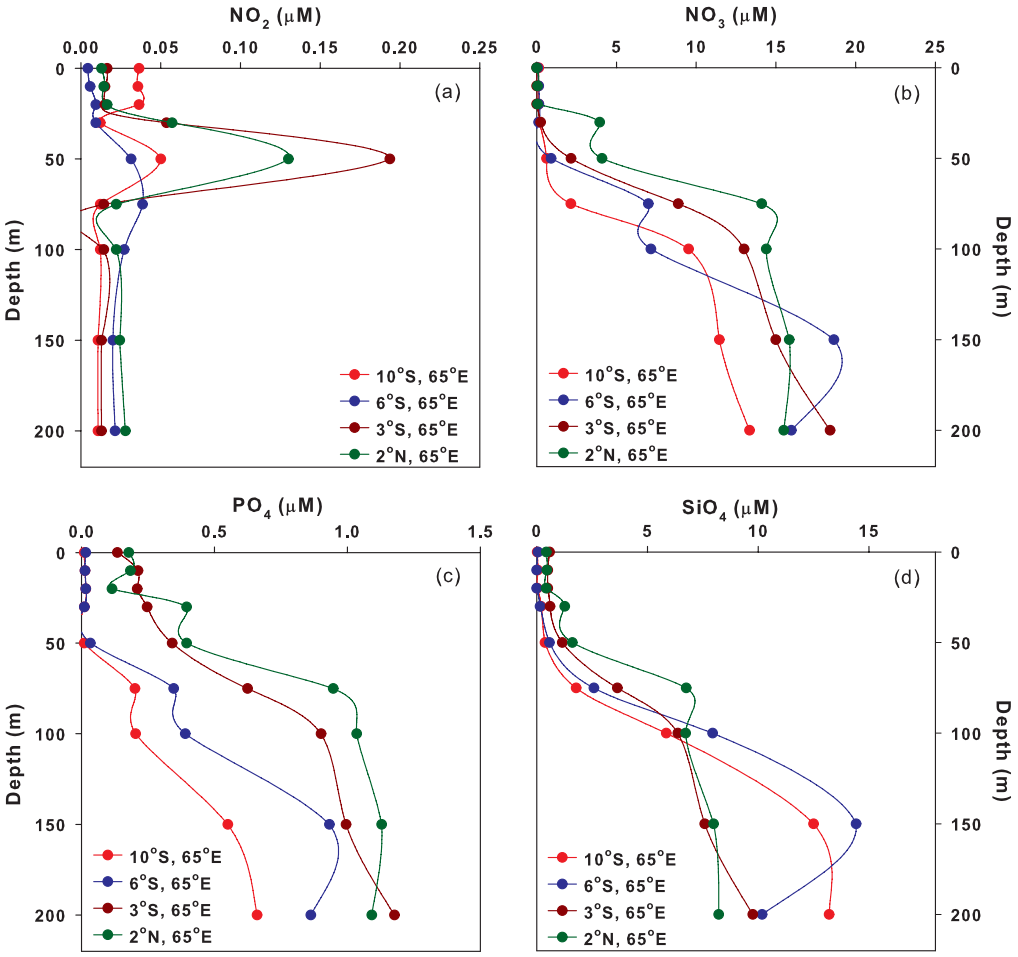

Figure 4.6: *Depth profiles of (a) NO_2, (b) NO_3, (c) PO_4, and (d) SiO_4 concentrations at different sampling locations in the EIO.*

NO_2 concentrations are lower throughout the upper 200 m waters at all the locations (Fig 4.6a). A sudden peak in NO_2 is observed at 50 m depth near the equator. This sub-surface maximum could be a signature of denitrified waters from the Arabian Sea. A progressive increase in the NO_3 concentrations with depth is found (Fig 4.6b). The upper 40 m waters are devoid of NO_3. Lower N:P ratio (below the Redfield Ratio) is observed at 50 m depth near the equator,

which also confirms the input of denitrified subsurface water from the Arabian Sea. Interestingly in the first 100 m, NO_3, PO_4, and SiO_4 concentrations are lower to the south. A nutrient depleted water mass is probably mixing there (Figs 4.6). The water mass is also pushing the thermocline upward (Fig 4.4a). Overall, the surface water in the EIO shows oligotrophic conditions during the study period. The pattern of PO_4 distribution to the south (Fig 4.6) shows marked changes compared to NO_3 with a steep rise in the surface as well as subsurface concentrations towards the equator. The signatures of physical forcings could be seen in the pattern of distribution of SiO_4 but such variations are limited to depths below 100 m.
At the transect average N:P ratio in surface is <3 during our observations. The ratio decreases sharply in subsurface layers and reaches <0.5 at 50 m depths in the south.

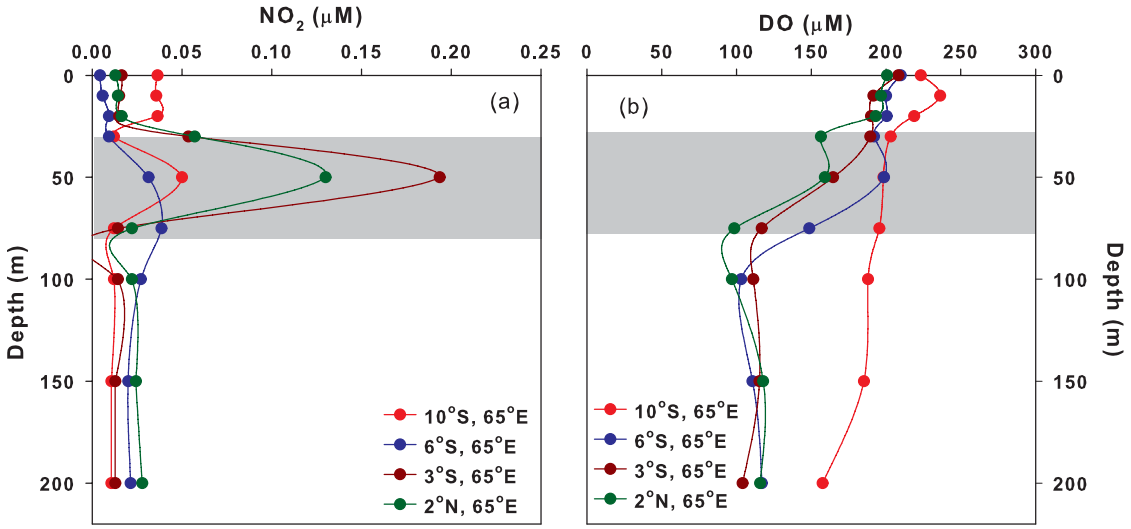

Figure 4.7: *Depth profiles of (a) NO_2, and (b) dissolved oxygen (DO) concentrations at different sampling locations in the EIO.*

The low N:P ratio indicates NO_3 deficit conditions even at the surface. This could be due to the influence of denitrified waters from the Arabian Sea. Depth profiles of NO_2 shown with the dissolved oxygen (DO) profiles are useful to verify this (Fig 4.7). A sharp increase in the NO_2 coincides with a slight decline in the DO (Fig 4.7). However, the decline in the DO values are not as prominent as observed

in NO_2. Nevertheless, this gives an indication of the influence of denitrified water in the subsurface layers. Arabian Sea denitrified waters in the subsurface of the equator region (upto 5^{o}S) have also been identified earlier (*Sardessai et al.*, 2010).

4.3 Carbon and Nitrogen uptake rates

Productivity measurements were conducted at 5 different stations, shown in Fig 4.2. At all the five locations total primary productivity measurements were carried out (using ^{13}C-labelled tracer), whereas, only at EIO-S2, EIO-S3 and EIO-S5, new and regenerated productivity measurements were carried out (using ^{15}N-labelled tracers).

4.3.1 Carbon uptake rates

Depth profiles of carbon uptake rates at different sampling locations are shown in Fig 4.8a. They vary from <0.2 μmol C L^{-1}d^{-1} to more than 1.0 μmol C L^{-1}d^{-1} in the surface waters. As PAR is found low (Table 4.1), no correction is made in the surface productivity values for the effect of incubation during different times of the day (as found in the NE-AS during late winter in this study).

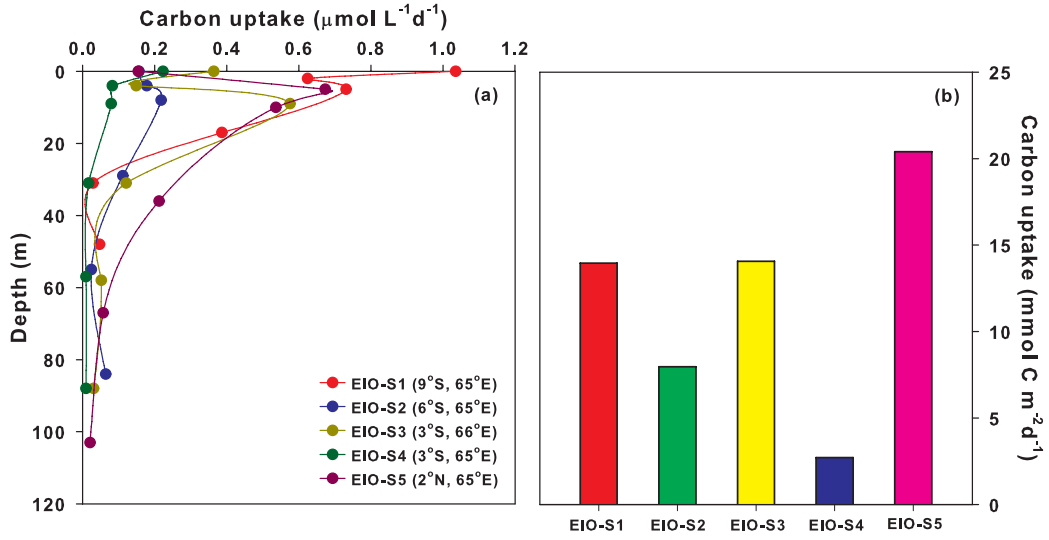

Figure 4.8: *Carbon uptake rates (a) depth profiles and (b) euphotic-depth-integrated values at different sampling locations in the EIO.*

The average surface carbon uptake is 0.4 μmol C $L^{-1}d^{-1}$. The highest surface carbon uptake is at the southernmost station (9^{o}S 65^{o}E), while the lowest is at the northern most station (2^{o}N 65^{o}E). Although nutrient concentrations are lower in the surface, most of the carbon uptake is confined to the upper 10 m (Fig 4.8a). In contrast, layers below 10 m, which contain higher nutrients, show almost an order of magnitude less carbon uptake rates. The decrease in carbon uptake with depth could be due to the reduced availability of light at different depths as light intensity decreases exponentially with depth. Overall, the depth variation in carbon uptake rates can be attributed to light variations. However, surface carbon uptake rate shows the opposite trend, it decreases with increase in surface light intensity (Fig 4.9). Euphotic-depth-integrated carbon uptake rates varied from 2.8 to 20.4 mmol C $m^{-2}d^{-1}$ (33 to 245 mg C $m^{-2}d^{-1}$). Average uptake is 11.0 mmol C $m^{-2}d^{-1}$ (131 mg C $m^{-2}d^{-1}$).

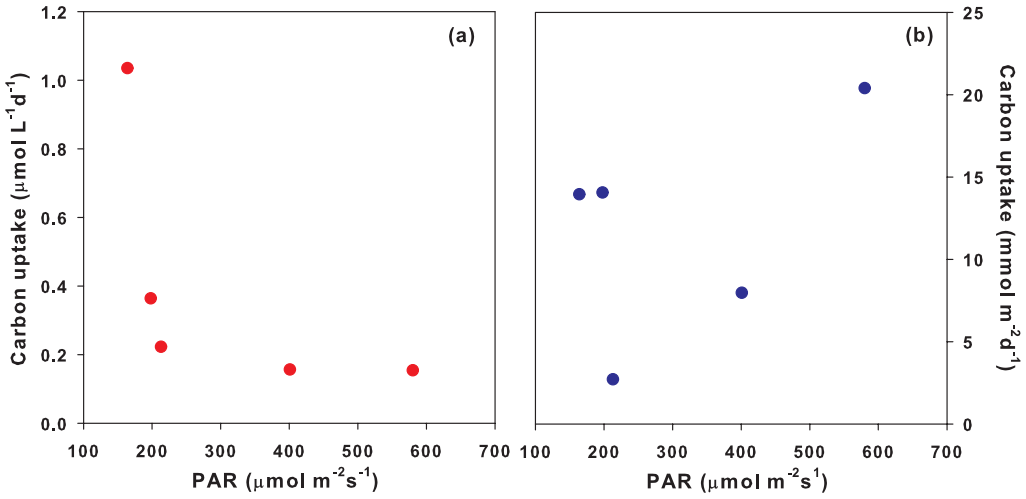

Figure 4.9: *Variation of (a) surface carbon uptake rate and (b) euphotic-depth-integrated carbon uptake rates with PAR at different sampling locations.*

The highest integrated carbon uptake is found at the northern most station (2^{o}N 65^{o}E). Surprisingly, at this location surface carbon uptake rate is the lowest among all the stations. At 2^{o}N 65^{o}E, MLD and euphotic depth, and surface PAR are the highest among all the stations. This indicates that higher PAR enhances

the column productivity. On the other hand, surface productivity is suppressed by high surface light intensity. The lowest column carbon uptake rate is found at the nearby location, 3^oS 65^oE. There are not much differences in the availability of nutrients and MLD at these two locations (Fig 4.6; Table 4.1). However, surface PAR value at the latter location is almost one third of the value observed at the former. This supports the above inference that higher PAR value increases column productivity, while other parameters remain constant. Overall, the surface productivity decreases with increasing surface light intensity (Fig 4.9a). In general, column productivity increases with surface light intensity (Fig 4.9b). Although PAR is lower EIO-S1 (9^oS 65^oE) and EIO-S3 (3^oS 66^oE) show relatively higher column productivity. This could be due to the support from the other favorable parameters such as nutrients.

Ryther et al (1966) reported productivities of 20 to 310 mg C $m^{-2}d^{-1}$ (with an average 158 mg C $m^{-2}d^{-1}$) for the period Jun-Aug based on ^{14}C method for the region. Our values are comparable with values reported by *Ryther et al* (1966). *Qasim* (1977) compiled data from 45 cruises and observed that productivity in the equatorial region is between 150-250 mg C $m^{-2}d^{-1}$. Most of our sampling stations confirm the range reported by *Qasim* (1977). The comparison of the present data with the earlier data indicates that productivity in the EIO has not changed very significantly even after decades. Overall, the EIO is low productive even during the summer monsoon, which the enhances productivity up to 2500 mg C $m^{-2}d^{-1}$ in the Arabian Sea. Generally, productivity is mainly controlled by the availability of nutrients and light. Nutrient dynamics in the region are mainly controlled by the mixing of water masses of different origins. Such processes are highly variable on spatial as well as seasonal scales. Denitrified water from the Arabian Sea and low saline water from the Bay of Bengal have been identified in the study area. Apart from the nutrients, it has been found in the present study that the surface light intensity plays a significant role in controlling surface as well as column productivity.

4.3.2 Nitrogen uptake rates

New productivity (NO_3 uptake rate) and regenerated productivity (the sum of NH_4 and urea uptake rates) measurements were carried out (using ^{15}N-labelled tracer) at EIO-S2, EIO-S3 and EIO-S5.

New productivity

Depth profiles of nitrate uptake rate at different sampling locations are shown in Fig 4.10a. The new productivity varies from <0.04 μmol N $L^{-1}d^{-1}$ to 0.05 μmol N $L^{-1}d^{-1}$ in the surface waters. The highest surface new productivity is at EIO-S2 (6^oS 65^oE), while the lowest is found at northern most station EIO-S5 (2^oN 65^oE).

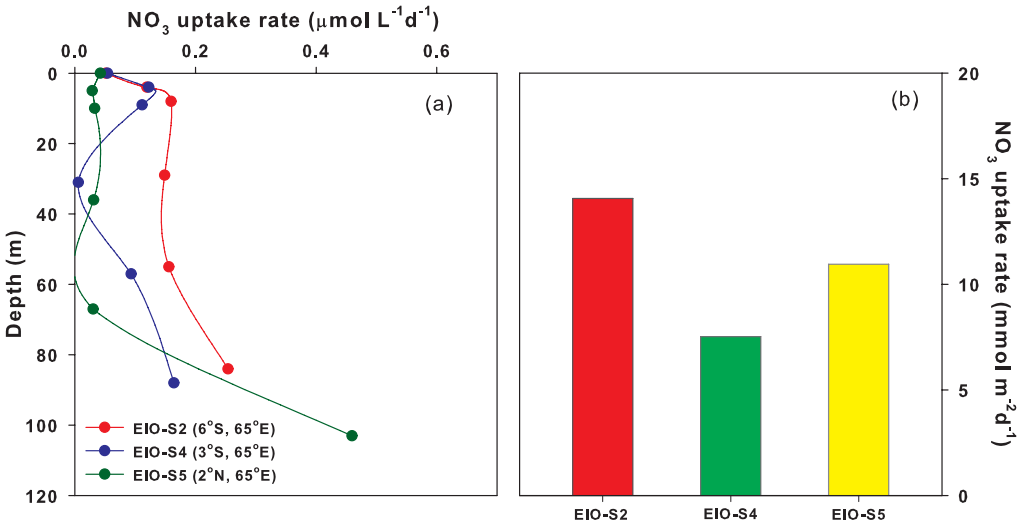

Figure 4.10: *NO_3 uptake rates (a) depth profiles and (b) euphotic-depth-integrated values at different sampling locations in the EIO.*

The average surface new productivity is 0.05 μmol N $L^{-1}d^{-1}$. In contrast to the carbon uptake rate, new productivity is higher in the subsurface waters. At all the locations, the highest new productivity is associated with the lowest light level. The pattern follows the variation of NO_3 (Fig 4.6b) rather than variation in light. This suggests the control of nutrient availability on the new productivity in the region.

Euphotic-depth-integrated new productivity varies from 7.5 to 14.1 mmol N

$m^{-2}d^{-1}$ (with an average 10.8 mmol N $m^{-2}d^{-1}$) (Fig 4.10b). The highest column new productivity is at EIO-S2 (6^oS 65^oE), which shows the highest surface new productivity too. This is in contrast to the data on the uptake of carbon. In carbon uptake rate, the highest column productivity location shows the lowest surface value.

Prakash (2008) measured new productivity in the EIO at two transects, 77^oE and 83^oE during pre monsoon 2005. He found very high new productivity, 12 to 160 mmol N $m^{-2}d^{-1}$, across the equator. The northern part showed higher new productivity along the 83^oE transect, while the southern part exhibited higher values along the 77^oE transect. In the present study, new productivity measurements are limited to the south of the equator. New productivity values from the present study are far below that obtained by *Prakash* (2008). The discrepancy could be because the present study and *Prakash* (2008) study were carried out in different seasons (summer monsoon vs. pre monsoon) and also along different longitudinal transects (65^oE versus 77^oE and 83^oE). He also found a large variability in new productivity between 77^oE and 83^oE transects. It is very unlikely that the discrepancy between the present data and those of *Prakash* (2008) is due to climate change, as the time lag between these two studies is not much. In addition, carbon uptake data show no sign of change; our values in are comparable to those obtained more than 3 decades ago by *Ryther et al* (1966) and *Qasim* (1977).

Regenerated productivity

As earlier, the rates given here are conservative estimates for NH_4 and urea uptake. Depth profiles of NH_4 uptake rates at different sampling locations are shown in Fig 4.11a. Surface uptake rate of NH_4 does not show much variation and remains between 0.01 and 0.02 μmol N $L^{-1}d^{-1}$ (with an average of 0.01 μmol N $L^{-1}d^{-1}$). The values are 3 times lower than those of observed for NO_3 uptake. The highest surface NH_4 uptake is found at EIO-S5 (2^oN 65^oE), which shows the lowest surface NO_3 uptake. No trend has been observed for NH_4 uptake with depth. The NH_4

uptake profile at EIO-S2 is quite different from the profiles at EIO-S3 and EIO-S5. At all the locations, the maximum NH_4 uptake rate is associated with the lowest light level. Nevertheless, at EIO-S2 and EIO-S3, comparable values with the maximum values are found at mid-depths. Euphotic-depth-integrated NH_4 uptake rates are shown in Fig 4.11b.

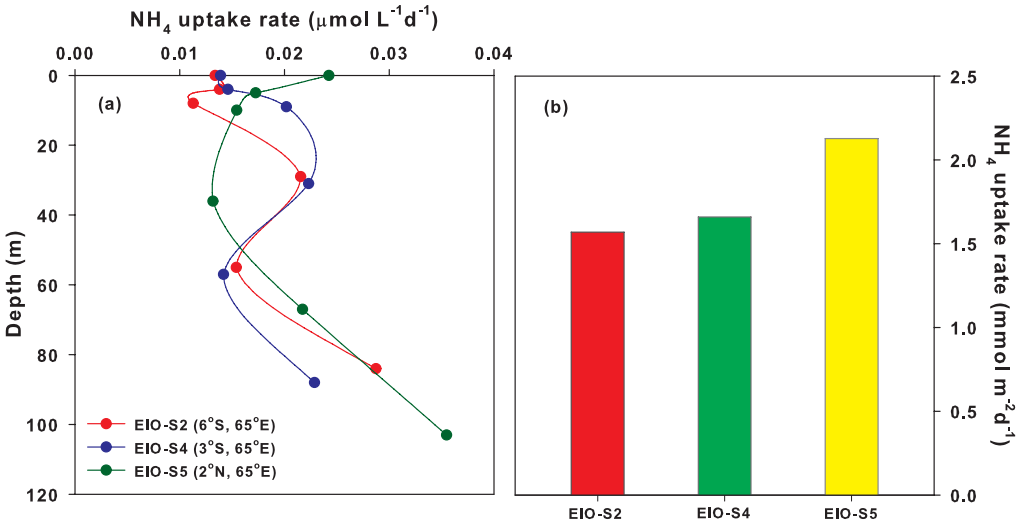

Figure 4.11: *NH_4 uptake rates (a) depth profiles and (b) euphotic-depth-integrated values at different sampling locations in the EIO.*

Depth-integrated uptake rate of NH_4 decreases to the south. It varies from 1.5 to 2.1 mmol N $m^{-2}d^{-1}$ (with an average mmol N $m^{-2}d^{-1}$), and is 6 times lower than that of NO_3. The highest integrated uptake rate is observed at EIO-S5 (2^oN 65^oE), which also shows the highest surface uptake. *Prakash* (2008) reported NH_4 uptake rates from 1.14 mmol N $m^{-2}d^{-1}$ to 2.17 mmol N $m^{-2}d^{-1}$ along 77^oE transect and from 1.26 mmol N $m^{-2}d^{-1}$ to 2.44 mmol N $m^{-2}d^{-1}$ along the 83^oE transect in the EIO during pre monsoon 2005. NH_4 uptake rates from the present study are in good agreement with his values. This is in contrast with the comparison of NO_3 uptake rates from both the studies.

Depth profiles of urea uptake rates at different sampling locations are given in Fig 4.12a. They vary between 0.02 and 0.03 μmol N $L^{-1}d^{-1}$ (with an average of 0.03 μmol N $L^{-1}d^{-1}$), and are less than those of NO_3 uptake, but higher than those of

NH_4 uptake.

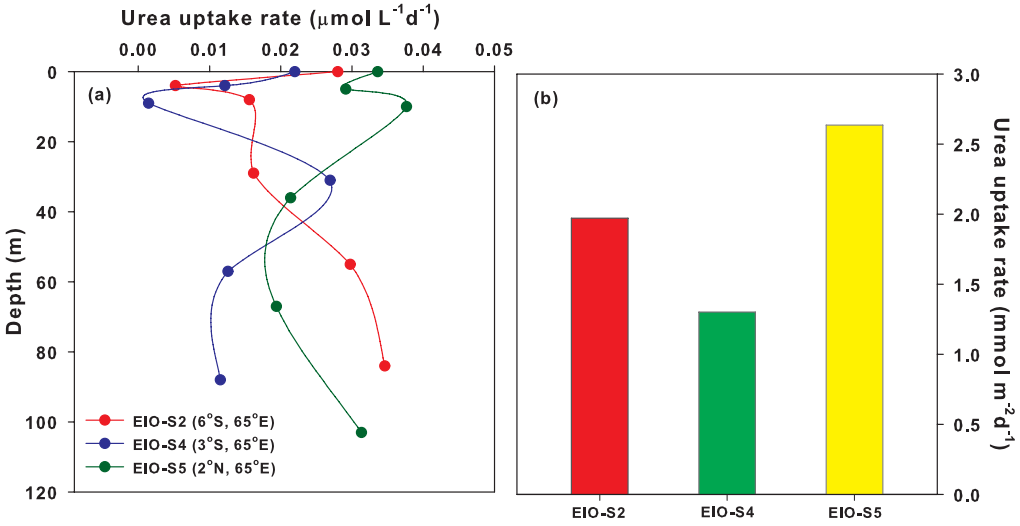

Figure 4.12: *Urea uptake rates (a) depth profiles and (b) euphotic-depth-integrated values at different sampling locations in the EIO.*

The highest surface urea uptake is at EIO-S5 (2^oN 65^oE), which shows the lowest surface NO_3 uptake and the highest surface NH_4 uptake. Like NH_4 uptake, no trend has been seen for the urea uptake with depth. In general, maximum urea uptake rate is associated with mid-depths, while the maxima in NO_3 and NH_4 uptake rate are found at the lowest light levels. This suggests that all the three nitrogenous nutrients show a large variability in the absolute values as well as the variations with depth.

Euphotic-depth-integrated urea uptake rates are shown in Fig 4.12b. They vary from 1.3 to 2.6 mmol N $m^{-2}d^{-1}$ (with an average 1.9 mmol N $m^{-2}d^{-1}$), and more than 5 times lower than those of NO_3 uptake, as in the case of NH_4 uptake. The highest integrated urea uptake rate is at EIO-S5 (2^oN 65^oE), which shows the highest surface uptake as well. *Prakash* (2008) reported urea uptake rates from 1.19 mmol N $m^{-2}d^{-1}$ to 2.53 mmol N $m^{-2}d^{-1}$ along 77^oE transect and from 1.14 mmol N $m^{-2}d^{-1}$ to 2.52 mmol N $m^{-2}d^{-1}$ along 83^oE transect in the EIO during pre monsoon 2005. Similar to the NH_4 uptake rates, urea uptake rates from the present study are in good agreement with his values.

The regenerated productivity (the sum NH_4 and urea uptake rates) varies from 0.03 to 0.05 μmol N $L^{-1}d^{-1}$ (with an average 0.04 μmol N $L^{-1}d^{-1}$). These values are comparable to the surface uptake of NO_3. The highest regenerated productivity is observed at EIO-S5 (2^oN 65^oE), which also shows the lowest surface new productivity. Euphotic-depth-integrated regenerated productivity varies between 2.9 and 4.8 mmol N $m^{-2}d^{-1}$ (with an average 3.7 mmol N $m^{-2}d^{-1}$). The average regenerated productivity is almost 3 times less than the new productivity. It can be concluded that the new productivity dominates the overall productivity in the EIO. As the NH_4 and urea uptake rates are conservative estimates, the conclusion drawn is preliminary.

f-ratio

The surface f-ratio varies from 0.4 to 0.6 (with an average 0.5). The lowest f-ratio is at EIO-S5, which also shows the highest surface NH_4 and urea uptake rates. Nevertheless, in general, more than 50% of the productivity is governed by NO_3 uptake and thus, new productivity dominates in the surface waters of the EIO. Euphotic-depth-integrated f-ratio varies from 0.7 to 0.8 with the highest value at the location EIO-S2 (6^oS 65^oE). The results indicate that the EIO is capable of high new/export production. The observed new productivity and f-ratios are comparable to those of Arabian Sea during winter (this study, *Prakash et al.*, 2008; *Kumar et al.*, 2010), except during bloom conditions. The values are also comparable to those obtained from the Bay of Bengal during spring and fall season (this study). The present values of new productivity are even higher than those reported from the Arabian Sea and Bay of Bengal during spring and pre monsoon, respectively (this study; *Kumar et al.*, 2004). However, the observed f-ratios are lower than those reported by *Prakash* (2008) (>0.9) for the EIO. New productivity values measured during the present study are lower than those of *Prakash* (2008) and the measured regenerated productivity values by both the studies are comparable, which is the reason for the difference in the f-ratios.

4.3.3 C:N consumption ratio

Fig 4.13 shows the ratio of carbon to nitrogen uptake rates (C:N) variation with depth at different sampling locations. The ratio at surface is around 2 at all the locations (Fig 4.13), which is much lower than the Redfield ratio (C:N = 6.6). At locations EIO-S2 (6^{o}S 65^{o}E) and EIO-S3 (3^{o}S 65^{o}E), the ratio decreases with depth.

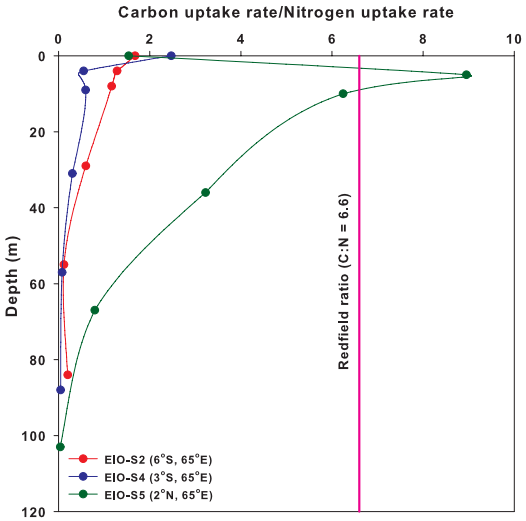

Figure 4.13: *The ratio of the observed C to N uptake rate at different sampling locations in the EIO. Vertical pink line represent the Redfield ratio (C:N = 6.6).*

The depth profile of the ratio is completely different at EIO-S5 (2^{o}N 65^{o}E). At this location the ratio reaches a maximum (8.9) at a depth of 10 m and then decreases with depth. Variation in the ratio is mainly controlled by the available nutrients, composition of plankton present, and microbial metabolism (e.g., N_2 fixation, denitrification and anammox etc.) (*Arrigo*, 2005). Plankton composition data are not available for the present study. Therefore, it is difficult to examine the role of plankton composition over the C:N uptake ratio. *Arrigo* (2005) suggests that in a low nitrogen environment, nitrogen may be assimilated in a higher proportion than the Redfield ratio. The ratio of euphotic-depth-integrated uptake rates of carbon and nitrogen varies between <1 and 2. This indicates the presence of plankton of low consumption ratio and/or nitrogen limited conditions. The uptake

rate of NO_3 follows the pattern of ambient NO_3 (Figs 4.6b, 4.10a), supporting the above inference. Carbon assimilation is also influenced by the availability of light. The nutrient dynamics is a function of mixing of waters masses of different origins in the EIO. Therefore, not only the overall productivity, the proportions of different elements during photosynthesis could also controlled by such mixing.

4.4 Conclusion

The seasonal mixing of waters masses of different origins in the EIO mainly controls hydrodynamic conditions, which ultimately governs nutrient dynamics. The present study indicates that surface light intensity along with nutrient availability decides the productivity in the EIO. Higher surface light intensity reduces the surface productivity but on the other hand, it enhances the overall depth-integrated productivity in the EIO. Both the above parameters control the consumption ratio of C:N by phytoplankton during photosynthesis. In general, the EIO is low productive. Higher concentrations of NO_3 in the subsurface layers support higher new productivity. Although NH_4 and urea uptake rates are lower than that of NO_3, they contribute significantly to the total productivity. The region shows comparable new productivity and *f*-ratios to that obtained at other parts of the Indian Ocean. Comparison with the results of *Prakash* (2008) reveals that new productivity varies significantly seasonally and spatially, but regenerated productivity does not. Overall, the EIO shows the potential for higher export production as do other parts of the Indian Ocean. The present study, along with *Prakash* (2008), enhances our understanding of the new and regenerated productivity in the EIO over two seasons (pre and summer monsoon) to some extent. A comparison with the findings of *Ryther et al* (1966) and *Qasim* (1977) with the present study rules out any significant trend in the productivity here over the past 3-decades. Efforts are needed to initiate a program in the EIO, similar to JGOFS in the Arabian Sea, to understand the biogeochemistry of this basin and its role in the global carbon budget.

Chapter 5

New and Primary productivity in the Indian sector of the Southern Ocean

5.1 Introduction

The Southern Ocean (SO) comprises the southernmost waters of the world ocean, generally taken to be south of 60^{o}S latitude and encircling Antarctica (Fig 5.1). It accounts for more than 12% of the total area of the world ocean. It includes the Antarctic Circumpolar Current (ACC, which circulates around Antarctica), the Amundsen Sea, Bellingshausen Sea, parts of the Drake Passage, Ross Sea, Cooperation Sea, the Cosmonaut Sea, a small part of the Scotia Sea, and Weddell Sea. It differs from the other oceans in that its largest boundary, the northern boundary, does not adjoin a landmass, but merges into the Atlantic, Indian and Pacific Oceans. It is one of the most important components of the Earth's climate, as it influences atmospheric composition and circulation, the global heat budget, and ocean circulation. It plays a major role in the present global climate system. The water mass characteristics of over 50% of the world ocean by volume are due to processes that occur within the SO. It acts as a physical link between the

Pacific, Indian and Atlantic oceans, transferring heat and momentum, and is the major source for the densest deep water in the global ocean (*Caldeira and Duffy*, 2000; *Matear and Hirst*, 1999). A brief description of winds, temperature, water circulation, and different water masses of the SO is presented in this section.

5.1.1 Climatic conditions

Winds

Zonal circulation of the wind pattern is more intense and constant in the SO than in any other region of the globe. Wind system of the SO comprises three main components: a southeasterly component near the coast, a zone of easterly flow encircling the continent and extending north to about 65^{o}S, and a wide zone of westerlies reaching as far north as about 40^{o}S (*Squire*, 1987). A ring of low pressure surrounds the Antarctic continental plateau, while tropical anti-cyclones lie to the north. Winds in the SO blow towards the trough of low pressure, but are directed to the left by the Earth's rotation (Coriolis effect). As a result, at about 50^{o}S of the SO, westerly winds occur. The westerlies within this circumpolar belt are quite strong, with a maximum intensity in the region of the ACC. It is this wind that drives the SO circulation. Superimposed upon this westerly circulation are northwest-southeast moving depressions (*Squire*, 1987).

Temperature

The SO is colder than most other oceans. Across the Polar Frontal Zone (PFZ) the temperature ranges between 4 and 8 ^{o}C in summer, and between 1 and 3 ^{o}C in winter. Surface waters south of the PFZ have an average temperature of about 1-2 ^{o}C in winter and 3-5 ^{o}C in summer, while further south, near the continent, temperatures range from only about -1.0 to -1.9 ^{o}C. Temperature differences between colder surface and bottom layers and intermediate, warmer, layers is less than 5 ^{o}C; thus the total annual range does not exceed 4-5 ^{o}C and is considerably less for the greater part of the region (*Knox*, 2006).

Solar radiation

In the far south near the continent, total darkness remains during half of the year, while daylight shines during the other half. This seasonal light regime is in contrast with the diurnal cycles of lower latitudes. The amount of light penetrating the surface waters of SO is mainly controlled by its intensity, angle of incidence, surface reflection, absorption by suspended particles, and by the presence of sea ice and snow cover. Light penetration is also influenced by the transparency of the atmosphere. In the region of the ACC, there is a continuous passage of low pressure systems and a predominance of cloudy weather resulting in lower insolation relative to areas closer to the continent (*Holm-Hansen et al.*, 1977). Oceanic waters surrounding Antarctica are typically blue and highly transparent with a maximum *Secchi* depth (the depth at which a standard *Secchi* disc becomes invisible) of about 40 m (*Slawyk*, 1979). The 1% light level is relatively deeper at about 100 m.

5.1.2 Oceanic circulation

Antarctic Circumpolar Current (ACC)

The Antarctic Circumpolar Current (ACC) is the most important current in the Southern Ocean, and the only current that flows completely around the globe. The ACC, as it encircles the Antarctic continent, flows eastward through the southern portions of the Atlantic, Indian, and Pacific Oceans (Fig 5.1).

Despite its relatively slow eastward flow of less than 20 cm s^{-1} in regions between the fronts, the ACC transports more water than any other current (*Klinck and Nowland*, 2001). The ACC extends from the sea surface to depths of 2000-4000 m and its width varies from less than 200 km south of Australia to over 1,000 km in the Atlantic. This tremendous cross-section allows for the current's large volume transport. The Antarctic Circumpolar Current's eastward flow is driven by strong westerly winds. The average wind speed between 40^{o}S and 60^{o}S is 15 to

24 knots (1 knot = 1.85 km h^{-1}) with strongest winds typically between 45^{o}S and 55^{o}S. Historically, the ACC has been referred as the 'West Wind Drift' because the prevailing westerly wind and current are both eastward. Although the predominant movement is towards the east, there is a strong northerly component.

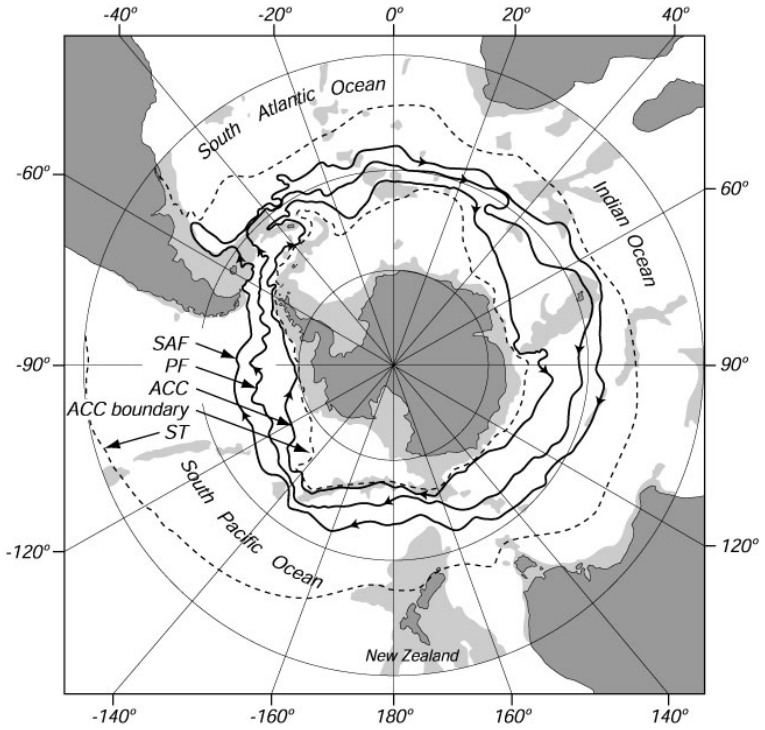

Figure 5.1: *Distribution of the Sub-antarctic and Polar Fronts and associated currents in the Antarctic (Source: Orsi et al., 1995).*

Circumpolar Frontal Zones

In the SO, zonal variations in specific water properties have been used to classify regions whose edges are defined by fronts, where there are rapid changes in water properties that occur over a short distance (*Gordon et al.*, 1977). The SO contains several oceanic frontal systems, viz., the North Subtropical Front (NSTF), Agulhas Retroflection Front (ARF), South Subtropical Front (SSTF), Subantarctic Front (SAF) and Polar Front (PF) (*Orsi et al.*, 1995; *Belkin and Gordon*, 1996). The southern ACC front (SACCF) is the third circumpolar front south of the PF (*Orsi et al.*, 1995). North of the ACC is the Subtropical Convergence or Subtropical

Front (STF), usually found between 35^{o}S and 45^{o}S, where the average Sea Surface Temperature (SST) changes from about 12 ^{o}C to 7-8 ^{o}C and salinity decreases from greater than 34.9 to 34.6 or less. The Antarctic Convergence is approximately 200 km south of the Polar Front.

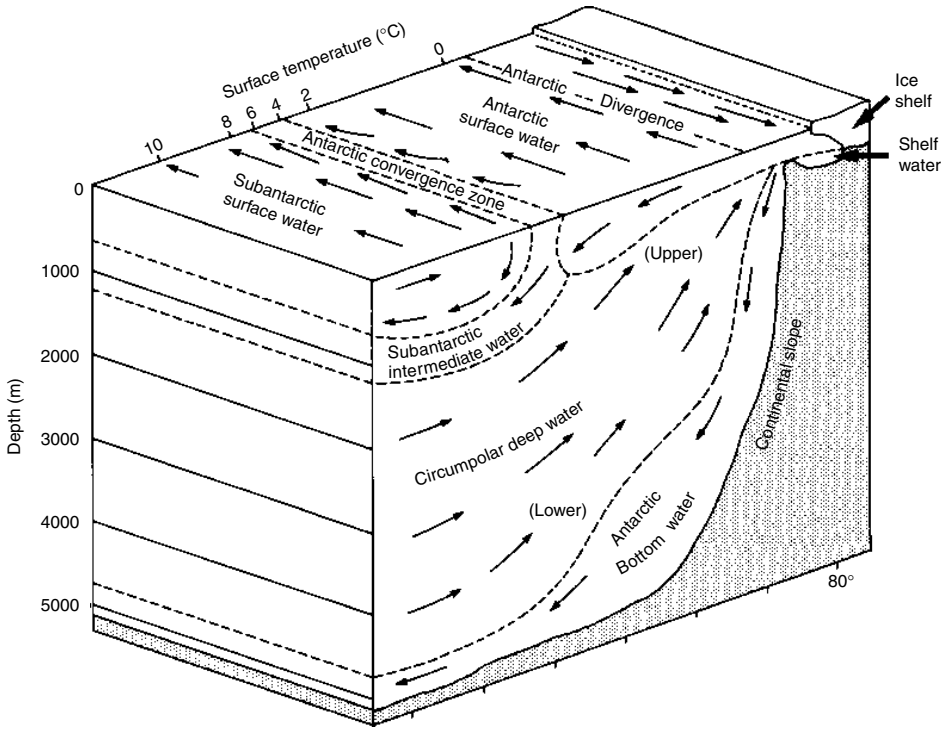

Figure 5.2: *Schematic diagram of the meridional and zonal flow and water masses of SO. The diagram represents average summer conditions. (Source: Knox, 2006).*

In the Antarctic Convergence, summer SST varies between 3 ^{o}C and 5 ^{o}C, while winter SST varies between 1 ^{o}C and 2 ^{o}C. North of the SAF, average SST is greater than 4 ^{o}C, while south of the Polar front, average SST is less than 2 ^{o}C. The eastward flow of the SAF, found between 48^{o}S and 58^{o}S in the Indian and Pacific Oceans and between 42^{o}S and 48^{o}S in the Atlantic Ocean, defines the ACC's northern boundary. A region of upwelling, the Antarctic Divergence, occurs at the Southern Front. *Orsi et al* (1995) define the southern boundary of the ACC as the poleward edge of the Upper Circumpolar Deep Water (T >1.8 ^{o}C). The mean ACC temperature ranges from -1 to 5 ^{o}C, depending on the time of the year and

location. The mean surface salinity decreases poleward, in general, from 34.9 at 35^{o}S to 34.7 at 65^{o}S. Typical salinity values are between 33.5 and 34.7, poleward of 65^{o}S. This temperature-salinity signature is due to a combination of water masses that meet in the SO and are mixed and redistributed by the Antarctic Circumpolar Current.

In the Indian Ocean sector the Agulhas Return Front (ARF) marks the southern extent of the subtropical gyre and is formed from the retroflection of the Agulhas Current south of Africa. The Agulhas Return Front is identified in surface water as far east as 56^{o}E (*Holliday and Read*, 1998). These frontal systems subdivide the sector into zones with different biogeochemical characteristics, viz., the Subtropical Zone (STZ), Subtropical Frontal Zone (STFZ), Subantarctic Zone (SAZ) and Polar Frontal Zone (PFZ). A fourth zone, the Continental Zone, and the westward flowing Antarctic Coastal (or Polar) Current are located even further poleward, between the Southern Front and the Antarctic continent. SST poleward of 65^{o}S is about -1.0 ^{o}C (*Deacon*, 1984).

The surface water masses of the SO can be divided into Subtropical, Subantarctic and Antarctic (Fig 5.2). North of the Agulhas Return Front the surface waters have their origin in the subtropical gyre of the Indian Ocean. South of the STF, the surface waters are carried by the Antarctic Circumpolar Current (ACC) around the Southern Ocean and can be subdivided into Subantarctic and Antarctic. The warmest water in this region is Tropical Surface Water (TSW) with temperature greater than 23 ^{o}C and relatively low salinities (*Gordon et al.*, 1987). Subtropical Surface Water (STSW) extends southwards to the ARF and has temperature-salinity range of 15 ^{o}C, 35.50 to 24 ^{o}C, 34.60 (*Darbyshire*, 1966). The coastal water of the Agulhas Current (AgulhasWater, AW) is slightly cooler (14-17 ^{o}C) and has a lower salinity (35.20-35.35) than the STSW (*Darbyshire*, 1966). The water between the ARF and the STF has its origins in AW, Indian STSW, Atlantic STSW and water from the subantarctic zone (*Read and Pollard*, 1993). The Agulhas Retroflection plays a role in the exchange of water between the Indian Ocean and

South Atlantic Ocean (*Gordon et al.*, 1987). Subantarctic Surface Water (SASW) is found between the STF and the SAF and has a wide range of temperatures and salinities varying with season (lower temperature in winter) and latitude (lower salinity to the south) (e.g. *Read and Pollard*, 1993). South of the PF lies the Antarctic Surface Water (AASW), which again shows seasonal and latitudinal variation in SST and salinity (highest salinity in the winter and highest temperature in the summer towards the north).

5.1.3 Previous studies on productivity in the SO

The SO primary productivity is low in large areas (*El-Sayed*, 1984), where nanophytoplankton cells (<20 μm) may sometimes comprise more than 50% of the phytoplankton biomass (*von Brockel*, 1981; *Koike et al.*, 1986) and more than 90% of the primary production (*von Brockel*, 1985). Primary productivity in the SO is spatially and temporarily highly variable (*Sullivan et al.*, 1993). During spring and summer, phytoplankton blooms are frequently observed in coastal regions, near the ice edge, in polynas, and at frontal zone systems. Despite the high level of major nutrients in surface waters, the main body of the Antarctic Circumpolar Current is characterized by low levels of biomass and primary productivity, <0.5 mg chl a m^{-3} and 300 mg C m^{-2} d^{-1}, respectively (e.g., *Holm-Hansen et al.*, 1977; *El-Sayed*, 1978; *Sakshaug and Holm-Hansen*, 1984; *Holm-Hansen and Mitchell*, 1991). In the Indian Sector of the SO, different zones show a wide range of productivity during austral summer (*Jasmine et al.*, 2009). The STZ, and NSTF are low productive ($\sim$200 mg C $m^{-2}d^{-1}$). The STFZ, ARF, SAF, and SAZ have productivity between 300-400 mg C $m^{-2}d^{-1}$. The SSTF shows the highest productivity (>900 mg C $m^{-2}d^{-1}$) with the lowest is found at the SPF, and PFZ (<200 mg C $m^{-2}d^{-1}$). Despite the high concentrations of N and P throughout the year, the regions south of SSTF exhibit low productivity. Therefore, these regions of the SO, like the subarctic Pacific and the equatorial Pacific, are termed as high-nutrient, low chlorophyll (HNLC) areas (*El-Sayed*, 1984).

A few studies are carried out in the region to estimate new and regenerated productivity. *Slawyk* (1979) was the first to use ^{13}C and ^{15}N tracers to measure nitrogen and carbon uptake rates in the Kerguelen Island area of the SO. Despite the high concentration of NO_3 (>20 μM) a very low C uptake (<1 mg C $m^{-2}h^{-1}$) was found. In addition, very low NO_3 uptake rates, varying from 0.03 to 0.12 mmol N $m^{-2}d^{-1}$ were recorded. The specific uptake rate of NO_3 was related to the temperature. No light limitation effect over C and N uptake rates was observed (*Slawyk*, 1979). Phytoplankton prefer NH_4 over NO_3 during late summer in the Scotia Sea, despite the high abundance of NO_3. Utilization of NO_3 only accounts for <40% of the total nitrogen utilization, if NH_4 concentration is >1 μM (*Glibert et al.*, 1982b). *Goeyens et al* (1991) observed that marginal ice zone ecosystem shifts from predominantly new productive (highest *f*-ratio 0.83) to regenerated productive (lowest *f*-ratio 0.30) after ∼3 weeks in the Weddell Sea. This transition corresponds with the change from a higher diatom population to a higher flagellate population in the Weddell Sea. Although NO_3 was found to be about 40 times higher than NH_4, the latter was consistently the preferred substrate for the plankton assemblage, accounting for over half of the nitrogen taken up during the austral winter in the marginal ice zone of the Weddell-Scotia Sea (*Cota et al.*, 1992).

Mengesha et al (1998) found oligotrophic conditions, with a large spatial variation of phytoplankton biomass and community structure, in the Indian sector of the SO. A pronounced seasonal variation was also observed in the nitrogen uptake rates (*Mengesha et al.*, 1998). During spring, the specific and absolute uptake rates of NO_3 dominate NH_4 and urea uptakes. While during summer NH_4 uptake was higher than that of NO_3. They observed a shift from new to regenerated productivity for the seasonal transition from spring to summer, as did *Goeyens et al* (1991) and *Cota et al* (1992). They also concluded that seasonal shift in N uptake regime can occur with, as well as without, marked changes in community structure. Such seasonal shift in the N uptake regime was also observed by *Semeneh et al* (1998) in the Atlantic and Indian sectors of the SO. They noticed that a pre-

dominantly NO_3 based, diatom dominated assemblage, thriving in a stable water column at the beginning of the season was transformed into a mainly NH_4 based, flagellate dominated assemblage, towards the end of the season in the Marginal Ice Zone areas of the Weddell Sea and adjacent areas. The change in phytoplankton community structure was caused by selective grazing by large grazers and reduced stability of the water column and the shift in uptake regime was due to increased NH_4 availability and changes in community structure. In contrast, they observed a shift in uptake regime in the absence of a big change in phytoplankton community structure in the Coastal and Continental Shelf Zone and Open Oceanic Zone of the Indian sector. The excess net removal of SiO_4 over NO_3 was observed in certain provinces of the SO (*Semeneh et al.*, 1998).

Sambrotto and Mace (2000) reported that NO_3 uptake rates were the greatest south of the Antarctic Polar Front (APF), exceeding 10 mmol N $m^{-2}d^{-1}$ in December near the retreating ice edge. In February, NO_3 uptake rates were an order of magnitude lower. Rates of NH_4 uptake in both periods were greater in the warmer waters north of the front; *f*-ratios varied from 0.50 to less than 0.05, with larger values associated with the >5 μm size fraction at the ice edge and generally lower values north of the APF. In these NO_3-replete waters, light/mixing conditions in the surface water accounted for over 50% of the variance in NO_3 uptake rates. They concluded that the marginal ice zone of the SO is an important region for export production.

Savoye et al (2004) distinguished three regions viz., (1) Sub-Antarctic Zone (SAZ) and Sub-Antarctic Front (SAF), (2) Polar Front Zone (PFZ) and Inter-Polar Front Zone (IPFZ), and (3) Southern Antarctic Zone (AZ-S) and Seasonal Ice Zone (SIZ), on the basis of N uptake rate and community structure. Region (1) is characterized by low N-uptake rate (4.4±0.3 mmol N $m^{-2}d^{-1}$), low new production (6.2±1.8 mmol C $m^{-2}d^{-1}$) and by dominance of small phytoplankton cells (<20 μm) over a time scale of one month. The region witnessed a shift from a system dominated by regenerated production (*f*-ratio = 0.38±0.05) to a system dominated

by new production (*f*-ratio = 0.82) within one month. Region (2) is characterized by slightly higher N uptake rates (5.6±0.1 mmol N $m^{-2}d^{-1}$), low new production (5.9±2.5 mmol C $m^{-2}d^{-1}$) and dominance of small phytoplankton. N-uptake is slightly dominated by NO_3 uptake (*f*-ratio = 0.56±0.01) in the region. While region (3) is characterized by high *f*-ratio (0.61±0.08). Large phytoplankton (>20 μm) dominated the community. *Prakash* (2008) found large spatial variations in the new productivity, from 0.9 to 7.7 mmol N $m^{-2}d^{-1}$, with the highest value at the Antarctic coast during austral summer in the Indian sector of the SO. In general, a large spatial and temporal variability is observed in the N uptake regime, community structure, and over all productivity in the region.

Sabine et al (2004) reported that about 60% of the total oceanic anthropogenic CO_2 inventory is stored in the Southern Hemisphere oceans, roughly in proportion to its larger ocean area. Antarctic Intermediate Water and sub-Antarctic Mode Water masses appear to take up large amounts of anthropogenic CO_2 from the atmosphere. These subducted intermediate and mode waters contain high concentrations of anthropogenic CO_2. This transport plus the large volumetric contribution of the water masses to the Southern Hemisphere thermocline leads to high anthropogenic CO_2 inventories, estimated to exceed 20 Pg C (*Sabine et al.*, 2004). Despite the importance of the SO to world climate, its unique ecosystem and associated resources, its role in climate and climate change, and the functioning of its ecosystem are not well understood. New productivity measurements in the region are sparse in both space and in time. The present study is an attempt to gain some knowledge regarding the C and N uptake rates in the region.

5.2 Hydrographic and meteorological parameters in the SO (austral summer 2009)

Strong winds, cyclones, precipitation, snow fall, and often cloudy conditions were found in the region. Icebergs were seen to the south of 65^{o}S. Pancake ice over the

sea surface was also seen in the first week of Mar 2010 near the Antarctic coast, an indication of the beginning of freezing. Environmental parameters observed at sampling locations (Fig 5.3) are listed in Table 5.1.

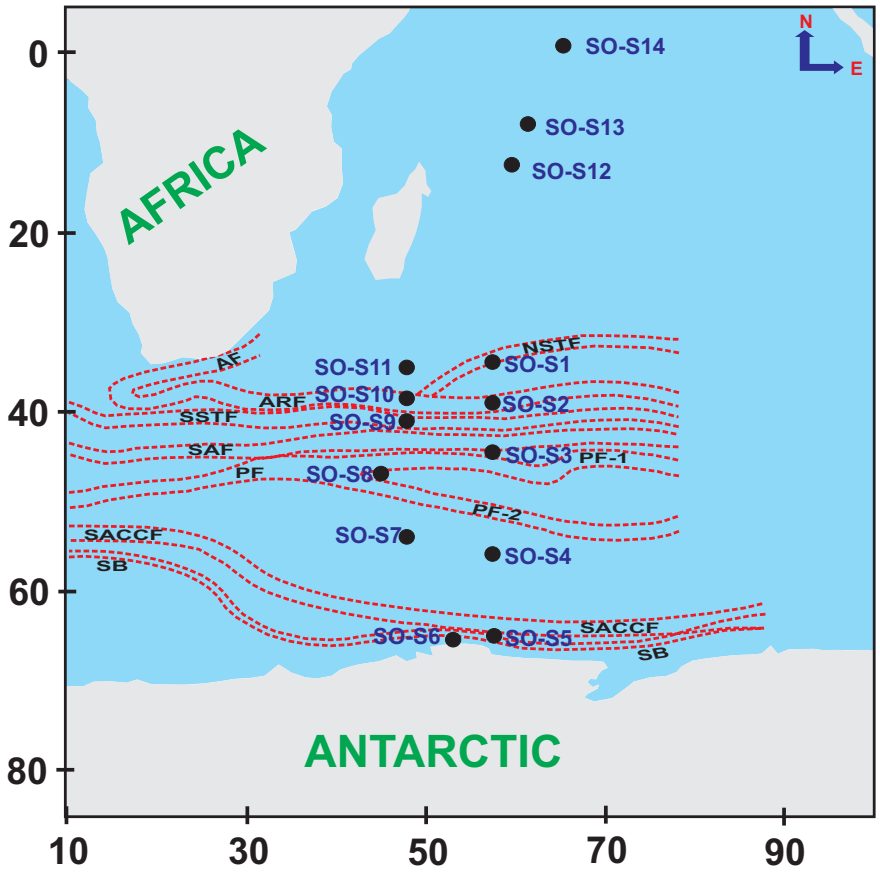

Figure 5.3: *Sampling locations shown with different frontal zones in the SO. Details of the zones are given in the text. Fronts are redrawn from Holliday and Read (1998).*

Winds were generally very strong and varied from 3.6 to 19.5 ms^{-1}. We encountered a big storm (sea state >10; Atmospheric pressure = 962 mbar; V_w = 60 ms^{-1}) to the south of 55^{o}S along the 48^{o}E. Therefore, sea water sampling using CTD rosette sampler could not be performed between 64^{o}S and 55^{o}S. Almost an order of magnitude variation was observed in photosynthetically active radiation (PAR) values, from 170 to 1390 μmol $m^{-2}s^{-1}$ (Table 4.1). The large variation was a consequence of the varying cloudiness. PAR measurements could not carried out

after the sampling location SO-S6 as our portable CTD was lost into the sea during a storm. Euphotic depth varied from 75 to 125 m during the period. After SO-S6 location, euphotic depth was estimated by a *Secchi* disk. Mixed layer depth (MLD) was found to be always shallower than the euphotic depth (except at SO-S7), and varied between 15 and 110 m. The lowest MLD was found in a location near the equator. Overall, MLD in the SO was higher.

Table 5.1: *Station code, sea surface temperature (^oC; SST), surface salinity, mixed layer depth (m; MLD), euphotic depth (m; ED), Photosynthetically active radiation ($\mu mol\ m^{-2}s^{-1}$; PAR), and surface wind speed (ms^{-1}; V_w) at different sampling locations.*

Station code	Lat (^{o}N)	Lon (^{o}E)	SST	Salinity	MLD	ED	PAR	V_w
SO-S1	-34.5	57.5	19.5	35.6	45	95	1390	10
SO-S2	-39.0	57.5	17.5	35.3	60	95	180	18
SO-S3	-44.5	57.5	13.0	34.8	54	85	321	3.6
SO-S4	-56.0	57.5	2.5	33.8	65	75	170	11.5
SO-S5	-65.0	57.5	0.0	34.0	30	95	1120	7
SO-S6	-65.5	53.0	-1.5	33.7	55	75	450	19.5
SO-S7	-35.0	48.0	2.0	33.8	110	75	ND	9.3
SO-S8	-38.0	48.0	8.0	33.9	70	85	ND	8.5
SO-S9	-41.0	48.0	16.0	35.3	75	85	ND	10.5
SO-S10	-47.0	45.0	20.0	35.5	80	85	ND	7.5
SO-S11	-54.0	48.0	20.5	35.5	25	95	ND	6
SO-S12	-12.5	59.7	29.0	34.2	15	125	ND	7.5
SO-S13	-7.9	61.4	30.0	33.8	30	125	ND	5.5
SO-S14	1.0	59.7	29.5	35.2	40	125	ND	6.5

ND-no data available (see text for explanation).

5.2.1 Temperature and salinity

During the present study, sampling was done mainly along two longitudinal transects viz., 57.5^{o}E and 48^{o}E, to observe any meridional and zonal variations in the C and N uptakes during austral summer. Meteorological parameters were recorded at every 3 hour interval. Sea water samples for hydrological parameters were collected at every degree latitude interval, except during stormy conditions.

Latitudinal variations in sea surface temperature (SST) along 57.5^{o}E and 48^{o}E longitudinal transects are shown in the Fig 5.4.

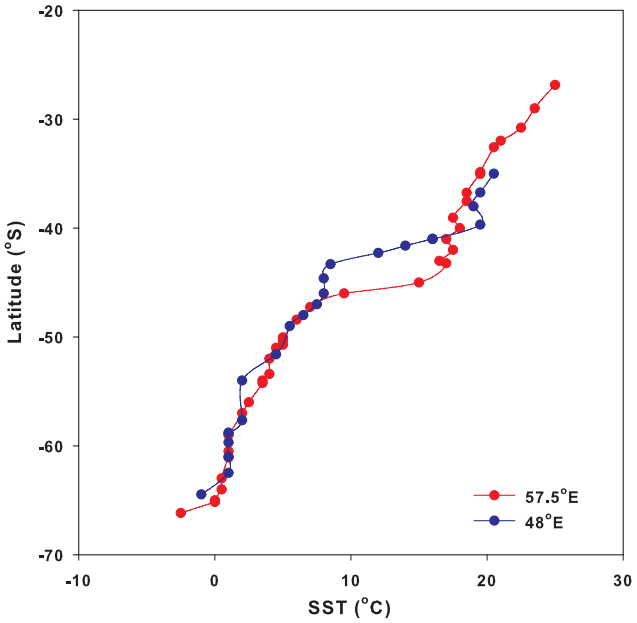

Figure 5.4: *Latitudinal variation of SST in the SO along 57.5^{o}E and 48^{o}E.*

A general decreasing trend in SST is observed along both the transects towards the south. Along the transect 48^{o}E, the SST decrease by 0.75 ^{o}C per degree latitude between 35-65^{o}S towards south. The decrease is much sharper (>4.5 ^{o}C per degree latitude) between the 40-42.5^{o}S latitudinal belt. Similar to the 48^{o}E transect, along the 57.5^{o}E transect, SST decreases by 0.75 ^{o}C per degree latitude between 28-66^{o}S towards the south. Here also, a sharp decrease (>1.5 ^{o}C per degree latitude) is seen between 42.5-47.5^{o}S latitudes. The differences noticed are: (i) decline in the SST is much sharper on 48^{o}E than on 57.5^{o}E, and (ii) the higher gradient in the SST is shifted a little southwards at 57.5^{o}E compared to 48^{o}E transect. Such observations are also reported earlier (e.g. *Carmack*, 1992).
Latitudinal variations in surface salinity along 57.5^{o}E and 48^{o}E are shown in Fig 5.5. Unlike in SST, the decreasing trend in surface salinity towards the south is not observed along either transect. However, a sharp change in the surface salinity is observed on both the transects, as was found in SST.

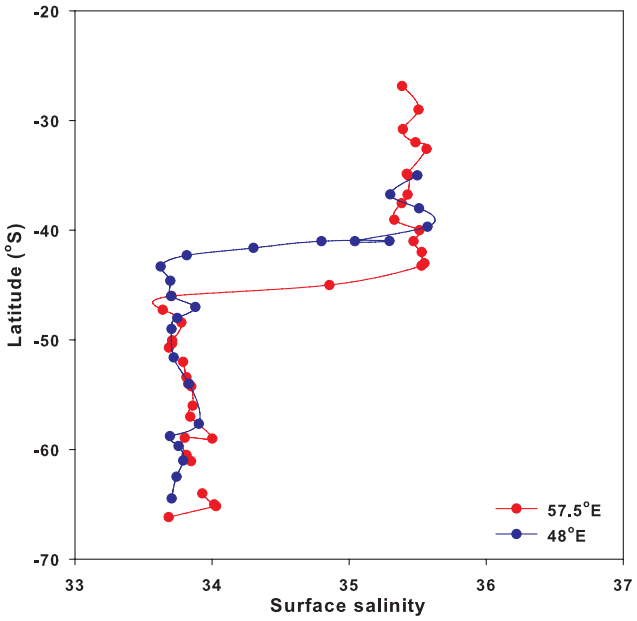

Figure 5.5: *Latitudinal variation of surface salinity (in psu) in the SO along 57.5^{o}E and 48^{o}E. (psu = practical salinity unit).*

Along 48^{o}E, the surface salinity decreases by 1 psu per degree latitude between 40-42.5^{o}S towards the south. Similarly, along 57.5^{o}E, the surface salinity decreases by 0.5 psu per degree latitude between 42.5-47.5^{o}S, towards the south. As seen in SST, the differences noticed are that (i) decline in the surface salinity is much sharper on 48^{o}E than on 57.5^{o}E, and (2) the higher gradient in the surface salinity is shifted a little southwards on 57.5^{o}E relative to 48^{o}E.

Such a large variability in SST and salinity is the special feature of the polar front which divides the SO into two distinct regions. An abrupt increase in salinity and SST towards the north near 40^{o}S is associated with the Sub-Tropical convergence, where the sub-Antarctic water meets the warm sub-tropical water. The differences related to the SST and salinity variations across the STF along the monitored transects (57.5^{o}E and 48^{o}E) suggest non uniformity of the boundary of the Sub-Tropical convergence in the Indian Sector (Fig 5.3). Either side of the polar front, water masses have very different characteristics in SST, salinity, phytoplankton abundance, nutrients, weather, etc. Variations in other related parameters across

such boundaries are discussed in the following sections.

Depth profiles of temperature are shown in Fig 5.6. A general increasing trend in vertical mixing is seen towards south. Temperature based mixed layer depth (MLD) varies between 30-65 m and 25-110 m along the 57.5^{o}E and 48^{o}E longitudes, respectively (Table 5.1). Temperature profiles across the SO show large variability. The southernmost location shows a hump in the temperature profile which could be associated with the sinking of the Antarctic coastal water.

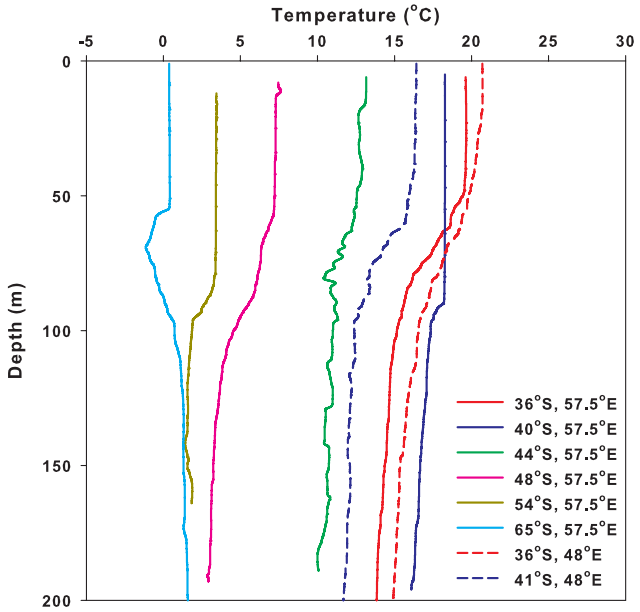

Figure 5.6: *Depth profiles of temperature at different sampling locations in the SO.*

A signature of rigorous mixing is seen in the depth profiles of salinity (Fig 5.7), particularly at 44^{o}S, 65^{o}E. Such increase in salinity of surface as well as in sub-surface waters is expected here as this location is situated in the north of the polar front. To the south of the polar front, not much variation is observed between the latitudes, at different longitudes (36^{o}S, 57.5^{o}E and 36^{o}S, 48^{o}E), while in the north of the polar front nearby latitudes at the same longitude (40^{o}S, 57.5^{o}E and 41^{o}S, 48^{o}E) show a large variability (Fig 5.7). This suggests the nonuniformity of the boundary of the Sub-Tropical convergence in the Indian sector (Fig 5.3).

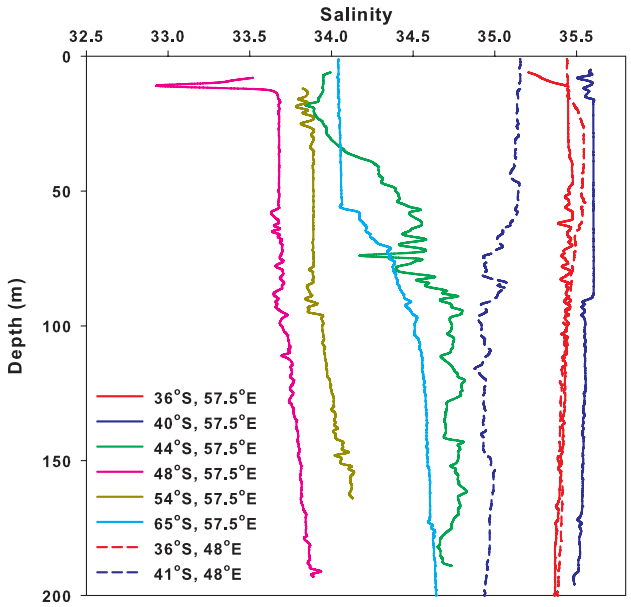

Figure 5.7: *Depth profiles of salinity (in psu) at different sampling locations in the SO.*

5.2.2 Nutrients

In general, the concentration of nutrients in surface waters south of the Polar Front are much higher than those in other oceanic waters (*Knox*, 1970; *El-Sayed*, 1978). Nutrient rich water upwells at the Antarctic Divergence, spreading out to ultimately downwell at the Polar Front. *Kuramoto and Koyama* (1982), and *Watanabe and Nakajima* (1982) found a completely asymmetric distribution of nutrients along 45^{o}E longitude transect. They found a decreasing trend in surface concentration of NO_3 between 67^{o}S and the Subtropical Convergence (41-43^{o}S), however, the decline was not sharp and its concentration remained $\geq$20 μM. While SiO_4 was very high ($\sim$50 μM) at 67^{o}S and it decreased to very low values ($\sim$1 μM) near the Subtropical Convergence (41-43^{o}S).

Latitudinal variations of surface concentrations of different nutrients (NO_2, NO_3, PO_4, and SiO_4) along the 57.5^{o}E and 48^{o}E transects are shown in Fig 5.8. All the nutrients show higher concentrations to the south of the polar front. At the Subtropical Convergence, NO_2 and SiO_4 are very low, while NO_3 and PO_4 remain

significantly higher (Fig 5.7), reflecting its assimilation and polymerization by diatoms and silico-flagellates. For a given latitude, values of nutrients on 48°E are higher than that on 57.5°E. The increase in SST and salinity are also more abrupt on 48°E than on 57.5°E. This suggests that all the nutrient inventory is closely related to the circulation, water masses and their boundaries.

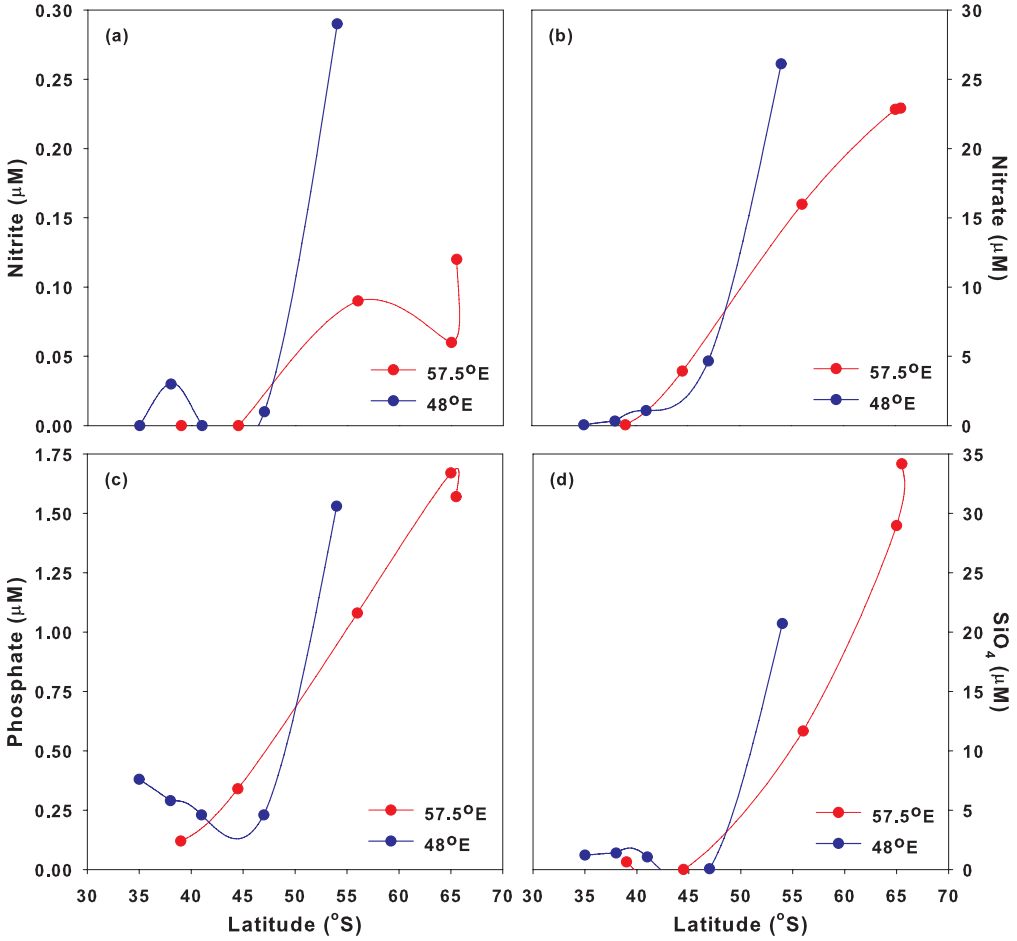

Figure 5.8: *Latitudinal variation of surface concentrations of (a) NO_2, (b) NO_3, (c) PO_4, and (d) SiO_4 in SO along 57.5°E and 48°E.*

The distribution of NO_2 and NO_3 down to the euphotic depth at different locations are shown in Fig 5.9. Along 57.5°E, south of the polar front, both NO_2 and NO_3 are high and decrease towards north. Higher concentrations of NO_2 and NO_3 indicate the underutilization of these substrates by phytoplankton probably due

to the lack of micro-nutrients (e.g., Fe) in the region. Fe in suspended particulate matter varies between 4 and 11 μg L^{-1} (*Dessai et al.*, 2010).

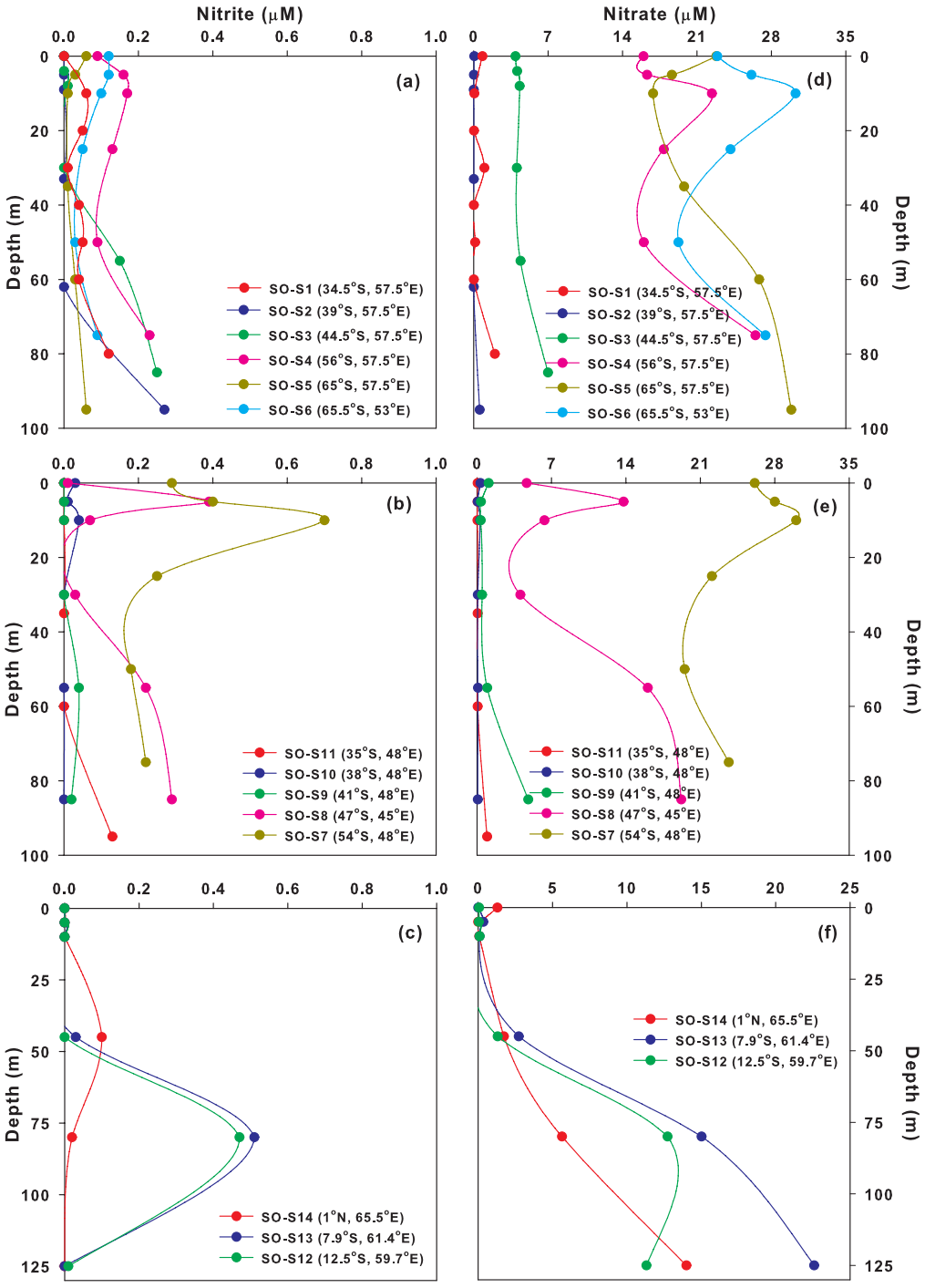

Figure 5.9: *Depth profiles of NO_2 (a, b, and c) and NO_3 (d, e, and f) at different locations, given in the legend.*

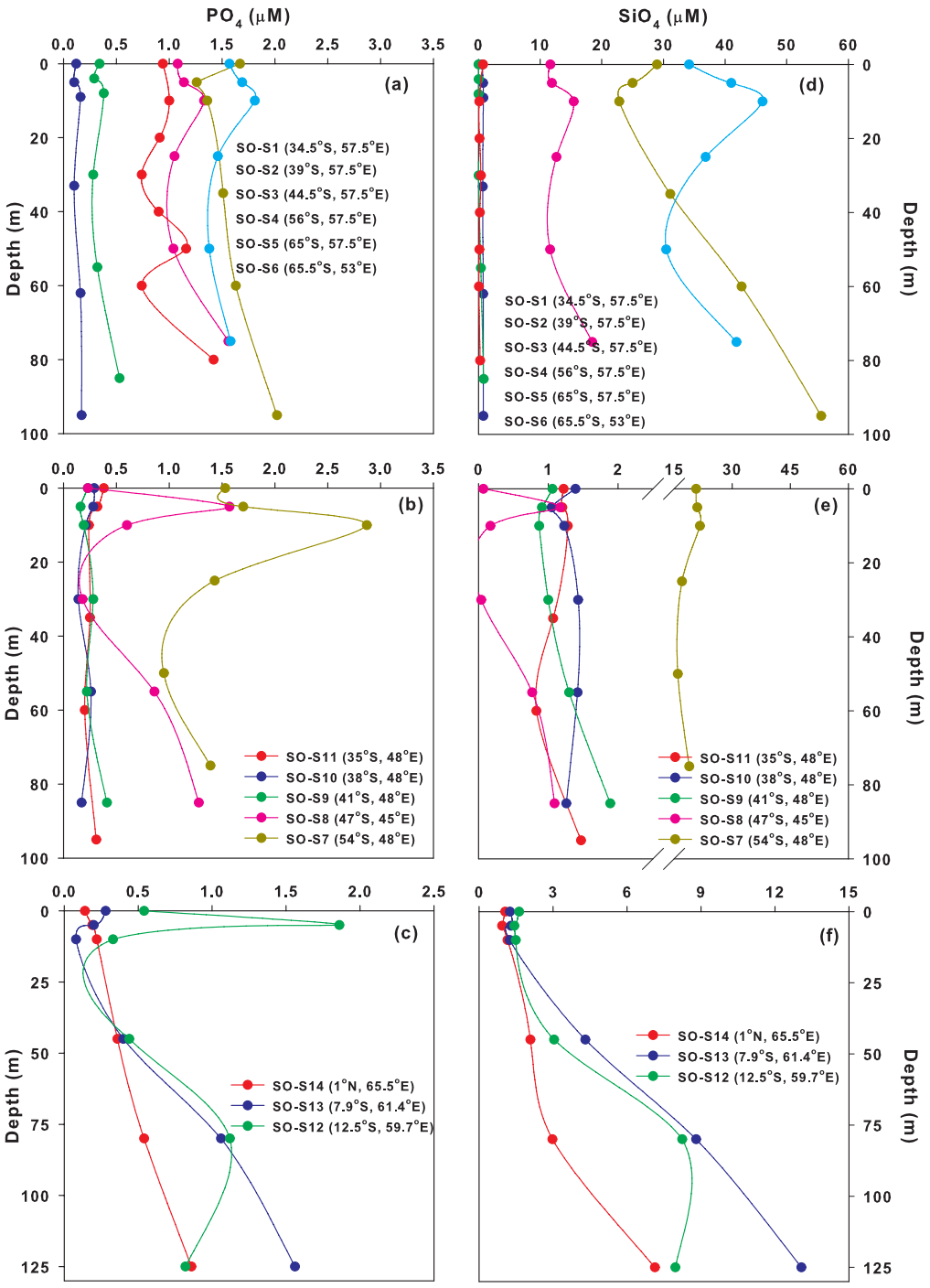

Figure 5.10: *Depth profiles of PO_4 (a, b, and c) and SiO_4 (d, e, and f) at different locations, given in the legend.*

It is widely accepted that Fe limitation is the main cause for the observed low chlorophyll and higher NO_3 in the region (e.g., *Martin et al.*, 1991). A similar

scenario is observed along the 48^{o}E transect. The only difference observed is that relatively higher NO_2 and NO_3 values are found on 48^{o}E than on 57.5^{o}E (Fig 5.9) (e.g., 56^{o}S, 57.5^{o}E vs. 54^{o}S, 48^{o}E). Apart from these two transects, samples are collected at three locations near the equator. Depth profiles of NO_2 and NO_3 show that the surface layer is devoid of these nutrients. Similar patterns were observed during the boreal summer 2008 (see chapter 4). This suggests that nutrient availability more or less remains same during both the seasons (austral and boreal summer) in this region.

The distribution of PO_4 and SiO_4 down to the euphotic depth at different locations are shown in Fig 5.10. Similar to NO_2 and NO_3 profiles, along 57.5^{o}E, south of the polar front, both PO_4 and SiO_4 are high and decrease towards the north. Here also, the limitation of Fe could be the reason for the observed higher PO_4 and SiO_4 towards the south. At 44.5^{o}S, 57.5^{o}E, decrease in SiO_4 is more pronounced than in NO_3, which indicates the dominance of diatoms and/or silico-flagellates here.

Data on 48^{o}E also show a similar pattern as on 57.5^{o}E. Here too, the only difference observed is that relatively higher PO_4 and SiO_4 are found on 48^{o}E than on 57.5^{o}E (Fig 5.9) (e.g., 56^{o}S, 57.5^{o}E vs. 54^{o}S, 48^{o}E). In locations near the equator, unlike NO_2 and NO_3, PO_4 and SiO_4 are significantly higher in the surface layers (Fig 5.10). Similar observations were also reported by *Sardessai et al* (2010). They attributed such enrichment in nutrients in surface water with the highest enrichment of SiO_4 to bubble, or atmospheric input (via dry and wet deposition, and bubble scavenging).

5.2.3 Chlorophyll

Surface as well as depth profiles of chlorophyll *a* (chl *a*) are different along the two transects (Fig 5.11). The highest surface chl *a* (>0.5 mg m^{-3}) is found at the Subtropical convergence along 57.5^{o}E. On either side of the Subtropical convergence, surface chl *a* is lower. Marginally higher values (>0.3 mg m^{-3}) are observed to the south of the polar front (>65^{o}S). A similar pattern was also reported by *Odate and*

Fukuchi (1995) in the Indian Sector of the SO. Due to a storm, data could not be collected beyond 55^{o}S along 48^{o}E, which restricts the comparison of chl *a* between the two transects.

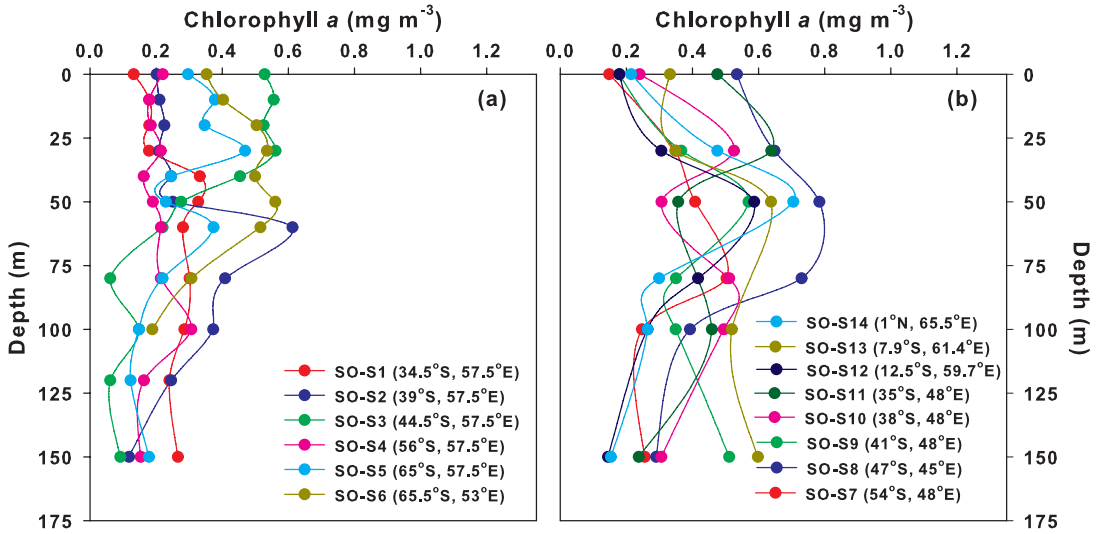

Figure 5.11: *Depth profiles of chlorophyll-a at different locations (a) along 57.5^{o}E, and the Antarctic coast, (b) along 48^{o}E, near Crozet island, and near the equator.*

Nevertheless, the highest surface value of chl *a* is also seen at the Subtropical convergence along 48^{o}E, but slightly northward. This again is the consequence of non-uniformity of the boundary of the Subtropical convergence in the region, also observed in the SST, salinity and nutrients. The supply of Fe near the Subtropical convergence could be a reason of the observed higher chl *a* there.

The Antarctic bottom water moves northward and meets the subtropical water at the Subtropical convergence, which might carry Fe along with other nutrients from the Antarctic continent. ARF could also be a source of Fe at this region as this front is identified in surface water as far as 56^{o}E (*Holliday and Read*, 1998). Further north, this water mixes with the subtropical water (nutrient-poor water), which limits the higher chl *a* values to this latitudinal belt.

Depth of Deep chl *a* Maximum (DCM) varies from 30 to 100 m and 30 to 80 m along 57.5^{o}E and 48^{o}E, respectively. All the three locations near the equator show DCM

at around 50 m depth. Depth of DCM increases towards the north along 48^{o}E. Such trend could be related to the movement of Antarctic bottom water and associated changes with the nutrients inventory. In addition, surface light intensity also plays a significant role. PAR data are not available for all the locations. Nevertheless, euphotic depth decreases in general towards north along 48^{o}E (Table 5.1). No such trend was found in the other transect. With the available information it is difficult to pin point the exact mechanism governing such variations.

5.3 Carbon and Nitrogen uptake rates

Productivity measurements were conducted at 14 different stations (Table 5.1), shown in Fig 5.3. Out of 14, five locations were along 57.5^{o}E, four along 48^{o}E, three near the equator, one near the Antarctic coast and the last was just outside the exclusive economic zone (EEZ) of Crozet island. At all the 14 locations total primary productivity (using ^{13}C-labelled tracer), new and regenerated productivity measurements (using ^{15}N-labelled tracer) were carried out.

5.3.1 Carbon uptake rate

Surface C uptake along 57.5^{o}E, varies between 0.3 and 1.8 μmol C L^{-1}d^{-1} with the highest value at SO-S3 (44.5^{o}S, 57.5^{o}E). The coastal location, SO-S6 (65.5^{o}S, 53^{o}E) also shows a significantly higher surface productivity (0.9 μmol C L^{-1}d^{-1}). Along 48^{o}E, surface productivity varies between 0.3 and 4.3 μmol C L^{-1}d^{-1}. Here too, the highest productivity is found at the Subtropical convergence. Surface C uptake rates vary from 0.3 to 1.5 μmol C L^{-1}d^{-1} at locations near the equator, comparable to those observed during boreal summer 2008 in this region (see Chapter 4).
Some common features are observed in the depth profiles of C uptake rates, higher in the surface (Fig 5.12), and lower on either side of the Subtropical convergence. The variations could be attributed to the variation of temperature, PAR, and availability of macro or micro nutrients. *Sakshug and Slagstad* (1991) suggested that low productivity in the SO is mainly because of low temperature but later it

was revised as due to the unavailability of Fe (*Martin et al.*, 1991).

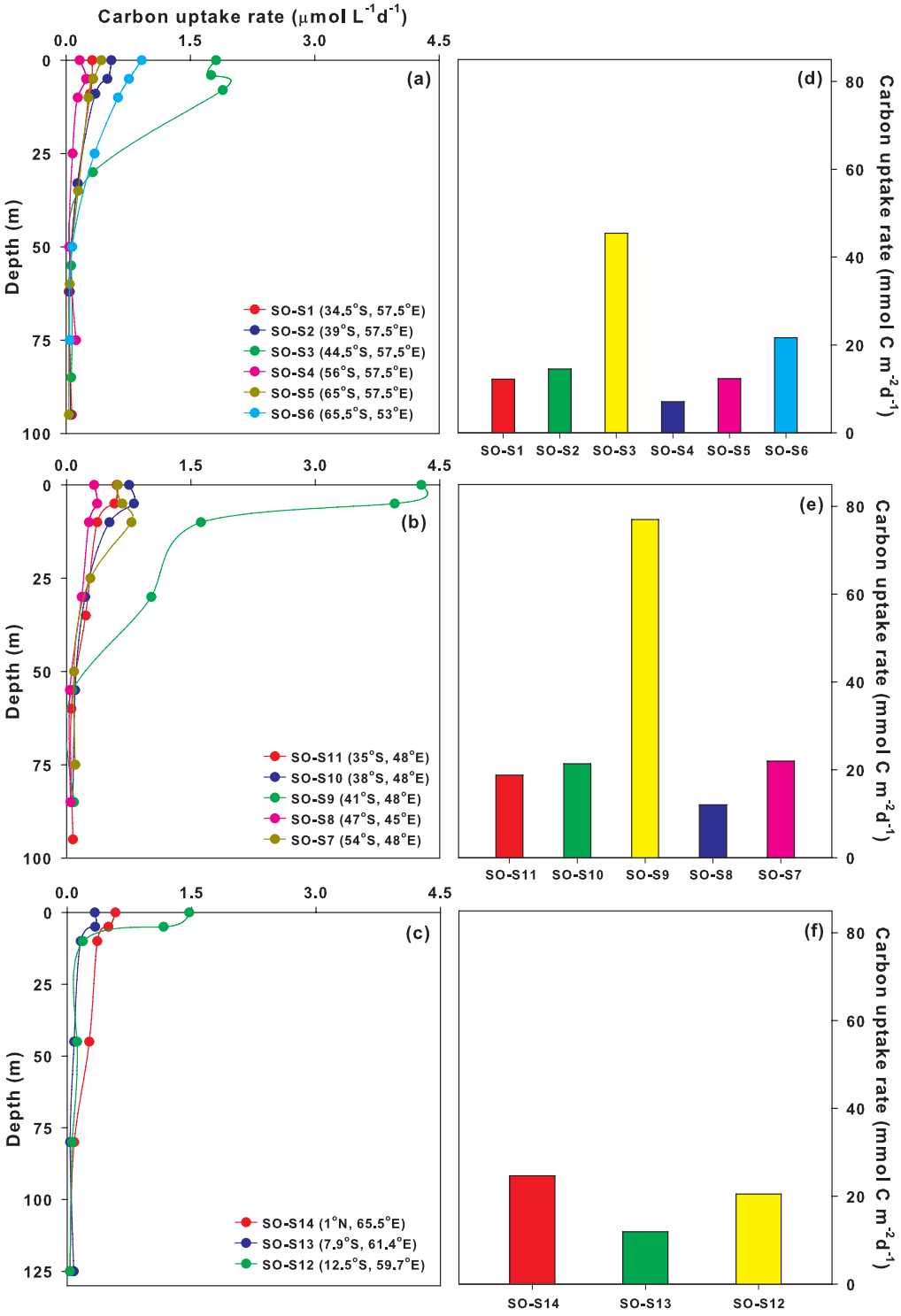

Figure 5.12: *Depth profiles of carbon uptake (a, b, and c) and euphotic-depth-integrated values (d, e, and f) at different locations in the SO.*

Insufficient solar energy (*Nelson and Smith*, 1991), strong winds that stir the water and result in deepening of the mixed layer and convection (*Sakshaug et al.*, 1991), and grazing by zooplankton (*Dubischar and Bathmann*, 1997) could be the other possible factors for low productivity in the region. In the present study, SO-S6 shows significantly higher productivity despite the very low SST (-1.5 ^{o}C). Higher productivity near the Subtropical convergence is supported by the supply of Fe from the the Antarctic bottom water that upwells and mixes with Subtropical water here, as suggested by *Boyd et al* (2007).

Euphotic-depth-integrated C uptake rate varies between 7.1 and 45.4 mmol C $m^{-2}d^{-1}$ (85 to 545 mg C $m^{-2}d^{-1}$) with the highest value at SO-S3, along 57.5^{o}E. The 48^{o}E transect is relatively more productive, C uptake rates vary from 18.8 to 77.0 mmol C $m^{-2}d^{-1}$ (225 to 924 mg C $m^{-2}d^{-1}$). Here too, the highest productivity is in the location near the Subtropical convergence (SO-S9). Overall, the region can be divided into five zones (from south to north) viz., (i) between the Antarctic continent and the polar front (Antarctic zone; ANZ), (ii) between the polar and SubAntarctic fronts (Polar frontal zone; PFZ), (iii) between the SAF and ARF (South Subtropical front; SSTF), (iv) Subtropical frontal zone (STFZ), and (v) between the ARF and North Subtropical front (Subtropical zone; STZ) (Fig 5.3).

SSTF (SO-S9) is found to be the most productive (productivity >900 mg C $m^{-2}d^{-1}$) and STZ (includes SO-S1, and SO-S11), the least productive (average productivity of ∼185 mg C $m^{-2}d^{-1}$; n=2) (Fig 5.13). The ANZ (includes SO-S4, SO-S5, SO-S6 and SO-S7) is also very low productive (∼190 mg C $m^{-2}d^{-1}$; n=4), while the STFZ (includes SO-S2, and SO-S10) and PFZ (includes SO-S3, and SO-S8), show an average productivity of ∼215 mg C $m^{-2}d^{-1}$ and ∼340 mg C $m^{-2}d^{-1}$, respectively.

The observed variation in the productivity for different zones is consistent with the observations of *Jasmine et al* (2009) along the 45^{o}E in 2004. At the ANZ, mixing between the Subtropical water and Subantarctic bottom water takes place at the

SSTF, which enhances the nutrient levels and productivity in this region. *Odate and Fukuchi* (1995) also found higher chl *a* in the region. Nutrient limitation at the STZ results in low productivity, while light limitation could be the reason for low productivity at ANZ (*Jasmine et al.*, 2009). The region PFZ, south of the SSTF show low productivity despite the presence of higher N and P in the surface. Grazing by zooplankton probably checks productivity in this zone (*Jasmine et al.*, 2009).

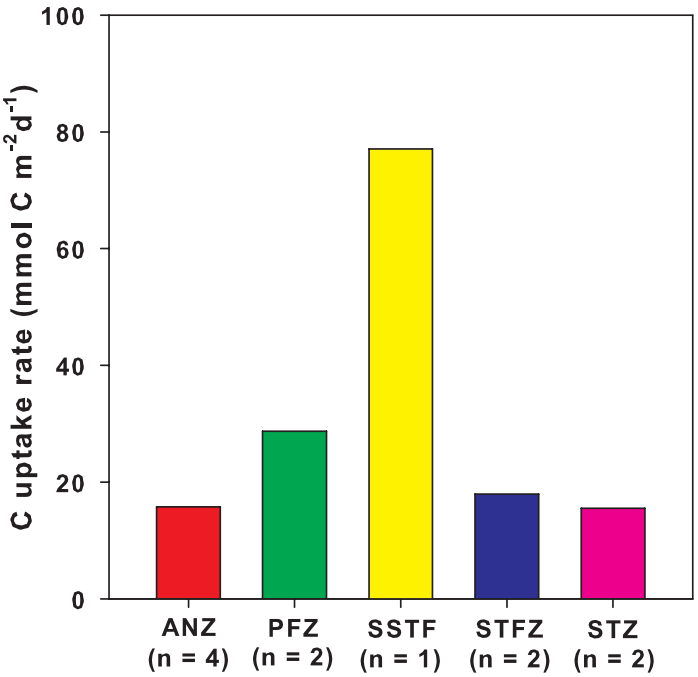

Figure 5.13: *Average carbon uptake rates in different zones (ANZ, PFZ, SAZ, and STZ; see text for the details) of SO. Number of sampling locations (n) for the respective zones are shown on the X-axis.*

The region STFZ, north of the SSTF, mostly shows characteristics of subtropical water (low nutrients) and low productivity. Locations near the equator show productivity between 12.0 and 24.7 mmol C $m^{-2}d^{-1}$ (143 to 296 mg C $m^{-2}d^{-1}$). The northernmost location (SO-S14) shows the highest productivity among the three locations, comparable to that observed here during boreal summer 2008 (see Chapter 4).

5.3.2 Nitrogen uptake rate

New productivity (NO_3 uptake rate) and regenerated productivity (the sum of NH_4 and urea uptake rates) results (using ^{15}N-labelled tracers) at 14 locations are shown in Figs 5.14, 5.15, and 5.16.

New productivity

Depth profiles of new productivity are shown in Fig 5.14. Surface new productivity varies between 0.01-0.03 μmol N $L^{-1}d^{-1}$ and 0.01-0.8 μmol N $L^{-1}d^{-1}$ on 57.5^{o}E and 48^{o}E, respectively, while near the equator it varies from 0.02 to 0.1 μmol N $L^{-1}d^{-1}$. Along both the transects, most new productivity is confined to the top 5-10 m layer (Fig 5.14). Locations (SO-S3 and SO-S9) near the Subtropical convergence show higher new productivity along both the transects. In addition, the location near the Antarctic coast (SO-S6) also shows significantly higher new productivity.
Overall, 48^{o}E shows higher new productivity values than 57.5^{o}E. These variations are in accordance with those observed in C uptake rates (discussed in the previous section).
Euphotic-depth-integrated new productivity varies from 0.6-2.4 mmol N $m^{-2}d^{-1}$ (with an average of 1.3 mmol N $m^{-2}d^{-1}$) on 57.5^{o}E. A significant higher new productivity is also observed near the Antarctic coast (SO-S6). New productivity on 48^{o}E varies between 0.3-4.1 mmol N $m^{-2}d^{-1}$ (with an average of 1.7 mmol N $m^{-2}d^{-1}$). The average new productivity on 48^{o}E is higher that on 57.5^{o}E. Our values are lower than those reported for the Antarctic polar front (0.9-12.5 mmol N $m^{-2}d^{-1}$; *Sambrotto and Mace*, 2000) and for the Pacific sector (0.9-7.6 mmol N $m^{-2}d^{-1}$; *Savoye et al.*, 2004). *Prakash* (2008) observed new productivity from 0.9 to 7.7 mmol N $m^{-2}d^{-1}$ during austral summer 2006 in the Indian Sector, which are also higher than the present values; nevertheless, comparable those obtained by *Cota et al* (1992) for the Scotia/Weddell Sea. Despite the similarity of the study region and season with *Prakash* (2008), our new productivity values are quite different. The difference signifies inter-annual variability in the new productivity

in the Indian Sector of the SO. Among the five zones, the highest new productivity is found to be 4.1 mmol N $m^{-2}d^{-1}$ for the SSTF and the lowest value (0.4 mmol N $m^{-2}d^{-1}$) is associated with the STZ (Fig 5.17).

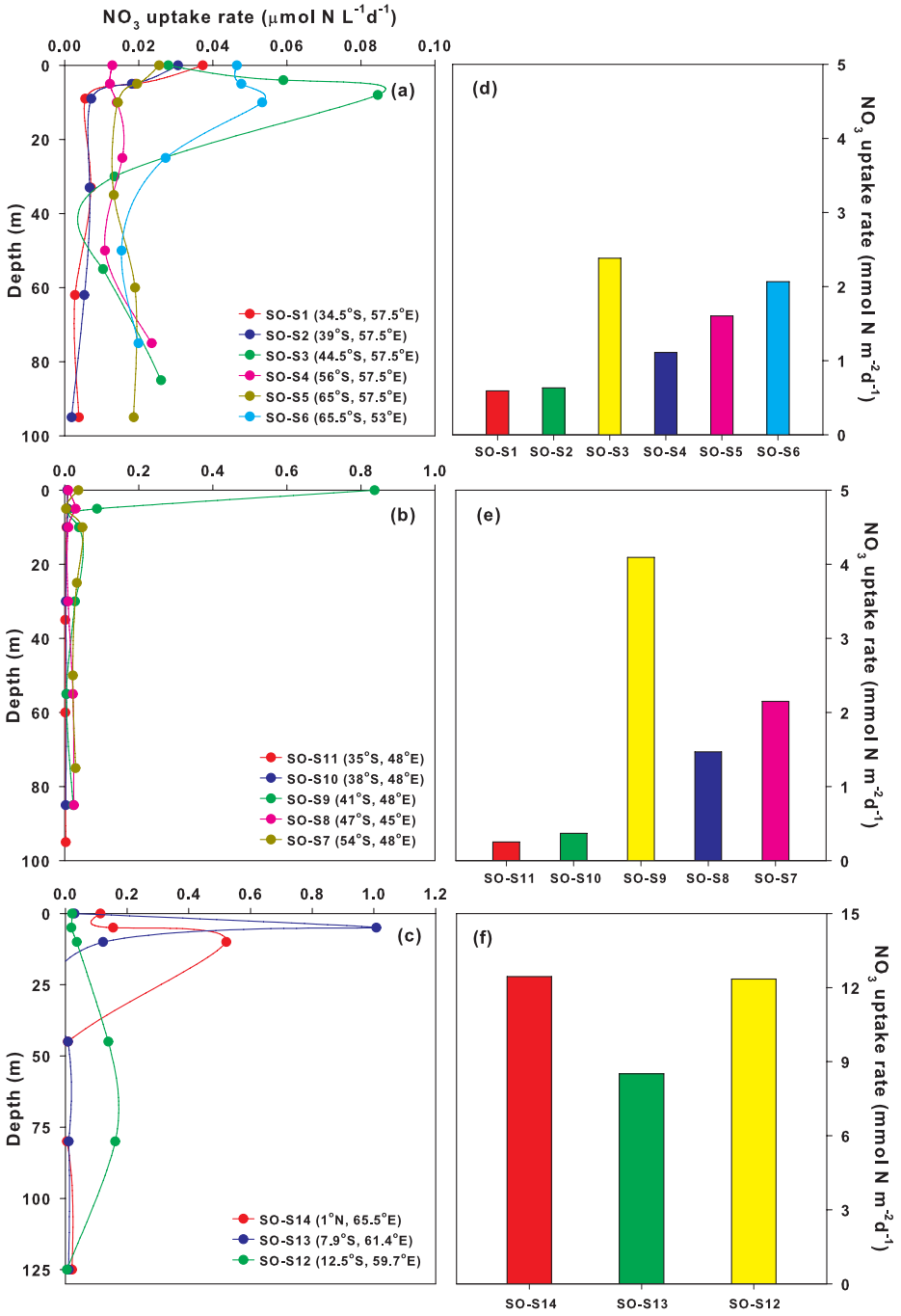

Figure 5.14: *Depth profiles of NO_3 uptake rate (a, b, and c) and their euphotic-depth-integrated values (d, e, and f) at different locations in the SO.*

C uptake rates are also the highest and the lowest at the SSTF and STZ, respectively (Fig 5.13). Such higher new productivity values associated with the front have also been reported by *Sambrotto and Mace* (2000) and *Savoye et al* (2004). New productivity of the SSTF is similar to the reported by *Savoye et al* (2004) for the same zone. The ANZ and PFZ show moderate new productivity despite the limiting factors such as light (for the latter) and Fe (for the former). Unavailability of NO_3 is the main factor of the observed very low new productivity at the STFZ and STZ regions.

Regenerated productivity

Ambient NH_4 and urea measurements were not done during the present study and hence conservative estimates of NH_4 and urea uptake rates are presented here. Depth profiles of NH_4 uptake rate are shown in Fig 5.15. Not much variation is observed in the surface NH_4 uptake rate ($\sim$0.01 μmol N $L^{-1}d^{-1}$) along both the 57.5^{o}E and 48^{o}E transects, while near the equator, it varies from 0.02 to 0.09 μmol N $L^{-1}d^{-1}$. Unlike new productivity, the NH_4 uptake is not confined to the upper layer but shows almost uniform values throughout the euphotic zone (Fig 5.15). Euphotic-depth-integrated NH_4 uptake rate varies from 0.8-1.6 mmol N $m^{-2}d^{-1}$ (with an average of 1.1 mmol N $m^{-2}d^{-1}$) along 57.5^{o}E, and between 0.8-1.5 mmol N $m^{-2}d^{-1}$ (with an average of 1.1 mmol N $m^{-2}d^{-1}$) along 48^{o}E. This indicates that no significant longitudinal variation exists for the NH_4 uptake rates, unlike in new productivity. Instead NH_4 uptake shows a latitudinal variation, it decreases towards south along both the transects. Overall, NH_4 uptake is 20% and 40% lower than that new productivity along the 57.5^{o}E and 48^{o}E transects, respectively (Figs 5.14 and 5.15). The values are much lower than those reported for the Antarctic polar front (12.2-54.8 mmol N $m^{-2}d^{-1}$; *Sambrotto and Mace*, 2000), for the Pacific sector (2.1-3.0 mmol N $m^{-2}d^{-1}$; *Savoye et al.*, 2004), and for the Scotia/Weddell Sea (0.7-9.7 mmol N $m^{-2}d^{-1}$; *Cota et al.*, 1992). *Prakash* (2008) observed NH_4 uptake rate 0.5 to 3.3 mmol N $m^{-2}d^{-1}$ for the Indian Sector, which are also higher

than the present values. As in the case of new productivity, despite the similarity in the study region and season with *Prakash* (2008), NH_4 uptake values are quite different in both the studies. Here too, the difference probably signifies inter-annual variability in the NH_4 uptake rate in the Indian Sector of the SO.

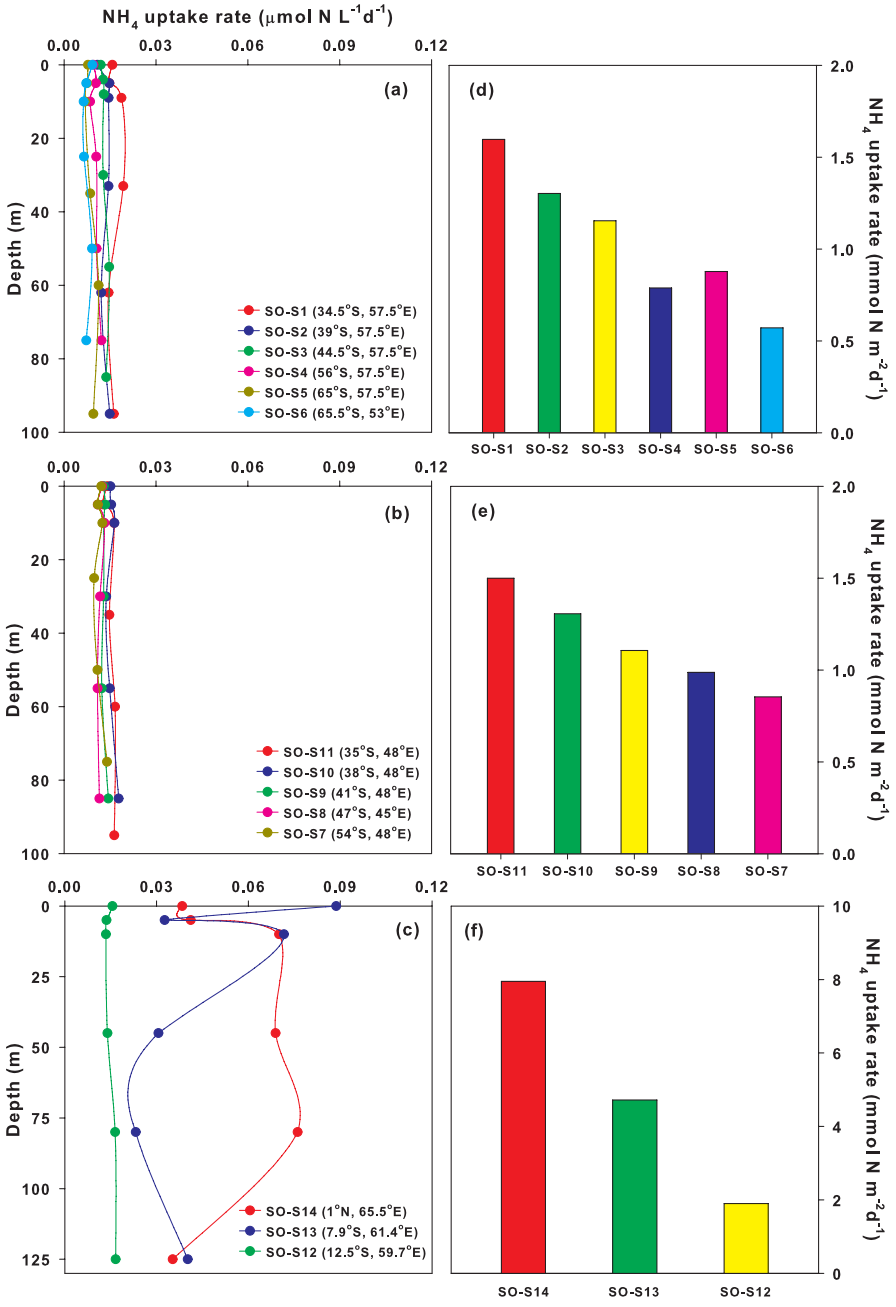

Figure 5.15: *Depth profiles of NH_4 uptake rate (a, b, and c) and their euphotic-depth-integrated values (d, e, and f) at different locations in the SO.*

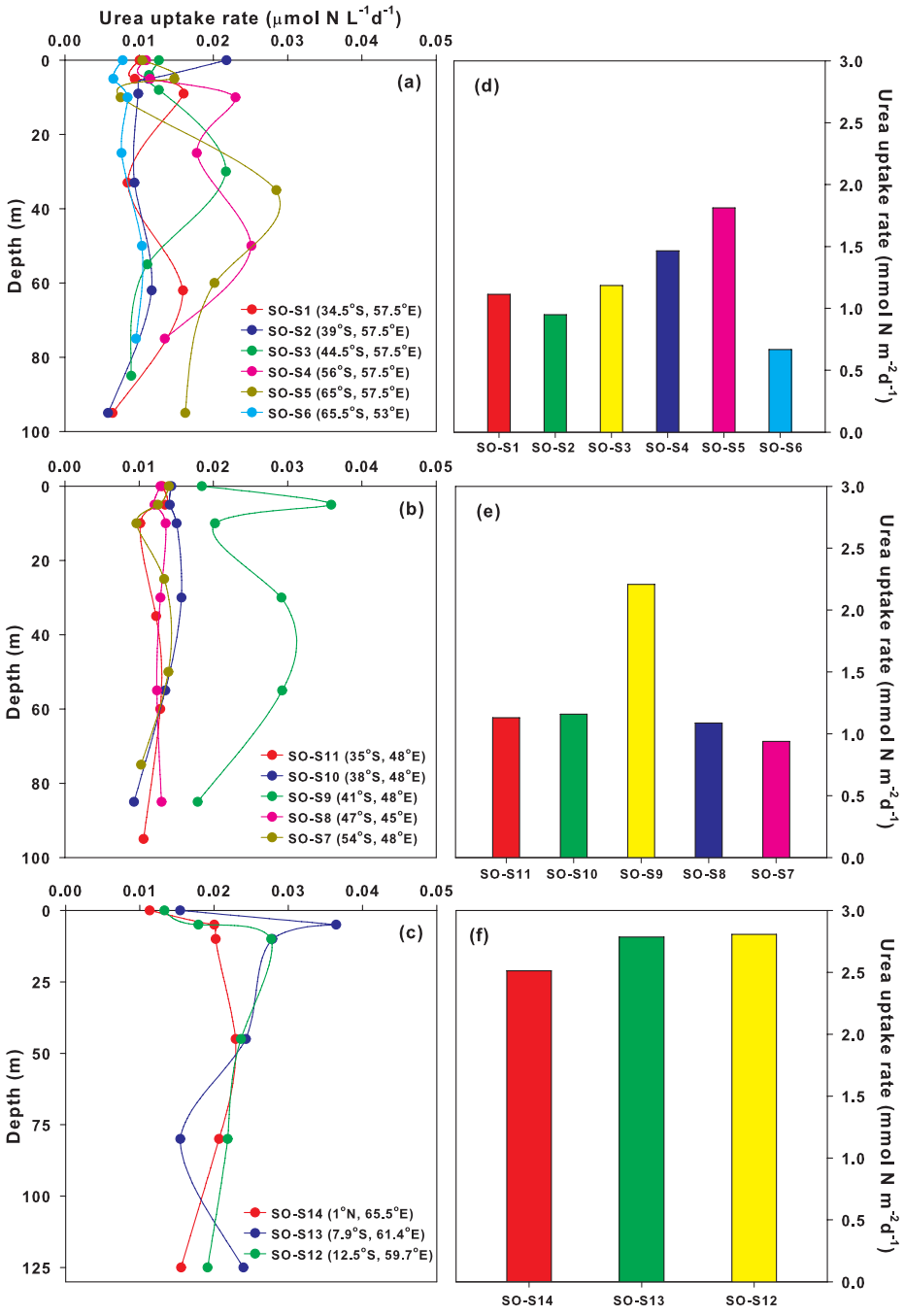

Figure 5.16: *Depth profiles of urea uptake rate (a, b, and c) and their euphotic-depth-integrated values (d, e, and f) at different locations in the SO.*

The highest NH_4 uptake rate is found to be 1.5 mmol N $m^{-2}d^{-1}$ for the STZ and the lowest (0.8 mmol N $m^{-2}d^{-1}$), associated with the ANZ (Fig 5.17). NH_4 uptake rate increases from zone 1 towards zone 5 (Fig 5.17). Near the equator,

integrated NH_4 uptake rate varies a lot, from <2 to >8 mmol N $m^{-2}d^{-1}$; unlike new productivity, NH_4 uptake rates are higher than those observed during boreal summer 2008 in this region (see chapter 4).

Depth profiles of urea uptake rate are shown in Fig 5.16. Surface urea uptake rate varies from 0.01-0.02 μmol N $L^{-1}d^{-1}$ along both the transects. Locations near the equator also show similar values (Fig 5.16). Similar to the NH_4 uptake, the urea uptake is almost uniform throughout the euphotic zone (Fig 5.16), except at SO-S6 and SO-S9, while locations near the equator show large variations in urea uptake with depth.

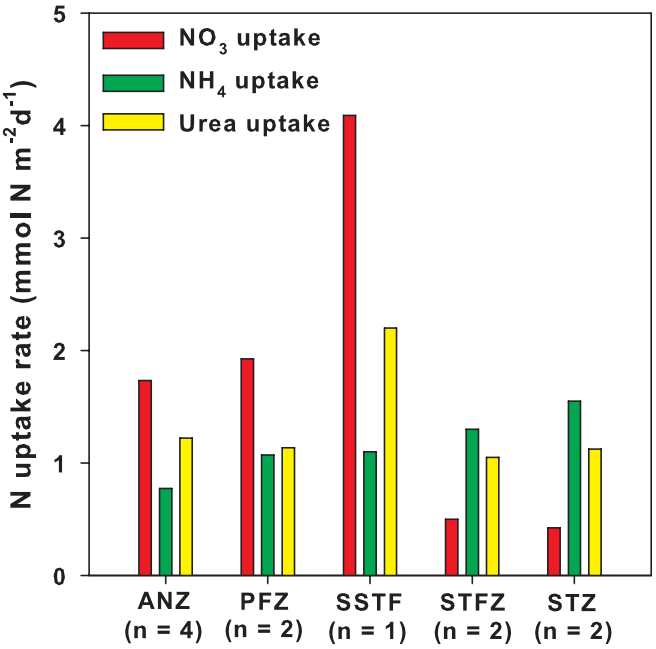

Figure 5.17: *Average nitrogen (NO_3, NH_4 and Urea) uptake rates in different zones (ANZ, PFZ, SAZ, and STZ; see text for the details) of SO. Number of sampling locations in the respective zones are marked on the X-axis.*

Euphotic-depth-integrated urea uptake rate varies from 0.9-1.8 mmol N $m^{-2}d^{-1}$ (with an average of 1.3 mmol N $m^{-2}d^{-1}$) along 57.5^{o}E. It varies between 0.9-2.2 mmol N $m^{-2}d^{-1}$ (with an average of 1.3 mmol N $m^{-2}d^{-1}$) along 48^{o}E. This indicates that no significant longitudinal variation exists in the urea uptake rate, as in the case of NH_4 uptake. Urea uptake also shows a latitudinal variation

but unlike NH_4 uptake, it increases towards the south along 57.5^{o}E (Fig 5.16). However, though SO-S6 shows the lowest urea uptake, it shows the highest NH_4 uptake. Along 48^{o}E, urea uptake rates are comparable at all locations, except at SO-S9. Locations near the equator also show comparable urea uptake rates (Fig 5.16). Overall, urea uptake rates are comparable to new productivity and higher than NH_4 uptake along both the transects. All the four zones show comparable urea uptake rates (Fig 5.17).

Urea uptake rates presented here are comparable to the values reported for the Pacific Sector (0.5-1.8 mmol N $m^{-2}d^{-1}$; *Savoye et al.*, 2004) and for the Indian Sector (0.2-1.9 mmol N $m^{-2}d^{-1}$; *Prakash*, 2008). Overall, the comparison suggests that urea uptake rates do not show much spatial as well as inter-annual variations. The total regenerated productivity (the sum of NH_4 and urea uptake rates) varies from 2.3-2.7 and 1.8-3.3 mmol N $m^{-2}d^{-1}$ along 57.5^{o}E and 48^{o}E, respectively. The highest total regenerated productivity (3.3 mmol N $m^{-2}d^{-1}$) is associated with the SSTF, which also shows the highest new productivity. The regenerated productivity varies from 2.0 to 2.6 mmol N $m^{-2}d^{-1}$ in the other four zones with an increasing trend from north to south (Fig 5.17). It varies between 4.7-10.5 mmol N $m^{-2}d^{-1}$ for the locations near the equator. The regenerated productivity values are slightly higher than new productivity over the SO, but lower than new productivity at equatorial locations.

f-ratio

As the NH_4 and urea uptake rates calculated in this work are conservative estimates, they are somewhat approximate. The surface *f*-ratio varies from 0.4 to 0.6 (with an average of 0.5) and 0.2-0.9 (with an average of 0.4) along 57.5^{o}E and 48^{o}E, respectively. By excluding SO-S9, the average *f*-ratio on 48^{o}E is only 0.3, lower than on 57.5^{o}E. The surface *f*-ratio over the locations near the equator varies from 0.2-0.7. The lowest *f*-ratio is found at the location SO-S10, and the highest at SO-S9. Overall, the surface *f*-ratio is close to 0.5. This suggests that 50% of the

productivity is induced by NO_3 and thus, new productivity is significantly high in the surface waters of the SO.

Euphotic-depth-integrated *f*-ratio varies from 0.2 to 0.5 with the highest value at the location SO-S3 along 57.5^{o}E, while the *f*-ratio varies from 0.1 to 0.6, with the highest value at SO-S7 along 48^{o}E. The location near the Antarctic coast (SO-S6) also shows a higher *f*-ratio (0.6). The values are significantly lower than the values reported by *Collos and Slawyk* (1986) for the Indian Sector along 66.5^{o}E. They reported *f*-ratios as high as 0.98 from a station at 43^{o}S. In the present study, higher *f*-ratio (0.6) is observed near the Subtropical convergence, but is much lower than that reported by *Collos and Slawyk* (1986). Values reported here are comparable to those of the Pacific (0.5-0.6; *Savoye et al.*, 2004) and the Indian sectors (0.2-0.6; *Mengesha et al.*, 1998). *Prakash* (2008) also reported a mean *f*-ratio of 0.5 for the Indian Sector. Locations near the equator show *f*-ratios between 0.5 and 0.7, lower than those observed here during the boreal summer 2008 (see chapter 4).

The SSTF exhibits the highest *f*-ratio (0.6); the lowest value, 0.1, is observed over STZ. The PFZ and SAZ show similar *f*-ratios (0.5), while the STFZ shows a very low (0.2) *f*-ratio. Unavailability of NO_3 could be the reason for the observed very low *f*-ratios in the STZ and STFZ. Different plankton populations (species and size) between different zones could also be a factor for the observed variation in the *f*-ratios (*Savoye et al.*, 2004). Their physiological characteristics, such as preference for NO_3 or NH_4, could vary considerably, even within the groups, which would probably lead to the differences. In general, *f*-ratio (0.5) indicates that the SO is capable of significant new/export production.

5.3.3 C:N consumption ratio

The depth variation of the ratio of carbon to nitrogen uptake rates (C:N) at different locations along 57.5^{o}E and 48^{o}E and near the equator are shown in Fig 5.18. The ratio at surface is more than 12 along both the transects (Figs 5.18a, 5.18b), much higher than the Redfield ratio (C:N = 6.6). It gradually decreases with depth

at all the locations. Except SO-S11, locations near the equator show values lower than the Redfield ratio throughout the euphotic zone (Fig 5.8c).

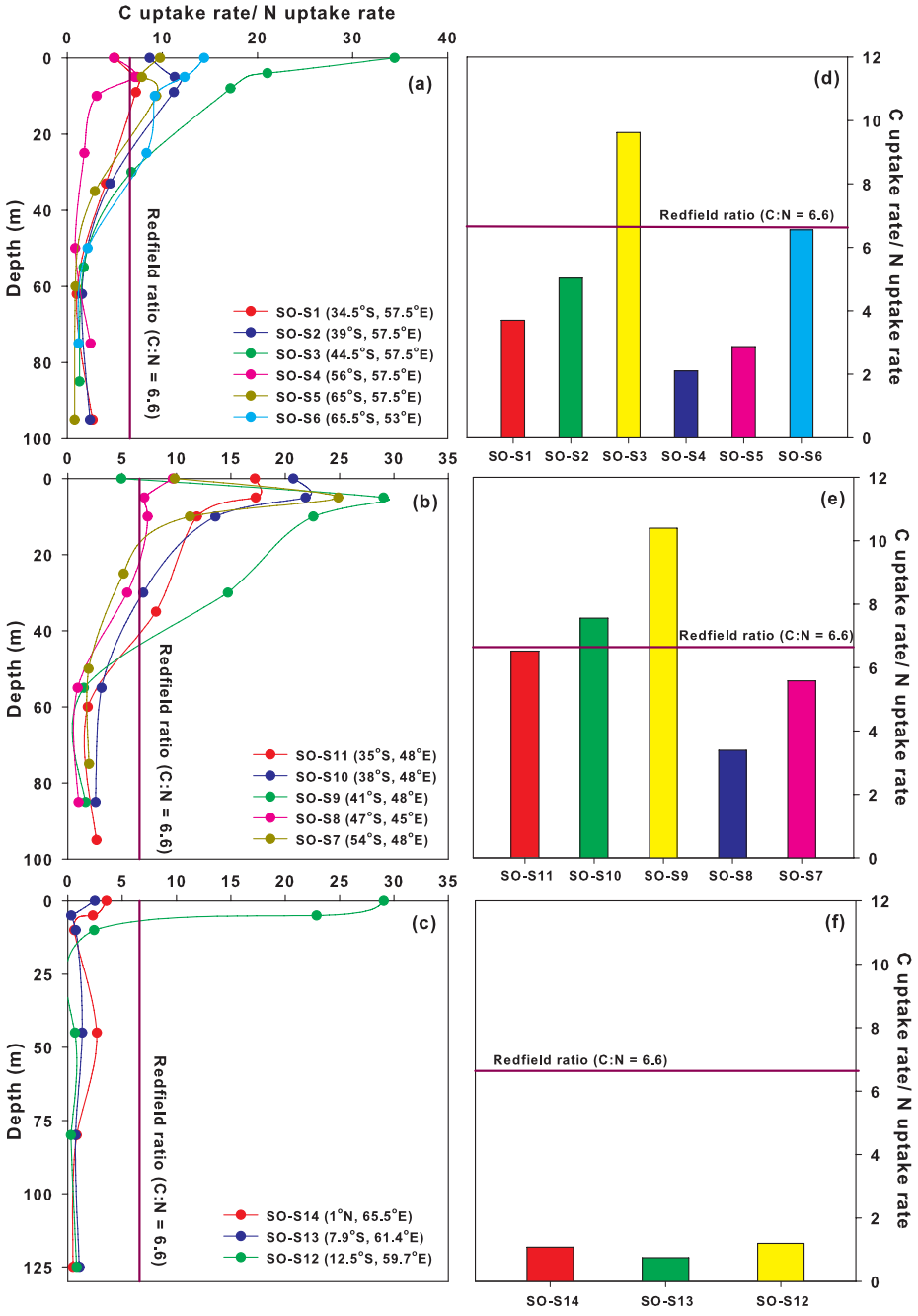

Figure 5.18: *Depth profiles of the ratio of the observed C to N uptake rates (a, b, and c) and the ratio of the observed euphotic-depth-integrated C to N uptake rates at different locations in the SO (d, e, and f). Pink lines represent the Redfield ratio (C:N = 6.6).*

Euphotic-depth-integrated C:N ratio for all the sampling locations are shown in Fig 5.18. Most of the locations on 57.5^{o}E, exhibit C:N ratio lower than the Redfield ratio (Fig 5.18d). In contrast, most of the locations on 48^{o}E, exhibit C:N ratios comparable to the Redfield ratio (Fig 5.18e). *Slawyk* (1979) also observed a wide range from 0.1 to 25.1 for the C:N uptake ratio for the Indian Sector. It was attributed to the variation in light intensity. The effect of surface light intensity is not found in the present study as a wide range of PAR values (170 to 1390 μmol $m^{-2}s^{-1}$) are associated with even wider ranges of C:N uptake ratios (5.0 to 34.1). In addition, ANZ, which is supposed to be light limited, shows a ratio (6.5) very close to the Redfield ratio. The SSTF exhibits a very high ratio (>10.0). Nevertheless, the ratio varies (from 4.3-6.5) marginally and stays close to the Redfield ratio in the other four zones. The composition of phytoplankton (for the ANZ and PFZ) and unavailability of NO_3 (for the STZ and STFZ) could be the main controlling factors here for the marginal shift in the ratio (*Arrigo*, 2005). *Odate and Fukuchi* (1995) observed large variation of plankton populations (species and size) between different regions of the Indian sector along a similar transect. Locations near the equator show C:N values much lower than the Redfield ratio (Fig 5.18f), similar to the boreal summer 2008 observations (see chapter 4).

5.4 Conclusion

The different water masses in the SO, along with their unique characteristics, control the nutrient dynamics, which ultimately decides the level of biological productivity. The present study shows that the availability of nutrients, surface light intensity, supply of Fe from the Antarctic continent together are the main controlling factors in deciding productivity in the SO. The Antarctic bottom water carries dissolved Fe towards the north and upwells at the SSTF and supports high productivity. Productivity is found to be different on different longitudes. The zonal variations in productivity accompany variations in SST, salinity and nutrients. In general, the SO is low productive. Zonal variations observed in the productivity

corroborate earlier data of *Jasmine et al* (2009). The new productivity covaries with the overall productivity, while uptake of reduced forms of nitrogen (NH_4 and urea) show opposite trends. On the basis of the C and N uptake data the entire region can be divided into five zones (from south to north).

(i) The ANZ is characterized by low productivity (∼190 mg C $m^{-2}d^{-1}$) and high new productivity (1.7 mmol N $m^{-2}d^{-1}$) and moderate *f*-ratio (close to 0.5). Here NO_3 is the preferred nitrogenous compound, followed by urea and NH_4. However, the sum of urea and NH_4 uptake rates is slightly higher than the NO_3 uptake. The region shows C:N ratios close to the Redfield ratio. Light limitation could be responsible for the low productivity here. (ii) The PFZ is characterized by low productivity (∼345 mg C $m^{-2}d^{-1}$) and moderate new productivity (1.9 mmol N $m^{-2}d^{-1}$) and *f*-ratio comparable to that at ANZ. Here too, NH_4 is the least preferred nitrogenous compound. NO_3 is the dominant nitrogen substrate for phytoplankton here. Overall, new productivity and regenerated productivity are roughly balanced here. As suggested by *Jasmine et al* (2009), grazing by zooplankton could keep the productivity low in this zone. (iii) The SSTF is characterized by the highest productivity (∼925 mg C $m^{-2}d^{-1}$) with the highest new productivity (4.1 mmol N $m^{-2}d^{-1}$), and the *f*-ratio slightly higher (0.6) than in the previous two zones. Higher urea uptake here controls the *f*-ratio. Here too, NO_3 is the most preferred nitrogenous compound, followed by urea and NH_4. The higher productivity and new productivity are the consequence of the supply of key micro-nutrients (Fe) here by subantarctic bottom water. (iv) The STFZ is characterized by low productivity (∼215 mg C $m^{-2}d^{-1}$) with low new productivity (0.5 mmol N $m^{-2}d^{-1}$), and very low *f*-ratio (0.2). The reduced forms of nitrogen mainly fuels the productivity here. Here, NH_4 is the most preferred nitrogenous compound and the least preferred is NO_3. Unavailability of NO_3 is the main cause for low productivity, new productivity and *f*-ratios in this zone. Overall, this zone shows oligotrophic characteristics. (v) The STZ is characterized by the least productivity (∼185 mg C $m^{-2}d^{-1}$) and the lowest new productivity (0.4 mmol N $m^{-2}d^{-1}$) and *f*-ratio (0.1). The N uptake

regime is more or less similar to that observed at STFZ; NH_4 is the most preferred nitrogenous compound, followed by urea and NO_3. Plankton composition likely differs between these different zones. Therefore, one would expect a difference in the preference for nitrogen species, and this probably explains the observed differences. The variation in the N regime controls the consumption ratio of C:N by phytoplankton during photosynthesis (*Arrigo*, 2005). The overall productivity variations are similar to the data of *Jasmine et al* (2009). Comparison with the results of *Prakash* (2008) reveals that the NO_3 and NH_4 uptake rates show some inter-annual variability, while such variability is not observed in the urea uptake. The observed new productivity values are generally lower than those reported earlier from different parts of the SO. Nevertheless, the latitudinal variation in the new productivity observed in the present study corroborates previous reports from the region, as do the observed *f*-ratios. There is a need to monitor the effect of global warming over the new productivity of the region, as the available data are too limited to draw definitive conclusions.

Chapter 6

Summary and scope for future work

New and total productivity measurements have been carried out in different oceanic regions viz., the Arabian Sea (AS), the Bay of Bengal (BOB), the equatorial Indian Ocean (EIO), and the Indian sector of the Southern Ocean (SO) during different seasons between 2006 and 2009. Each of these regions represents a different productivity regime. The AS is one of the most productive regions of the world's ocean (*Madhupratap et al.*, 1996; *Prasanna Kumar et al.*, 2001) as well as intense oxygen minimum and denitrification zones (*Naqvi*, 1987). In contrast, productivity in the BOB is lower (*Prasanna Kumar et al.*, 2002), and it exhibits a relatively thinner and less intense oxygen minimum zone with no evidence of significant denitrification (*Rao et al.*, 1994; *Sardessai et al.*, 2007). However, the EIO neither has an intense oxygen minimum zone nor any denitrification (*Sardessai et al.*, 2010). In terms of biological productivity, satellite ocean color data suggest that the equatorial Atlantic and Pacific are more productive compared to the EIO. In the Indian Sector of the SO, different zones show wide ranges of productivity (*Jasmine et al.*, 2009). Despite the high concentrations of N and P throughout the year, the region exhibits low productivity. Therefore, the SO, like the subarctic Pacific and the equatorial Pacific, is termed as high-nutrient, low chlorophyll (HNLC) region (*El-Sayed*, 1984). A summary of measured carbon and different nitrogen (NO_3, NH_4 and urea) uptake rates along with the f-ratios are given in Table 6.1.

Table 6.1: *Summary of the measured uptake rates of carbon (mmol C $m^{-2}d^{-1}$; ρC), NO_3 (ρNO_3), NH_4 (ρNH_4), and urea ($\rho Urea$) and f-ratios during the present study at different regions and seasons using the ^{13}C and ^{15}N tracer techniques. Nitrogen uptake rates are in the unit of mmol N $m^{-2}d^{-1}$*

Region	**Season**	ρ**C**	ρ**NO$_3$**	ρ**NH$_4$**	ρ**Urea**	***f*-ratio**
AS	Spring	ND	0.2-1.3	0.1-0.4	0.1-0.15	0.5-0.8
	Late winter	1.8-19.6	1.6-9.0	0.1-0.4	0.1-0.6	0.8-0.9
BOB	Spring	0.03-0.25*	3.2-6.6	0.1-0.6	0.3-9.6	0.3-0.9
	Early winter	16.9-35.8	24.2-69.5	3.8-4.3	1.0-1.4	0.8-0.9
EIO	Summer	2.8-20.4	7.5-14.1	1.5-2.1	1.3-2.6	0.4-0.6
SO	Austral summer	7.1-45.4	0.3-4.1	0.8-1.6	0.9-2.2	0.1-0.6

* *Only surface carbon uptake (μmol C $L^{-1}d^{-1}$) was measured; ND-no data available.*

6.1 Results from the Arabian Sea

The major findings of the present study from the AS are listed below.

6.1.1 Results during spring 2006

- During spring, diatoms dominate plankton population in the NE-AS (more than 50%). Cyanobacteria is the next most abundant plankton and mostly dominates in the coastal region. Both *Trichodesmium erythraeum* and *Trichodesmium thibautii* are found in the region, with a slight dominance of the former.

- The region is well stratified in spring and most of the NO_3 uptake takes place below the mixed layer. Nitrate is the most preferred nitrogenous nutrient, followed by NH_4 and urea.

- As *Trichodesmium* is abundant in the coastal region, the associated N_2-fixation rate (estimated from the abundance and cell specific uptake rate) is also higher than at open ocean regions. N_2-fixation rate is mostly confined to the first few meters of the surface. At coastal locations, NO_3 uptake and

N_2-fixation dominate as a major factor of new production below the mixed layer and surface layers, respectively.

- The lowest δ^{15}N of surface PON coincides with the highest *Trichodesmium* abundance at surface, suggesting that *Trichodesmium* fixes atmospheric N_2 ($\delta^{15}N = 0$) and adds new nitrogen to the ocean.

- The annual input of nitrogen from the growth of *Trichodesmium* is estimated to be ∼0.9 Tg N.

- δ^{15}N of surface PON suggests that the recently fixed nitrogen contributes to as high as ∼79 % of the nitrogen in the surface suspended particles.

6.1.2 Results from late winter 2007

- During late winter, diatoms dominate the plankton population in the region (more than 60%). However, at two locations, *Noctiluca miliaris* dominates over other plankton (more than 80% in the surface waters).

- On the basis of earlier findings and the present data, no significant signature for any shift of plankton community from diatoms to a *Noctiluca miliaris*-dominated community is observed. Further, the results suggest that the north-western AS is known to be dominated by *Noctiluca miliaris* blooms and the eastern AS, dominated by diatoms.

- A large variation in productivity is observed between two nearby latitudes (21^oN and 22^oN), which is also evidenced by SeaWiFS chlorophyll images. The northern locations are more productive than the southern one.

- The surface cell concentration affects light penetration and thus the depth of the euphotic zone, and thereby, the column integrated productivity.

- The present study provides the first evidence of photo-inhibition in the surface waters of the region using time course as well as varying light intensity

experiments. When light intensity exceeds from 1200 μmol $m^{-2}s^{-1}$ surface productivity decreases due to the effect of photo-inhibition.

- In an another experiment, the highest specific uptake rate is found in the morning, followed by the evening and the noon.

- A comparison of the present results with the earlier reported values indicates that new productivity varies during winter and the preference for different nitrogenous substrates varies from the west to the east.

6.2 Results from the Bay of Bengal

The major findings of the present study from the BOB are listed below.

6.2.1 Results during spring 2007

- In the BOB, the light reaching to the sea surface is mainly controlled by clouds. Photosynthetically active radiation (PAR) varies from 200 to 1690 μmol $m^{-2}s^{-1}$ during the study period. However, clear day surface light intensity is found to be comparable to that observed during the spring in the NE-AS (present study).

- The Deep Chlorophyll Maxima (DCM) is invariably situated between 50 and 70 m at all the locations. The availability of nutrients is the key factor which controls surface productivity, as light remains moderate. Higher chlorophyll at mid-depths are the consequence of moderate light and higher nutrients at those depths.

- Like in the NE-AS, east-west variation in productivity is observed in the BOB with the western part exhibiting higher productivity.

- NO_3 is found to be the most preferred nitrogen compound followed by urea and NH_4 by phytoplankton.

- A comparison of the present results with the earlier findings reveals that the BOB has a larger contribution relative to the NE-AS in the sequestration of CO_2 from the atmosphere, particularly during spring.

6.2.2 Results during early winter 2007

- In the present study, an eddy is identified at 17.8 ^{o}N, 87.5 ^{o}E, with the help of sea surface height anomaly image.

- Although the SST is similar at eddy and non-eddy locations, a large variation in the surface NO_3 concentration has been observed. NO_3 concentration in the upper 20 m at the center of the eddy is found to be six times higher that outside of the eddy.

- Eddy-pumping supplies nutrients from the deep and enhances the new productivity. Integrated new productivity is more than twice higher at the center of the eddy than outside.

- NH_4 and urea uptake rates are found to be very low compared to NO_3 uptake. Overall, in the eddy region, NO_3 is the most preferred nitrogenous substrate.

- Higher new productivity and f-ratios observed in the eddy region suggests that eddies are capable of exporting most of the total production to the deep.

6.3 Results from the Equatorial Indian Ocean

The major results obtained during summer 2008 from the EIO are listed below.

- Sea state was 8 (near "Gale" conditions) and the sea very rough, particularly to south of the equator during summer 2008. Strong cloudiness suppressed PAR in the region. PAR is found to be as low as 164 μmol m^{-2}s^{-1} at the southern most sampling location.

- A signature of denitrified waters from the Arabian Sea is seen in the region.

- The present study indicates that the surface light intensity along with the nutrient availability decides the productivity in the EIO.
- Higher surface light intensity reduces the surface productivity but on the other hand, it enhances the column productivity in the EIO.
- The region shows comparable new productivity and *f*-ratios to that obtained from the other parts of the Indian Ocean. Further, the region shows the potential for higher export production as other parts of the Indian Ocean.
- A comparison with the earlier findings with the present study rules out any significant change in productivity in the region over the past 3-decades.

6.4 Results from the Indian sector of the Southern Ocean

The major results obtained during the austral summer 2009 from the SO are listed below.

- In the SO, strong winds, cyclones, precipitation, snow fall, and often cloudy conditions are found during the austral summer 2008. Icebergs were seen to the south of 65^{o}S. A big storm is faced (sea state >10; Atmospheric pressure = 962 mbar; V_w = 60 ms^{-1}) to the south of 55^{o}S along the 48^{o}E.
- A general decreasing trend in SST is observed towards the south along both 48^{o}E and 57.5^{o}E longitudes. However, some notable differences are: (i) decline in the SST is much sharper on 48^{o}E than on 57.5^{o}E, and (ii) the higher gradient in the SST is shifted a little southwards at 57.5^{o}E compared to the 48^{o}E transect. This suggests the nonuniformity of the boundary of the Sub-Tropical convergence in the Indian sector
- All the nutrients NO_3, NO_2, SiO_4 and PO_4 show higher concentrations to the south of the polar front. At the Subtropical Convergence, NO_2 and SiO_4

are very low, while NO_3 and PO_4 remain significantly higher, reflecting its assimilation by diatoms and silico-flagellates. For a given latitude, values of nutrients on 48^{o}E are higher than that on 57.5^{o}E. This suggests that all the nutrient inventory is closely related to the circulation, water masses and their boundaries.

- The highest surface chl *a* (>0.5 mg m^{-3}) is found at the Subtropical convergence along 57.5^{o}E. On either side of the Subtropical convergence, surface chl *a* is lower.

- Depth of DCM varies from 30 to 100 m and 30 to 80 m along 57.5^{o}E and 48^{o}E, respectively.

- The new productivity covaries with the overall productivity, while uptake of reduced forms of nitrogen (NH_4 and urea) shows opposite trends. On the basis of the C and N uptake data, the entire region can be divided in five zones (from south to north) viz., (i) between the Antarctic continent and the polar front (Antarctic zone; ANZ), (ii) between the polar and SubAntarctic fronts (Polar frontal zone; PFZ), (iii) between the SAF and ARF (South Subtropical front; SSTF), (iv) Subtropical frontal zone (STFZ), and (v) between the ARF and North Subtropical front (Subtropical zone; STZ).

- ANZ is characterized by low productivity (∼190 mg C $m^{-2}d^{-1}$) and high new productivity (1.7 mmol N $m^{-2}d^{-1}$) and moderate *f*-ratio (close to 0.5). Here NO_3 is the preferred nitrogenous compound, followed by urea and NH_4. Light limitation could be responsible for the low productivity here.

- PFZ is characterized by low productivity (∼345 mg C $m^{-2}d^{-1}$) and moderate new productivity (1.9 mmol N $m^{-2}d^{-1}$) and *f*-ratio comparable to that at ANZ. Here too, NH_4 is the least preferred nitrogenous compound. As suggested by *Jasmine et al* (2009), grazing by zooplankton could keep the productivity low in this zone.

- SSTF is characterized by the highest productivity (∼925 mg C $m^{-2}d^{-1}$) with the highest new productivity (4.1 mmol N $m^{-2}d^{-1}$), and the *f*-ratio slightly higher (0.6) than in the previous two zones. Here, higher urea uptake controls the *f*-ratio. The higher productivity and new productivity are the consequence of the supply of key micro-nutrients (Fe) here from the subantarctic bottom water.

- STFZ is characterized by low productivity (∼215 mg C $m^{-2}d^{-1}$) with low new productivity (0.5 mmol N $m^{-2}d^{-1}$), and very low *f*-ratio (0.2). The reduced forms of nitrogen mainly fuels the productivity here. This zone shows oligotrophic characteristics.

- STZ is characterized by the least productivity (∼185 mg C $m^{-2}d^{-1}$) and the lowest new productivity (0.4 mmol N $m^{-2}d^{-1}$) and *f*-ratio (0.1). The N uptake regime is more or less similar to that observed at STFZ; NH_4 is the most preferred nitrogenous compound and followed by urea and NO_3.

The present study is an attempt to provide comprehensive data on oceanic productivity (total, new and regenerated) and *f*-ratios for the different oceanic basins. The results presented here are useful to test/validate biogeochemical models. This further can be combined with remote sensing data to elucidate the vital role of marine biological productivity in the global carbon cycle. However, to obtain large scale estimations for the carbon export fluxes, sustained observations over several years of ^{13}C-^{15}N based primary and export productivity, coupled with biogeochemical models and remote sensing are called for.

6.5 Scope for future work

More work needs to be done on this topic with improvements for a better understanding of the nitrogen cycling and carbon fluxes between oceans and the atmosphere. Future work that could be undertaken in continuation of the present study are:

- *Trichodesmium* blooms are frequently seen in the Arabian Sea and the Bay of Bengal (*Devassy et al.*, 1978, *Capone et al.*, 1998, *Parab et al.*, 2006; *Jyothibabu et al.*, 2003). In addition to the *Trichodesmium* blooms, presence of diazotrophic γ-proteobacteria in the Arabian Sea has also been reported (*Bird et al.*, 2005), which are thought to release fixed nitrogen to the ocean water, which becomes then available to the other non-diazotrophic species (*Letelier and Karl*, 1996). Only one study is reported in which direct measurements of N_2-fixation was measured in the central Arabian Sea, more than a decade ago. Therefore, it is important to estimate rates of N_2-fixation in the northern Indian Ocean to better constrain the nitrogen gain to the ocean from the atmosphere.

- The role of denitrification is somewhat better quantified in the Arabian Sea but the other possible loss mechanism of nitrogen to the atmosphere, viz., anammox, is yet to be evaluated.

- Both modeling (*Wiggert et al.*, 2006) and field measurements (*Naqvi et al.*, 2010) show that the primary productivity is limited by the availability of Fe in the nutrient-replete upwelled water in parts of the western Arabian Sea during the late summer monsoon. The biogeochemical and ecological implications of such Fe deficiency in the Arabian Sea and in other parts of the Indian Ocean need to be investigated in detail.

- The northern Indian Ocean is subject to significant riverine inputs, with globally significant annual freshwater discharges mostly during the summer monsoon. The freshwater is accompanied by terrigenous inputs such as dissolved inorganic nutrients, dissolved and particulate organic carbon and other elements (P,N,Fe) (*Seitzinger et al.*, 2005). The riverine inputs of both dissolved and particulate nitrogen to the ocean are poorly quantified, and no information is available on submarine groundwater flow so far. In the climate change scenario, the effect of the variation of the fresh water influx over the

nitrogen and carbon biogeochemistry of coastal seas and estuaries need to be investigated.

- It has also been hypothesized that the shift to a high CO_2/low pH ocean may significantly affect nitrogen cycling in anticipated and unanticipated ways such as the balance between nitrification/denitrification (*Huesemann et al.*, 2002) and nitrogen inputs due to N_2-fixation (*Hutchins et al.*, 2007). In this respect, the Arabian Sea and the Bay of Bengal are going to be very important basins to study such changes as they continuously experience continental influence.

- High CO_2/low pH condition is also likely to affect coastal communities. The past few decades have seen a significant change from inorganic nutrient loading to organic nutrient loading, and it has been suggested that this change in the primary nitrogen agents leading to eutrophication may be selecting for harmful and nuisance algal species (e.g., *Anderson et al.*, 2002). However, not much work has done in the Indian coastal areas to see such changes and its broader implications on the health of the coastal ecosystem.

- Equatorial Indian Ocean is still undersampled for its biological productivity, particularly the nitrogen uptake. Including the present study, only two studies are so far available for the region. Moreover, the Indian Ocean is warming faster than any other ocean basin (*Levitus et al.* 2000) and thus may serve as a sentinel for low latitude oceanic response to global warming. Therefore, to obtain large scale estimations for the carbon export fluxes, sustained observations over several years are needed.

- It has become apparent that the availability of Fe is a major factor limiting phytoplankton growth in the deep, open ocean regions of the Southern Ocean. Fe regulates the capability of phytoplankton to utilize NO_3 that is normally found in excess in the SO. However, the role of Fe over the uptake

of other nitrogenous nutrients such as NH_4 and urea in the SO are yet to be documented.

- Uptake studies on bulk phytoplankton communities have shown that a variety of nitrogen compounds are used simultaneously by phytoplankton. It is also known that there are inherent differences in the capabilities of organisms and their flexibility in acquiring nitrogen from different forms available in the environment, but little is known about cell-specific and taxa-specific uptake of nitrogen substrates. Therefore, it is important to undertake nitrogen uptake studies targeting specific cells and taxa for a better understanding of nitrogen cycling. This can provide a vital information about the f-ratios in natural environments in a better way, which has a direct bearing on the carbon budget of surface ocean.

References

References:

Anderson D. M., Glibert P. M., Burkholder J. M., 2002. Harmful algal blooms and eutrophication: Nutrient sources, composition, and consequences. *Estuaries* 25, 704-726.

Arrigo K. R., 2005. Marine microorganisms and global nutrient cycles. *Nature* 437, 349-355.

Aufdenkampe A. K. et al, 2002. Biogeochemical controls on new production in the tropical Pacific. *Deep Sea Research II* 49, 2619-2648.

Babu M. T., Prasanna Kumar S., Rao D. P., 1991. A subsurface cyclonic eddy in the Bay of Bengal. *Journal of Marine Research* 49, 404-410.

Babu M. T. et al, 2003. On the circulation in the Bay of Bengal during northern spring inter-monsoon (March-April) 1987. *Deep-Sea Research II* 50, 855-865.

Banse K., McClain C. R., 1986. Winter blooms of phytoplankton in the Arabian Sea as observed by the Coastal Zone Color Scanner. *Marine Ecological Progress Series* 34, 201-211.

Bates N. R., Pequigent A. C., Sabine C. L., 2006. Ocean carbon cycling in the Indian Ocean: 2. Estimate of net community production. *Global Biogeochemical Cycles* 20, GB3021 doi: 10.1029/2005GB002492.

Beaufort L., Bassinot F., Vincent E., 1999. Primary production response to the orbitally induced variations of the southern ossilation in the equatorial Indian Ocean. *In Reconstructing Ocean History: A window into the future* edited by Abrantes and Mix, Kluwer Academic/Plenum Publishers, New York. pp 245-294.

Belkin I. M., Gordon A. L., 1996. Southern Ocean fronts from the Greenwich Meridian to Tasmania. *Journal of Geophysical Research* 101, 3675-3696.

Bhattathiri P. M. A. et al, 1996. Phytoplankton production and chlorophyll distribution in eastern and central Arabian Sea in 1994-1995. *Current Science* 71, 857-862.

Bird C. et al, 2005. Spatial Distribution and Transcriptional Activity of an Uncultured Clade of Planktonic Diazotrophic γ-Proteobacteria in the Arabian Sea. *Applied And Environmental Microbiology* 71 (4), 2079-2085.

Boyd P. W. et al, 2007. Mesoscale iron enrichment experiments 1993-2005: Synthesis and future directions. *Science* 315, 612-617.

Brandes J. A. et al, 1998. Isotopic composition of nitrate in the central Arabian Sea and eastern tropical North Pacific: a tracer for mixing and nitrogen cycles. *Limnology and Oceanography* 43, 1680-1689.

Bronk D. A., Gilbert P. M., Ward B. B., 1994. Nitrogen Uptake, Dissolved Nitrogen Release, and New Production. *Science* 265, 1843-1846.

Buesseler K. O., 1991. Do upper-ocean sediment traps provide an accurate record of particle flux?. *Nature* 353, 420-423.

Buesseler K. O. et al, 1998. Upper ocean export of particulate organic carbon in the Arabian Sea derived from Thorium-234. *Deep Sea Research II* 45, 2461-2487.

Buesseler K. O. et al, 2007. An assessment of the use of sediment traps for estimating upper ocean particle fluxes. *Jouranl of Marine Research* 65, 345-416.

Burkill P. H., Mantoura R. F. C., Owens N. J. P., 1993. Biogeochemical cycling in the northwestern Indian Ocean: a brief overview. *Deep Sea Research II* 40, 643-649.

Bury S. J. et al, 2001. Size-fractionated primary production and nitrogen uptake during a North Atlantic phytoplankton bloom: Implications for carbon export estimates. *Deep Sea Research I* 48, 689-720.

Caldeira K., Duffy P. B., 2000. The role of the Southern Ocean in uptake and storage of anthropogenicc arbon dioxide. *Science* 287, 620-622.

Capone D. G. et al, 1997. Trichodesmium: a globally significant marine cynobacterium. *Science* 276, 1221-1229.

Capone D. G. et al, 1998. An extensive bloom of the N2 fixing cyanobacterium Trichodesmium erythraeum in the central Arabian Sea. *Marine Ecological Progress Series* 172, 281-292.

Capone D. G. et al, 2005. Nitrogen fixation by Trichodesmium spp.: An important source of new nitrogen to the tropical and subtropical North Atlantic Ocean. *Global Biogeochemical Cycles* 19, GB2024, doi:10.1029/2004GB002331.

Carmack E. C., 1992. Large-scale physical oceanography of polar oceans. in *Polar Oceanography, Part A: Physical Sciences*, Smith W.O., Jr., Ed., 171-222.

Chen Y. L., Chen H. Y., 2006. Seasonal dynamics of primary and new production in the northern South China Sea: THe significance of river discharge and nutrient advection. *Deep Sea Research I* 53, 971-986.

Codispoti L. A., Friedrich G. E., Hood D. W., 1986. Variability in the inorganic carbon system over the southeastern Bering Sea shelf during spring 1980 and sprin-summer 1981. *Continental Shelf Research* 5, 133-160.

Codispoti L. A., 2007. An oceanic fixed nitrogen sink exceeding 400 Tg N a^{-1} vs the concept of homeostasis in the fixed-nitrogen inventory. *Biogeosciences* 4, 233-253.

Cota G. F. et al, 1992. Nutrient and biogenic particulate distributions, primary productivity and nitrogen uptake in the Weddell-Scotia Sea marginal ice zone during winter. *Journal of Marine Research* 50, 155-181.

Cullen J. J., 1991. Hypotheses to explain high nutrient, low chlorophyll conditions in the open sea. *Limnology and Oceanography* 36, 1578-1599.

Collos Y., Slawyk G., 1986. 13C and 15N uptake by marine phytoplankton. IV. Uptake ratios and the contribution of nitrate to the productivity of Antarctic waters (Indian Ocean sector). *Deep Sea Research* 33, 1039-1051.

Darbyshire M., 1966. The surface waters near the coasts of Southern Africa. *Deep Sea Research* 13, 57-81.

Deacon G., 1984. The Anarctic circumpolar ocean. *Cambridge University Press*, pp. 180.

Denman K. L. et al, 2007: Couplings Between Changes in the Climate System and Biogeochemistry. In: Climate Change 2007: The Physical Science Basis. Contribution of Working Group I to the Fourth Assessment Report of the Intergovernmental Panel on Climate Change [Solomon, S., Qin D., Manning M., Chen Z., Marquis M., Averyt K. B.,Tignor M. and Miller H. L. (eds.)]. Cambridge University Press, Cambridge, United Kingdom and New York, NY, USA.

Dessai D. V. G. et al, 2010. Reading source and processes from the distribution of suspended particulate matter and its selected elemental chemistry in the Southern and Indian Oceans. *Current Science* (in the press).

Devassy V. P., Bhattathiri P. M. A., Qasim S. Z., 1978. *Trichodesmium* Phenomenon. *Indian Journal of Marine Sciences* 7, 168-186.

Dickson M. et al, 2001. Production and respiration rates in the Arabian Sea during the 1995 Northeast and Southwest Monsoons. *Deep Sea Research II* 48, 1199-1230.

Donald K. M. et al, 2001. Uptake of carbon, nitrogen and phosphorus by phytoplankton along the 20^{o}W meridian in the NE Atlantic between 57.5^{o}N and 37^{o}N. *Deep Sea Research II* 48, 873-897.

Dubischar C. D., Bathmann U. V., 1997. Grazing impact of copepods and salps on phytoplankton in the Atlantic sector of the Southern Ocean. *Deep Sea Research II* 44, 415-433.

Dugdale R. C., Goering J. J., 1967. Uptake of new and regenerated forms of nitrogen in primary productivity. *Limnology and Oceanography* 12, 196-206.

Dugdale R. C., Goering J. J., Ryther J. H., 1964. High nitrogen fixation rates in the Sargaso Sea and the Arabian Sea. *Limnology and Oceanography* 9 (4), 507-510.

Dugdale R. C., Wilkerson F. P., 1986. The use of 15N to measure nitrogen uptake in eutrophic oceans: Experimental considerations. *Limnology and Oceanography* 31, 673-689.

Dwivedi R. M. et al, 2006. Influence of northeasterly trade winds on intensity of winter bloom in the Northern Arabian Sea. *Current Science* 90 (10), 1397-1406.

Elskens M. et al, 2008. Primary, new and export production in the NW Pacific subarctic gyre during the vertigo K2 experiments. *Deep Sea Research II* 55, 1594-1604.

El-Sayed S. Z., 1978. Primary productivity and estimates of potential yields on the Southern Ocean. in *Polar Research: To the Present and the Future*, AAAS Selected Symposia 7, Whinnie, M.A., Ed., American Association for the Advancement of Science, Washington, DC, 141-160.

El-Sayed S. Z., 1984. Productivity of Antarctic watersa reappraisal, in *Marine Phytoplankton and Productivity*, HolmHansen O., Bolis L., Gilles R., Eds., Springer, Berlin, 19-34.

Eppley R. W. et al, 1977. Nitrogen assimilation by phytoplankton and other microorganism in the surface waters of the central North Pacific Ocean. *Marine Biology* 39, 111.

Eppley R. W., Petersen B. J., 1979. Particulate organic matter flux and planktonic new production in the deep ocean. *Nature* 282, 677-680.

Eppley R. W., Koeve W., 1990. Nitrate use by plankton in the eastern subtropical North Atlantic, March-April 1989. *Limnology and Oceanography* 35, 1781-1788.

Evans W., Strutton P. G., Chavez F. P., 2009. Impact of tropical Instability waves on nutrient and chlorophyll distributions in the equatorial Pacific. *Deep Sea Research I* 56, 178-188.

Falkowski P. G. et al, 1991. Role of eddy pumping in enhancing primary production in the ocean. *Nature* 352, 55-58.

Falkowski P., Barber R. T., Smetacek V., 1998. Biogeochemical controls and feedbacks on ocean primary productivity. *Science* 281, 200-206.

Falkowski P. et al, 2000. The Global Carbon Cycle: A test of our knowledge of Earth as a system. *Science* 290, 291-296.

Fernandez C. et al, 2005. An estimation of annual new production and carbon fluxes in the northeast Atlantic Ocean during 2001. *Journal of Geophysical Research* 110, C07S13, doi:10.1029/2004JC002616.

Fernndez C., Raimbault P., 2007. Nitrogen regeneration in the NE Atlantic Ocean and its impact on seasonal new, regenerated and export production. *Marine Ecology Progress Series* 337,79-92.

Fischer J., Schott F. A., Stramma L., 1996. Currents and transports of the Great Whirl-Socotra Gyre system during the summer monsoon August 1993. *Journal of Geophysical Research* 101, 3573-3587.

Fu Fei-Xue, Bell P. R. F., 2003. Factors affecting N_2 fixation by the cyanobacterium *Trichodesmium* sp. GBRTRLI101 FEMS. *Microbiology Ecology* 45 (2), 203-209.

Gauns M. et al, 2005.Comparative accounts of biological productivity characteristics and estimates of carbon fluxes in the Arabian Sea and the Bay of Bengal. *Deep Sea Research II* 52, 2003-2017.

Glibert P. M. et al, 1982a. Isotope dilution models of uptake and remineralization of ammonium by marine plankton. *Limnology and Oceanography* 27, 639-650.

Glibert P. M., Biggs D. C., McCarthy J. J., 1982b. Utilization of ammonium and nitrate during austral summer in the Scotia Sea. *Deep Sea Research* 29, 837-850.

Goes J. I. et al, 2005. Warming of the Eurasian Landmass in making the Arabian Sea more productive. *Science* 30, 545-547.

Goeyens L. et al, 1991. Spatiotemporal variability of inorganic nitrogen stocks and uptake fluxes in the Scotia-Weddell Confluence area during November and December 1988. *Marine Ecology Progress Series* 77, 7-19.

Gomes H. R., Goes J. I., Saino T., 2000. Infuence of physical processes and freshwater discharge on the seasonality of phytoplankton regime in the Bay of Bengal. *Continental Shelf Research* 20, 313-330.

Gomes H. R. et al, 2008. Blooms of Noctiluca miliaris in the Arabian SeaAn in situ and satellite study. *Deep Sea Research I* 55, 751-765.

Gordon, A. L., Taylor H. W., Georgi D. T., 1977. Antarctic oceanographic zonation. *Polar Oceans, Proceedings of the Polar Oceans Conference* Arctic Institute of North America. 44-76.

Gordon A. L., Lutjeharms J. R. E., Grundlingh M. L., 1987. Stratication and circulation at the Agulhas Retroection. *Deep Sea Research* 34, 565-599.

Grunseich G. S. et al, 1980. Sample conversion, mass spectrometry, and calculations for 15N analysis of phytoplankton nutrient uptake. Coastal Upwelling Ecosystem Analysis (CUEA) Tech. Rep. 44.

Harrison W. G., Platt T., Lewis M. R., 1987. f-ratio and its relationship to ambient nitrate concentration in coastal waters. *Jouranl of Plankton Research* 9, 235- 248.

Harrison, W. G. et al, 1992. Nitrogen dynamics at the VERTEX time-series site. *Deep Sea Research I* 39, 1535-1552.

Harrison W. G., Harris L. R., Irwin B. D. R., 1996. The kinetics of nitrogen utilization in the mixed layer: Nitrate and ammonium interactions at nanomolar concentrations. *Limnology and Oceanography* 41 (1), 16-32.

Holliday N. P., Read J. F., 1998. Surface oceanic fronts between Africa and Antarctica. *Deep Sea Research I* 45, 217-238.

Holm-Hansen O. et al, 1977. Primary production and the factors controlling phytoplankton growth in the Southern Ocean, in Adaptations within Antarctic Ecosystems, Llano, G.A., Ed., Smithsonian Institution, Washington, DC, 11-73.

Holm-Hansen O., Mitchell B. G., 1991. Spatial and temporal distribution of phytoplankton and primary production in the western Bransfield Strait. *Deep Sea Research* 38, 961-980.

Houghton R. A., 2007. Balancing the Global Carbon Budget. *Annu. Rev. Earth Planet. Sci.* 35, 313-347.

Hu S. H., Smith W. O., 1998. The effects of irradiance on nitrate uptake and dissolved organic nitrogen release by phytoplankton in the Ross Sea. *Continental and Shelf Research* 18, 971-990.

Huesemann M. H., Skillman A. D., Crecelius E. A., 2002. The inhibition of nitrification by ocean disposal of carbon dioxide. *Mar. Pollut. Bull.* 44, 142-148.

Hutchins D. A. et al, 2007. CO_2 control of Trichodesmium N_2-fixation, photosynthesis, growth rates, and elemental ratios: Implications for past, present, and future ocean biogeochemistry. *Limnology and Oceanography* 52, 1293-1304.

Ittekkot V. et al, 1991. Enhanced particle fluxes in Bay of Bengal induced by injection of fresh water. *Nature* 351, 385-387.

Jasmine P. et al, 2009. Hydrographic and productivity characteristics along 45E longitude in the southwestern Indian Ocean and Southern Ocean during austral summer 2004. *Marine Ecology Progress Series* 389, 97-116.

Jobbagy E. G., Jackson R. B., 2000. The vertical distribution of soil organic carbon and its relation to climate and vegetation. *Ecol. Applicat.* 10, 423-436.

Johansen A. M., Hoffmann M. R., 2003. Chemical chracterization of ambient aerosol collected during the northeast monsoon season over the Arabian Sea: Labile-Fe(II) and other trace metals. *Journal of Geophysical Research*, doi: 10.1029/2002JD003280.

Jyothibabu R. et al, 2003. Intense blooms of Trichodesmium erythraeum (Cyanophyta) in the open waters along east coast of India. *Indian Journal of Marine Sciences* 32(2), 165-167.

Jyothibabu R. et al, 2008. Seasonal variation of microzooplankton (20-200 μm) and its possible implications on the vertical carbon flux in the western Bay of Bengal. *Continental Shelf Research* 28, 737-755.

Karl D. M. et al, 1995. Ecosystem changes in the North Pacific subtropical gyre attributed to the 1991-92 El Nino. *Nature* 373, 230-234.

Karl D. M. et al, 2002. Dinitrogen fixation in the world's oceans, *Biogeochemistry* 57, 47- 98.

Klinck J. M., Nowland Jr. W. D., 2001. Antarctic Circumpolar Current. *Encyclopedia of Ocean Science, Academic Press* 1st Edition, 151-59.

Knox G. A., 1970. Antarctic marine ecosystems, in *Antarctic Ecology* Vol. 1, Holdgate M.W., Ed., Academic Press, London, 69-96.

Knox G. A., 2006. Biology of the Southern Ocean. Second Edition. Taylor and Fransis Group, ISBN: 0-8493-3394-6.

Koike I., Holm-Hansen O., Biggs D. C., 1986. Inorganic nitrogen metabolism by Antarctic phytoplankton, with special reference to ammonia cycling, *Marine Ecology Progress Series* 30, 105-116.

Kumar S., 2004. Biogeochemistry of Nitrogen isotopes in Northern Indian Ocea. PhD Thesis. M. S. Univeristy of Baroda, Vadodara, INDIA.

Kumar S. et al, 2004. High new production in the Bay of Bengal: Possible causes and implications. *Geophysical Research Letters* 31, L18304, doi:10.1029/2004GL021005.

Kuamr S., Ramesh R., 2005. Productivity measurements in the Bay of Bengal using ^{15}N tracer: Implications to the global carbon cycle. *Indian Journal of Marine Sciences* 34(2), 153-162.

Kumar S. et al, 2010. Nitrogen uptake in the northeastern Arabian Sea during winter cooling. *International Journal of Oceanography* (in the press).

Kuramoto S., Koyama K., 1982. Preliminary report of the oceanographic observations on the 22nd Japanese Antarctic Research Expedition (1980-1981), *Mem. Natl. Inst. Polar Res.* Special Issue 23, 5-12.

Laws E. A. et al, 2000. Temperature effects on export production in the open ocean. *Global Biogeochemical Cycles* 14 (4), 1231-1246.

Lee K., 2001. Global net community production estimated from the annual cycle of surface water total dissolved inorganic carbon, *Limnology and Oceanography* 46, 1287-1297.

Letelier R. M., Karl D. M., 1996. Role of *Trichodesmium* spp. in the productivity of the subtropical North Pacific Ocean. *Marine Ecology Progress Series* 133, 263-273.

Levitus S., Boyer T. P., 1994. World Ocean Atlas 1994, Vol. 5, Temperature. *NOAA Atlas NESDIS*, Vol. 4. US Government Printing Office, Washington, DC, 117pp.

Levitus S et al, 2000. Warming of the world ocean. *Science* 287, 2225-2229.

Levitus S., Burgett R. Boyer T. P., 1994. World Ocean Atlas 1994, Vol. 5, Salinity. *NOAA Atlas NESDIS*, Vol. 3. US Government Printing Office, Washington, DC, 99pp.

Lewis M. R. et al, 1986. Vertical nitrate fluxes in the oligotrophic ocean. *Science* 234, 870- 873.

Lipschultz F. 2001. A time-series assessment of the nitrogen cycle at BATS. *Deep Sea Research II* 48, 1897-1924.

Lipschultz F. et al, 2002. New production in the Sargasso Sea: History and current status, *Global Biogeochemical Cycles* 16 (1), doi: 10.1029/2000GB001319.

Luz B., Barkan E., 2000. Assessment of Oceanic Productivity with the Triple-Isotope Composition of Dissolved Oxygen. *Science* 288, 2028-2031.

MacIsaac J. J., Dugdale R. C., 1972. Interactions of light and inorganic nitrogen in controlling nitrogen uptake in the sea. *Deep Sea Research* 19, 209-232.

Madhu N. V. et al, 2002. Enhanced biological production off Chennai triggered by October 1999 super cyclone (Orissa). *Current Science* 82 (12), 1472-1479.

Madhu N. V. et al, 2006. Lack of seasonality in phytoplankton standing stock (chlorophyll *a*) and production in the western Bay of Bengal. *Continental Shelf Research* 26, 1868-1883.

Madhupratap M. S. et al, 1996. Mechanism of the biological response to winter cooling in the northeastern Arabian Sea. *Nature* 384, 549-552.

Martin J. et al, 1991. The case of Iron. *Limnology Oceanography* 36(8), 1793-1802.

Matear R., Hirst A. C., 1999. Climate change feedback on the future oceanic CO2 uptake. *Tellus* 5, 722-733.

Matondkar S. G. P. et al, 2006. Setellite and ship studies of phytoplankton in the Northeastern Arabian Sea during 2000-2006 period. *Proceedings of SPIE* 6406, doi: 10.117/12.693693.

MacCarhty J. J., Carpenter E. J., 1979. *Oscillatoria* (*Trichodesmium*) *thiebautii* (Cyanophyta) in the central North Atlantic Ocean. *Journal of Phycology* 15, 75-82.

McCarthy J. J. et al, 1996. Newproduction along 140^{o}W in the equatorial Pacific during and following the 1992 El Nino event. *Deep Sea Research II* 43, 1065-1093.

McCarthy J. J., Garside C., Nevins J., 1999. Nitrogen dynamics during the Arabian Sea northeast monsoon. *Deep Sea Research II* 46, 1623-1664.

Mengesha S. et al, 1998. Seasonal variation of phytoplankton community structure and nitrogen uptake regime in the Indian Sector of the Southern Ocean. *Polar Biology* 20, 259-272.

Mengesha S. et al, 1999. Phytoplankton nitrogen nutrition in the Western Indian Ocean: Ecophysiological adaptations of Neritic and Oceanic assemblages to ammonium supply. *Extuarine, Coastal and Shelf Science* 48, 589-598.

Minas H. J., Minas M., Packard T. T., 1986. Productivity in upwelling areas deduced from hydrographic and chemical fields, *Limnology and Oceanography* 31, 1180-1201.

Montoya J. P., Voss M., 2006. Nitrogen cycling in suboxic waters: isotopic signatures of nitrogen transformation in the Arabian Sea oxygen minimum zone, in: *Past and present Water column Anoxia*. (ed. L. N. Neretin) Springer, Netherlands, pp. 259-281.

Murtugudde, R. et al, 1999. Ocean color variability of the tropical Indo-Pacific basin observed by SeaWIFS during 199798. *Journal of Geophysical Research* 104, 18351-18366.

Murty V. S. N., Suryanarayana A., Rao D. P., 1993. Current structure and volume transport across 121^oN in the Bay of Bengal. *Indian Journal of Marine Sciences* 22, 12-16.

Nair R. R. et al, 1989. Increased particle flux to the deep ocean related to monsoons. *Nature* 338, 749-751.

Naqvi S. W. A., 1987. Some aspects of the oxygen deficient conditions and denitrification in the Arabian Sea. *Journal of Marine Research* 45, 1049-1072.

Naqvi S. W. A. et al, 1996. Respiration rates in subsurface waters of the northern Indian Ocean: Evidence for low decomposition rates of organic matter within the water column in the Bay of Bengal. *Deep Sea Research I* 43, 73-81.

Naqvi S. W. A. et al, 2010. The Arabian Sea as a high-nutrient, low-chlorophyll region during the late Southwest Monsoon. *Biogeosciences Discuss* 7, 25-53.

Narvekar J., Prasanna Kumar S., 2006. Seasonal variability of the mixed layer in the central Bay of Bengal and associated changes in nutrients and chlorophyll. *Deep Sea Research I* 53, 820-835.

Neess J. C. et al, 1962. Nitrogen metabolism in lakes, Measurement of nitrogen fixation with 15N, *Limnology and Oceanography* 7, 163-169.

Nelson D. M., Smith W. O. Jr., 1991. Sverdrup re-visited: critical depths, maximum chlorophyll levels, and the control of Southern Ocean productivity by the irradiance-mixing regime. *Limnology and Oceanography* 36, 1650-1661.

Nielsen S. E., 1952. The use of radioactive Carbon (14C) for measuring organic production in the sea. *J. Cons. Int. Explor. Mer.* 18, 117-140.

Odate T., Fukuchi M., 1995. Distribution and community structure of picophytoplankton in the Southern Ocean during the late austral summer of 1992. *NIPR Symp. Polar Biology* 8, 86-100.

Orsi A. H., Whitworth T., Nowlin W. D., 1995. On the meridional extent and fronts of the Antarctic Circumpolar Current. *Deep Sea Research* 42(5), 641-673.

Owens N. J. P. et al, 1993. Size-fractionated primary production and nitrogen assimilation in the northwestern Indian Ocean. *Deep Sea Research II* 40(3), 607-709.

Parab S. G. et al, 2006. Monsoon driven changes in phytoplankton populations in the eastern Arabian Sea as revealed by microscopy and HPLC pigment analysis, *Continental Shelf Research* 26, 2538-2558.

Pena M. A., Harrison W. G., Lewis M. R., 1992. New production in the central equatorial Pacific. *Marine Ecology Progress Series* 80, 265-274.

Planas D. et al, 1999. Nitrate uptake and diffusive nitrate supply in the central Atlantic. *Limnology and Oceanography* 44, 116-126.

Planas D. et al, 1999. Nitrate uptake and diffusive nitrate supply in the central Atlantic. *Limnology and Oceanography* 44, 116-126.

Platt T. et al, 1989. Biological production of the oceans: The case for a consensus. *Marine Eclogical Progress Series* 52, 77-89.

Platt T., Jauhari P., Sathyendranath S., 1992. The importance and measurement of new production, in *Primary Productivity and Biogeochemical Cycles in the Sea*, edited by Falkowski P. G. and Woodhead A. D., pp. 273- 284, Springer, New York.

Plattner G. K., Gruber N., Frengel H., McWilliams J. C., 2005. Decoupling marine export production from new production. *Geophysical Research Letters* 32, L11612 doi: 10.1029/2005GL022660.

Poulton A. J., Stinchcombe M. C., Quartly G. D., 2009. High numbers of *Trichodesmium* and diazotrophic diatoms in the southwest Indian Ocean. *Geophysical Research Letters* 36, L15610, doi:10.1029/2009GL039719.

Prakash S., 2008. Role of the ocean in the Global carbon cycle. PhD. thesis. The Maharaja Sayajirao University of Baroda Vadodara, India.

Prakash S., and Ramesh R., 2007. Is the Arabian Sea getting more productive?. *Current Science* 92(5), 667-671.

Prakash S. et al, 2008. Quantification of New Production during a winter Noctiluca scintillans bloom in the Arabian Sea. *Geophysical Research Letters* 35, doi: 10.1029/2008GL033819.

Prasad T. G., 1997. Annual and seasonal mean buoyancy fluxes for the tropical Indian Ocean. *Current Science* 73, 667-674.

Prasanna Kumar S., Prasad T. G., 1996. Winter cooling in the northern Arabian Sea. *Current Science* 71 (11), 834-841.

Prasanna Kumar S. et al, 2001. Physical forcing of biological productivity in the Northern Arabian Sea during the Northeast Monsoon. *Deep Sea Research II* 48, 1115-1126.

Prasanna Kumar S. et al, 2002. Why is the Bay of Bengal less productive during summer monsoon compared to the Arabian Sea?. *Geophysical Research Letters* 29, 22-35.

Prasanna Kumar S. et al, 2004. Are Eddies nature's trigger to enhance biological productivity in the Bay of Bengal?. *Geophysical Research Letters* 31, L07309, doi:10.1029/2003Gl019274.

Prasanna Kuamr S., Narvekar J., 2005. Seasonal variability of the mixed layer in the Arabian Sea and its implication on nutrients and primary productivity. *Deep Sea Research II* 52, 1848-1861.

Prasanna Kuamr S. et al, 2007. Eddy-mediated biological productivity in the Bay of Bengal during fall and spring intermonsoons. *Deep Sea Research I* 54, 1619-1640.

Qasim S.Z., 1977. Biological productivity of the Indian Ocean, *Indian Jouranl of Marine Sciences* 6, 122-137.

Radhakrishna K., 1978. Primary productivity of the Bay of Bengal during March-April 1975. *Indian Journal of Marine Science* 7, 58-60.

Raimbault et al, 1999. Carbon and nitrogen uptake and export in the equatorial Pacific at 150^{o}W: Evidence of an efficient regenerated production cycle. *Journal of Geophysical Research* 104 (C2), 3341-3356.

Ramasastry A. A., Balaramamurty C., 1957. Thermal fields and oceanic circulation along the east coast of India. *Proceedings of the Indian Academy of Science* 46, 293-323.

Ramaswamy V., Nair R.R., 1994. Fluxes of material in the Arabian Sea and Bay of Bengal-Sediment trap studies. *Proceedings of the Indian Academy of Sciences (Earth and Planetary Sciences)* 103, 189-210.

Ramaswamy V., Sarin M. M., Rengarajan R., 2005. Enhanced export of carbon by salps during the northeast monsoon period in the northern Arabian Sea. *Deep Sea Research-II* 52, 1922-1929.

Rao C. K. et al, 1994. Hydrography of the Bay of Bengal: Possible reasons for a different water-column cycling of carbon and nitrogen from the Arabian Sea. *Marine Chemistry* 47, 279-290.

Read J. F., Pollard R. T., 1993. Structure and transport of the Antarctic circumpolar current and Agulhas Return current at 40E. *Journal of Geophysical Research* 98, 12281-12295.

Reuer M. K. et al, 2007. New estimates of Southern Ocean biological production rates from O_2/Ar ratios and the triple isotope composition of O_2. *Deep Sea Research I* 54, 951-974.

Ryther J. H. et al, 1966. Primary organic production in relation to the chemistry and hydrography of the western Indian Ocea. *Limnology and Oceanography* 11, 371-380.

Sabine C. L. et al, 2004. The Oceanic Sink for Anthropogenic CO_2. *Science* 305, 367-371.

Sakshaug E., Holm-Hansen O., 1984. Factors governing pelagic production in polar oceans. in *Marine Phytoplankton and Productivity* Holm-Hansen O., Bolis, O.L., Gilles, R., Eds., Springer, Berling/ Heidelberg, 1-18.

Sakshaug E., Slagstad D., 1991. Light and productivity of phytoplankton in polar marine systems: A physiological view. in *Pro Mare Symposium on Polar Marine Ecology*, Trondheim, Sakshaug E., Hopkins C. C. E., Eds., Polar Research, 69-85.

Sakshaug E., Slagstad D., Holm-Hansen O., 1991. Factors controlling the development of phytoplankton blooms in the Antarctic Oceana mathematical model. *Marine Chemistry* 35, 259-271.

Sambrotto R. N., 2001. Nitrogen production in the northern Arabian Sea during the Spring Intermonsoon and Southwest Monsoon seasons. *Deep Sea Research II* 48, 1173-1198.

Sambrotto R. N., Mace B. J., 2000. Coupling of biological and physical regimes across the Antarctic Polar Front as refected by nitrogen production and recycling. *Deep Sea Research II* 47, 3339-3367.

Sardessai S. et al, 2007. Influence of environmental forcings on the seasonality of dissolved oxygen and nutrients in the Bay of Bengal. *Jouranl of Marine Research* 65, 301-316.

Sardessai S. et al, 2010. Nutrient characteristics of the water masses and their seasonal variability in the eastern equatorial Indian Ocean. *Marine Environmental Research*, 10.1016/j.marenvres.2010.05.009.

Sarma V. V. S. S., 2004. Net plankton community production in the Arabian Sea based on O_2 mass balance model. *Global Biogeochemical Cycles* 18, 10.1029/2003GB002198.

Sarma V. V. S. S., Kumar M. D., George M. D., 1998. The eastern and Central Arabian Sea as a perennial source for atmospheric carbon dioxide. *Tellus* 50B, 179-184.

Sarma V. V. S. S. et al, 2003. Carbon budget in the eastern and central Arabian Sea: An Indian JGOFS synthesis. *Global Biogeochemical Cycles* 17 (4), doi:10.1029/2002GB001978.

Sarma V. V. S. S., Kumar M. D., Saino T., 2006. Impact of sinking carbon flux on accumulation of deep-ocean carbon in the Northern Indian Ocean. *Biogeochemistry*, DOI 10.1007/s10533-006-9055-1.

Sarmiento J. L., Siegenthaler U., 1992. New Production and Global Carbon Cycle, in *Primary Productivity and Biogeochemical Cycles in The Sea*, Edited by Falkowski P. G. and Woodhead A. D., 317-332, Springer, New York.

Savoye N. et al, 2004. Regional variation of spring N-uptake and new production in the Southern Ocean. *Geophysical Research Letters* 31, L03301, doi:10.1029/2003GL018946.

Schott F., 1983. Monsoon response of the Somali current and associated upwelling. *Progress in Oceanography* 12, 357-381.

Schott F., McCreary J. P., 2001. The monsoon circulation of the Indian Ocean. *Progress in Oceanography*, 51, 1-123.

Seitzinger S. P. et al, 2005. Sources and delivery of carbon, nitrogen, and phosphorus to the coastal zone: An overview of global nutrient export from watersheds (NEWS) models and their application. *Global Biogeochemical Cycles* 19, Art. No. GB4S01, doi: 10.1029/2005GB002606.

Seki M. P. et al, 2001. Biological enhancement at cyclonic eddies tracked with GOES thermal imagery in Hawaiian waters. *Geophysical Letters* 28, 1583-1586.

Semeneh M. et al, 1998. Nitrogen uptake regime and phytoplankton community structure in the Atlantic and Indian sectors of the Southern Ocean. *Jouranl of Marine Systems* 17, 159-177.

Senan R., Sengupta D., Goswami B. N., 2003. Intraseasonal "monsoon jets" in the equatorial Indian Ocean. *Geophysical Research Letters* 30, doi:10.1029/2003GL017583.

Sengupta D., Bharath Raj G. N., Shenoi S. S. C., 2006. Surface freshwater from Bay of Bengal runoff and Indonesian Throughflow in the tropical Indian Ocean, *Geophysical Research Letters* 30, doi:10.1029/2006GL027573.

Shankar D., Vinaychandran P. N., Unnikrishnan A. S., 2002. The monsoon currents in the north Indian Ocean. *Progress in Oceanography* 52, 63-120.

Shetye S. R. et al, 1990. Hydrography and circulation off the west coast of India during the southwest monsoon 1987. *Journal of Marine Research* 48, 359-378.

Shetye S. R. et al, 1991. Wind-driven coastal upwelling along the western boundary of the Bay of Bengal during the southwest monsoon. *Continental Shelf Research* 11, 1397-1408.

Shetye S. R. et al, 1993. The western boundary current of the seasonal subtropical gyre in the Bay of Bengal. *Journal of Geophysical Research* 98, 945-954.

Slawyk G., Collos Y. , Auclair J. C., 1977. The use of the 13C and 15N isotopes for the simultaneous measurement of carbon and nitrogen turn over rates in marine phytoplankton. *Limnology and Oceanography* 22, 925-932.

Slawyk G., 1979. ^{13}C and ^{15}N uptake by phytoplankton in the Antarctic upwelling area: Results from the Antipord I cruise in the Indian Ocean Sector. *Australian Journal of Marine and Freshwater Research* 30, 431-448.

Slawyk G., Raimbault, P., 1995. Simple procedure for simultaneous recovery of dissolved inorganic and organic nitrogen in 15N-tracer experiments and improving the isotopic mass balance. *Marine Ecology Progress Series* 124, 289-299.

Smith R. L., Bottero J. S., 1977. On upwelling in the Arabian Sea. In: *A voyage of discovery* (Ed) M. Angel, pp. 291-304, Pergamon Press.

Smith W. O., 1993. Nitrogen Uptake and New Production in the Greenland Sea' The Spring Phaeocystis Bloom. *Journal of Geophysical Research* 98, 4681-4688.

Smith W. O., 1995. Primary productivity and new production in the Northeast Water (Greenland) Polynya during summer 1992. *Journal of Geophysical Research* 100, 4357-4370.

Smith W. O. et al, 1997. New production in the Northeast Water Polynya: 1993. *Jouranl of Marine Systems* 10, 199-209.

Spencer D., Broecker W. S., Craig H., Weiss R. F., 1982. GEOSECS Indian Ocean Expedition, Vol. 6, Sections and Profiles. *National Science Foundation*, 140pp, Washington DC.

Squire V. A., 1987. The physical oceanography and sea ice characteristics of the Southern Ocean, Primer Symposium Espanol de Estudios Antarcticos, Pama de Mallorca, 30 June-July 1985, 12.

Subramanian V., 1993. Sediment load of Indian Rivers. *Current Science* 64, 928-930.

Sullivan C. W. et al, 1993. Distribution of phytoplankton blooms in the Southern Ocean. *Science* 262, 1832-1837.

Tyrrell T. et al, 2003. Large-scale latitudinal distribution of *Trichodesmium* spp. in the Atlantic Ocean. *Journal Plankton Research* 25, 405-416.

UNESCO, 1994. "Protocols for the Joint Global Ocean Flux Study (JGOFS) core measurements", Manual and guides, 170, Scientific Committee on Oceanic Research, 29. pp 120.

Varela D. E., Harrison P. J., 1999. Seasonal variability in nitrogenous nutrition of phytoplankton assemblages in the northeastern subarctic Pacific Ocean. *Deep Sea Research II* 46, 2505-2538.

Varela M. et al, 2005. Nitrogen uptake and dissolved organic nitrogen release in planktonic communities characterized by phytoplankton size structure in the central North Atlantic. *Deep Sea Research I* 52, 1637-1661.

von Brockel K., 1981. The importance of nanoplankton within the pelagic Antarctic ecosystem, Kieler Meeresforschung Sonderheft, 5, 61-67.

von Brockel K., 1985. Primary production data from the south-eastern Weddell Sea, *Polar Biology* 4, 75.

Wafar M. V. M. et al, 1986. Nitrogenous nutrients and primary production in a tropical oceanic environment. *Bulletin of Marine Science* 38 (2), 273-284.

Watanabe K., Nakajima Y., 1982. Vertical distribution of chlorophyll a along 458 E in the southern ocean, 1981. *Mem. Natl. Inst. Polar Res.* Special Issue 23, 73-86.

Watts L. J., Owens N. J. P., 1999. Nitrogen assimilation and f-ratio in the north-western Indian Ocean during an Intermonsoon period. *Deep Sea Research II* 46, 725-743.

Westberry T. K., Siegel D. A., 2006. Spatial and temporal distribution of Trichodesmium blooms in the world's oceans. *Global Biogeochemical cycles* 20, GB4016, doi: 10.1029/2005GB002673.

Wheeler P. A., 1993. New production in the subarctic Pacific Ocean: net changes in nitrate concentrations, rates of nitrate assimilation and accumulation of particulate nitrogen. *Progress in Oceanography* 32, 137-161.

Wiggert J. D., Murtugudde R. G., Christian J. R., 2006. Annual ecosystem variability in the tropical Indian Ocean: Results of a coupled bio-physical ocean general circulation model. *Deep Sea Research II* 53, 644-676.

Wilkerson F. P., Dugdale R. C., 1992. Measurements of nitrogen productivity in the equatorial Pacific. *Journal of Geophysical Research* 97, 669-679.

Wyrtki K., 1973. An equatorial jet in the Indian Ocean. *Science* 181, 1331-1338.

Wyrtki K., 1988. Oceanographic Atlas of the International Indian Ocean Expedition. *Amerind Publishing Co. Pvt. Ltd.*, New Delhi, India.

Yool A. et al, 2007. The significance of nitrification for oceanic new production. *Nature* 447, 999-1002.

You Y., Tomczak M., 1993. Thermohaline circulation and ventilation in the Indian Ocean derived from water mass analysis. *Deep Sea Research I* 40 (1), 13-56.

List of Publications

1. *Estimation of Decomposition Rates of Peat Deposits using Radiocarbon*
   M. G. Yadava, **Naveen Gandhi** and R. Ramesh
   Indian Journal of Geochemistry, 22(1), 57-64, 2007.

2. *Nitrogen sources for new production in the NE Arabian Sea during spring*
   Naveen Gandhi and R. Ramesh
   Eleventh ISMAS Triennial Conference on mass spectrometry 2009, Hyderabad, INDIA, pp. 261-263, 2009.

3. *Nitrogen uptake rates and new production in the northern Indian Ocean*
   Naveen Gandhi, S. Prakash, R. Ramesh and S. Kumar
   Indian Journal of Marine Sciences, 2010 (accepted).

4. *Improving the estimation of new production using the ^{15}N tracer technique: a case study from the northern Indian Ocean*
   Naveen Gandhi
   National Academy Science Letters, 2010 (accepted).

5. *Nitrogen uptake rates during spring in the NE Arabian Sea*
   Naveen Gandhi, R. Ramesh, R. Srivastava, M. S. Sheshshayee, R. M. Dwivedi, and Mini Raman
   International Journal of Oceanography, 2010 (under review).

6. *Nitrogen sources for new production in the NE Arabian Sea*
   Naveen Gandhi, R. Ramesh, S. Prakash, and S. Kumar

Journal of Sea Research, 2010 (under review).

7. *Measurement of marine productivity using ^{15}N and ^{13}C tracers: some methodological aspects*
   Naveen Gandhi, S. Kumar, R. Ramesh and M. S. Sheshshayee
   Journal of Earth System Science, 2010 (under review).

8. *First direct measurements of N_2 fixation during Trichodesmium bloom in the eastern Arabian Sea*
   Naveen Gandhi, A Singh, S. Prakash, R. Ramesh, Mini Raman, M. S. Sheshshayee and Suhas Shetye
   Global Biogeochemical Cycles, 2010 (under review).

9. *Role of atmospheric deposition in new productivity in the northern Indian Ocean*
   A. Singh, **Naveen Gandhi** and R. Ramesh
   Atmospheric Science Letters, 2010 (under review).

10. *Nitrogen sources for new production in the NE Indian Ocean*
    Naveen Gandhi, A. Singh and R. Ramesh
    Advances in Geosciences, 2010 (under review).